October 15, 1979

Final Report of Research Performed Under the Contract NASW-3053

Analysis of Time Dependent Phenomena Observed with the LPSP OSO-8 Instrument.

Prepared by:

John W. Leibacher

Lockheed Palo Alto Research Laboratory
3251 Hanover Street
Palo Alto, California 94304

For NASA Headquarters

TABLE OF CONTENTS

I) Introduction

This program studied the dynamics of the solar photosphere and chromosphere. Observations obtained by the Laboratoire de Physique Stellaire et Planetaire's ultra-violet spectrometer onboard the OSO-8 spacecraft were analyzed and two papers presenting results were published. Three reviews on different topics concerning the theory of stellar atmospheric dynamics were presented and published. Dynamical models of the chromosphere and the emitted resonance line spectrum were calculated, and one article has been accepted for publication and another is in preparation. Three contributed papers were delivered at scientific conferences. These publications are attached.

II) Discussion

Repeated spectral scans of strong, optically thick resonance lines formed in the solar chromosphere were analyzed for indications of oscillatory velocities and intensities. Figure 1 displays Lyman alpha data obtained during one orbit, which has had data losses replaced by interpolation. These spectra were taken away from active regions, near the center of the disk, with a spatial resolution of 4 x 10 arcseconds. They show only the central absorbtion reversal and one of the adjacent emission peaks, and succeeding scans are displaced vertically for viewing "clarity". One can see the geocoronal Lyman alpha absorbtion near grating position 898 and the blue peak near 928 (wavelength increases to the left). A slow displacement of the profile to the left can also be seen. Figure 2 shows the average profile for this orbit, after the correction for the wavelength drift has been applied.

Among other indicators of velocity which were studied, the blue peak is reasonably well defined, and the position of a parabola fitted by the method of least squares was used to define it. Figure 3 shows a series of spectra and the fitted parabolae, and Figure 4 shows the resulting variation of the peak's position. A sine wave, whose period equals the satellite's orbital period, has been drawn through the measurements, and the positions of data losses indicated by arrows. The residuals are shown on Figure 5, and (apart from the measurement at 560 seconds where the data was fit by a parabola with a minimum, rather than a maximum) one sees the indication of a variation with a period near one thousand seconds. All of the Lyman alpha data had this same characteristic oscillatory behaviour. Figure 6 presents the variation of the intensity of the blue peak and the curvature of the peak.

After the first flush of excitement over the discovery of this "900 second" oscillation - for that was its mean period - had passed and references to other observations of chromospheric oscillations with similar periods were dredged out of the literature, the real discovery was made that the observed periods corresponded precisely to the beat period between the repetition rate of the spectra (10.24 seconds) and the rotation rate of the spacecraft (10 seconds on the average, with slow drifts of several seconds). The amplitude of the intensity fluctuation is too large to be accounted for by displacements of the pointing axis, and it appears that it results from a modulation of the transmission with the period of the spacecraft rotation. Extensive additional observations and analysis by the P.I. team have demonstrated that the effect does not manifest itself in the other channels of the spectrometer, and the intermittency of the effect and its lack of correlation with the operational mode of the LPSP instrument suggests that it arises from another component of the spacecraft. Efforts to identify and correct for the modulation have been unsuccessful to date.

More positive results using statistical methods are contained in attachments B, C, and D.

A major effort of this program was devoted to the dynamical modeling of the solar chromosphere with the dual goals of improving our understanding of 1) the dynamical processes themselves and 2) spectral line formation in the dynamic chromosphere. As these lines provide the principal diagnostic tool for chromospheric measurements, the calculation of the diagnostics combined with the complete knowledge of the physical conditions giving rise to these diagnostics gives us a means of evaluating the efficacy (and veracity) of the measurement techniques. The combination of hydrodynamics and radiative

transfer in this way offers some exciting new insights into the behaviour of the Sun as we see briefly below. The results of this work will be published in two papers in collaboration with R.F. Stein of Michigan State University and P. Gouttebroze of LPSP.

A one dimensional, non-linear dynamical model of the solar atmosphere from 1.6 megameters below the visible surface to 3 megameters above was excited from below by pulses or oscillations in a series of calculations performed at LPSP. Figure 7 shows the velocity (solid lines) and pressure (dotted lines) at a number of different altitudes as a function of time for a typical calculation. The important points to note are the standing wave (pressure and velocity 90° out of phase) formed in the lower atmosphere (the zero of altitude corresponds to the visible surface) and the less regular, shorter period, standing wave formed in the chromosphere (1200 to 2000 kilometers). The photospheric oscillation is the well known "300 second" oscillation, and the chromospheric oscillation is the - slightly less - well known "200 second" oscillation. Variation of the structure of the chromosphere and the amplitude of the motions has shown that the chromospheric oscillation results from a trapped, interfering wave - much as the 300 second oscillation does - rather than from a ringing at the cut-off for propagating acoustic waves, as had been previously thought.

Figure 8 shows a series of magnesium resonance line profiles calculated for a dynamical model similar to those in Figure 7. A rather low amplitude motion was studied so that differences from the better understood, static line profiles would not be too great for an initial study. Displacements and intensity fluctuations of the emission peaks as well as of the central absorption reversal are evident. Figure 9 shows the variation of intensity at different wavelengths

as a function of time. The photospheric 300 second oscillation dominates further than 0.5 Angstroms from line center, while closer to the center the 200 second oscillation dominates. The intensity variations of the emission peaks as well as the displacements of the central absorbtion stand out clearly. The intensity fluctuation at each wavelength has been expressed as a fractional change about the mean at that wavelength, and the fluctuation at each wavelength has been normalised to unity. The fractional fluctuation at each wavelength is indicated at the right. In the blue peak, the intensity varies by over a factor of two, even for this model with its relatively low chromospheric velocities.

Figures 10 and 11 show the results of fitting parabolae to the maxima and minima of the profiles. The central absorbtion is referred to as K3 and the emission peaks as K2 (violet and red). Because of the standing wave character of the dynamics, the perturbations remain in phase through a large range of heights in the chromosphere, and thus the two emission peaks are of equal intensity nearly simultaneously with the maximum of K3, and the zero crossing of the velocity. The very high vertical phase velocities result in diagnosed velocities which are remarkably close to those at the heights of formation of the spectral features. Perceptible differences in the phase of the three diagnosed velocities are nonetheless apparent.

The contribution to the emergent intensity as a function of altitude is shown in Figure 12, as a function of time, for a wavelength justly slightly to the blue of line center, within the central absorbtion feature. The variation in altitude of the emitting region results primarily from the motion of the matter up and down during the oscillation. Figure 13 plots the same contribution functions against the average height of the matter, so that the abscissa is

just the mass depth transformed to read in kilometers. The emission arises from essentially the same material independently of the time. One should note that only a very, very small range of altitudes contributes. The behaviour at the blue emission peak is slightly more surprising (Figure 14). Reasonably large variations of the altitude of the emitting material occur, which results from the doppler shifts of the absorption profile with very rapid wavelength dependence. Figure 15 shows another projection of the same information. The depth above which 0.1, 0.2, 0.3 ... 0.9 of the emission arises is plotted for the same wavelength as Figure 12, as a function of time. The variations of the thickness as well as the altitude of the emitting region are striking.

Finally, Figure 16 shows the contribution functions on the flanks of the emission peak where a dramatic alternation of the emitting material by over 1000 kilometers occurs. This is but the beginning of the understanding of this great wealth of information which promises to not only increase our knowledge of the formation of spectral lines and their use as diagnostics, but also to enable us to make testable predictions on the bases of various hypotheses concerning stellar atmospheric dynamics.

This work would not have been possible without the generous collaboration of the staff of the Laboratoire de Physique Stellaire et Planètaire. Access to the data, even after it had been taken, was possible only as a result of a tremendous effort on their part. The non-linear, hydrodynamic calculations and the radiative transfer calculations were carried out on the CDC 7600 computer of the Centre National d'Etudes Spatiale. The data analysis and analysis of the results of the dynamical and transfer calculations were carried out within the Space Astronomy Group of LMSC and profited greatly from their expertise. Finally, I wish to thank NASA for its support of this research program.

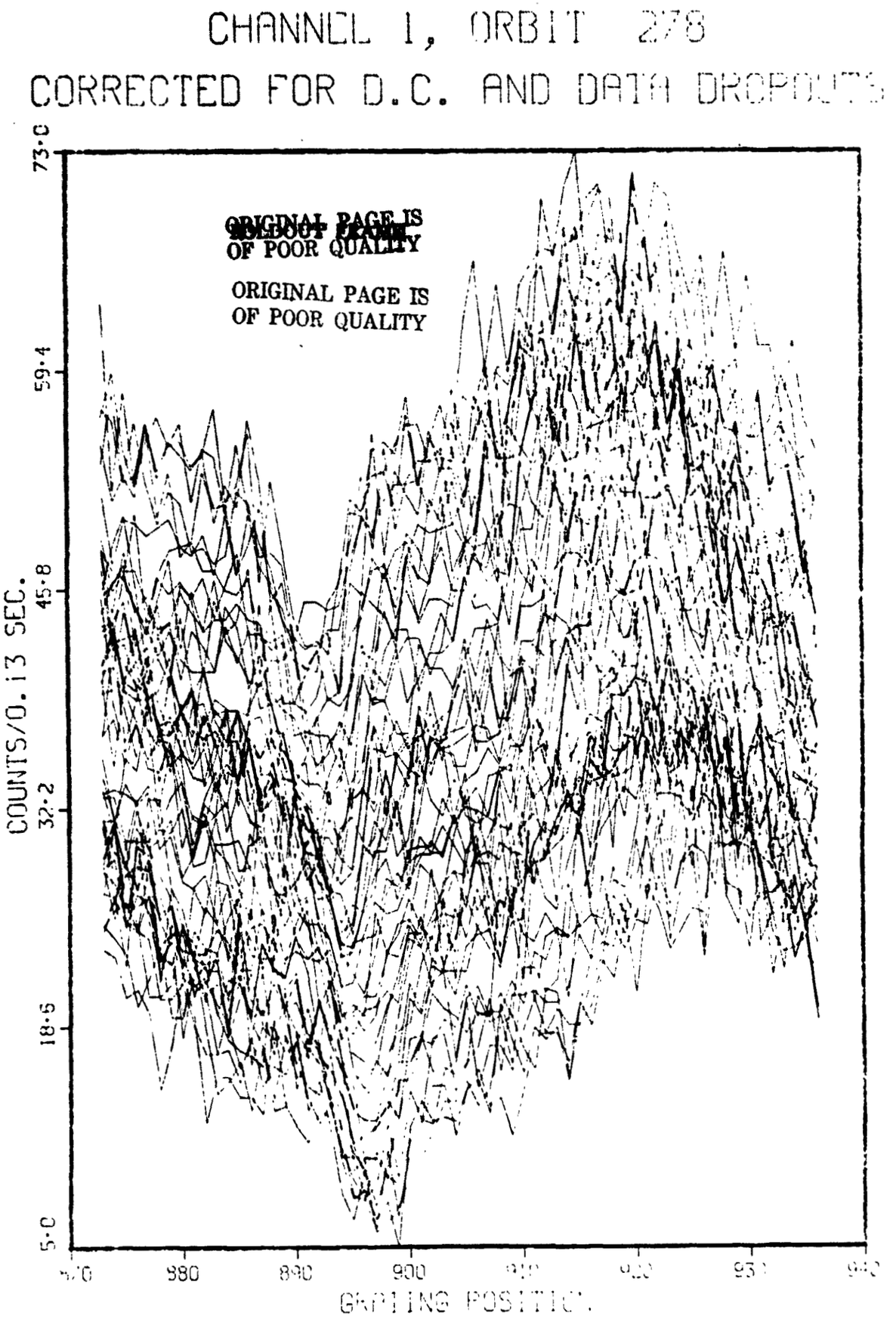
CHANNEL 1, ORBIT 278
CORRECTED FOR D.C. AND DATA DROPOUTS
ORIGINAL PAGE IS
OF POOR QUALITY
ORIGINAL PAGE IS
OF POOR QUALITY
COUNTS/0.13 SEC.
73·0
59·4
45·8
32·2
18·5
5·0
880
890
900
GRATING POSITIO

Figure 1

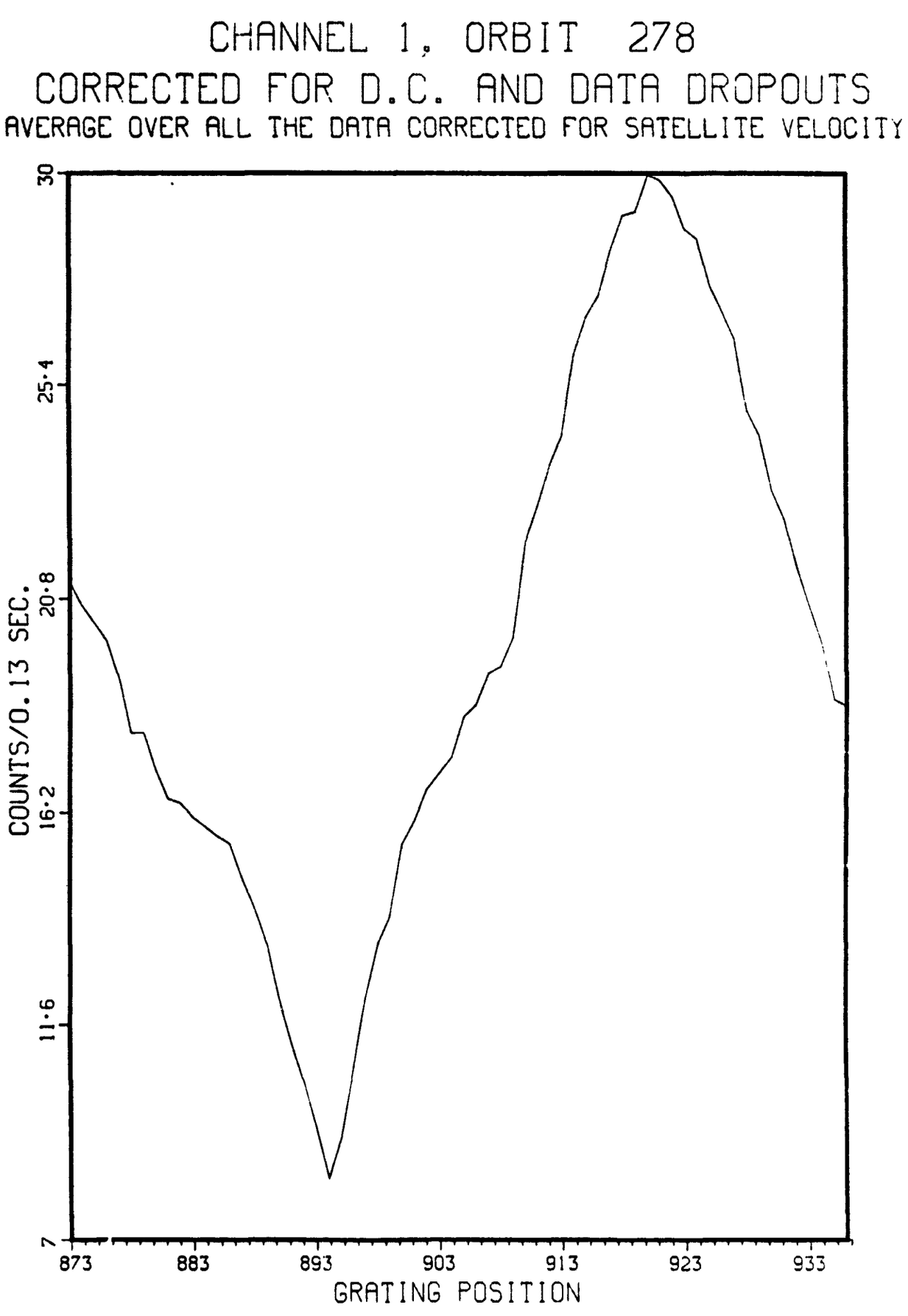
CHANNEL 1, ORBIT 278
CORRECTED FOR D.C. AND DATA DROPOUTS
AVERAGE OVER ALL THE DATA CORRECTED FOR SATELLITE VELOCITY
COUNTS/0.13 SEC.
30
25·4
20·8
16·2
11·6
7
873
883
893
903
913
923
933
GRATING POSITION

Figure 2

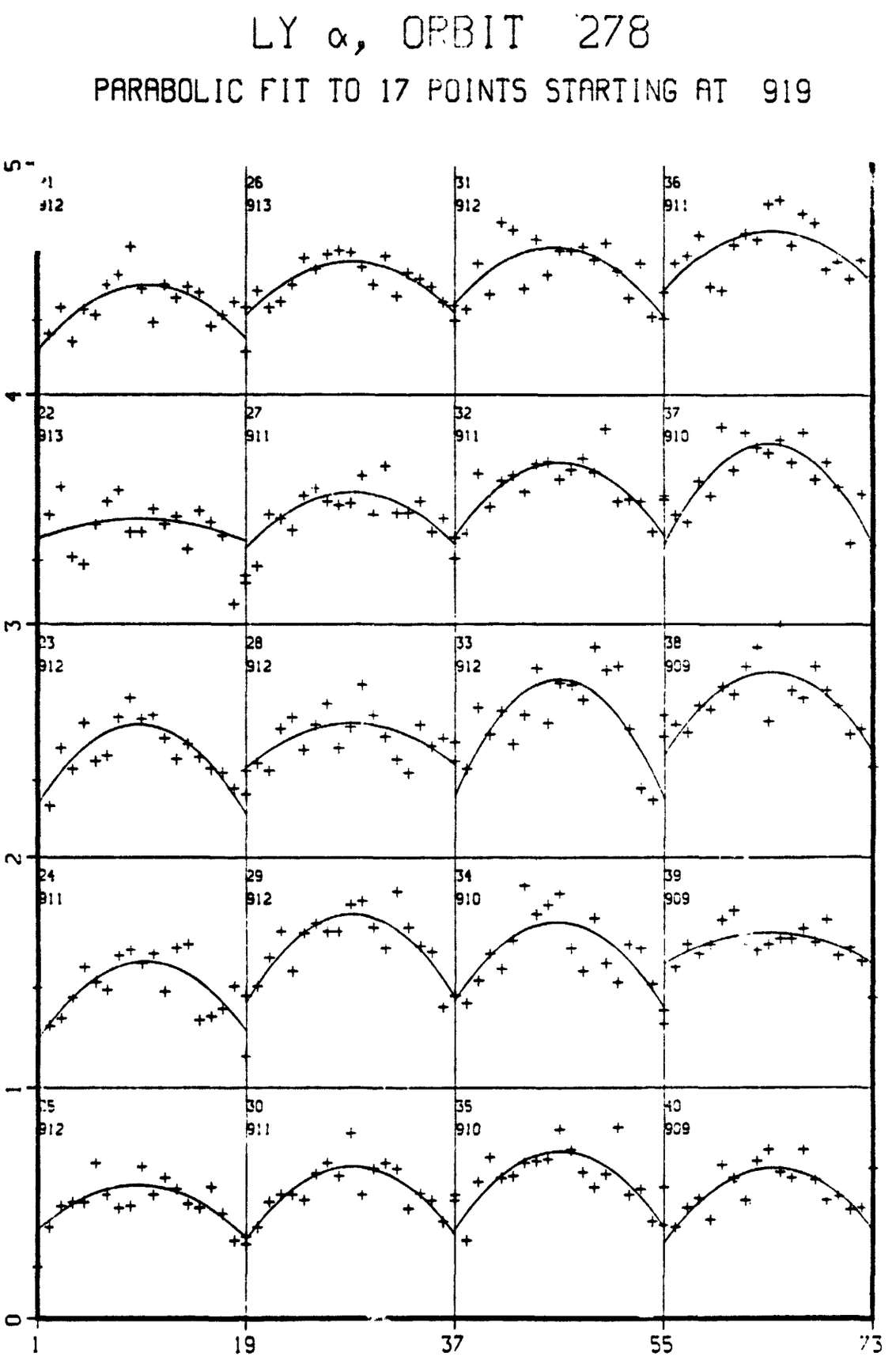
LY α, ORBIT 278
PARABOLIC FIT TO 17 POINTS STARTING AT 919
1
912
26
913
31
912
36
911
22
913
27
911
32
911
37
910
23
912
28
912
33
912
38
909
24
911
29
912
34
910
39
909
35
912
30
911
35
910
40
909
5
4
3
2
1
0
1
19
37
55
73

Figure 3

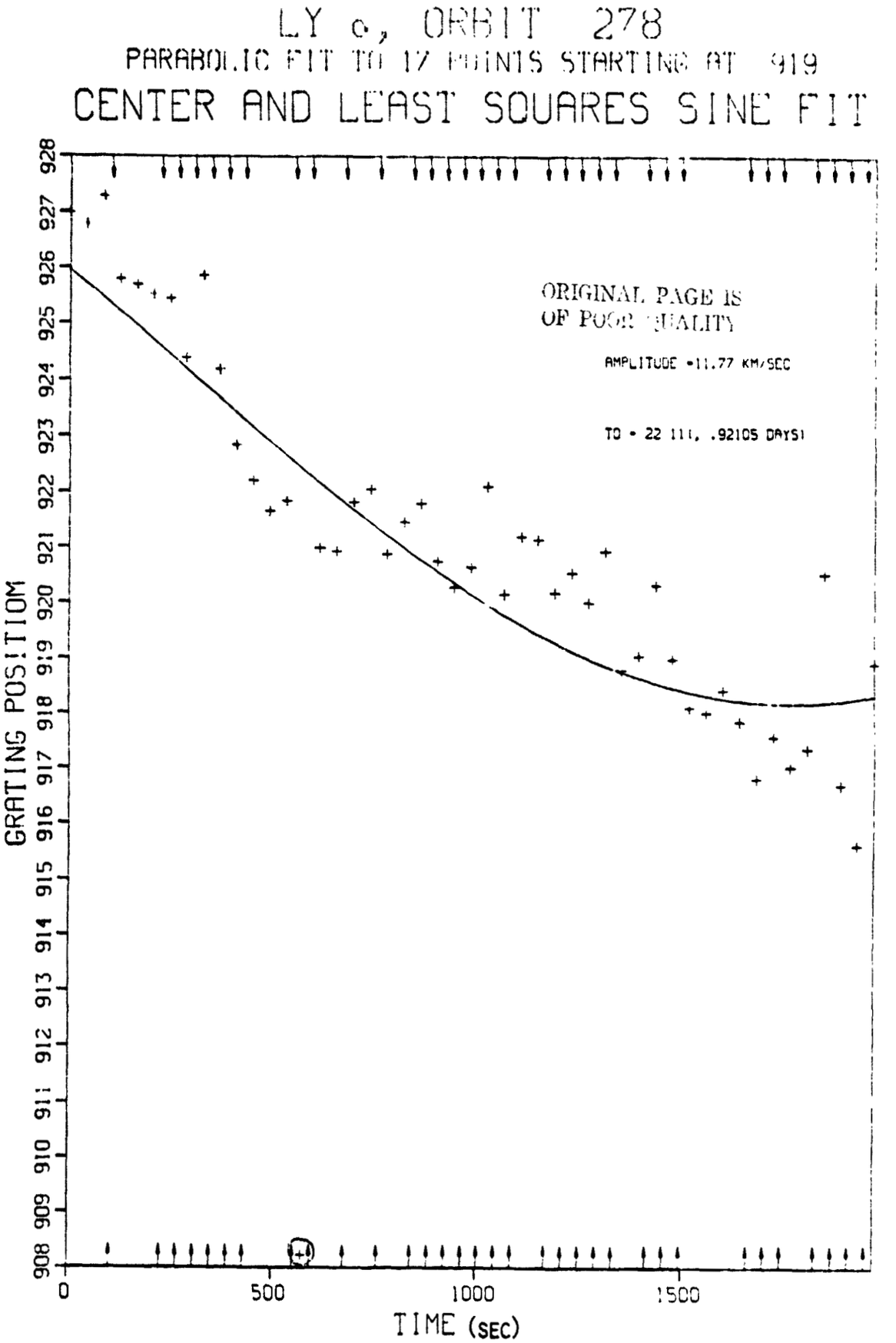
LY α, ORBIT 278
PARABOLIC FIT TO 17 POINTS STARTING AT 919
CENTER AND LEAST SQUARES SINE FIT
ORIGINAL PAGE IS
OF POOR QUALITY
AMPLITUDE =11.77 KM/SEC
TO = 22 111, .92105 DAYS)
GRATING POSITION
908 909 910 911 912 913 914 915 916 917 918 919 920 921 922 923 924 925 926 927 928
0
500
1000
1500
TIME (SEC)

Figure 4

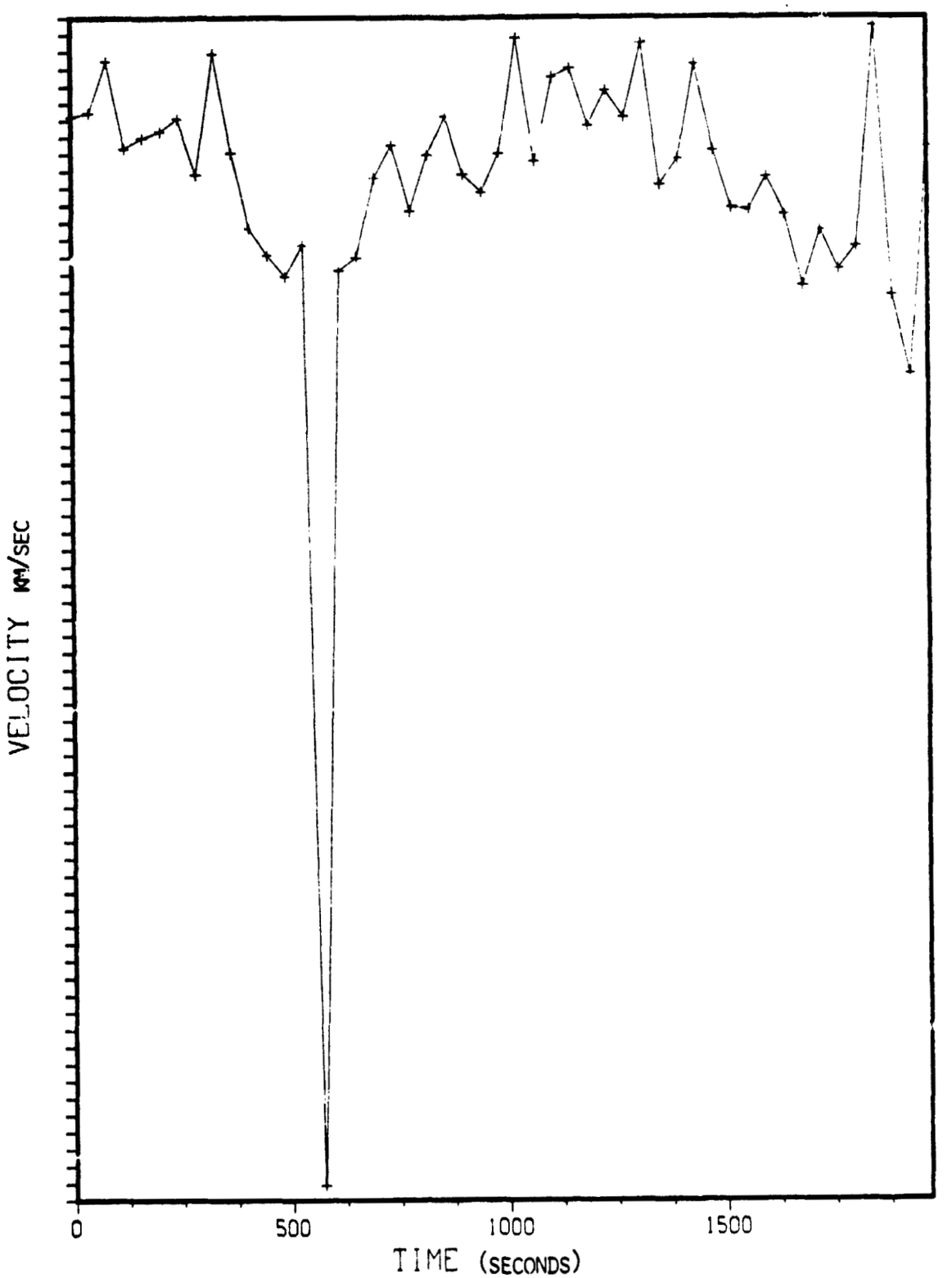
LY α, ORBIT 278
PARABOLIC FIT TO 17 POINTS STARTING AT 919
VELOCITY KM/SEC
0
500
1000
1500
TIME (SECONDS)

Figure 5

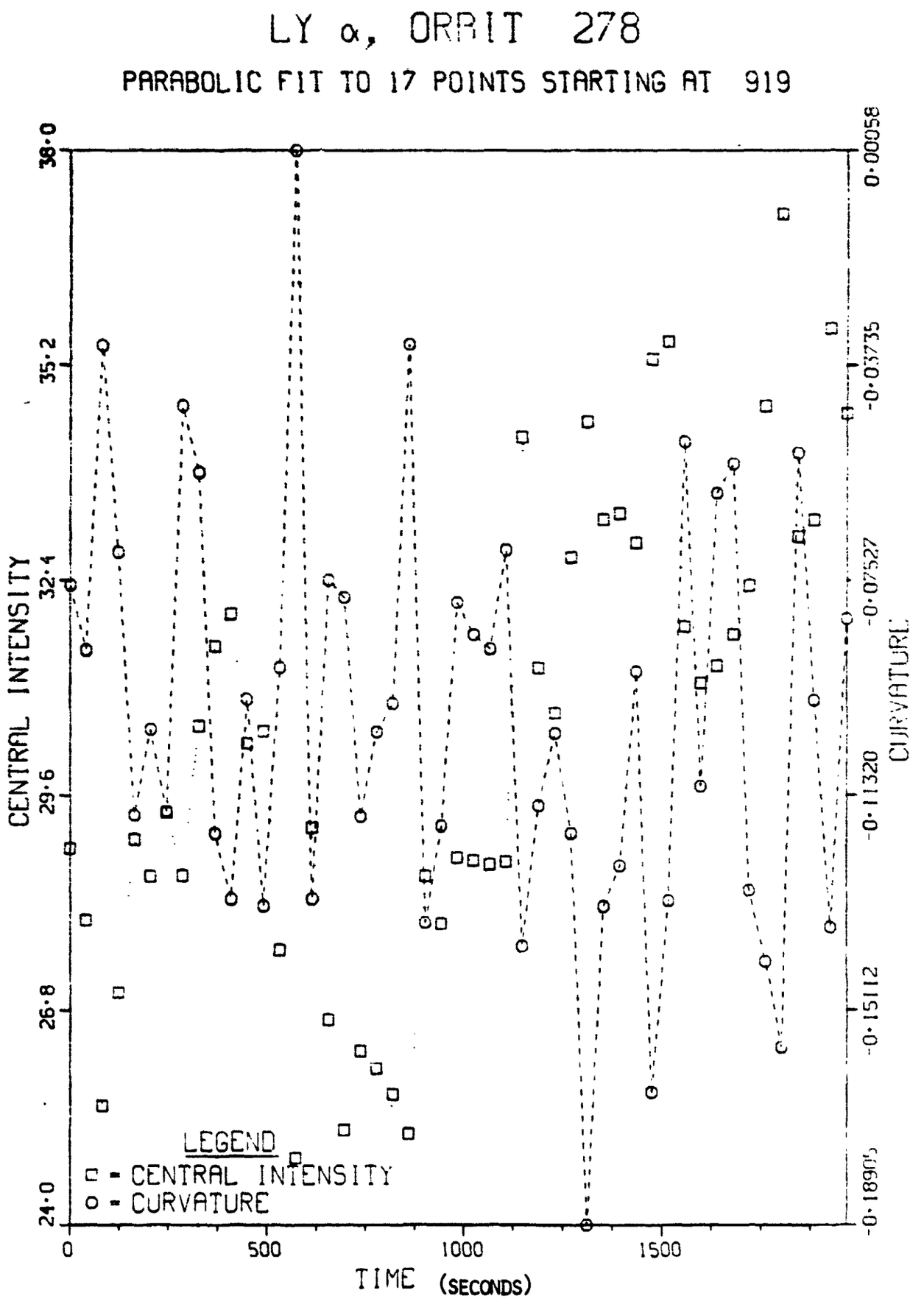
LY α, ORBIT 278
PARABOLIC FIT TO 17 POINTS STARTING AT 919
CENTRAL INTENSITY
38·0
35·2
32·4
29·6
26·8
24·0
CURVATURE
0·00058
-0·03735
-0·07527
-0·11320
-0·15112
-0·18905
0
500
1000
1500
TIME (SECONDS)
LEGEND
□ = CENTRAL INTENSITY
o = CURVATURE

Figure 6

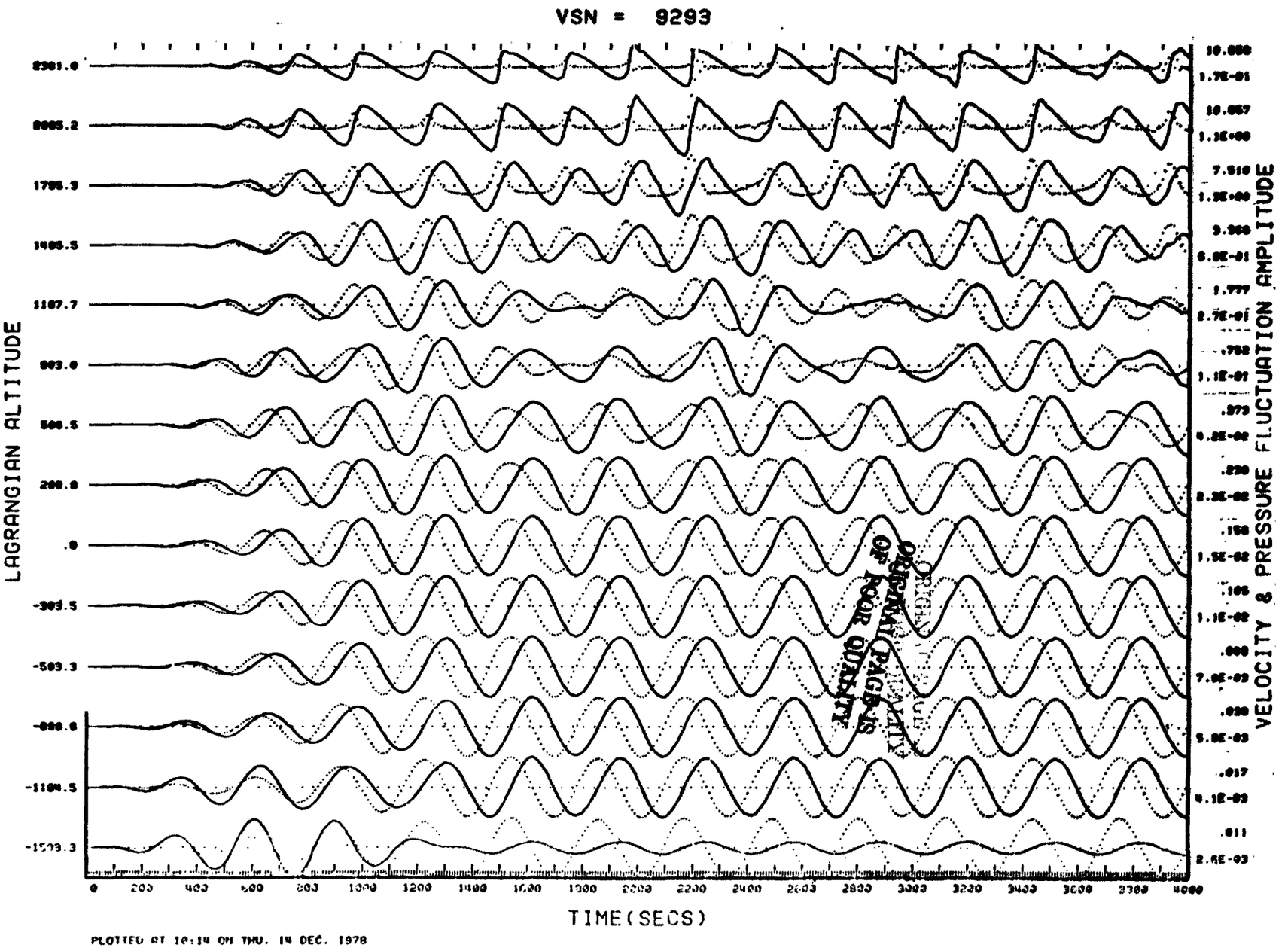

Figure 7

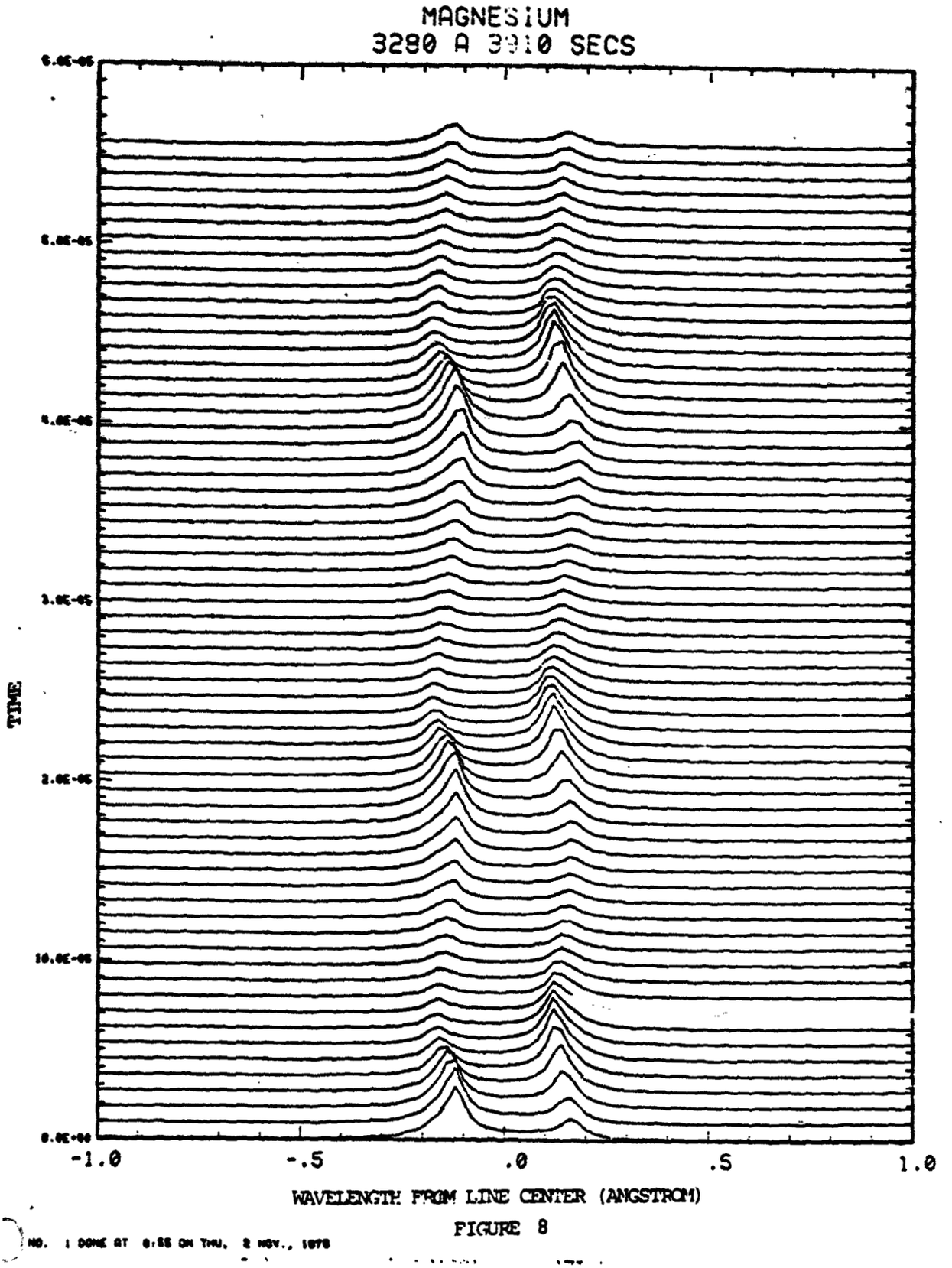

FIGURE 8

NO. 1 DONE AT 8:55 ON THU, 2 NOV., 1978

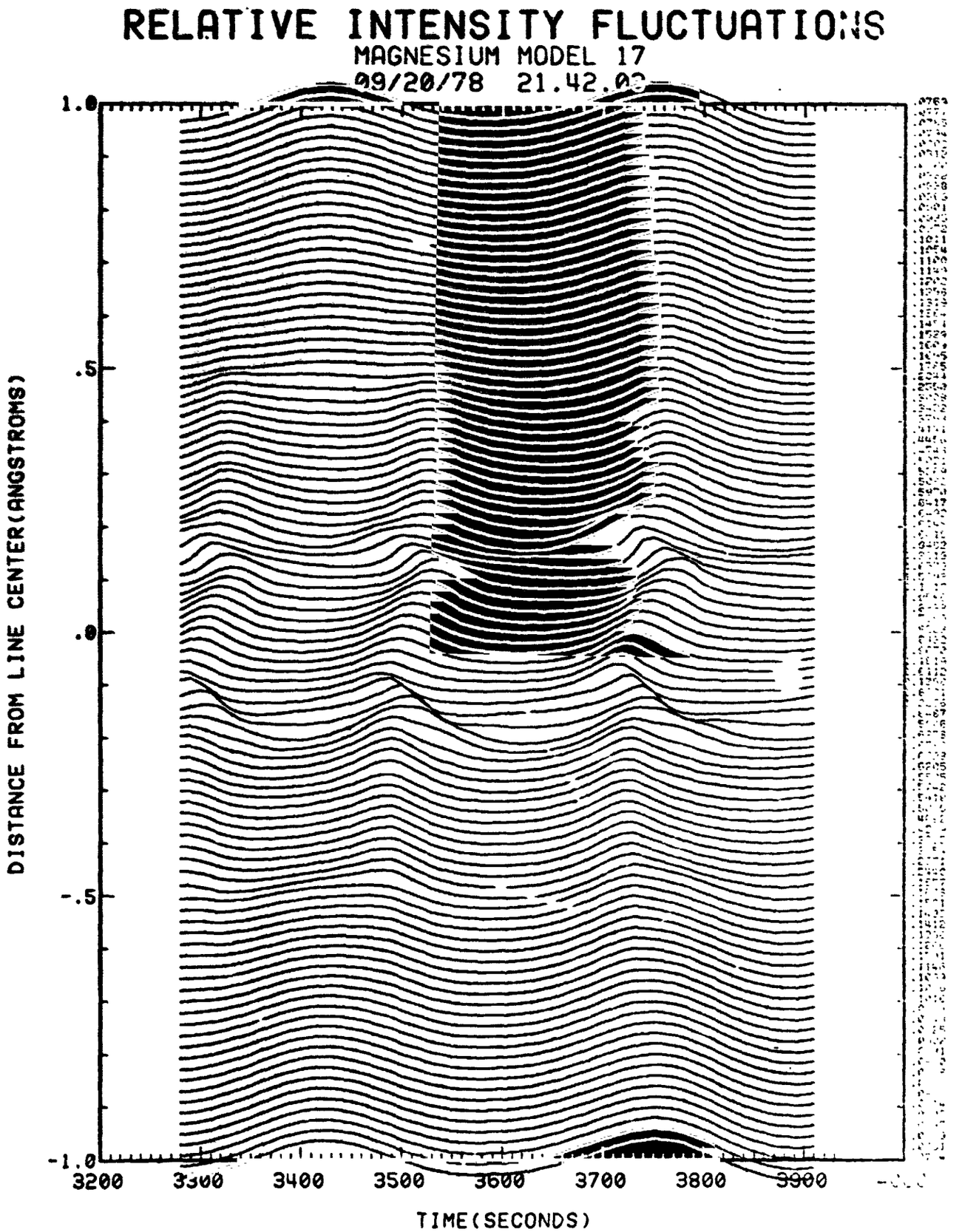
RELATIVE INTENSITY FLUCTUATIONS
MAGNESIUM MODEL 17
09/20/78 21.42.03
1.0
.5
.0
-.5
-1.0
DISTANCE FROM LINE CENTER(ANGSTROMS)
3200
3300
3400
3500
3600
3700
3800
3900
TIME(SECONDS)
PLOT NO. 1 DONE AT 23:43 ON THU, 4 JAN., 1979

Figure 9

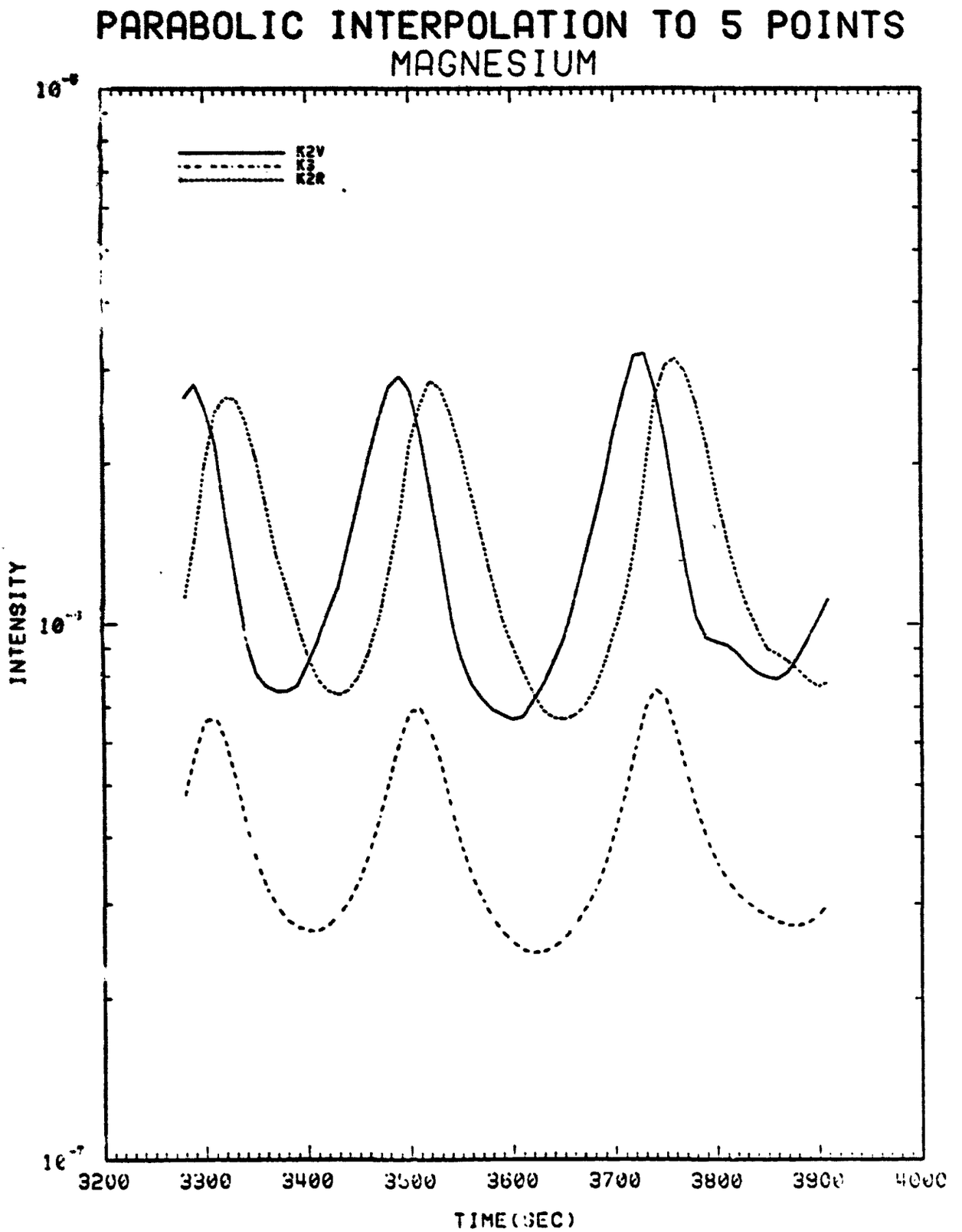
PARABOLIC INTERPOLATION TO 5 POINTS
MAGNESIUM
K2V
K3
K2R
INTENSITY
TIME(SEC)
3200
3300
3400
3500
3600
3700
3800
3900
4000

FIGURE 10

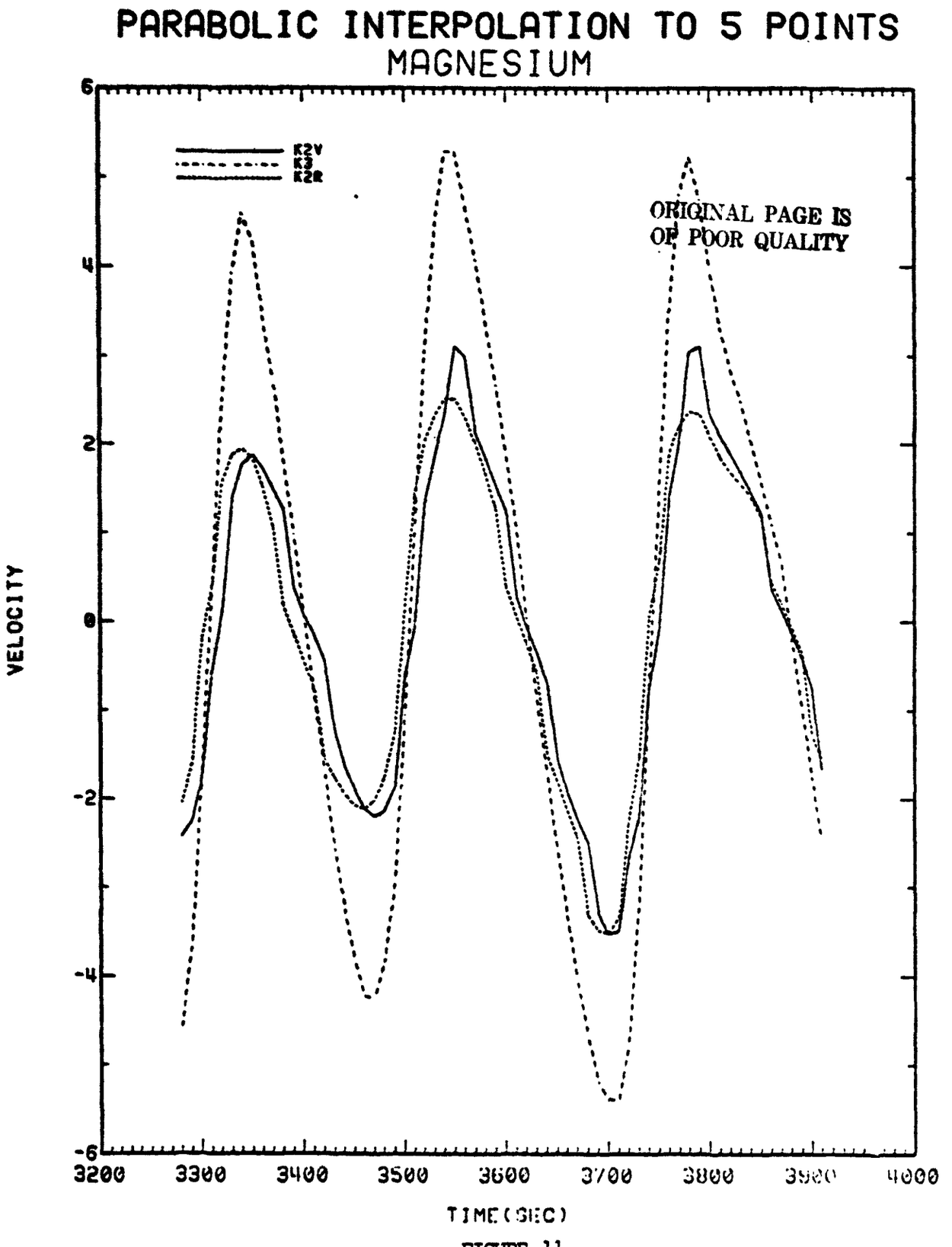
PARABOLIC INTERPOLATION TO 5 POINTS
MAGNESIUM
K2V
K2R
ORIGINAL PAGE IS
OF POOR QUALITY
VELOCITY
TIME(SEC)
6
4
2
0
-2
-4
-6
3200
3300
3400
3500
3600
3700
3800
4000

FIGURE 11

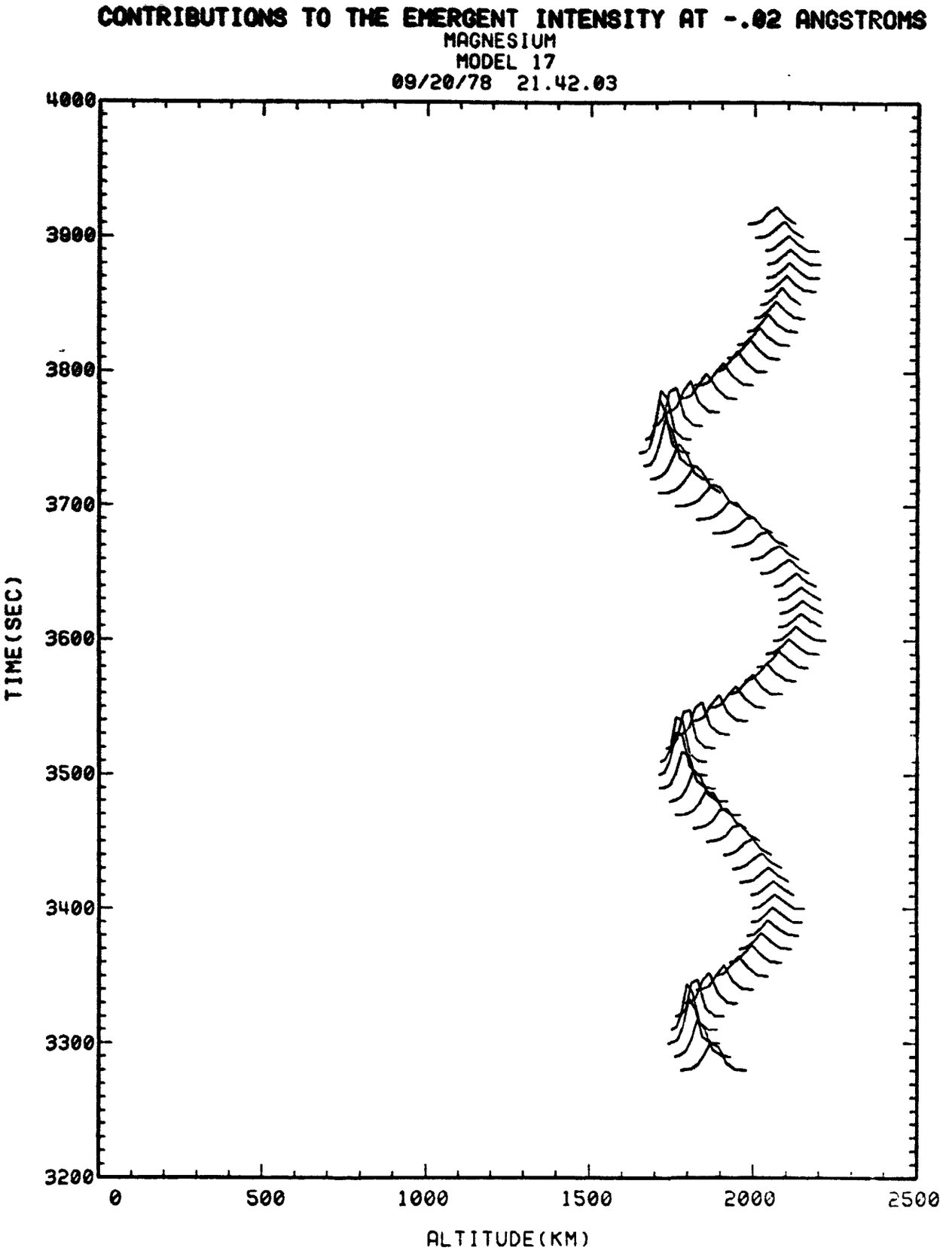
CONTRIBUTIONS TO THE EMERGENT INTENSITY AT -.02 ANGSTROMS
MAGNESIUM
MODEL 17
09/20/78 21.42.03
4000
3900
3800
3700
3600
3500
3400
3300
3200
TIME(SEC)
0
500
1000
1500
2000
2500
ALTITUDE(KM)
PLOT NO. 3 DONE AT 1:32 ON WED, 3 JAN., 1979

Figure 12

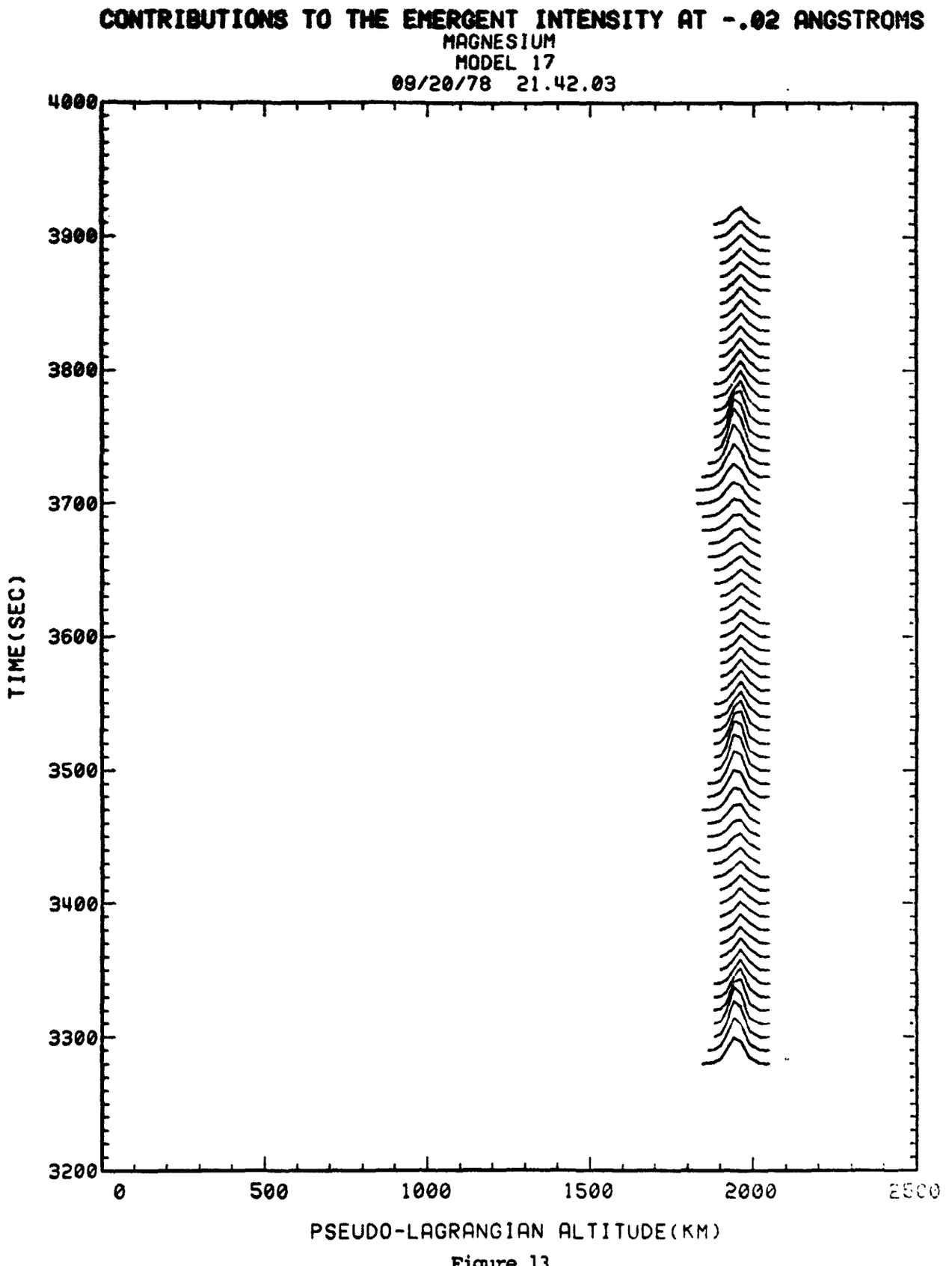
CONTRIBUTIONS TO THE EMERGENT INTENSITY AT -.02 ANGSTROMS
MAGNESIUM
MODEL 17
09/20/78 21.42.03
4000
3900
3800
3700
3600
3500
3400
3300
3200
TIME(SEC)
0
500
1000
1500
2000
2500
PSEUDO-LAGRANGIAN ALTITUDE(KM)
PLOT NO. 4 DONE AT 1:32 ON WED, 3 JAN., 1979

Figure 13

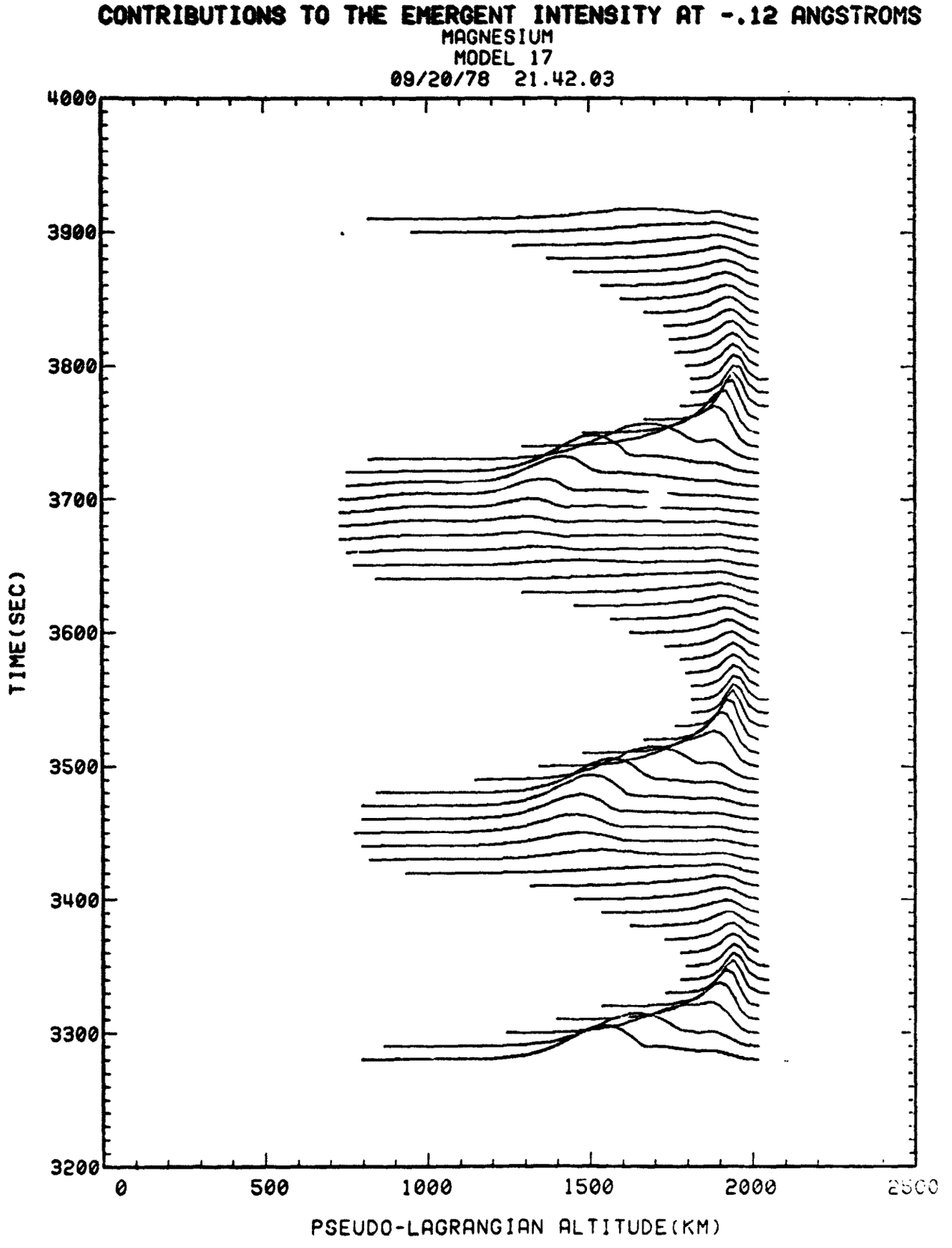
CONTRIBUTIONS TO THE EMERGENT INTENSITY AT -.12 ANGSTROMS
MAGNESIUM
MODEL 17
09/20/78 21.42.03
4000
3900
3800
3700
3600
3500
3400
3300
3200
TIME(SEC)
0
500
1000
1500
2000
2500
PSEUDO-LAGRANGIAN ALTITUDE(KM)
PLOT NO. 4 DONE AT 11: 0 ON WED, 3 JAN., 1979

Figure 14

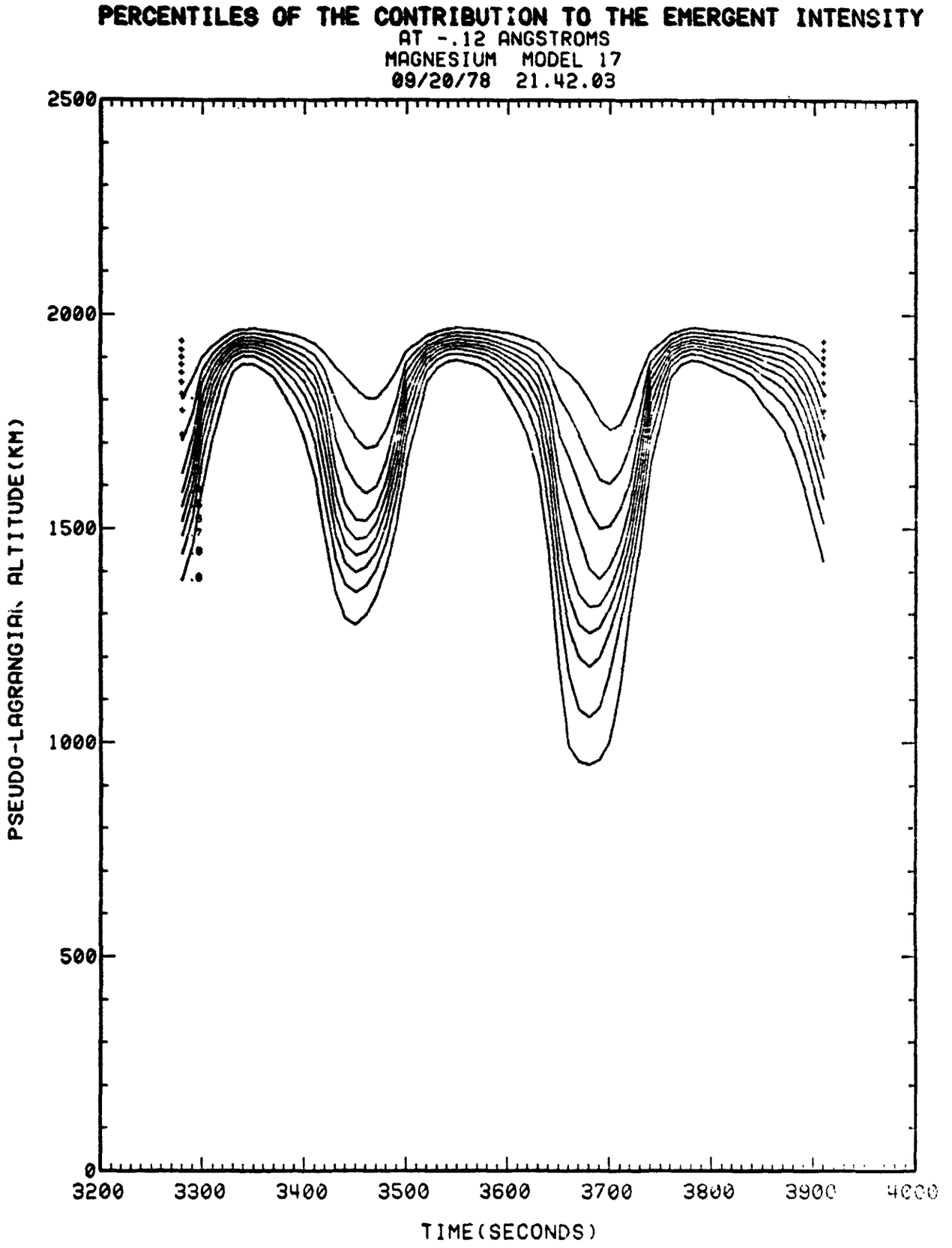
PERCENTILES OF THE CONTRIBUTION TO THE EMERGENT INTENSITY
AT -.12 ANGSTROMS
MAGNESIUM MODEL 17
09/20/78 21.42.03
2500
2000
1500
1000
500
0
PSEUDO-LAGRANGIAN ALTITUDE(KM)
3200
3300
3400
3500
3600
3700
3800
3900
4000
TIME(SECONDS)
PLOT NO. 4 DONE AT 2:51 ON WED, 3 JAN., 1979

Figure 15

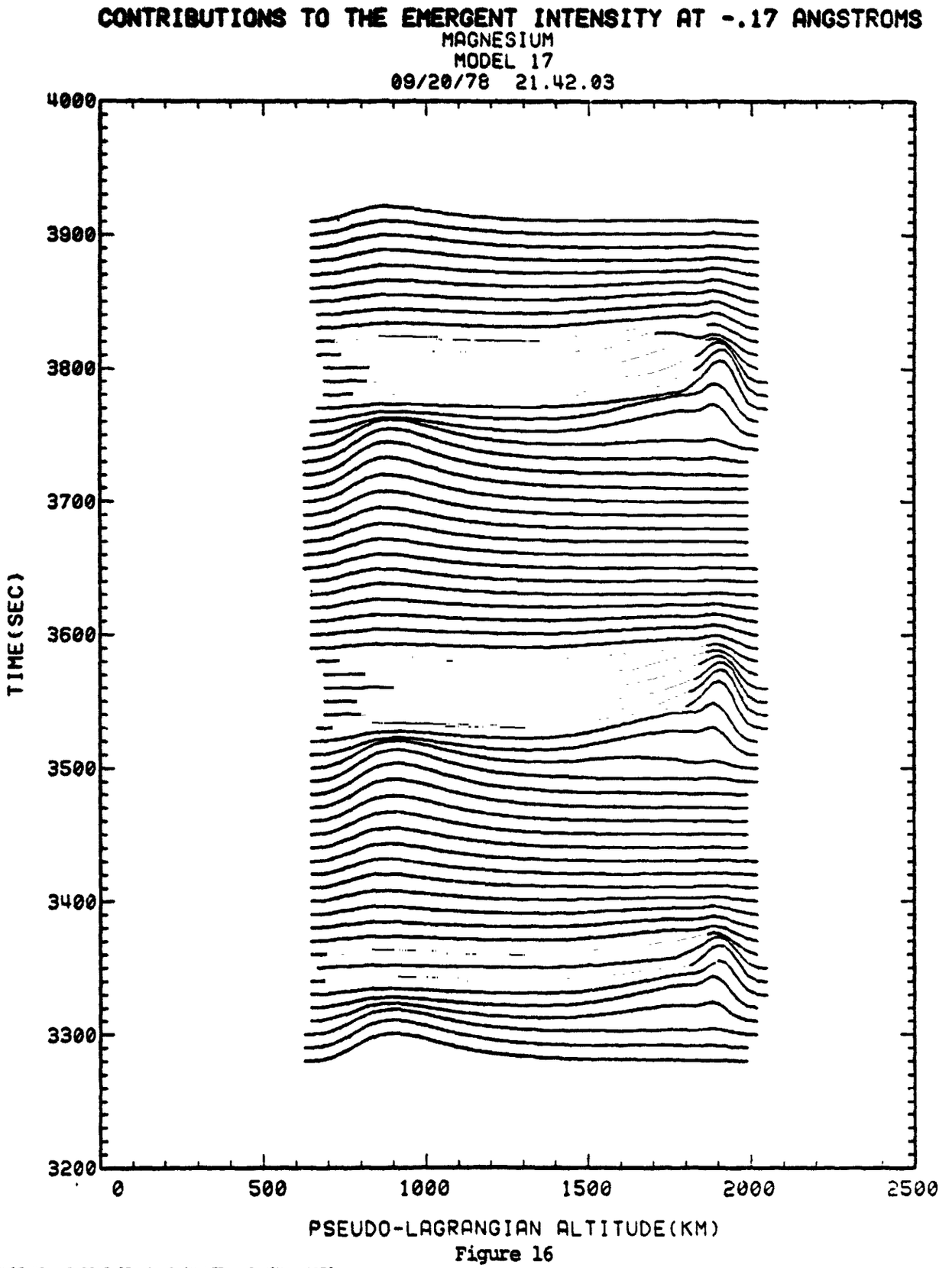

Figure 16

PLOT NO. 2 DONE AT 1: 0 ON WED, 3 JAN., 1979

Attachment A

Published in the Proceedings of the November 1977 OSO-8 Workshop
Boulder, Colorado; pages 311-339

Theoretical Aspects of the 300 Second and Related Oscillations of the Solar Atmosphere

John Leibacher
Space Astronomy Group
Lockheed Palo Alto Research Laboratory
Palo Alto, California

I. Introduction

It seems to me that only extremely rarely does our knowledge of the behaviour of the Sun, and astronomical objects in general, advance in a nice, clear fashion at all similar to The Scientific Method, whose virtues were extolled back in high school physics courses. Only infrequently do real, testable predictions emerge from hypotheses formulated to describe known, but unexplained phenomena. Even less frequently is the physics sufficiently simple that one effect dominates and the predictions are unambiguously confirmed. Nonetheless, this has occurred recently in the interpretation of what for a long time was known as "wiggly line spectra" - the spatially and temporally resolved velocity field of the solar photosphere. It is thus with nostalgic pleasure that I undertake a description of the denouement of nearly twenty years of research into the nature of the "five-minute" oscillation of the solar atmosphere.

After briefly recalling what the problem was, I shall review the model of the "five-minute" oscillation which has demonstrated this predictive success - first, the atmospheric properties which determine the resonant frequencies, the variation of these frequencies with horizontal scale and the vertical structure of the resonant motions; and second, the mechanisms which have been proposed to drive these motions. While the detailed, numerical agreement between theoretical predictions of the resonant frequencies and observation has not only confirmed the model but allowed its application as a diagnostic of sub-surface conditions ("solar seismology"), our ideas about the excitation and damping mechanisms are in a much more preliminary state.

Then, I shall discuss the chromospheric concomitants of the observed photospheric motions. (Given the input of the photospheric oscillations, what do we expect to see in the chromosphere as a result ?) Although the mechanism for the decrease in energy of the "five minute oscillation" and the increase in energy of the "three minute oscillation" appears to be understood, attempts to model the temporal variation of optically thick lines have been largely unsuccessful. Although it is possible that our dynamical description is in error, it seems clear that the proper combination of hydrodynamic models and line formation diagnostics has not yet been used to derive appropriate predictions for comparison with observation. Finally, we are led to conclude that the most naive expectations of shock wave heating of the solar chromosphere and corona have not been fulfilled, and that while the observational quest must continue - guided by more realistic theoretical predictions - alternative heating mechanisms should be actively investigated.

II. Oscillatory Motions of the Solar Photosphere

Although the oscillatory motions of gravitationally stratified, compressible fluids - atmospheres - have been "well understood" since the work of Lamb at the beginning of the century, in the absence of specific problems posed by observation, astronomers seem not to have considered the consequences of the existence of such hypothetical motions. While Biermann and Schwarzschild had conjectured that running waves generated in the convection zone could transport the energy required to account for departures from radiative equilibrium in the outer layers of the solar atmosphere, it was assumed that these waves would span a broad spectrum of temporal and spatial scales commensurate with the "turbulent" convective motions thought to be responsible for generating them. When Leighton actually measured the time variation of the velocity at a point on the Sun, he found much to everyone's apparent surprise that instead of being a more or less random function, the velocity oscillated quite regularly with a period near five minutes. What is so special about five minutes? How does the Sun go about selecting just this one narrow range of periods?

It turns out, embarrassingly enough, that there are a lot of ways to do it - none so much as suspected before Leighton's observations directed attention to the problem - and within a decade half a dozen distinctly different, but "credible" models for the five minute oscillation emerged. (The interested reader is referred to reviews by Michalitsanos(1973) and Stein and Leibacher(1974)). Within the last two years observations have been obtained (Deubner, 1975) and corroborated (Rhodes, Ulrich and Simon, 1977) which confirm predictions made on the basis of one of these models, and thus in the current order of things this model has been elevated to the status of "astrophysical truth" - not to be confused with "astrophysical accuracy." Let me qualitatively describe the important aspects of this model.

The "truth" is that acoustic waves with periods greater than 200 seconds will be trapped within a limited region, some tens of megameters thick, just below the visible surface of the Sun where they couple to the thermal and dynamic state maintained by the outward convective transport of the solar flux. These trapped waves drive non-propagating, evanescent waves seen in the visible atmosphere. To describe this phenomenon, it behooves us to think a little about acoustic waves.

A change in the density of a gas, brought about by pushing on one end of it for example, generally causes a change in the pressure through the conservation of energy Since the pressure is just the internal energy density, compressing the gas increases the pressure. Since the pressure has not increased everywhere, only on the side where we pushed, a pressure gradient now exists which will in turn accelerate the gas towards the low pressure. This acceleration compresses the low pressure gas and we've gone around the loop and start once again: a density increase (via the conservation of energy) causes a pressure increase, a pressure gradient (via the conservation of momentum) causes an acceleration, an acceleration (via kinematics) causes a displacement, a differential displacement (via conservation of mass) causes a density increase. This compressional disturbance is propagated by the internal random, thermal motions of the particles at a speed $\sim\sqrt{kT/m}$, which is referred to as the speed of sound.

In fact, in an infinite, isothermal, homogeneous gas, the sound speed represents the only characteristic dimensional quantity, and it is just the signal propagation speed for small disturbances. If we look at a plane parallel sound wave, the wave crests move at the sound speed along the direction of propagation, and hence they must move faster than the sound speed along any other direction. (It's worth drawing a little sketch.) For example on a plane nearly perpendicular to the direction of propagation, the crests will move sideways at "nearly infinite" speed. The propagation speed of the crest (or trough, or node) is often referred to as the phase velocity. Interesting things occur at the interface between two regions of differing sound speed (i.e. different temperature). Waves which are propaging towards the region of higher sound speed with an arbitrary period and wavelength (just the product of the period and the sound speed) will maintain their period and wavelength along the interface (that is, the phase velocity along the interface is the same on both sides of the interface). But in the region of higher sound speed, the wavelength corresponding to a given period must increase and hence the wavelength perpendicular to the interface must increase (since the wavelength parallel to the interface is fixed by continuity). This is just the same as saying that the direction of propagation changes, in the sense that the wave propagates more nearly parallel to the interface. Which is all just equivalent to Snell's law in optics - waves propagating into a region of decreasing index of refraction (increasing speed of light) are refracted away from the normal. The "interesting things" happens when the temperature increases so that the sound speed in the higher temperature region equals, or exceeds, the horizontal phase velocity of the incident wave. The wave can no longer propagate perpendicular to the interface in the hot region, and it is reflected ("total internal reflection"). In general, the wave doesn't stop abruptly at the interface, but it's energy falls off exponentially into the hot region. This "evanescent wave" is curious in that although at any point the velocity varies sinusoidally in time, there is no phase propagation away from the interface. The velocity reaches a maximum (or minimum) everywhere simultaneously, so it might be more appropriate to think of the phase velocity perpendicular to the interface as being infinite. Furthermore, in contrast to the propagating wave where the pressure and velocity fluctuate in phase - which is just what is required for the right amount of work to be done

around one cycle - the pressure and velocity are ninety degrees out of phase, so that no energy is transmitted.

A wave propagating at some angle to the temperature stratification in the direction of increasing temperature will eventually get to a region (temperature) where the sound speed equals the horizontal phase velocity and the wave will be turned around. It is worth noting that if we look at waves of the same frequency but varying angle of propagation with respect to the temperature stratification, or equivalently varying horizontal wavelength if we think of a "vertical" temperature stratification, the more nearly horizontally propagating waves will be reflected first (at the lowest temperature) and the sound speed to which the waves can propagate is just proportional to the horizontal wavelength; or inversely proportional to the sine of the angle to the vertical. Thus waves propagating "straight in", that is waves with infinite horizontal wavelength, will never be reflected. The existence of such reflections is of interest in that it can exclude waves from the high temperature region (the deep interior of the sun) and, more significantly in the present context, in that two reflections will form a cavity, or duct (an organ pipe or cello string) in which interference will occur and certain frequencies will be selected from a broad band excitation. For example, one of the first models for the "five minute oscillation" - proposed by F.D. Kahn but later shown to be unacceptable on several points - was based upon the trapping of sound waves near the temperature minimum by the higher temperatures above and below.

Other "interesting things" happen to sound waves when they propagate in a region of changing density - such as occurs in the presence of a gravitational field, but which would also occur if the mean molecular weight were stratified for example. If this "atmosphere" were displaced upwards or downwards "slowly", then sound waves would run back and forth, and after they damp out and the atmosphere would return to its stratified equilibrium. That is all well and good, but what is "slowly"? Whereas the isothermal gas we considered above had only a characteristic velocity associated with it, the density stratification introduces a characteristic length - the scale height. If we move the atmosphere periodically up and down with a period sufficiently long

so that a small density fluctuation would travel many ("many" turns out to equal 4π) scale heights in one period, then the atmosphere more or less stays together and moves up and down in phase. However, if we jiggle the atmosphere up and down very rapidly - more rapidly than the atmosphere can respond - then waves zip on up at the sound speed. Since the sound speed remains constant, these waves propagate without reflection. However, since the atmospheric density varies, the velocity amplitude must vary inversely to maintain the constant flux of energy ($\rho v^2 c$, where c is the velocity of sound). Thus waves propagating upwards, into less dense gas will increase in amplitude as $\rho^{-\frac{1}{2}}$. As the period increases to that at which the atmosphere can respond in phase - the cut-off period for propagation - the energy propagation velocity decreases to zero and the wavelength increases to infinity. For periods slightly longer than the cut-off, the atmospheric fluctuations vary exponentially rather than sinusoidally with height, and these waves are again referred to as "evanescent."

If the gas is stratified gravitationally, the scale height is inversely proportional to the temperature, so the time for a density disturbance to propagate a scale height is just proportional to $T/\sqrt{T}$ or $\sqrt{T}$. Once again, the propagation characteristics change with a change in temperature so that when a wave propagates into a cooler part of the atmosphere - with a smaller scale height - waves of sufficiently long period will no longer propagate, that is they will be reflected. Thus a sound wave propagating into a region of continuingly decreasing temperature will eventually reach a region where its period times the sound speed equals 4π times the density scale height, at which point energy will be propagated no further. If sound waves covering a range of periods propagate into a region of decreasing temperature, the longest period waves will be reflected first and the short period high frequency waves will propagate down to low temperatures (small scale height). Combining this behaviour with the reflection that occurs at high temperature (when the sound speed equals the horizontal phase speed) we see (I hope) that in an atmosphere there exists a range of temperatures within which a given acoustic mode (specified pair of period and horizontal wavelength) may propagate. Whereas we have already seen how a cavity capable of trapping acoustic waves is formed at the temperature minimum, we now have discovered that there exist additional cavities in the rising temperature

regions above and below the temperature minimum. In fact, the second model for the "five minute oscillations" - proposed by Bahng and Schwarzschild but alas, also shown to be unacceptable on several points - suggested that waves trapped in the chromospheric temperature rise could account for the observations.

There followed many other descriptions; some using running acoustic waves, others buoyancy waves trapped in the temperature minimum; before the importance of acoustic waves trapped in the temperature rise towards the solar interior was pointed out by R. Ulrich and independently by Bob Stein and myself. As simple as this description now seems, it took an embarrassingly long time to arrive at it. In my own case, I was considering a very different aspect of the problem and was extremely annoyed that the model developed beautiful five minute oscillations long before it had a chance to develop what I wanted to study. After a lot of hard work trying to make the oscillations go away, I conceded defeat and accepted what the model was trying to tell us. Ulrich recounts a similar serendipitous experience, having originally thought that the "overstability", or growing amplitude of the oscillations was a numerical difficulty of his computer program. But I am getting ahead of the story. Let us consider in a little more detail the properties of the sub-photospheric cavity, before discussing how these trapped waves are excited.

For any given wave mode (period and horizontal wavelength), in a propagating region, there exists two waves corresponding to upward and downward propagation. If a reflection exists somewhere, then the wave propagating away from the reflection is just the wave propagating towards it, but turned around. Of course, the wave experiences a phase change at the reflection. This would be the situation in a semi-infinite uniform gas with a wall at one end, for example. If we introduce a second reflection the situation becomes much more intersting. Consider an excitation operating within the cavity; a diaphragm moving up and down for example. For an arbitrary periodic excitation, the waves reflected back to the excitation will arrive somewhat out of phase with it and will impede the excitor. Thus the gas may be moving upward at the diaphragm while the diaphragm is trying to push the gas back down. Not a very efficient way to transfer energy, I hope we all can agree. For certain periods of excitation, however, the reflected wave will arrive back at the

driving exactly in phase with it and the excitor can put more energy into the gas and the wave will grow in amplitude. That is, the gas would be moving with the diaphragm. A slightly more concrete analogy, would be trying to push a child on a swing. If you don't push in phase with his swinging, it doesn't work very well. These resonant modes, often referred to as "normal modes", are of interest to us here just because of their resonant response to broad band excitation. That is, while waves spanning a broad range of periods and horizontal wavenumbers will be trapped in the sub-photospheric cavity, these resonant modes should be preferentially excited to large amplitudes.

In general, a cavity formed by two reflections will have many resonant modes, that is many wavelengths that can satisfy the requirement that after two reflections they arrive back at the "starting point" in phase. For example, the cello string has as resonant modes all of those sine waves which go to zero at both ends. Thus the longest wavelength, resonant mode consists of a half cycle of a sine wave, but 1, $1\frac{1}{2}$, 2, $2\frac{1}{2}$,..... cycles will also resonate. Thus each successively higher order resonant mode has an additional zero crossing along its length. Since the reflections at the end are indpendent of the wavelength (ideally), this cavity possesses an infinite number of resonant modes. In addition, for this simple system, the wavelength and the period of a wave motion are linearly related so that these resonances have a simple harmonic relationship between the periods. Such systems, for which waves of all periods propagate at the same speed are said to be "dispersionless", a packet of energy consisting of a range of wavelengths does not disperse as it propagates. As we have seen above, the propagation speed and reflection of acoustic waves in the solar atmosphere depend both upon the period and the horizontal wavelength. Hence they are dispersive. Thus while vertically propagating waves with periods of 300 and 400 seconds will be reflected downward just below the visible surface because the scale height gets too short, 200 second waves will just propagate into the visible atmosphere and 100 second waves will propagate right past the temperature minimum and on up into the chromosphere. So in fact, the cavity does not exist for these short period waves. Purely vertically propagating waves will go all the way in to the center of the sun without being reflected, so the cavity will be extremely thick for them, while waves propagating very obliquely will be reflected

back upwards before they have penetrated very deeply.

At a fixed horizontal wavelength, the longest vertical wavelength which resonates has the longest period, and higher harmonics have shorter periods. Since the downward reflection no longer exists for sufficiently short period waves, only a finite number of resonant modes exist below the solar surface - in contrast to the situation for the cello string. In addition, while for the nice, uniform cello string all of the higher order resonant modes had the wave energy distributed more or less uniformly along the string which, of course, has the same length for all of the harmonics, in the subphotospheric cavity the lower order resonant modes propagate more nearly horizontally than the higher order ones and thus they propagate in a more limited range of depths in the solar convection zone than the higher order (shorter vertical wavelength, shorter period) resonant modes. Of course the resonance will exist for other horizontal wavelengths, for which - because of the dependence of the vertical wavelength on the horizontal wavelength and the period - the resonant period will be different. The ensemble of resonant modes with the same number of vertical wavelengths trapped in the cavity is often referred to as a "vertical mode" and the number of zero crossing of the pressure fluctuation - for example - used as an index. The longest vertical wavelength mode - which has no zero crossings - is called the "fundamental". For a given vertical mode, longer horizontal wavelengths penetrate deeper in the solar convection zone to higher temperatures; thus the cavity is more extended, the vertical wavelength longer and hence the period longer. The precise functional dependence of the period upon the horizontal wavelength results from the detailed mathematical formulation, however the qualitative relationship can be arrived at quite simply. At any temperature in the atmosphere, the characteristic period - the acoustic cut-off period - is just proportional to the square root of the temperature, while the characteristic length - the scale height - is proportional to the temperature. Thus in an atmosphere with a more or less smoothly varying temperature, by keeping the ratio of the period to the characteristic period and horizontal wavelength to the characteristic length constant, that is since

$$P \sim \sqrt{T}$$

and

$$\lambda \sim T,$$

then

$$P \sim \sqrt{\lambda},$$

the resonant modes with the same number of vertical modes all "look the same", with the longer period, long horizontal wavelength ones just being shifted to higher temperatures - deeper in the convection zone. This square root dependence is, in fact, precisely the analytic result for an atmosphere consisting of a linear temperature increase, and it obtains as the large horizontal wavelength limit for the more complicated temperature distribution in the solar sub-photospheric cavity.

Figure 1 displays the low order resonant modes calculated analytically for a model solar atmosphere consisting of an isothermal temperature minimum of 4000°K, 1.5 Mm thick, between a linear rise of 100°/ km into the "corona" and a rise of 10° / km into the interior. (It is generally more convenient for theory and analysis to proceed using the Fourier transforms of the real variables, so reciprocal periods (frequencies) and reciprocal wavelengths (wavenumbers) are most commonly used.) Acoustic waves can propagate above the shaded band. The fundamental mode is evanescent everywhere, and it lies very close to the compressionless waves for which the divergence of the velocity vanishes. "Internal gravity" waves - corresponding to the buoyancy restoring force - exist in the lower shaded region, and the first three internal gravity wave modes are shown. Note the square root dependence of the frequency on the horizontal wavenumber for small wavenumbers. The observed oscillations correspond to horizontal wavenumbers of the order of several tenths of a Mm^{-1}, and the higher horizontal wavenumber behaviour - where the modal curves are open upward, rather than downward - which corresponds to a constant number of vertical wavelengths in the temperature minimum-region-has not been observed. The S - shaped bends in the higher harmonics

occur as the mode crosses a line corresponding to the same number of vertical wavelengths in the isothermal temperature minimum as a lower order mode. The detailed vertical variation of the energy density in the resonant modes is unfortunately not so amenable to a simple qualitative discussion. But it is interesting to note that while for horizontal wavelengths greater than 4 times the scale height at the temperature minimum the oscillatory energy of the fundamental mode is concentrated in the sub-photospheric cavity, for smaller horizontal wavelengths the energy concentrates in the chromospheric cavity - as suggested by Bahng and Schwarzschild. Furthermore, the maximum amplitude of the higher order modes alternates from the convection zone to the chromosphere from mode to mode.

Numerical calculations with temperature and density distributions given by realistic solar models have been carried out by Ando and Osaki (1975, 1977) and Ulrich and Rhodes (1977). Both groups draw attention to modes which are trapped in the chromosphere with a period near 240 seconds. As mentioned above, analytic studies predict a whole series of such chromospheric modes. Deubner has found some observational evidence suggesting the possible existence of power at this frequency. However, quite frankly, it would be somewhat surprising were this mode to exist because of the large amplitude of the motion at chromospheric heights. That is, the wave will significantly distort the resonating cavity. The least that one might expect is that the modes with different horizontal wavelengths, instead of being completely independent, would have their phases locked together. As we shall see below, the currently discussed excitation mechanisms all operate below the visible surface and hence the excitation of the chromospheric mode is not expected to be favored. However, it should be pointed out that for comparable amplitudes near the visible solar surface, the chromospheric mode should be much more visible in the chromosphere than the normal modes with their maximum in the sub-photospheric cavity. While the astounding coincidence with observations served to establish the sub-photospheric cavity model, more recently small remaining differences between observation and theory have been exploited as diagnostics of the thermal structure of the hydrogen convection zone. It may be that no plausible choice of a mixing length would be capable of precisely matching the observations, thereby vitiating the mixing length treatment of convection. The different depth distribution of the energy in

the different modes appears to be capable of providing a diagnostic of the variation of the solar rotation rate with depth (Deubner, Ulrich and Rhodes, in preparation).

While in what has been said up to now, any horizontal wavelength was as good as another; along a model curve, for every wavelength there corresponded a period. If , however, the oscillations last for a very "long" time, where now "long" is understood to be of the order of the time for the phase to propagate around the circumference of the Sun; then even though there are no reflections, the wave can interfere with itself after going all of the way around and once again only those modes with wavelengths which end up in phase with themselves will resonate. The necessary observational resolution to resolve the horizontal modes is not impossible to imagine, and the existence or non-existence of this secondary modal structure should be an exciting diagnostic of the lifetime of the modes. In any case, there are several hundred thousand modes which contribute to the observed "five-minute" oscillation!

While the fact that the observed structure of the "five minute" oscillations coincides so impressively with the normal modes of the sub-photospheric cavity gives us confidence in the appropriateness of the model, I haven't given the reader any reason to suppose that there is any means of putting energy into these modes; or in the lingo of the trade, to "excite" them. (Just because unicorns could exist, one is not compelled to assume that they do.) As often seems to be the case, there exist a plethora of mechanisms available and the problem seems to be more choosing amongst them. The different mechanisms differ not only in their dependence upon the period and horizontal wavelength of the mode, but also in their dependence on the structure of the atmosphere. Thus for other stellar types the relative importance of the different mechanisms will almost certainly change.

Two fundamentally different ways of putting energy into a wave, or oscillatory motion exist: internally or externally, via the energy equation or via the momentum equation. By pushing on the gas in a cavity - mechanically through a diaphragm, as discussed above, or via some other motion in the atmosphere - at one of its resonant frequencies,the gas will be excited to an

oscillation at the amplitude specified by the pushing ("driving" is the more commonly used lingo). The sound wave could exist at any amplitude in this formulation, the non-linearities having been neglected. Thus if a resonant mode was oscillating away at some amplitude and the driving was turned on at a lower amplitude, the driving would reduce the oscillation amplitude and thus would really be dissipation. Lighthill has formulated this approach in connection with the generation of sound waves by the turbulence in the exhaust from jet engines, and it has been used in astrophysics - primarily by Stein - to evaluate the flux of sound waves emitted by the "turbulent" flow in the hydrogen convection zone. "Turbulent flow" is the buzz word used to describe the velocities responsible for carrying the convective flux of energy - as specified by the mixing length treatment of convection. Given a characteristic velocity, which depends upon an assumed numerical and functional form for the mixing length, a turbulent spectrum of temporal and spatial scales is assumed. Unfortunately, the emitted flux is very sensitive to all of these assumptions. This flux is primarily at very short periods (less than 100 seconds) which are not trapped. Although these high frequency waves do not contribute to the "five-minute" oscillation, they may well be important in the heating of the lower solar chromosphere. Recently Goldreich and Keeley (1977) and Keeley (1977) have considered the same mechanism for the longer period, resonant modes and they find that although the turbulence acts primarily to dissipate the radial modes, it is capable of exciting the non-radial modes to amplitudes comparable with observation. This mechanism arises primarily in the upper parts of the convection zone where the convective velocities and the associated dynamical effects rise rapidly before falling to zero in the convectively stable photosphere. While this pushing acts on the wave through sources which appear in the momentum equation, periodic addition of internal energy has also been suggested as a means of exciting the resonant modes.

As the temperature and density of the gas vary throughout the oscillation, the interaction of the gas with the mean atmosphere will also vary. Depending upon the phase between the energy transfer and the temperature fluctuation, the effect will increase or decrease the amplitude of the wave. For example, if heat is lost when the gas is hot and gained when the gas is cold, the oscillatior

will be damped. By reducing the energy density when it is high we reduce the restoring force of the compresibility and hence the energy of the wave has been reduced. If on the other hand, the gas could be made to absorb more energy when it was hot and less energy when it was cool, the amplitude of the wave would increase. This occurs quite generally for any thermodynamic cycle: heat absorbed during the hot part of the cycle adds to the energy of the oscillator, heat added during the cool part of the cycle reduces the energy. When the energy added is proportional to the amplitude - often called a "linear instability" - the amplitude will grow exponentially in time. An oscillator whose amplitude increases exponentially in time is said to be "overstable" or "vibrationally unstable". The amplitude will continue to increase until some process whose importance depends non-linearly on the amplitude grows to dominate - a parabola, or higher order polynomial, starts rising from zero more slowly than any straight line but eventually will exceed it. These non-linearities may occur in the excitation or in the dissipation process. If the amplitude of the wave in the driving region becomes large, over part of the cycle the excitation may change to dissipation. Thus any further increase in the amplitude would increase the dissipation more rapidly than it increased the excitation and thus the growth of the oscillation would cease. This limitation is often referred to as a "saturation" of the excitation. Leakage from the cavity may also limit the amplitude. The sound waves penetrate slightly through the temperature minimum region and will be dissipated at greater heights. This dissipation increases rapidly in its efficiency with increasing amplitude; so that were nothing else occuring, the wave amplitude wool increase until the energy dissipated above the temperature minimum just equaled the energy put into the wave by the overstability.

Such overstabilities have been invoked for years to account for the Cepheid pulsation phenomenon. Although several effects are intimately combined, the increasing opacity with increasing temperature (at constant density) which prevails in the hydrogen and helium ionization zones of stellar envelopes takes energy from the outward thermal flux and transforms it to acoustic waves. Rather than controlling the deposition of energy into the wave, the opacity mechanism regulates the escape of energy through the wave; and, following Eddington, this distinction between periodic injection and periodic damming up

of a continuous flux is referred to as the "Eddington Value". This fluctuating opacity mechanism is often referred to as the "κ mechanism" in distinction to the contribution made by the fluctuation in the internal energy brought about by the fluctuating ratio of specific heats - the "γ mechanism". At temperatures above the maximum of ionization, further into the interior, the situation reverses and increasing temperature leads to a decreasing opacity, and thus fluctuations deep in the stellar interior are damped. Since the driving "changes sign" at high temperatures, as the temperature fluctuation in an oscillation grows with amplitude, eventually the driving will saturate and the amplitude will be limited. Resonant modes with large amplitudes in the damping region will not be excited, while those with large amplitudes in the outer regions, where hydrogen and helium are ionizing, will be excited. Thus, along a modal curve for-say-the first harmonic, since longer horizontal wavelength modes will resonate deeper in the interior they will grow less rapidly in time than shorter horizontal wavelength modes; and very long horizontal wavelength modes will most probably not be overstable. However, Provost (1973) has cautioned against such "intuitive" reasoning. Ando and Osaki (1975, 1977) have done extensive calculations of the variation of the growth rate with horizontal wavenumber for the different modes.

While this overstability arises in the outer region of the solar convection, zone, near the depths where the "Lighthill mechanism" is effective, the thermal rather than dynamical coupling to the mean atmosphere should uncouple the relative importance of these two mechanisms in other stars. Ando (1976) has calculated growth rates of the overstability in other stars.

Another physically distinct overstability, suggested long ago by Cowling, revived by Spiegel and discussed recently in detail by Graff (1976), derives energy from the super-adiabatic temperature gradient maintained by convection. Because the mean atmospheric temperature gradient is greater than that of the displaced gas in the sound wave, any dissipative mechanism - such as radiative transfer - will add heat when the fluctuation is displaced towards the interior; that is, compressed and heated; and remove it during the other half cycle. (This type of mechanism has also been suggested to generate MHD waves, particularly in connection with the problem of cooling sunspots. A recent article by Cowling (1977) is of interest here.) It appears that for

the Sun, the κ mechanism contributes much more than this "Cowling - Spiegel" to the overstability of acoustic modes in the sub-photospheric cavity. Because of the tremendous efficiency of convection in the Sun, the actual temperature gradient exceeds the adiabatic gradient by less than a part in a thousand throughout almost the entire convection zone. It is only in the outer scale height or two that substantially super-adiabatic gradients exist, and thus only a relatively small mass is available to participate in the driving. However, in other stars where convection may be less efficient and extended super-adiabatic zones present, this mechanism may contribute.

In concluding this section, let me repeat that the theoretical "action" in the near future appears to focus on the generation of these resonant modes whose existence has been established. To evaluate the amplitudes attained by the overstabilities for comparison with observation and to evaluate the energy loss by dissipation, a much more difficult non-linear problem must be attacked. In addition, having established a new paradigm, new observations must continue to test it. In particular, the interaction of a magnetic field, be it in a sunspot, an active region, or in the quiet sun network, with the resonant modes is of great interest. The observations reported on at this meeting by Livingston (see also Giovanelli, Livingston and Harvey, 1978) provide an excellent stimulus for this undertaking.

II. Chromospheric Dynamics

One of the principal programs of the pointed instruments onboard OSO-8 has been the observation of velocity and intensity fluctuation fields throughout the solar chromosphere and the transition to the solar corona. These fluctuating fields are of interest not only as phenomena in their own right but also because of their relation to the mechanical energy transport which has been speculated to be responsible for the heating of the chromosphere and corona. Because spatial inhomogeneities are known to be much greater in the chromosphere than in the photosphere and the effect of magnetic fields more important, we may anticipate that several processes may simultaneously contribute to the chromospheric dynamics and that the isolation and identification of the phenomenon may prove more difficult. Thus humbled, it behooves us to examine the apparent consequences for the chromosphere of the model of resonant modes trapped in the sub-photospheric cavity. We shall show that the frequencies which cannot propagate near the temperature minimum and are trapped in the convection zone, propagate once again in the higher temperature chromosphere. In addition, waves at the cut-off period are generated near the temperature minimum and these play an important role in the chromosphere. Finally , even for resonant oscillations with amplitudes smaller than those observed near the visible surface, the chromospheric amplitudes are sufficiently large that non-linear effects become important. These effects will be illustrated by the results of numerical calculations of the one dimensional response of the chromosphere.

The resonant modes trapped in the sub-photospheric cavity occur because waves of the frequencies of these modes cannot propagate at the temperature minimum where the scale height becomes too small. An evanescent, exponentially varying wave extends into the photosphere and the energy density decreases upwards towards the chromosphere. Although the energy density decreases, the velocity amplitude actually increases upwards, just not rapidly enough to overcome the effect of the rapidly decreasing density. Although the velocity becomes large, it is very difficult for these evanescent waves, with pressure and velocity out of phase, to dissipate, and they certainly will not form shock waves in the normal sense of the term. At large amplitude, they presumably couple to higher frequency waves which can propagate and dissipate. If the

low temperature region extended to infinty, the reflection would be perfect. However, after approximately seventeen pressure scale heights, the temperature rises and the resonant mode frequencies can once again propagate. If the amplitudes were very small; a resonant cavity similar to that in the hydrogen convection zone would exist - as discussed above - and the two cavities would be coupled by the evansecent waves in between. As we shall see below, the waves are sufficiently strong to distort the high temperature reflection region of the chromospheric cavity and the chromospheric resonance is destroyed. Thus somewhat higher than 2 megameters above the visible surfa the five minute oscillation will start propagating once again, but the amplitude of these modes is now quite large and as soon as they can propagate, they start to dissipate their energy.

Another process, whose existence might not have been anticipated from the modal analysis, seems to be of greater importance however. Lamb - who I indicated earlier discovered practically all of the basic physics of atmospheres over fity years ago - showed that when an isothermal atmosphere is subjected to a pulse of energy, a wake remains after the pulse,oscillating at the acoustic cut-off period. This is about 200 seconds for the solar temperature minimum region. Like the evansecent waves, this cut-off period wave transmits very little energy, and the pressure and velocity fluctuations are nearly ninety degrees out of phase. In contrast with the evanescent wave, the energy density does not decrease with altitude in the atmosphere. This wave appears to be excited by the 300 second evanescent wave in the solar photosphere, with which it enjoys a resonance - in that after two 300 second periods, three 200 second periods have elapsed. This is illustrated in Figure 2 where the non-linear response of a plane parallel solar atmosphere to a pulse started 1.6 megameters below the visible surface has been followed for 1400 seconds. A rigid lower boundary was raised about a kilometer in 50 seconds, so that the maximum upward velocity of the impulse was 0.05 km/sec. The resulting 300 second oscillation is rather weak only 0.1 km/sec at the surface. In contrast to the 300 second oscillation at negative altitudes, above the temperature minimum (550 km) a very regular 200 second oscillation has been established. Above 1000 kilometers the velocity oscillations become significantly asymmetric in time, and the pressure pulses narrow so that by 2400 kilometers the pulse

is only about twenty percent of the period. High in the chromosphere, the pressure more than doubles in these short pulses, so that the atmosphere is blasted upwards and then nearly free falls back down until the descent is arrested by the next upward blast. As low down in the chromosphere as 1800 km, the particle excursions are of the order of 600 km, that is to say several scale heights. Thus even for this relatively low amplitude sub-photospheric, resonant mode, there remains no semblance of a mean, equilibrium chromosphere. Another resonant mode, of infinitesimal amplitude, could no longer interact with an equilibrium atmosphere, but rather it would see drastic time changes.

Attempts have been made to understand the temporal evolution of strong chromospheric lines such as the calcium K resonance line (Heasley (1975), Cram (1976)) and the hydrogen Lyman α line (Kneer and Nakagawa, 1976) by calculating line profiles from the chromosphere as a pulse, like the one which initiates the motions in Figure 2, propagates upwards. Durrant, Grossman-Doerth and Kneer (1976) have argued that such an isolated pulse with pressure and velocity in phase, is not capable of reproducing the observed profile changes. In fact, one sees that the situation following the initial pulse is distinctly different, in that the pressure and velocity fluctuations are significantly out of phase - nearly ninety degrees. Thus in a real, dynamical atmosphere the 200 second pulses are always moving into an atmosphere far removed from equilibrium by the passage of the previous pulse. Of course, there may exist other sources of pulses with no special phase with respect to the 200 second oscillation - those generated by exploding granules for example. But these too will move into an atmosphere whose time averaged properties bear little resemblence to the equilibrium, static atmosphere - there is no way that a micro-turbulent pressure is going to model even the mean state of an atmosphere with motions greater than the scale height. Furthermore, because of the substantial motions of the atmosphere, the velocity at constant mass depth - that is, measured in a Lagrangian coordinate - which bears a closer relation to what a spectral line will "see" than the velocity at a constant geometrical depth, contains striking differences for the upper chromosphere. Figure 3 displays the Lagrangian fluctuations for the same calculation presented in Figure 2. The phase velocities are reduced high in the chromosphere because of the outward impulses. The pulses also tend to form

pairs, which is seen most clearly in the pressure fluctuation - the first pulse slows down the existing infall and the second re-accelerates the material outward. The resulting outward motion moves this mass depth away from the next outwardly moving pressure pulse, which as a result takes an increased length of time to catch up.

Although the most striking aspect of chromospheric dynamics - the decrease of the period of oscillation from 300 to 200 seconds - is easily accounted for within our present understanding of sub-photospheric resonant modes and propagation in the photosphere and chromosphere, the detailed evolution of optically thick spectral lines, which (presumably) provide us with much improved height resolution and a better constrained diagnostic, has not been satisfactorily described. While those who expected OSO-8 to observe beautiful N wave shock profiles to confirm the shock wave heating hypothesis (and deliver them their science on a silver platter) must feel somewhat disappointed, it certainly appears at this point that the ball has merely been placed back in the theoretician's court: it is incumbent on "us" to provide a meaningful expectation of the observable consequences of the "astrophysical truth" of the photosphere.

III. Chromospheric and Coronal Heating

The lack of unambiguous success in identifying propagating and dissipating shock waves in the chromosphere has certainly impeded the solution of the problem of chromospheric and coronal heating; but in addition to the diagnostic problem cited above, other theoretical aspects of a self-contained shock wave heating model remain to be resolved: total flux generated, distribution of the flux with period and horizontal wavelength, height distribution of the dissipation again as functions of the period and horizontal wavelength, effect of changes in the mean atmosphere on the generation and dissipation; to list but a few. It has been argued that the Sun is the ideal stimulus for attacking these questions not only because of the spatial and temporal resolution which its propinquity affords, but also because of the relative weakness of the chromosphere/corona phenomenon. Because only a very small fraction of the total flux appears to be required to heat the outer atmosphere above its radiative

equilibrium temperature, only very small modifications to the conditions in the convection zone - or wherever else the generation of a propagating mechanical energy flux from a thermal flux may occur - would seem necessary. That is, the structure in the generation region may be calculated neglecting the mechanical flux, which is then just calculated as a perturbation - it exerts no effect back on the local, thermally controlled structure, such as might exist if very efficient wave generation refrigerated the atmosphere. However, because of the weakness of the phenomenon it may well turn out that no one effect dominates and we may advance our understanding by studying the outer atmospheres of stars with more significant dynamical effects: cepheids or stars with more vigorous convection zones. Currently the situation is embarrassingly reversed; stellar astronomers seem to be taking unfounded solar hypothesis seriously and are applying them out of context. (See Linsky and Ayres (1977) for a critique).

These hypothesis have not changed significantly in recent years. Let me just outline them for the sake of completeness. Short period (less than 100 seconds) non-resonant waves generated by turbulence in the convection zone dissipate their energy by non-linear processes after propagating a shorter distance than the longer period, nearly resonant waves essentially because the short period waves have shorter wavelengths. Quite simply, they don't have to go so far in order to break. In addition to the horrible uncertainty in the power generated by this mechanism mentioned earlier, the short wavelengths - comparable to the region over which a spectral line is formed - have posed problems to the direct observation of these waves. Deubner (1977) has recently interpreted waviness in the temporal power spectra of photospheric oscillation at these periods as an indication of the existence of these short wavelengths. Ulmschneider and Kalkofen (1977) argue strongly in favor of the importance of this short wavelength heating, while Proderic and Thomas (1976) contest the treatment of radiative losses, Jordon (1976) supports Ulmschneider's position and Cram (1977) questions the whole edifice. These short wavelength waves would be primarily of importance in heating the low chromosphere, where they dissipate the remaining small fraction of their energy not lost by radiative damping as they propagate through the photosphere. Essentially none of their energy remains to heat the corona.

The model of heating by dissipation of sub-photospheric resonant modes in the corona has also suffered the difficulty of fundamental uncertainties in the energy generation rate. However, this appears to be in the process of being resolved. These modes have the advantage of being directly measured in the photosphere so that an observational normalisation is available. The direct calculation of the amplitude achieved by the overstability of non-vertically propagating modes is a challenging problem, which unfortunately has not been challenged. Since the amplitudes in the driving region are very small (less than one thousandth the sound speed), the oscillations will find it difficult to saturate the excitation mechanism. Calculation of the limitation of the amplitude growth by shock wave dissipation requires the coupled treatment of the overstability and of two dimensional shocks. While progress may be made using existing one dimensional shock wave computer programs, the determination of the importance of two dimensional effects must await development of the appropriate programs. According to Bob Stein, several groups are attacking this problem via different techniques.

Several authors have calculated the thermal structure to be expected from a balance between shock wave heating, radiative losses and thermal conduction using analytical expressions for the dissipation of the mechanical flux. Because the wavelengths are long compared to the scale height, approximate treatment of the propagation and dissipation of these waves by methods which assume the medium to be uniform are not valid. Nonetheless, a great deal of work and even more publications are based upon this invalid treatment. Stein and Schwartz (1972) have demonstrated the inappropriateness of applications of the "weak shock theory", which makes additional assumptions essentially equivalent to assuming that the shock doesn't exist, by comparing results with the full non-linear treatment.

In closing, it is appropriate to point out that while there remain many theoretical aspects of the hypothesis of shock wave heating of the outer solar atmosphere which require development before the hypothesis can be accepted or rejected, alternative hypotheses exist which may in time prove to be more successful in describing stellar chromospheres and coronae. In particular, very strong (greater than 1000 gauss), very small (less than an arc-second)

magnetic fields are known to exist in the super-granulation network boundaries all across the "quiet sun", and these will support magnetic wave modes with generation, propagation and dissipation properites quite distinct from the purely acoustic modes described here. The work of Defouw (1976), Piddington (1973), Uchida and Kaburaki (1974), Wentzel (1974) should be consulted. In addition, one can imagine that these fields are capable of dissipating their energy in either very small flare-like, "catastrophic" events, or more uniformly in time - to give plasma physicists an easy problem for a change. In any case, I hope that it is clear that theoreticians have before them a wide range of exciting, relatively well defined problems and they may take heart from the recent success in the prediction of the modal structure of the five minute oscillation - some problems actually do manage to get themselves solved!

It is a pleasure to thank Robert Stein and Pierre Gouttebroze for many useful discussions and Lise Ouvrard for correcting the grammar. The non-linear calculations were performed on the CDC 7600 of the Centre National de Etudes Spatiales. This work was supported in part by NASA contracts NASW-3055 and NAS8-32356, and the Lockheed Independent Research Program.

REFERENCES

Ando, H. 1976, Publ. Astron. Soc. Japan, 28, 517: "Overstability of Acoustic Modes in Late Type Stars and its Observational Implication."

Ando, H. and Osaki, Y. 1975, Publ. Astron. Soc. Japan, 27, 581: Nonadiabatic Nonradial Oscillations: An Application to the Five Minute Oscillations of the Sun.

Ando, H. and Osaki, Y. 1977, Publ. Astron. Soc. Japan, 29, 221: "The Influence of the Chromosphere and Corona on the Solar Atmospheric Oscillations".

Cowling, T.G. 1976, Mon. Not. Roy. Astron. Soc. 177, 409: "On the Thermal Structure of Sunspots".

Cram, L.W. 1976, Astron. Astrophys. 50, 263: A Multi-component Time-dependent Model for the Calculation of the Ca II K Line.

Cram, L.E. 1977, Astron. Astrophys. 59, 151: "On the Heating of the Solar Chromosphere"

Deubner, F.L. 1975, Astron. Astrophys. 44, 371: Observations of Low Wave-number Non-Radial Eigenmodes of the Sun.

Deubner, F.L. 1977, submitted to Astron. Astrophys: "Observations of Short Period Acoustic Waves Bearing on the Interpretation of "Microturbulence".

Defouw, R. 1976, Astrophys. J. 209, 266: "Wave Propagation Along a Magnetic Tube".

Durrant, C.J., Grossman-Doerth, and Kneer, F.J. 1976, Astron. Astrophys. "The Sun;s Chromospheric Velocity Field as inferred from the Ca II K Line".

Giovanelli, R.G., Livingston, W.C. and Harvey, J.W. 1977, Preprint: "Oscillations in Solar Magnetic Tubes".

Goldreich, P. and Keeley, D.A. 1977, Astrophys. J. 212, 243: "Solar Seismology II. The Stocastic Excitation of the Solar P-Modes by Turbulent Convection".

Graff, P. 1976, Astron. Astrophys, 49, 299: "A Study of Unstable Acoustic Waves in a Convective Zone".

Heasley, J.N. 1975, Solar Phys. 44, 275: Asymmetries of the Solar Ca II Lines.

Keeley, D.A. 1977, Symp. on Large Scale Motions on the Sun, Sacramento Peak Observatory: "Some Problems in the Theory of Global Solar Oscillations".

Kneer, F.J. and Nakagawa, Y. 1976, Astron. Astrophys. 47, 65: Radiative Hydrodynamics of Chromospheric Transients.

Leibacher, J.W. 1971, Harvard University Thesis: "Solar Atmospheric Oscillations".

Linsky, J. and Ayres, T.R. 1977, Preprint: "Stellar Model Chromospheric VII Empirical Estimates of the Chromospheric Radiative Losses of Late - Type Stars.

Michalitsanos, A.G. 1973, Earth Extraterr. Sci. 2, 125: Recent Theoretical Interpretations of the Solar Five-Minute Oscillation.

Piddington, J.H. 1973, Solar Phys. 33, 363: "Solar Atmospheric Heating".

Praderie, F. and Thomas, R.N. 1976, Solar Phys. 50, 333: Radiation Loss and Mechanical Heating in the Low Solar Chromosphere.

Prevost, J. 1973, Solar Phys. 33, 103: Note on the Response of an Atmosphere to a Localized Turbulent Source.

Stein, R.F. and Leibacher, J.W. 1974, Ann. Rev. Astron. Astrophys. 12 , 407: "Waves in the Solar Atmosphere".

Stein, R.F. and Schwartz,R.A. 1972, Astrophys. J. 177, 807: Waves in the Solar Atmosphere. II. Large Amplitude Acoustic Pulse Propagation.

Uchida, Y. and Kaburaki, O. 1974, Solar Phys. 35, 451: "Excess Heating of the Corona and Chromosphere above Magnetic Regions by Non-Linear Alfven Waves".

Ulmschneider, P. and Kalkofen, W. 1977, Astron. Astrophys. 57, 199: Acoustic Waves in the Solar Atmosphere. III. A Theoretical Temperature Minimum.

Ulrich, R.K. 1970, Astrophys. J. 162, 993: "The Five Minute Oscillations on the Solar Surface".

Ulrich, R.K. and Rhodes, E.J. 1977, preprint: "The Sensitivity of Non-Radial P Mode Eigenfrequencies to Solar Envelope Structure".

Wentzel, D.G. 1974, Solar Phys. 39, 129: "Coronal Heating By Alfven Waves".

FIGURE CAPTIONS

Figure 1: Resonant modes for a plane parallel atmosphere with a 1.5 megameter thick temperature minimum at 4000°K, a 100°/km temperature gradient above and a 10°/km gradient below. Limits for propagating acoustic and internal gravity waves in the temperature minimum region are shaded. The fundamental and first three acoustic and internal gravity resonant modes are shown.

Figure 2: Velocity (solid lines) and relative pressure (dotted lines) fluctuations as a function of time at various altitudes in a model solar atmosphere. Altitude (in kilometers) is measured from a zero at $\tau_{5000} = 1$ in the initial atmosphere. The energy equation is adiabatic with a constant $\gamma = 1.4$. The velocity and pressure normalisation at each altitude was chosen to exhibit the fluctuations after the atmosphere had recovered from the initial pulse, and points out of range have not been plotted.

Figure 3: Same as Figure 2, except the fluctuations are measured at constant mass depths, corresponding (approximately) to the altitudes displayed in Figure 2 for the initial atmosphere.

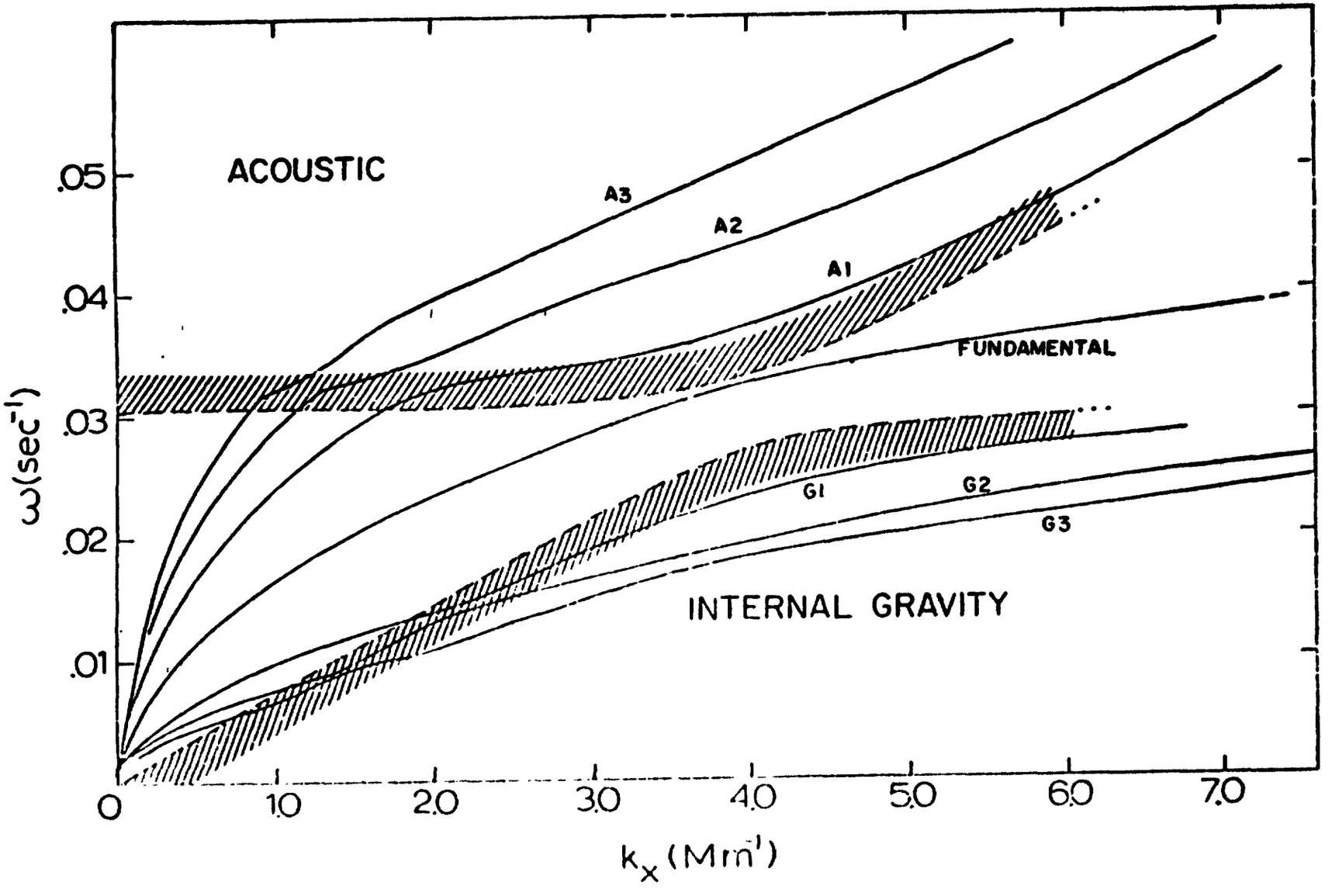
ACOUSTIC
A3
A2
A1
FUNDAMENTAL
G1
G2
G3
INTERNAL GRAVITY
.05
.04
.03
.02
.01
ω(sec⁻¹)
0
1.0
2.0
3.0
4.0
5.0
6.0
7.0
kx (Mm⁻¹)

Figure 1

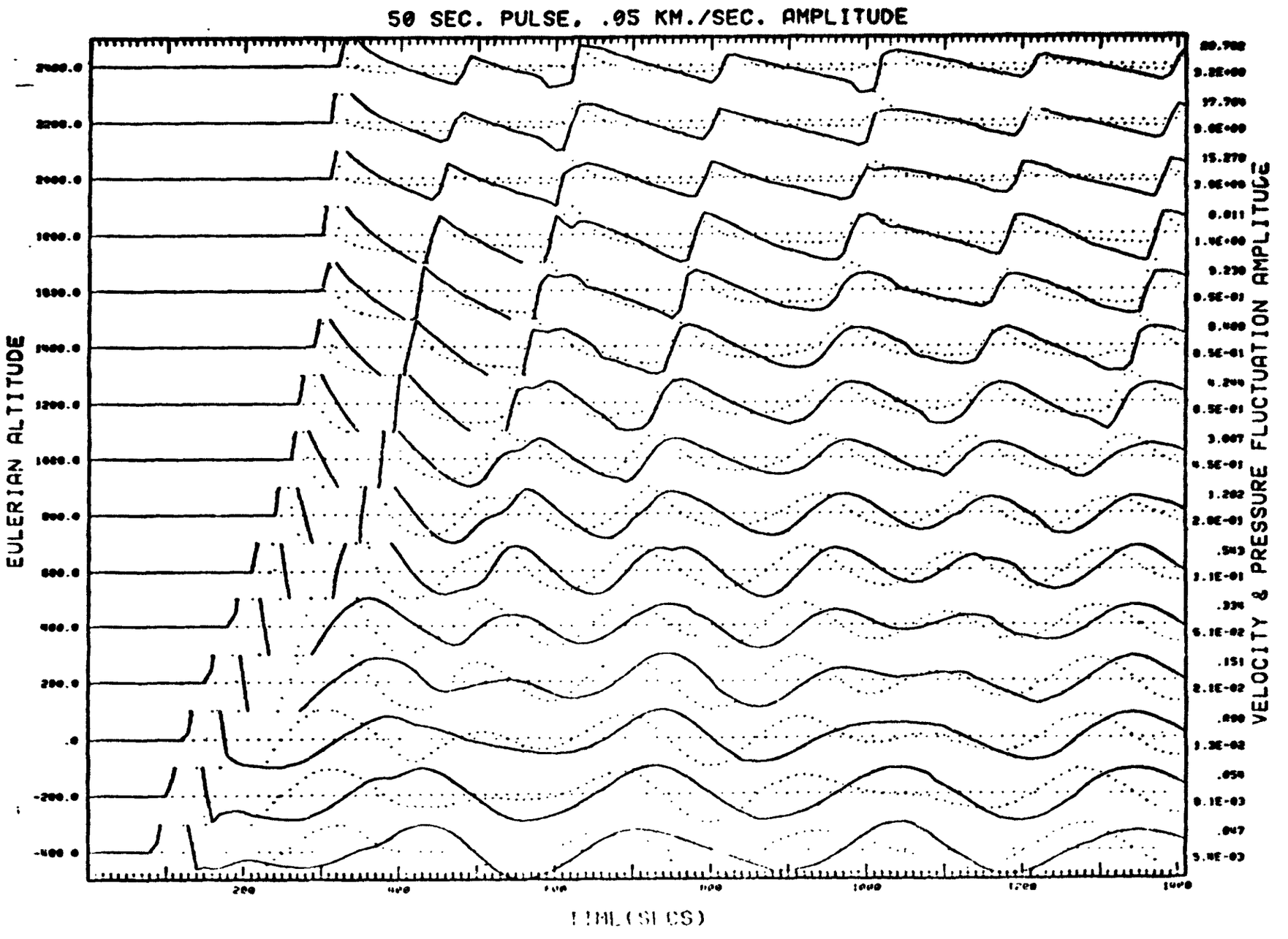
50 SEC. PULSE, .05 KM./SEC. AMPLITUDE
EULERIAN ALTITUDE
VELOCITY & PRESSURE FLUCTUATION AMPLITUDE
TIME(SECS)

Figure 2

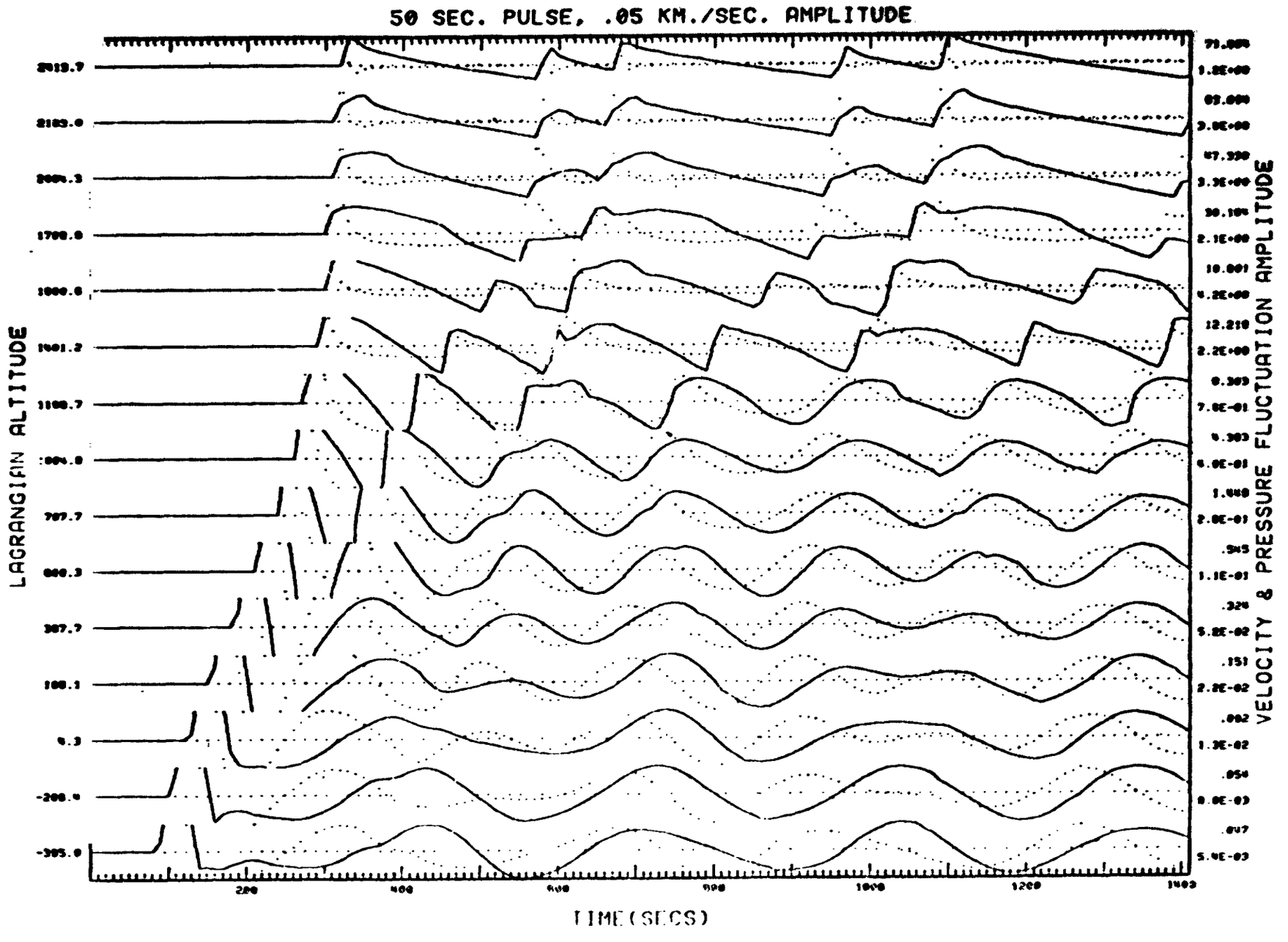
50 SEC. PULSE, .05 KM./SEC. AMPLITUDE
LAGRANGIAN ALTITUDE
VELOCITY & PRESSURE FLUCTUATION AMPLITUDE
TIME(SECS)
200
400
600
800
1000
1200
1400

Figure 3

Attachment B

Published in the Proceedings of the November 1977 OSO-8 workshop, p. 356

Observations of oscillations of the solar CaK, Mgk 2795 Å and H-Lyman α lines from OSO-8

G. Artzner, J.W. Leibacher*

Laboratoire de Physique Stellaire et Planétaire
CNRS - P.O. Box 10, 91370 Verrières-le-Buisson, France

*Lockheed Palo Alto Research Laboratory
Palo Alto, California 94304

ORIGINAL PAGE IS
OF POOR QUALITY

We have observed simultaneously the solar CaK (3933 Å), CaH (3969 Å), Mgk (2796 Å), Mgh (2803 Å), and H-Lyα 1216 Å solar lines with spatial, temporal and spectral resolutions of 1" x 10", 10 seconds and 0.02 Å, over time sequences ranging from 40 to 60 minutes.

When plotting as a function of time the integrated intensity of the Mgk line (over 1.09 Å), a clear quasi-periodic oscillation is visible on 48 out of 50 time-sequences ; 16 of the 48 measured periods are shorter than 197 seconds, 16 between 197 and 238 seconds, 16 greater than 238 seconds.

Within the 10 seconds resolution, the temporal evolutions of the intensity of the blue emission peak of the CaK and Mgk lines are correlated without phase shift.

A study of thepower spectrum of the temporal evolution of the intensity of the blue emission peak of the CaK and Mgk lines for 12 time sequences, indicates that strong, short period oscillations (< 200 seconds) occur over quiet areas of the sun, such as the center of the supergranulation cells, whereas weak, long period (>250 seconds) oscillations occur over areas with active CaK profiles.

For 7 time sequences we have computed the average Lyman-α profile corresponding to the "blue" and "red" phases of the solar oscillations (i.e., for a time sequence of 300 spectra, we add the 100 Lyα profiles measured simultaneously with the 100 Mgk profiles with the strongest blue peak, and repeat one other Lyα average corresponding to the 100 Mgk profiles with the weakest blue peak). The resulting "blue" and "red" Lyman-α profiles have the same total intensity, the same intensity at the emission peaks, whereas the corresponding CaK and Mgk profiles are strongly different. The central reversal of the average "blue" Lyα profile is shifted to the red with respect to the average "red" profile, indicating that the part of the solar atmosphere where this central reversal comes from oscillates somehow in phase with the lower chromosphere where the Mgk lines originates.

Attachment C

THE ASTROPHYSICAL JOURNAL, 221:1032–1061, 1978 May 1

THE LPSP INSTRUMENT ON *OSO 8*. II. IN-FLIGHT PERFORMANCE AND PRELIMINARY RESULTS

R. M. BONNET, P. LEMAIRE, J. C. VIAL, G. ARTZNER, P. GOUTTEBROZE, A. JOUCHOUX, J. W. LEIBACHER,* A. SKUMANICH,† AND A. VIDAL-MADJAR
Laboratoire de Physique Stellaire et Planétaire, C.N.R.S., France
Received 1977 August 29; accepted 1977 November 8

ABSTRACT

The in-flight performance for the first 18 months of operation of the French, pointed instrument on board *OSO 8* are described. The angular and spectral resolution, the scattered light level, and various other instrumental parameters are evaluated from the observed data and shown to correspond mostly to nominal design values. The properties of the instrument are discussed, together with their evolution with time. The distribution of the first 8363 orbits between various observing programs is given. Preliminary results are also described. They include studies of the chromospheric network, sunspots and active regions, prominences, oscillations in the chromosphere, chromosphere-corona transition lines, and aeronomy.

Subject headings: instruments — Sun: chromosphere — Sun: prominences — Sun: spectra — Sun: sunspots — ultraviolet: spectra

I. INTRODUCTION

One of the major goals of solar physics is to understand the nature, origin, and evolution of the various features present in the solar atmosphere. Some, like the granulation, represent dynamical responses to the convection zone. Others, like spots or the more dispersed magnetic flux tubes (e.g., network fragments), represent symptoms of a magnetic process. Any advance in our understanding of such interior processes must come from high angular and spectral resolution observations of the line profiles of such features.

The NASA orbiting solar satellite *OSO 8*, launched on 1975 June 21, carried in its pointed section two instruments designed for the highest angular and spectral resolution achieved by spacecraft to date. One of these instruments was the responsibility of the Laboratory for Atmospheric and Space Physics (LASP) of the University of Colorado, the other was that of the Laboratoire de Physique Stellaire et Planétaire (LPSP) of the Centre National de la Recherche Scientifique (France).

In this paper, we describe the performance achieved in orbit and outline the main results obtained with the LPSP instrument after 18 months of successful operation. Most of these results are in a preliminary state. A complete description of the instrumentation has been given in Artzner *et al.* (1977), hereafter referred to as Paper I.

* Lockheed Palo Alto Research Laboratory, Palo Alto, CA.

† High Altitude Observatory, National Center for Atmospheric Research; and University of Colorado, Boulder. The NCAR is sponsored by the NSF.

II. SUMMARY OF THE INSTRUMENT CAPABILITIES

Because of the limitations imposed by the size of the spacecraft (although considerably larger than the previous *OSO*s), the LPSP telescope was a Cassegrainian with a diameter of 30 cm. Consequently we limited our observations to the most intense chromospheric lines. Because the chromosphere is of limited depth, the spectrometer was designed so as to simultaneously observe six lines:

Ca II H (396.9 nm) and K (393.4 nm);

Mg II *h* (280.3 nm) and *k* (279.6 nm);

H I Lα (121.6 nm) and Lβ (102.5 nm).

A very rapid and versatile spectral scanner made it possible to also study the lines of O VI (103.2 nm) and Si III (120.6 nm) nearly simultaneously with those listed above and enabled us to study propagation effects and to obtain height resolution from the upper-photosphere to the lower corona. Table 1 summarizes the main characteristics of the spectrometer, which operates with two different spectral resolutions.

Two methods were available to make spectroheliograms. One was by means of spacecraft rasters: two image sizes were available, 44′ × 40′ and 2′.75 × 2′.3 (nominal). The reader is referred to Paper I (Table 2) for more details on these rasters. In addition, the LPSP telescope had an articulated secondary mirror which was moved by a two-axis stepping mechanism. Accordingly the solar image could be moved step by step. Each step was 1″ on the solar surface while the maximum area covered was 64″ × 64″.

A slit wheel mechanism, at the focus of the telescope, was used to select various slit sizes ranging

TABLE 1

DESIGN CHARACTERISTICS OF THE *OSO 8* LPSP SIX-CHANNEL HIGH-RESOLUTION SPECTROMETER

CENTRAL LINE	(nm)	SPECTRAL RESOLUTION (nominal) Low Mode (nm)	High Mode (nm)	High Mode $km\,s^{-1}$	MAXIMUM SPECTRAL RANGE (nm)	SPECTRAL INCREMENT PER GRATING STEP (nominal) (nm)
Ca II.....	396.9	0.1	0.0020	1.51	395.164–398.244	0.00149
Ca II K.....	[illegible]	0.02	0.0020	1.52	391.444–394.942	0.00169
Mg II h.....		0.1	0.0025	2.67	277.739–282.264	0.00219
Mg II k.....	279.6	0.02	0.0025	2.68	277.005–281.551	0.00220
H I Lα.....	121.6	0.02	0.0020	4.93	120.569–122.291	0.00083
H I Lβ.....	102.5	0.1	0.0060	17.65	101.686–103.229	0.00074

NOTE.—Wavelength units are nanometers (nm).

from 1″ × 1″ to 1″ × 40″ as well as [illegible] corresponding to 6″ × 2″.

III. IN-FLIGHT PERFORMANCE

Prior to launch, the instrument was submitted to numerous tests and calibrations, the results of which are given in Paper I. Here we present the actual performance measured in flight.

a) Angular Resolution

The ground tests of the telescope led us to expect an instrumental profile with a full width at half-maximum (FWHM) of 2″. Two methods have been used to estimate the angular resolution in orbit:

i) *Images of Limb Shape*

Repeated scans of the solar limb, as observed with a 1″ × 1″ aperture using the internal raster mode in the

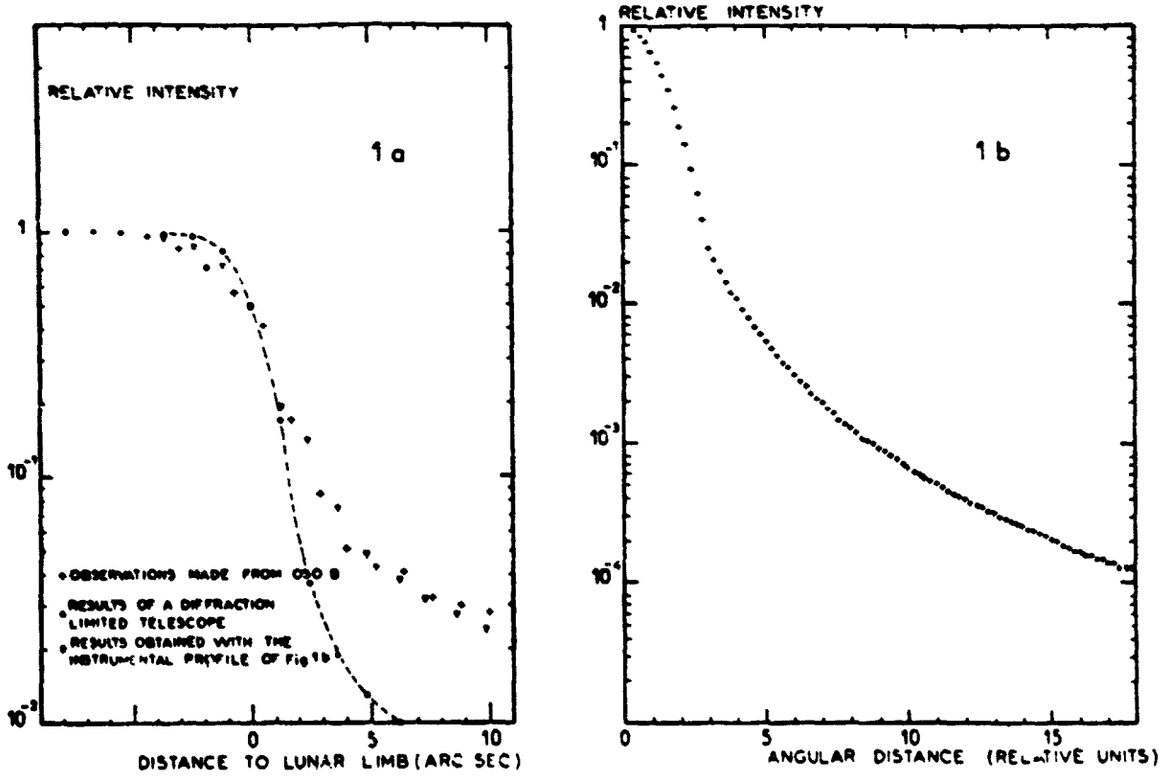

FIG. 1. (*a*) Internal raster scans across the lunar limb in Ca K. The dots show the results one would obtain assuming the telescope to be diffraction limited. The triangles show the results one obtains assuming the instrumental profile to be that represented on (*b*), the telescope instrumental profile.

far wings of the Ca II line, show a limb darkening with a 50% decrease over an angular distance of 2".

However, this method does not separate the resolution of the telescope from the jitter of the pointing system. Rapid, one-dimensional scan of the solar limb as well as other methods allowed us to estimate the amplitude of the rms jitter as 0".5.

ii) *Partial Solar Eclipses*

On 1976 April 29 and October 23, two partial eclipses of the Sun were visible from *OSO 8*. Figure 1*a* represents spatial scans laterally across the lunar limb measured in relative intensity units. The actual observations are compared with the results of a computation assuming the 16 cm Cassegrainian telescope to be diffraction limited, and to have an instrumental profile as given in Figure 1*b*. The fit using the profile of Figure 1*b* represents a good approximation. We therefore conclude that the instrumental profile has a FWHM of 2".5 ± 0".5.

b) Spectral Resolution

i) *Lα and Lβ Channels*

For these we take advantage of the narrow absorption line due to geocoronal hydrogen. By applying a method developed for the study of interstellar absorption lines (Vidal-Madjar *et al.* 1977), we obtain a spectral resolution in flight of 0.002 ± 0.0005 nm at Lα, and 0.006 ± 0.001 nm at Lβ.

ii) *Calcium and Magnesium Channels*

We compare the solar spectra obtained by our instrument with ground based (Ca II channels) and balloon- or rocket-borne observations (Mg II channels).

In Figure 2 we show the full range Ca II K and Mg II *k* spectra from *OSO 8*. The variation with wavelength of the sensitivity of the instrument has been corrected for, and the spectra are deconvoluted from the instrumental profile. The comparison with the spectrum of the Kitt Peak Preliminary Solar Atlas (Brault and Testerman 1972), which has a spectral resolution of 0.0024 nm, shows that our resolution in orbit is better than this value. In the case of the Mg II channels, comparison with the spectra of Lemaire and Skumanich (1973) and Kohl and Parkinson (1976) yields a resolution of 0.0025 ± 0.00025 nm. This value is equal to the nominal design value (cf. Table 1).

c) Dispersion and Grating Mechanism (Spectral Scanner) Stability

The dispersion law of the spectrometer was determined in orbit by measuring the position, in units of a grating step, of 11 solar absorption lines of known wavelengths in the Ca II and Mg II channels. For the Lβ channel we used the O I lines at 130.48 and 130.6 nm and N I at 119.9 nm (which appear in the 11th and 12th orders of diffraction).

Because of the lack of lines in the Lα channel, we deduce the dispersion law from that at Lβ. The absorption line of geocoronal hydrogen provides an absolute reference. This proved to be valuable due to the appearance of positioning uncertainties (± 1 grating step) in the movable Lα, Lβ exit slit mechanism. The dispersion law was measured repeatedly to check for long-term variations. Over 1 year we found that the correspondence between absolute wavelength and grating step number varied by no more than ± 3 grating steps (cf. last column of Table 1).

To check the mechanism stability over one orbit, we measured the position of the photospheric line 391.52 nm in the wings of Ca II K. Any departure from the orbital Doppler effect could be attributed to photospheric Doppler shifts and/or changes in the spectrometer. The result is shown on Figure 3. One can easily recognize the 300 s photospheric Doppler oscillations after removal of the orbital Doppler shift, measured for the first time from space. The amplitude of the residual noise on this curve amounts to ± 30 m s^{-1}. The stability of the mechanism over a full orbit day is better than one grating step and exceeds our design expectations. We are able to easily and accurately measure Doppler shifts of photospheric and chromospheric lines (see § Vc below).

d) Scattered Light Background and Dark Current

The level of scattered light in the telescope plus spectrometer was determined from partial eclipses of the Sun. From Figure 1 we see that at 11" from the lunar limb this level amounts to 2% of the intensity of the disk in the calcium channels. For Mg II it is 4%. For Lα and Lβ these figures become 10% and 20%, respectively, which indicates that the scattered light level may vary with wavelength, roughly as 1 λ^2.

No simple and unambiguous method was available to measure separately and give an absolute value for the amount of scattered light in the spectrometer due to wavelengths well away and near the wavelength of interest.

In the case of the Ca II and Mg II channels, we could compare the performance of our spectrometer with those of other ground-based or rocket-borne instruments. The result of this comparison appears in Table 2, where we give the ratio of intensities at Ca II H_1 and K_1, Mg II h_1 and k_1, relative to those of the Ca II and Mg II line wings. We notice that our performance is excellent for the Ca II channels, for which these ratios are smaller than those deduced from the Utrecht (Minnaert, Mulders, and Houtgast 1940) and the Air Force (Beckers, Bridges, and Gilliam 1976) atlases. We also compare our values with those of Linsky (1970) and of White and Suemoto (1968) who used particularly good optical systems. The Utrecht Atlas was used to evaluate the ratio of the H_3 and K_3 intensities relative to that of the continuum at 400.0 nm. The results are:

$$\frac{I_{H_3}}{I_{400.0}} = 0.053, \quad \frac{I_{K_3}}{I_{400.0}} E = 0.065, \quad \text{for } OSO\ 8,$$

while White and Suemoto (1968) find 0.071 ± 0.0015 and 0.061 ± 0.001, respectively, and Linsky (1970)

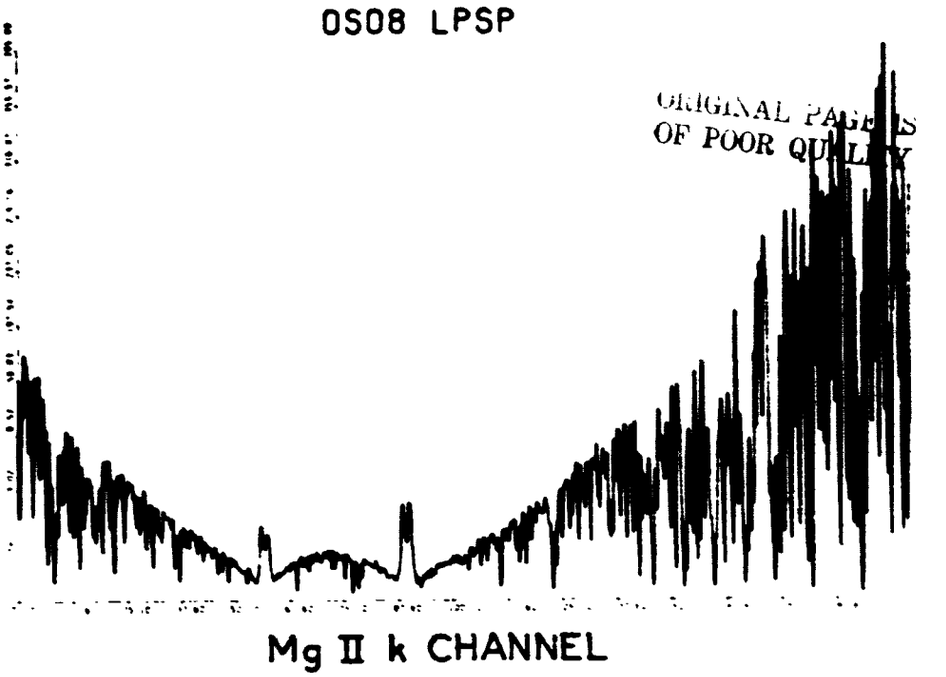

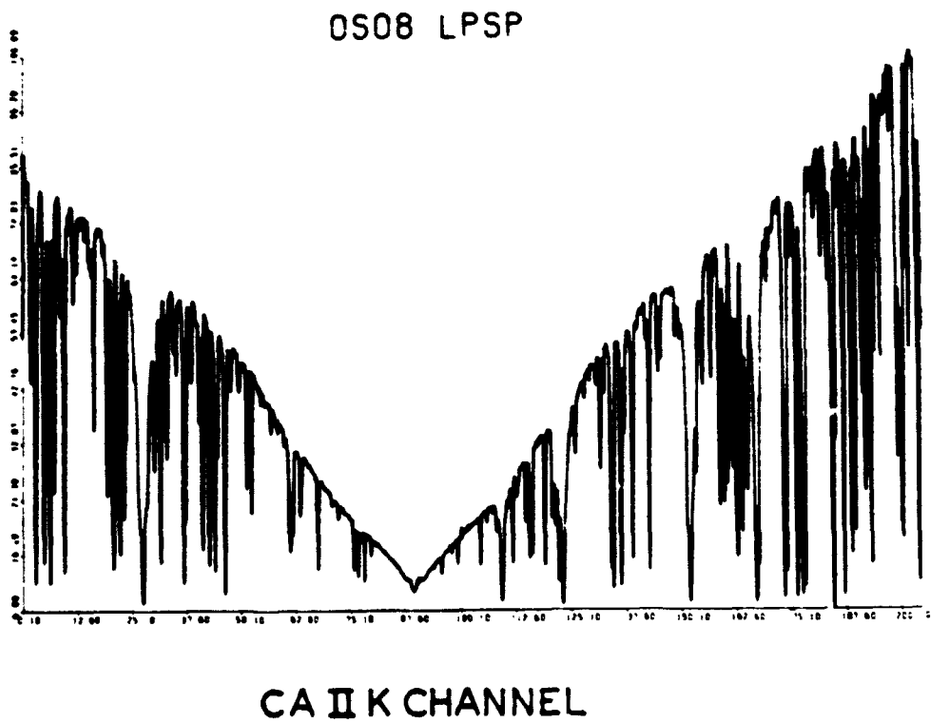

FIG. 2 Full range spectral scans in the Ca II K and Mg II *k* channels using a 1" × 3" entrance slit. The ordinates are counts per gate. Instrumental sensitivity variations over the wavelength range have been corrected for. Notice the reversed asymmetries in the Mg II *h* and *k* lines. It takes approximately 50 s to go from Mg II *k* to *h*, and the asymmetries reflect time variations in the line profiles over 50 s.

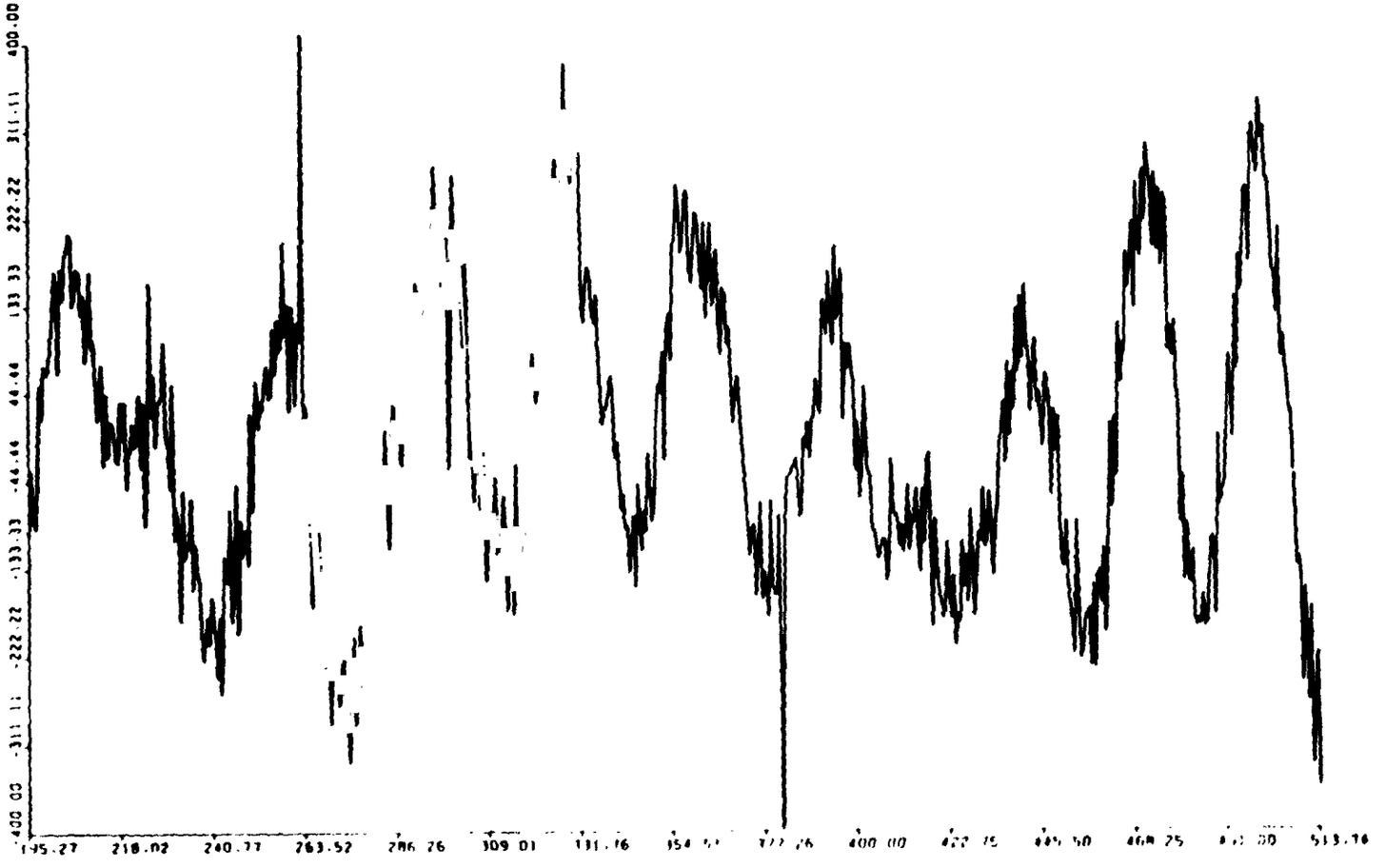

FIG. 3.—Relative velocity of the 391.52 nm photospheric line observed in the Ca II K channel. The 300 s oscillation is easily evidenced. The spacecraft Doppler shift has been removed. Spikes are identified as telemetry noise. The vertical scale is in m s^{-1}; the horizontal scale is in units of 10 s.

TABLE 2

RATIO OF INTENSITIES AT THE POSITIONS K_1, H_1, k_1, AND h_1 TO INTENSITIES MEASURED IN THE WINGS OF Ca II AND Mg II LINES IN THE *OSO 8* CHANNELS

Channel	Ratio	*OSO 8*	Utrecht Atlas (Minnaert *et al.* 1940)	Air Force Atlas (Beckers *et al.* 1976)	Kohl and Parkinson (1976)*
Ca II H.....	$I(395.18)/I(H_1)$	0.084	0.085	...	
	$I(398.13)/I(H_1)$	0.077	0.090	...	
Ca II K.....	$I(391.47)/I(K_1)$	0.078	0.088	0.087	...
	$I(394.85)/I(K_1)$	0.083	0.096	0.095	...
Mg II *h*.....	$I(h_1r)/I(277.73)$	0.079	...	...	0.048
	$I(h_1r)/I(282.01)$	0.063	...	...	0.045
	$I(h_1v)/I(277.73)$	0.046	...	...	0.028†
	$I(h_1v)/I(282.01)$	0.037	...	...	0.025†
Mg II *k*.....	$I(k_1r)/I(277.73)$	0.048	...	...	0.048
	$I(h_1v)/I(277.73)$	0.03	...	...	0.028†

NOTE.—The results are compared with the same ratios evaluated from Solar Atlases or available published data. *r* and *v* referred to the red and the blue part of the lines.

* We are indebted to Dr. J. Kohl for providing original records of his spectra.

† These values are probably uncertain due to the difficulty of measuring the solar intensity at k_1.

0.0409 ± 0.0022 and 0.0434 ± 0.0011 for the same ratios. Our results are intermediate between these two, confirming the very good performance of the Ca II channels.

For Mg II we have used the spectrum of Kohl and Parkinson for comparison. Excellent agreement is obtained in the *k* channel, our spectra indicating nearly exactly the same amount of scattered light as in the comparison spectrum. The agreement is, however, poor in the case of the *h* channel. Both the *h* and *k* lines can be observed in this channel together with the reference wavelength at 277.73 nm, allowing direct comparison between the two channels. As a result, we notice that the *h* channel has a much higher level of scattered light. This might be the result of degraded spectral resolution, due to a defective adjustment of the common coma and astigmatism corrector used in the Mg II channels whose delicate adjustment was optimized for the *k* channel.

For the Lα and Lβ channels we have made computations using the instrumental profiles, determined by ray tracing techniques, and the expected properties of the baffling inside the instrument; and we find that the level of scattered light is approximately 3% of the maximum flux in both channels.

Dark-current measurements were performed systematically each orbit during the first year and every 2 or 3 days in the second year. The dark current was found to be stable, with nearly no change during 18 months. The values are respectively 1.3, 1.1, and 0.1 counts s^{-1} for Mg II, Lα, and Lβ, respectively.

The calcium channel dark current was typically 200 counts s^{-1}. This comparatively bad performance is due to a leak in the enclosure system (skin).

e) Photometric Standardization

Photometric sensitivities have been measured regularly in orbit relatively to their values at launch. Such measurements are made every day or two with the 1" × 10" entrance slit at disk center quiet Sun, in the high spectral resolution mode for Ca II and Mg II and low resolution mode for Lα and Lβ. The number of counts at certain standard wavelengths (see below) measures the relative efficiency, whose variation as a function of time is shown in Figure 4.

The interpretation of these curves may be of interest to those who plan to utilize similar instruments in space. The telescope mirrors, the collimator, the grating, and all surfaces in the Lα, Lβ, and Mg II channels were coated at the Goddard Space Flight Center, with Al–LiF (Bradford *et al.* 1969). Elaborate precautions were taken in the storing and handling of optics throughout the mounting and calibration of the instrument. In fact, a special 300 square meter facility was built with air cleanliness and with temperature carefully controlled and humidity always kept below 30%. (Salvetat 1975). A loss of sensitivity such as the one reported here is very unlikely due to a contamination in the instrument before the launch and should rather be regarded as caused by the outgassing of the spacecraft and the instrument once placed in the space vacuum. In that case, the greater the number of reflections, the larger the degradation. The presence of steps which appear at nearly the same time on all the curves of Figure 4 is probably the signature of sudden outgassing periods. The significant differences noticeable between the individual curves, however, are indicative of causes of degradation proper to each channel, affecting either the mirrors, the filters, or the detectors.

The two Lyman channels show nearly the same behavior, with the larger loss at Lα attributed to the larger number of reflections in this channel (seven at Lα versus five at Lβ). At day 540, i.e., 18 months after launch, the sensitivity at Lα and Lβ was 10^{-3} and 5.10^{-3}, respectively, of the value at launch. Assuming that each reflection is affected equally by the contamination (which is certainly a crude approximation), these numbers indicate that each reflection has reached 35% at Lα and 37% at Lβ of its value at

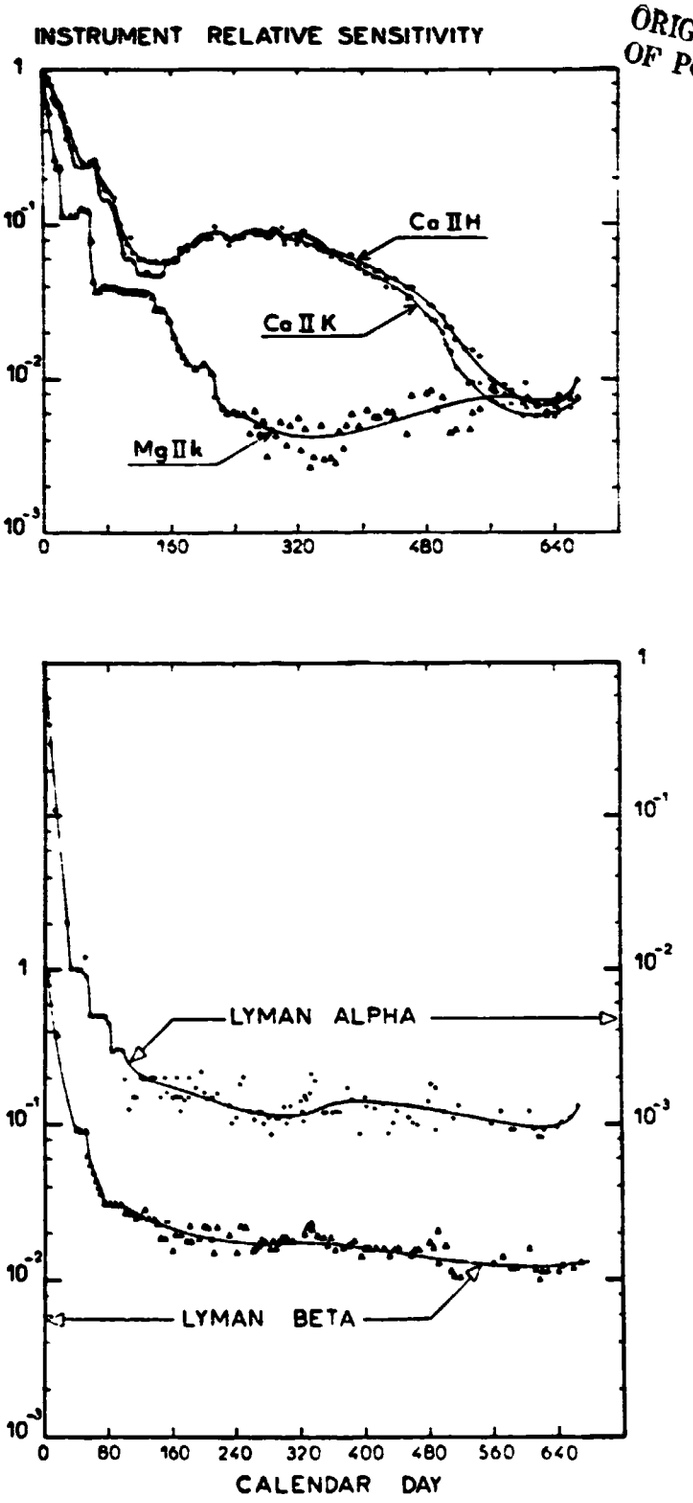

FIG. 4 Variations of the instrument sensitivity relative to its value at launch. Time is in days after launch.

day zero. Such results are not particularly dramatic when compared with the photometric behavior of other solar space instruments (Huber *et al.* 1973).

However, the combined effect of outgassing and the baking of the secondary mirror surface by a flux of more than 18 "solar constants" is likely to be responsible in a large proportion for the sensitivity loss. A simulation made a few weeks prior to launch at NASA on Al+LiF coated samples illuminated by 17 "solar constants" and placed in a normally outgassing environment showed a decay in efficiency from 63% to 58% and from 67% to 35% at Lα and Lβ, respectively, only 52 hours after pumpdown.

Obvious solutions, such as closing a shutter in front of the telescope during the first orbits when outgassing is high, were unfortunately not possible and would have delayed the launch several months.

Assuming, arbitrarily, that the secondary mirror is responsible for a loss of a factor 10 at both Lα and Lβ, each surface would have reached an efficiency of 46% of its value at launch, which is more or less normal.

Totally unexpected and more striking is the behavior of the Mg and Ca channels. Although of yet unknown origin, outgassing might also be responsible for the degradation observed in these channels, at least until day 160 when the sensitivity reaches 1/40 and 1/20, respectively, of the value at launch. This corresponds to an average loss per reflection of 48% and 55%. After day 160 the sensitivity in the two Ca channels rises again. At the same time a faster decay is observed in the Mg channels. This peculiar behavior is attributed to interference phenomena, probably complementary, in Ca and Mg within thin films of contaminant(s) deposited on any one of the optical surfaces. Deteriorations of the interference filters which are used in all these channels may also contribute. In the case of the Mg channel it is also very likely that the detector itself is responsible for the loss of sensitivity. This is apparently not the case for the two Ca channels since their sensitivity follows nearly the same variation with time, which more likely reflects a variation in the optics used in common.

The overall loss of sensitivity compromised certain aspects of the observing program. However, the versatility of the instrument made it possible to obtain scientific data of high quality and value throughout the mission.

f) Absolute Calibration

The calcium channels were calibrated by comparison with the data of Linsky (1970) and Livingston and White (1978) which represent average quiet Sun conditions. The absolute intensity at our standard wavelengths H_{1v} and K_{1v} were taken as 0.0751 and 0.0687, respectively, in units of the continuum intensity at 400 nm.

For the magnesium channels we attempted to improve Bonnet's 1967 results (Bonnet 1968) and designed a high spectral resolution instrument calibrated against a blackbody constructed by R. Peyturaux at the Institut d'Astrophysique de Paris. This instrument was launched twice on the LASP rockets number 21029 on 1975 July 28, and 21030 on 1976 February 18, but because of malfunctions in the electronics it did not give reliable results. We prefer therefore to rely on other recent measurements—e.g., those of Kohl and Parkinson (1976). The absolute intensity at the standard wavelengths h_{1v} and k_{2v} were taken as 8 and 6×10^{-12} ergs cm^{-2} s^{-1} sr^{-1} cm^{-1}, respectively.

For the Lyman channels we also used the above rocket program to carry packages consisting of ⅛ m Ebert-Fastie spectrometers, measuring the integrated solar disk to calibrate the LASP and LPSP instruments separately. Only the second flight yielded good calibration data. The results are given in Table 3 and are compared there with other measurements. The LPSP values are somewhat high; however, they are in the direction suggested by geophysicists (Levasseur *et al.* 1977). To use these integrated intensities in Lα and *Lβ*, we used quiet Sun average profiles computed for the whole disk (Fig. 5). We have taken into account the center-to-limb variation in an approximate way that will ultimately be improved upon by means of entire Sun raster-generated profiles (i.e., profiles constructed from spectroheliograms), when these become available from the data tapes. The absolute flux at the standard wavelength (core of the line) used to monitor the Lα relative sensitivity was taken to be 3×10^{10} photons cm^{-2} s^{-1} nm^{-1}.

IV. REAL TIME OPERATION AND PROBLEMS

The various modes of operation of the instrument have been described in Paper I. Here we discuss the "real-time" operation mode which allowed one, for

TABLE 3

INTEGRATED SOLAR FLUX MEASUREMENTS OBTAINED WITH CALIBRATION ROCKETS AT Lα AND Lβ

CALIBRATED FLUX	CALIBRATION ROCKETS			*OSO 5*†	AE-C‡
	1975 July 28 LASP*	1976 Feb 18 LPSP	1976 Feb 18 LASP*	1975 Aug 8	1975 Apr. 11
F(10.7 cm) (10^{-22} W m^{-2} Hz^{-1})	75.5	70.1	70.1	70	
F(Lα) (ergs cm^{-2} s^{-1})	4.02	5.46 ± 20%	4.05 ± 20%	4.25	none
F(Lβ) (ergs cm^{-2} s^{-1})	none	0.078 ± 20%	none	none	0.050

* Rottman 1977.

† Vidal-Madjar 1977.

‡ Hinteregger 1976.

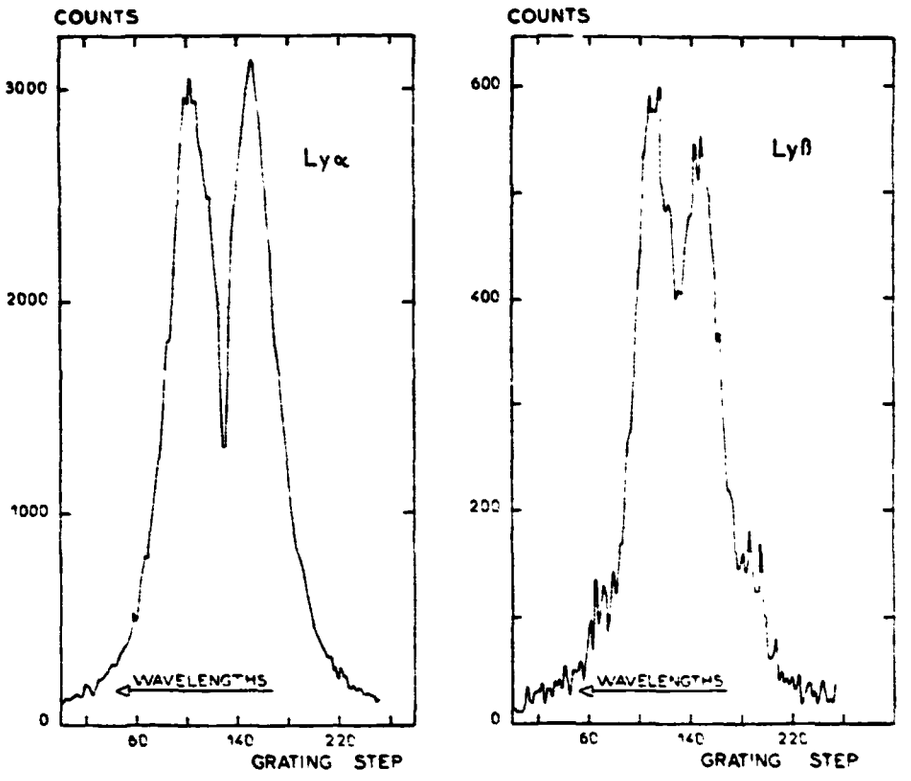

FIG. 5.—Full Sun average Lα and Lß profiles. Wavelengths increase to the left. The conversion into λ units can be made using the values of the last column of Table 1.

the first time, to point from an orbiting observatory with an absolute accuracy of nearly 1". The LPSP and LASP instruments were both operated from LASP (Boulder, Colorado) with "resident" LPSP scientists and guest investigators involved in the daily operations. Target selection alternated daily between LPSP and LASP until 1976 April and then weekly. For a more complete description of the operations command generation and quick-look facilities, see Jouchoux and Hansen (1978).

a) Pointing System Problems

The pointing system of the "sail" section of *OSO 8* uses either one of two Sun sensors (SEAS), designed by Hughes Aircraft Company, mounted on each instrument. These devices coalign the SEAS pointing axis with the optical axis of the associated telescope. This corrects for drifts of the optical axis with respect to the mechanical structure of the instruments.

Because of an electronic problem, the SEAS on the LPSP instrument failed after 56 days in orbit and all subsequent operations made use of the other SEAS. Consequently thermal and other drifts between the LPSP axis and the LASP axis had to be known. To determine these, we measure relative positions ($\pm X$, $\pm Y$) of the solar limb (in the X-Y frame of the satellite) during one orbit using images from the internal raster mode. We corrected for these drifts by programming the secondary mirror when it was necessary to stay within 1" of the target.

Variations in the SEAS scale factor and zero point (Sun-center line of sight) proved to be more troublesome. A weekly determination of the absolute four positions of the solar limb in the X-Y frame of the satellite was necessary. Using such data, from spacecraft and internal rasters, an extrapolated scale and zero point could be found for the particular day of observation. This proved to be successful, and we were able to position targets at the very center of our field of view, often without the need for corrections. Finally, the repeatability of the pointing system at the limb was found to be within 1" or 2", but with occasional jumps of 5".

b) Target Acquisition

Nearly 80% of the orbits under LPSP control were dedicated to studies of selected targets, often as small as a few seconds of arc. This mode of observation from an unmanned observatory involves a fairly complex procedure which requires considerable care and dispatch from the observer. We illustrate this in Figure 6 and describe the acquisition of the core of a sunspot.

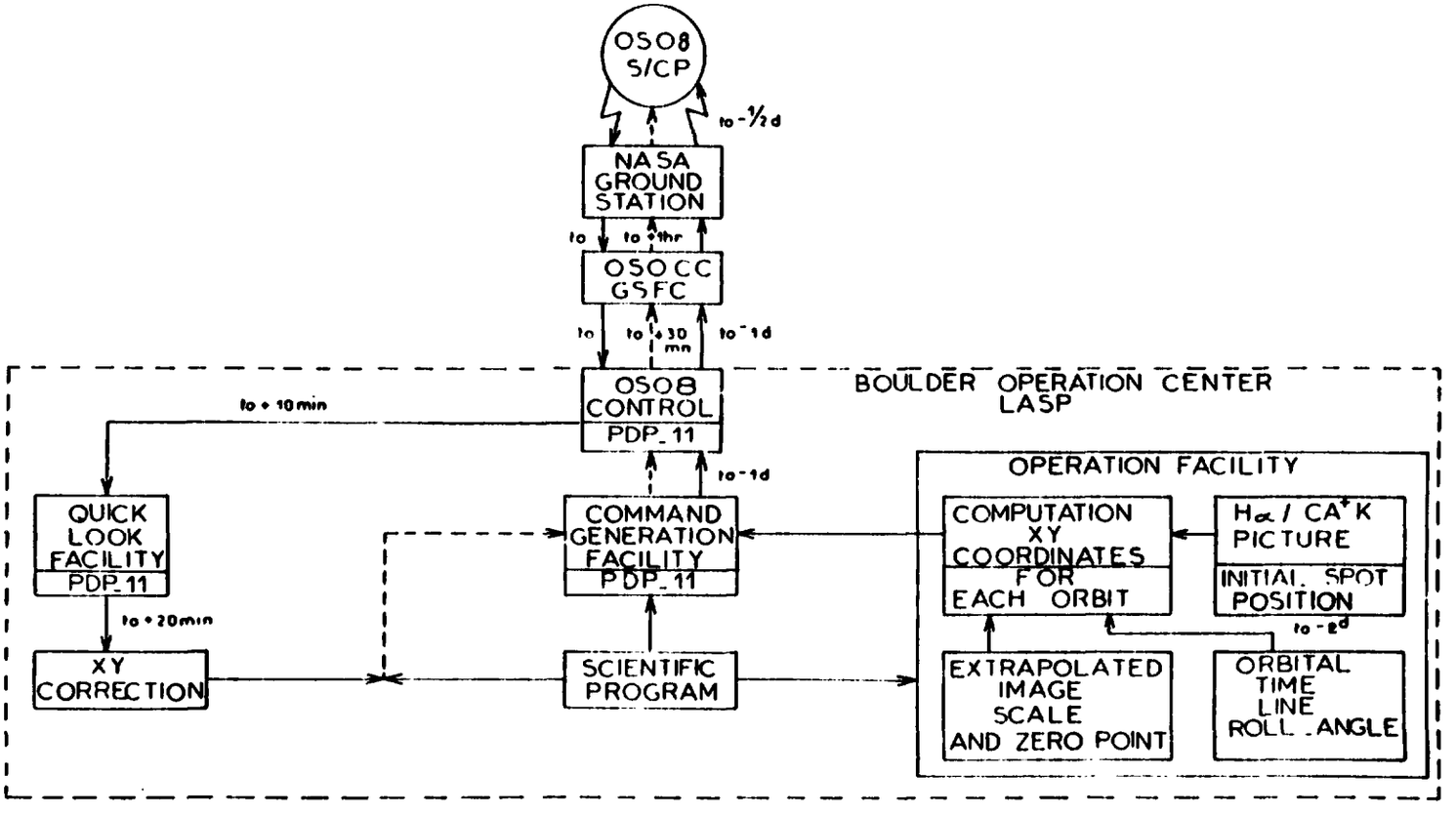

FIG. 6. - Block diagram showing the circuitry of telemetry and telecommand data between Boulder and NASA and illustrating "real-time" acquisition of a solar target (t_0 is the execution time).

As soon as a spot is visible on either a Hα picture (taken daily by NOAA/NBS in Boulder) or the Ca II K picture transmitted by telephone from Sacramento Peak Observatory, we determine its Stonyhurst coordinates for the time of the photograph. These coordinates are then transformed and oriented into the satellite spin frame of reference for the projected time of observation. Finally the scale distortion of the pointing system is corrected for. The instrument commands and associated pointing commands are generated and sent to NASA on the day before the date of observation. During the day of observation an internal image of the spot, 64″ × 64″, is executed in the far wings of Ca II or Mg II during a real-time pass of the satellite over a ground station. These real-time data are received by telephone via GSFC on the PDP 11 computer at Boulder, where they are subsequently decoded and displayed as an image. Any corrections to the position of the spot are determined from the image and are sent by telephone to NASA who uplink the corrections to the spacecraft. The time delay between the real-time pass and execution of pointing corrections can be as short as the time interval between two successive ground station passes, namely, 1½ hours. This apparently straightforward operation is made more difficult because of the need to extrapolate the scale distortion parameters and to correct for the drifts of the line of sight already mentioned.

c) Lα *Modulation*

The Lα signal was discovered to be occasionally modulated with an amplitude which may reach 10% of the signal at precisely the rotation period of the spacecraft wheel except during the first 2 minutes after sunrise when sometimes a period distinctly shorter than the wheel period was found.

All attempts made to detect a similar phenomenon in the other channels have failed, suggesting that it is not caused by a pointing problem. Indeed we have sometimes observed oscillations in the pointing axis with periods equal to that of the wheel rotation and an amplitude of 0.5, but these affect all channels at the same time.

The phenomenon has to be taken into account when analyzing time series and profiles of the Lα line. As described in Paper I, the duration of every individual measurement is the product of 0.16 s gate time by a power of 2, and the most commonly used values are 10.24 s (64 grating steps) and 20.48 s (128 grating steps). The period of rotation of the wheel of the spacecraft varies from 10.7 to 9.5 s and for spectral scans with a time base equal to or larger than 10.24 s, the modulation induces a "beat" of period ranging from infinity to 131 s.

Figure 7 plots the raw data for the first moment of the wavelength of the line versus time. A strong 800 s period is evident. If the individual data points are corrected for the modulation with a period equal to that of the wheel and the first moment is recomputed, then the circles in Figure 7 show that the 800 s oscillation is suppressed.

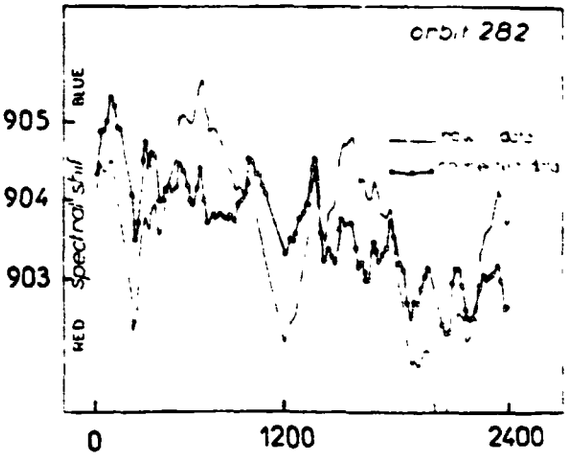

FIG. 7.—Variation with time of the position of the first moment of Lα. The solid line variation shows a strong oscillation of ~800 s period. Circles represent the same data after correcting the Lα profiles for the instrumental modulation: the 800 s oscillations have vanished. Abscissa is time (in seconds); ordinate is grating step number.

This proves without ambiguity that the phenomenon is purely instrumental and that the possibility of its solar origin, should be definitely disregarded.

V. PRELIMINARY RESULTS

Spacecraft (playback) data are sent by NASA to Boulder by telephone line and recorded there on magnetic tapes. Mass production tapes of this data are prepared by NASA and mailed to the Centre National d'Etudes Spatiales (CNES) (Toulouse, France), which is in charge of the processing and distribution of the final data tapes to the LPSP investigators and guest investigators. The results presented below have been obtained mostly from playback data at Boulder.

a) *Observational Program*

Table 4 presents a summary of the various types of observations that were programmed during the first 8363 orbits. No distinction is made in the table with regard to pointing control. Orbits with problems in either the instrument, the spacecraft, or the command system represent only 2% of the total.

The column headings in the table describe the modes of operation of the instrument while the rows indicate the scientific question or the solar feature under study.

Orbits labeled "Line Profiles" usually correspond to spectral scans ranging from 64 to 512 grating steps centered at either the six chromospheric lines or the O VI line at 103.2 nm. The "Others" columns indicate studies in either the wings of the Ca II and Mg II lines or the O V and Si III lines at 121.8 nm, 120.6 nm, respectively. Other lines such as O I, N I, etc., were observed in the Lβ channel by making use of the different grating orders. During these orbits the satellite was in the pointed mode.

TABLE 4

SCIENTIFIC PROGRAM OF THE FIRST 8363 ORBITS

PARAMETER	LINE PROFILES			SPECTROHELIOGRAMS			VELOCITY FIELDS AND OSCILLATIONS	TRANSIENTS	LARGE λ SCANS	GUEST OBSERVER ORBITS
	6 Lines	O VI 103.2	Others	6 Lines	O VI 103.2	Others				
Quiet Sun:										
Chromospheric network	554	194	...	465	80		310	257	254	463
Limb studies	483	180	25	208	126	95				
Active regions	583	175	31	276	209	7	132	138	30	249
Sunspots	455	107	8	120	184	1	20	56	2	117
Coronal holes	42	87	14	25	40	11	...	...	4	5
Prominences	63	23	3	33	20	1	...	...	...	25
Filaments	55	23	...	26	35	...	...	...	...	...
Full Sun images:										
R 128s	High resolution (20")			73	87	16	...	...	...	...
R 128f				13	2	3	...	...	...	...
R 64	Low resolution (40")			135	1	...	...	...	...	...
Photometric and pointing calibration	360	...	...	...	123	...	...	...	...	...
Instrumental tests and miscellaneous	...	...	...	...	421	...	...	...	...	...

NOTE.—Numbers represent full day orbits.

Under "Spectroheliograms" we classify orbits for which most of the time is spent rastering, using either the internal or the satellite raster mode. Morphology and long-term variability studies of solar features were of interest here.

During orbits labeled "Velocity Fields and Oscillations" we spent most of the time in the pointed mode studying rather small areas of the disk, not more than 64" × 1". Here, special spectral scans were made. For example, short-period waves ($T < 40$ s) were searched for by scanning rapidly through the line profiles using wavelength position separated by 16 grating steps.

Under "Transients" are grouped orbits observed with the fast, low-resolution satellite rasters. The short time constant of such modes allows one to observe rapidly propagating shocks and any other rapid phenomena.

"Large λ Scans" represent the full scanning capability of the grating and were performed either to study lines in the low orders of the Lβ channel or to standardize the Mg II and Ca II line cores with respect to their far wings.

For most orbits, sunset and sunrise experiments were performed in order to measure atmospheric extinction at various wavelengths of interest (see § Vg below).

"Chromospheric Network Studies" include not only morphology and time evolution but also line profiles for center-to-limb and cell-network comparisons. "Limb Studies" include orbits dedicated to the shape of the limb, spicules, and the vertical extension of the solar atmosphere in various lines.

"Photometric Calibration" has already been described in § III; for these orbits the satellite is pointed at disk center in a quiet region.

The last five rows of Table 4 include scientific as well as instrument or satellite calibration orbits. Also included are orbits devoted to eclipse observations, to studies of the geocoronal hydrogen line, and to the search for lines such as Fe XIII 121.64 nm and He II 102.5 nm.

b) Quiet Sun and Chromospheric Studies

Figure 8 (Plate 21) represents an example of our study of the network and the quiet Sun. Such internal raster images along with associated profiles will permit an intercomparison of cell and network properties.

Figure 9 compares profiles obtained at the center of a cell and in a network fragment. One can notice the strong variation in intensity, particularly in Mg II *k* and Lα, between the two regions. This is due partly to a decreasing line background contribution as well as differential temperature sensitivity. The asymmetry of Lα is always much less pronounced than in the case of Mg II *h* and *k*, presumably because of smaller velocity gradients at the Lα height of formation.

Figure 10 shows average quiet Sun profiles of Lα and Lβ taken with a 6" × 2' slit at disk center and near the limb ($\mu = 0.14$). Notice the two lines of O I at 130.48 and 130.59 nm in the wings of Lβ (observed in the 11th order). By the insertion into the light beam of a MgI$_2$ filter one can block out all photons below 115 nm and observe only the two O I lines. Differencing permits one to reconstruct the Lβ profile. The result of this procedure is shown on Figure 11. The remaining slight anomaly at grating step 180, might be due to the Hβ line of He II (102.57 nm). Center-to-limb measurements at the corresponding wavelength show appreciable limb brightening. Investigations are under way to confirm this observation.

The variation of the distance between peaks of the Lα and Lβ lines from center to limb is apparent together with the variation of the ratio of the peak to core intensities (see Table 5). The values in Table 5 at $\mu = 0.14$ are close to those calculated by Vernazza (1972).

One noticeable feature is the reversed intensity asymmetry between the Lα and Lβ shortward and longward peaks at the disk center. In Lα the shortward peak is generally higher than the longward peak while the reverse holds in Lβ. At the limb, both Lα and Lβ profiles become symmetrical. It is possible that this effect may not be intrinsic but is either an instrumental effect or the effect of unresolved lines at Lβ. The matter is under study.

To study the morphology of network fragments and their evolution in time, monochromatic images have been obtained simultaneously in the six lines alternately with broad-band images in O VI (103.2 nm) for a number of observing sequences (Fig. 12). Preliminary analysis of a 20 hr sequence shows that significant evolutionary changes can occur over a 12 hr period. The larger size K_{2v} fragments are easily identified in the Lα + Lβ (= H Lyman) and O VI images where they do not appear as extended as indicated by the ATM data (Reeves 1976). This is supported by an analysis of the Lα brightness distribution. Applying the method of Skumanich, Smythe, and Frazier (1975) to both the present *OSO 8* sequence and ATM data, one finds a fractional Lα network area of 37% and 41%, respectively. The ratio of mean network to mean cell brightness proved to be 1.9 and 2.1, respectively. For comparison the *OSO 8* Ca II distribution yielded a fractional area of 27% and brightness ratio of 1.3.

c) Quiet Chromospheric Oscillation and Transients

We have already mentioned in § IIIc (cf. Fig. 3) our successful detection of the 300 s oscillation of photospheric lines in the wings of Ca II H and K.

TABLE 5

CENTER-TO-LIMB COMPARISONS OF THE DISTANCE BETWEEN THE BLUE AND RED PEAKS AND OF THE RATIO BETWEEN THE AVERAGE PEAK INTENSITY AND THE CORE INTENSITY OF THE Lα AND Lβ LINES

LINE	SEPARATION OF PEAKS (nm)		I_{peak}/I_{core}	
	$\mu = 1.0$	$\mu = 0.14$	$\mu = 1.0$	$\mu = 0.14$
Lα	0.043	0.05	1.3 ± 50%	2.2
Lβ ..	0.027	0.031	1.4 ± 50%	1.5

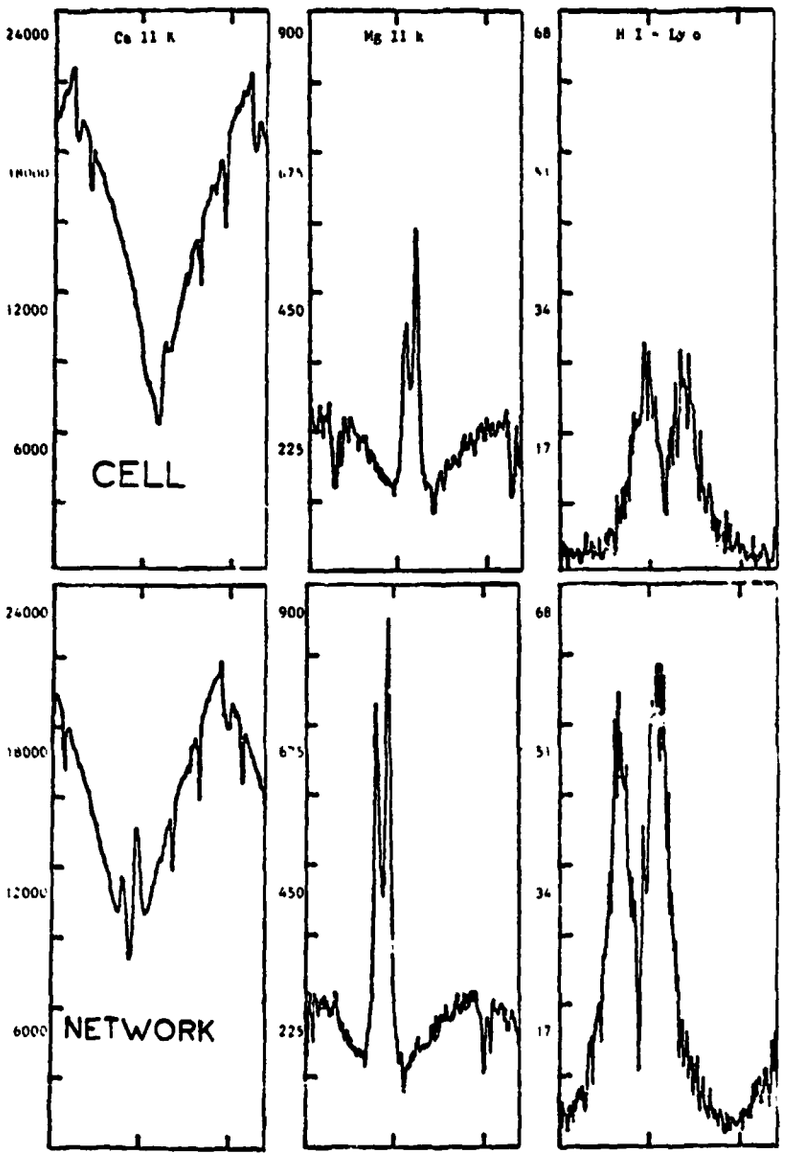

FIG. 9.– Comparison between simultaneous observations of Ca II K, Mg II *k*, and Lα profiles in the network and at the center of a supergranulation cell. The slit size is 1" × 10". Units are counts per counting gate.

The Mg II *k* and Ca II K lines (Fig. 13) show oscillations of ~200 s period. We parametrize the profile of Mg II *k* as a difference of two Gaussians:

$$I(\lambda) = E_1 \exp\left(\frac{\lambda - E_2}{E_3}\right)^2 \left[1 - A_1 \exp\left(\frac{-A_2}{A_3}\right)^2\right],$$

where E_1 and A_1 represent the intensities of the emission and absorption components of the profile, respectively, and E_2 and A_2 the average wavelength position (or "first moment of the wavelength") of the emission and absorption components. We should point out that no physical meaning is to be attached to this parametrization. The time behavior of these various parameters is shown on Figure 14.

The oscillation of the parameter E_2 or average emission position covers a range of ± 0.00186 nm or ± 2 km s^{-1}. For A_2 or average absorption position, this value is doubled. This clear difference might be interpreted as the amplification, with increasing height in the atmosphere, of a wave, if one assumes, as usual, that the core of Mg II *k* is formed at a higher altitude than the wings. The average "bluer" position of E_2 (emission) compared to A_2 (absorption) reflects the

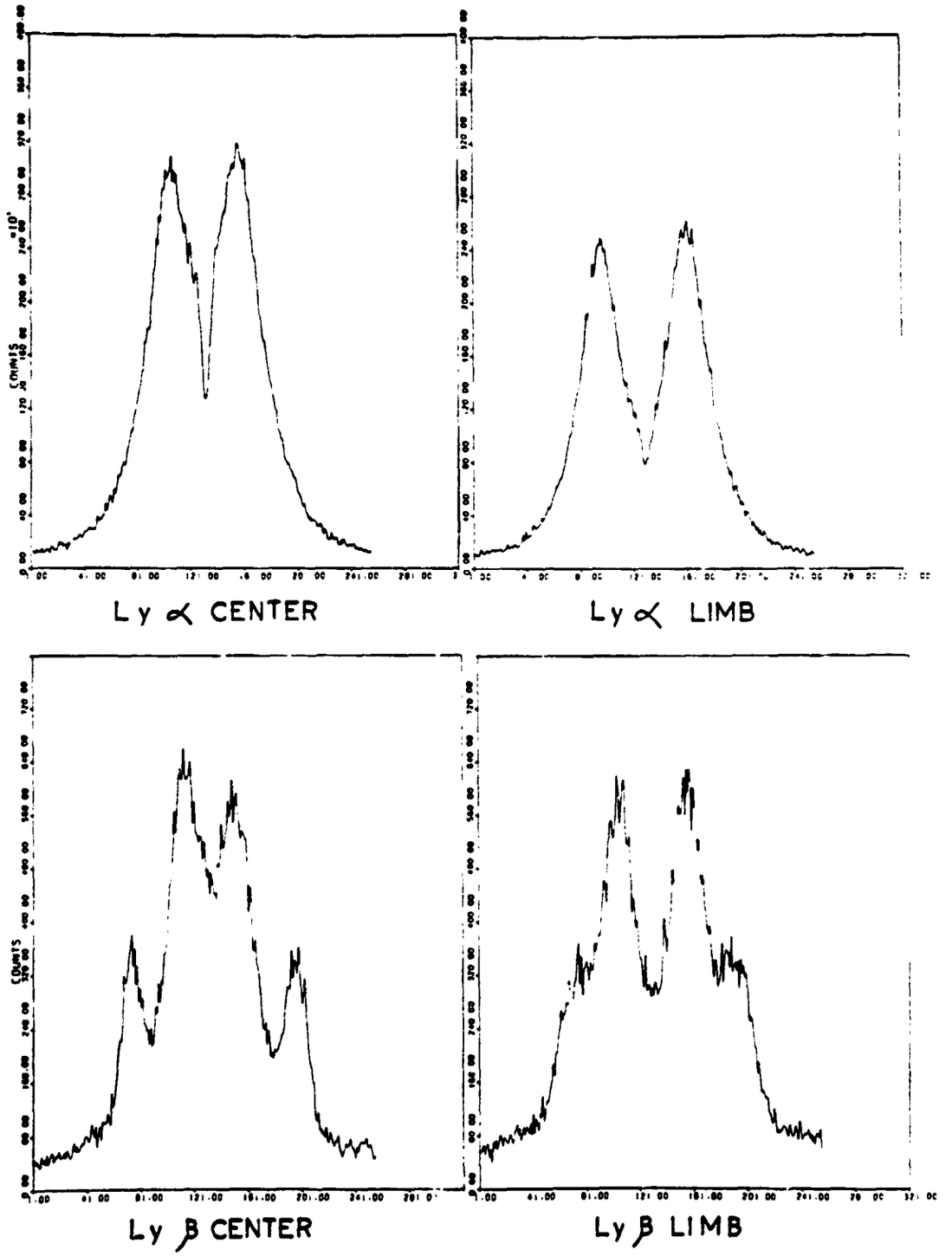

FIG. 10.– Lα and Lβ profiles at the center and at the limb of the Sun obtained with a 6" × 2' resolution. The two lines in the wings of Lβ are O I 130.48 nm and 130.59 nm appearing in the 11th order of diffraction. Wavelengths increase to the left. The abscissae are grating step numbers. For conversion in λ units, see Table 1.

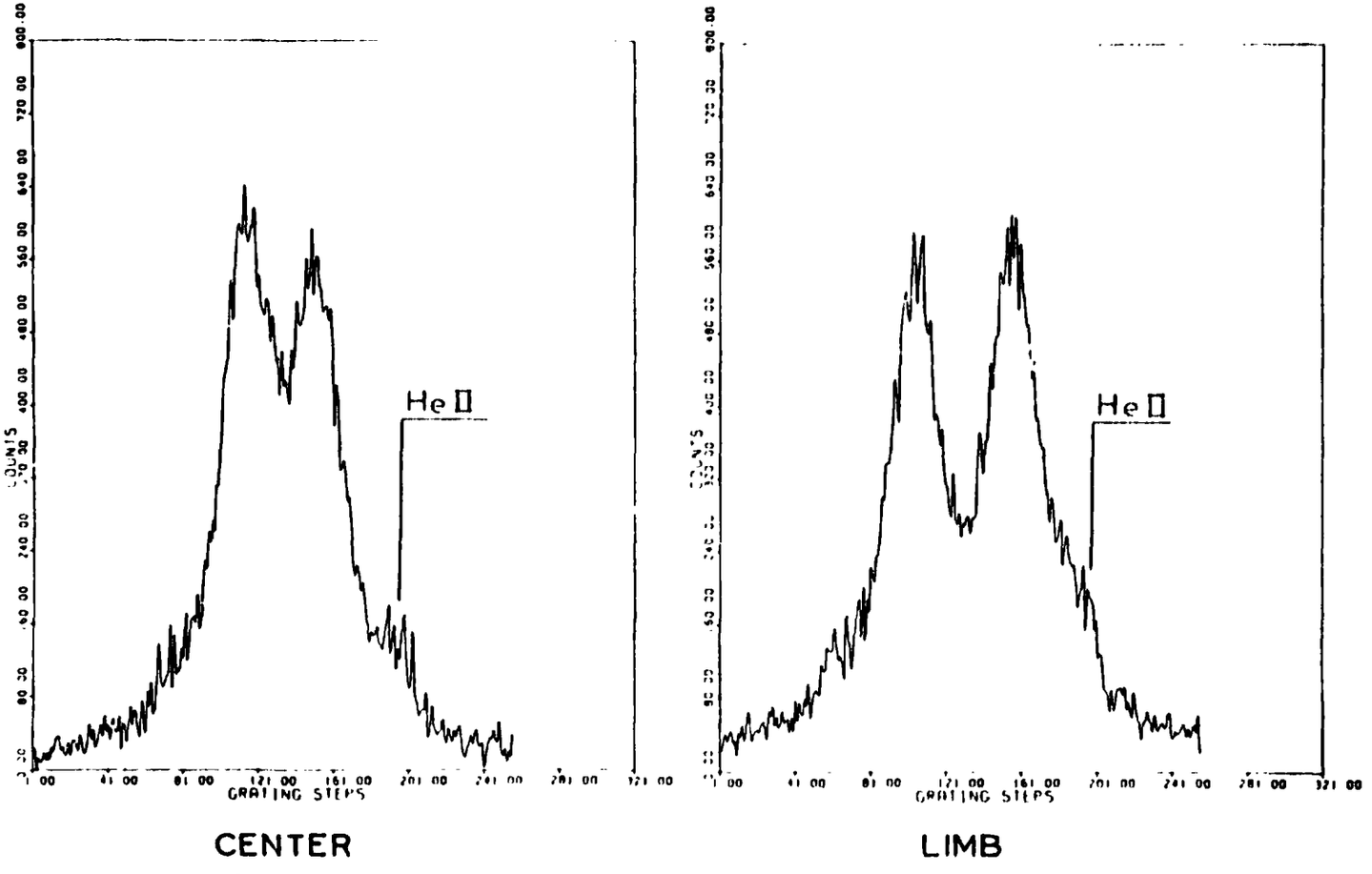

FIG. 11.– 1.β profiles after the subtraction of the O I lines made by inserting a MgF_2 filter in the beam. Wavelengths increase to the left. For conversion into λ units, see Table 1.

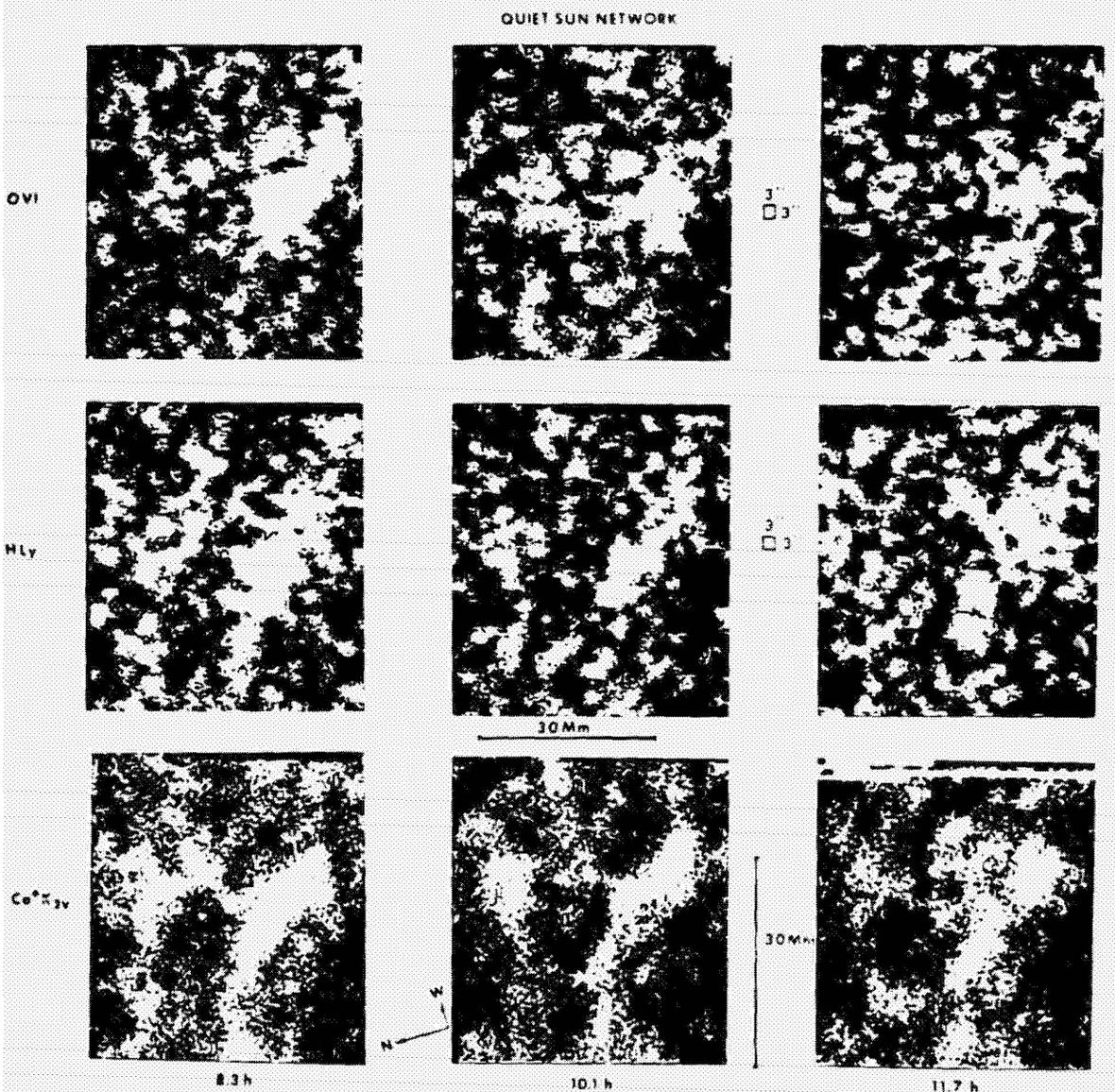

FIG. 12.—Evolution with time of network fragments, observed with 64″ × 64″ internal rasters in O VI, Lα, and Ca II lines

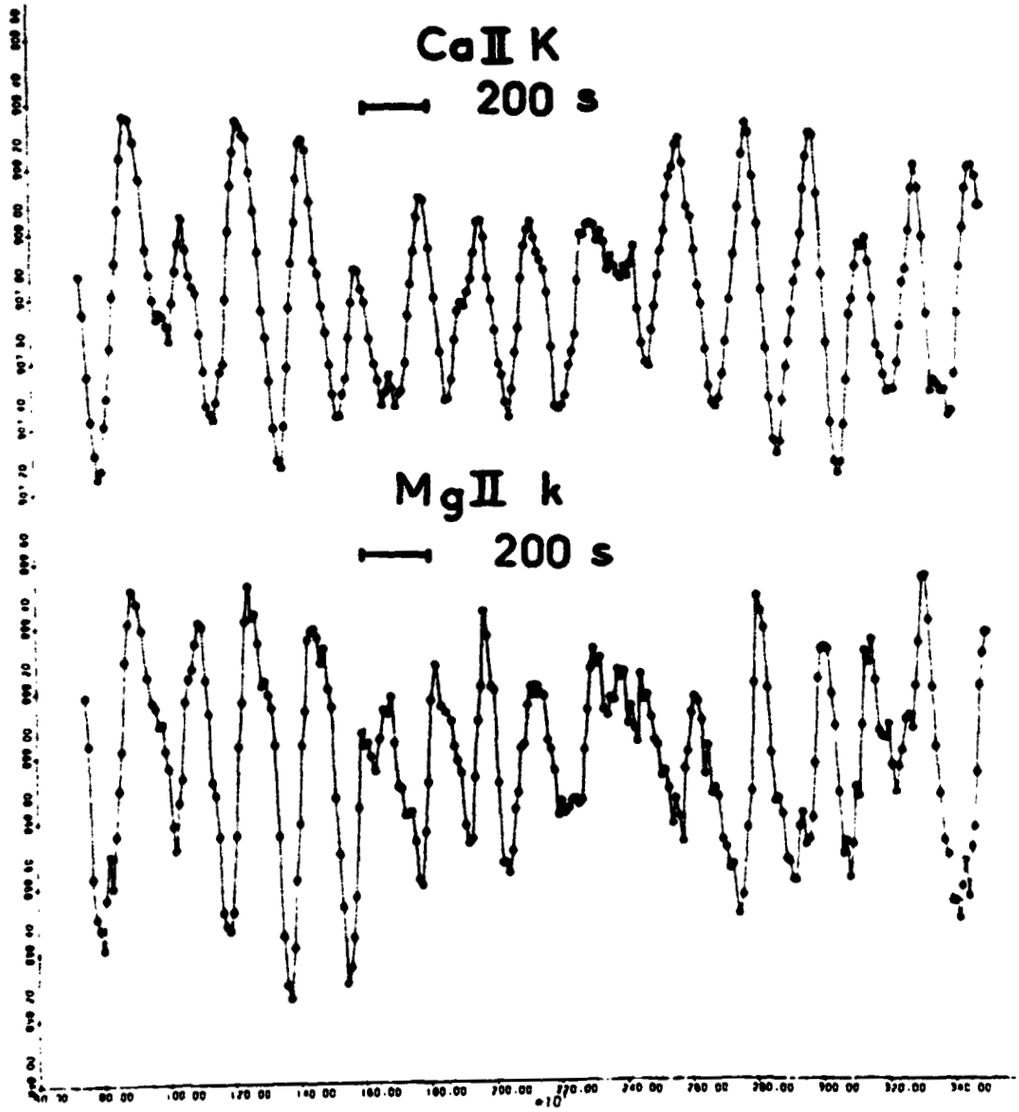

FIG. 13.—Oscillations of the center of symmetry of the Ca II (*upper curve*) and Mg II (*lower curve*) emission components. Horizontal units are multiples of 10 s.

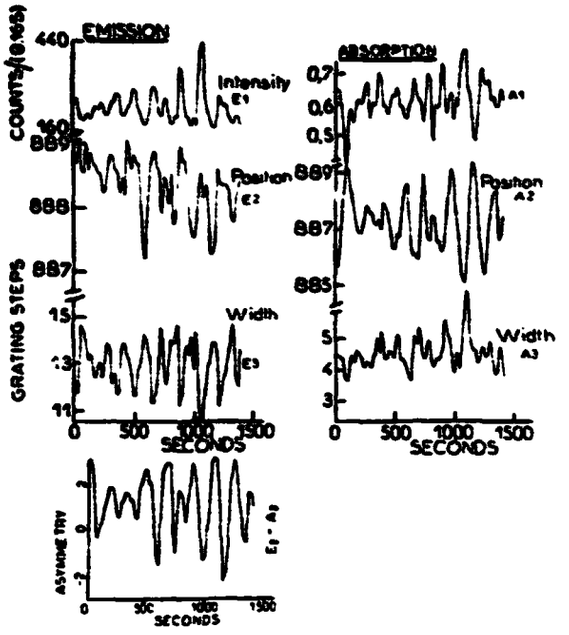

FIG. 14.—Time variations of the various parameters of the analytical function used to represent Mg II *k*. Observations are made at disk center.

fact that the average Mg II *k* profile in the Sun is asymmetric, with k_2v stronger than k_2r. This is illustrated also on Figure 15, where we see that the line shape varies from a strongly asymmetrical profile ($k_2v > k_2r$) to a nearly perfect symmetrical profile ($k_2v = k_2r$).

In Figure 16 we see the variation over 40 s of the Mg II and Ca II K profiles observed simultaneously.

The Mg II lines exhibit the same periods as the Ca II lines. We have a broad set of observations which contain wave trains lasting in general no longer than a few cycles with periods ranging from 250 s down to 130 s. A search for shorter periods was undertaken, in particular by guest observers, but no clear evidence has yet emerged from these investigations at this early stage of data analysis.

The good results obtained in Mg II encouraged us to search for a possible oscillation of Lα. The large contribution function of the line, which tends to smooth out the effects of any wave on the profile, together with the low photon count in this channel made this observation a particularly difficult one. We first tried to detect intensity fluctuations by integrating the number of photons over ±0.025 nm from line center. We did not find any obvious evidence of variations, other than random, a result in accord with the previous attempts made from studies of *Skylab* results (Vernazza *et al.* 1975).

To overcome the low photon statistics problem, we tried to correlate the shape of Lα with that of Mg II *k* profiles. We definitely see evidence for a correlation, the bluer *k* profiles corresponding to redshifted Lα profiles. The amplitude of the shift is of the order of 2 grating steps (3 km s^{-1}). More work is under way, but we may state at this stage that the oscillations seen in Mg II *k* have an influence higher in the chromosphere, at the altitudes where Lα is formed (Artzner *et al.* 1978).

Several orbits were devoted to the study of oscillations in the O I, Si III, and O VI lines, but have not yet been analyzed. Transient and short time phenomena have been observed. Numerous tachograms dedicated

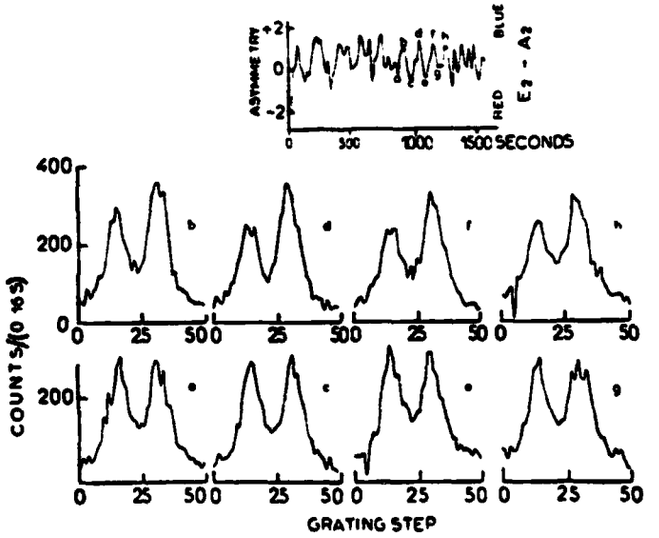

FIG. 15.—Mg II *k* profiles observed at the maxima and minima of the oscillations of the line center of gravity, showing obvious occurrence of asymmetrical blue peaked profiles at maxima and symmetrical or slightly asymmetrical red peaked profiles at minima. Wavelengths increase to the left.

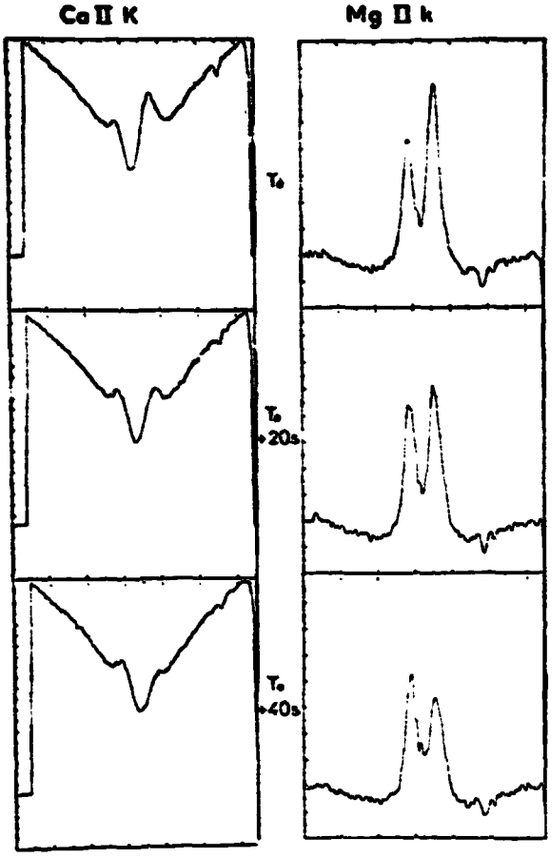

FIG. 16.—Observation of a temporal event, simultaneously in Ca II K and Mg II *k* as it propagates through the line profile. Wavelengths increase to the left. Vertical scale is in relative units.

to the investigation of transients and other flows in the chromosphere have been programmed and are under study.

d) Study of Sunspots and Active Regions

Sequences of high-resolution images and spectra taken 1" apart show the evolution of spot morphology and profiles in space and time. Umbral flashes have been observed as well as oscillations. Nearly simultaneous observations of lines from the photosphere to the transition region should allow us to study the vertical structure of spots.

A preliminary analysis of spacecraft rasters made with the 1" × 10" entrance slit, and LPSP internal rasters made with the 1" × 1", 1" × 3" entrance slit, show that regions of strongly enhanced O VI 103.2 nm emission very often tend to be distributed other than directly above sunspot umbrae. This is the case both for some unipolar single spots as well as multipolar spot groups. However, we do find circumstances when single spots show the transition region "plume" directly over the spot as reported by Foukal *et al.* (1974).

Figure 17 shows this phenomenon, where isophotes are represented in photospheric light, Lα, and O VI.

We have also found examples of steplike changes in the distribution of the enhanced O VI emission (Fig. 18). If we assume that the enhanced O VI emission is associated with a specific magnetic field connectivity, then our results imply "step" changes in field connectivity. The general O VI emission in the active region was found to be approximately 10 times brighter, with strongly enhanced features approximately 100 times brighter, than the average quiet Sun. Simultaneous observations in Lα, Lβ, Mg II, and Ca II also show the general active-region enhanced emission as well as strongly enhanced features. The Lα and Lβ features are identical, but show systematic horizontal displacement with respect to the Ca II and Mg II emission features. Little or no correlation is found with the O VI structures. With regard to the profiles of the resonance lines, the self-reversal is weak or absent above regions as shown on Figure 19. Presumably the line-forming region has reduced opacity.

e) Studies of Prominences

Temporal evolution of, and velocity field in, prominences were studied with consecutive monochromatic spacecraft rasters. Figure 20 shows, at the top, Ca II images at wavelengths ranging from −0.012 nm to +0.03 nm from line center. The main loop is clearly visible only at line center; this is confirmed by spectra constructed from the different monochromatic images of the prominence which show a single emission peak with a FWHM of 0.020 nm which is typical of quiescent prominences (Engvold and Livingston 1971). This is consistent with a mean turbulent velocity of 9 km s^{-1} and a temperature T_e = 8500 K. At the bottom of Figure 20 are two simultaneous Lα and Lβ images.

Several observations were made to study the thermal structure and evolution of active and eruptive prominences. Figure 21 shows an internal raster performed with a slit of 1" × 1" above active region McMath No. 14127.

The first three simultaneous images in Lα, Lβ, and Ca II K_2V show a loop system with a rather faint contrast in K_2V as compared to the plage at the limb, but a higher contrast in Lα (and Lβ). The next three images are separated by 11 minutes (raster repetition rate) and are made in O VI 103.2 nm. They trace out the high-temperature evolution of the region (O VI being formed at approximately 350,000 K). The first O VI image shows a faint high loop, the second some residual brightness around the foot of the loop, and the third an important enhancement at this same point. Then within 20 min the loop disappeared, as can be seen on the next three images in Lα, Lβ, and Ca II K.

Many images and spectra have been obtained that will allow the study of temperature, density, and velocity variations during loop evolution (Vial *et al.* 1978).

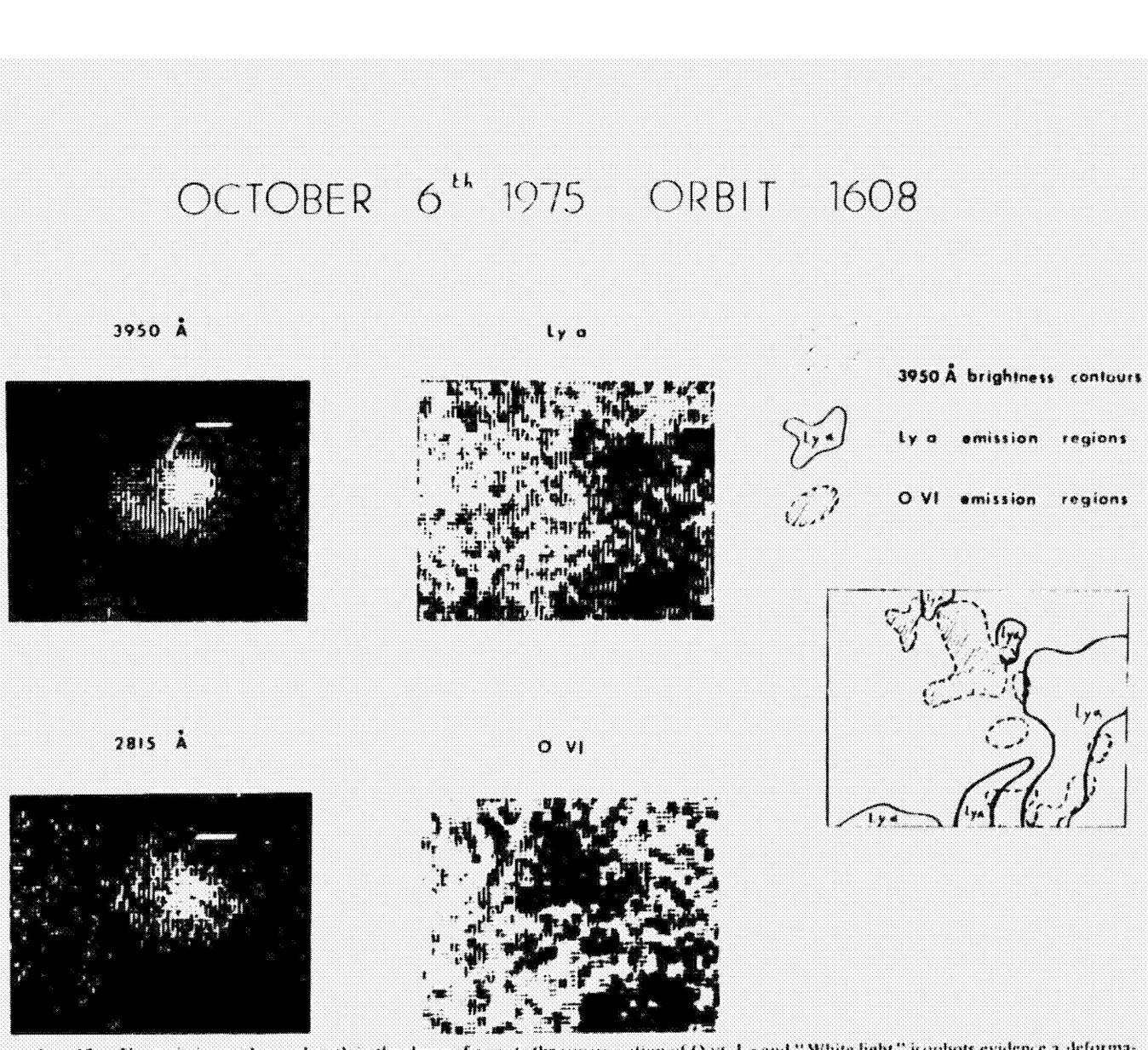

FIG. 17.—The variation with wavelength in the shape of a spot; the superposition of O VI, Ly α and "White light" isophots evidence a deformation with height in the solar atmosphere.

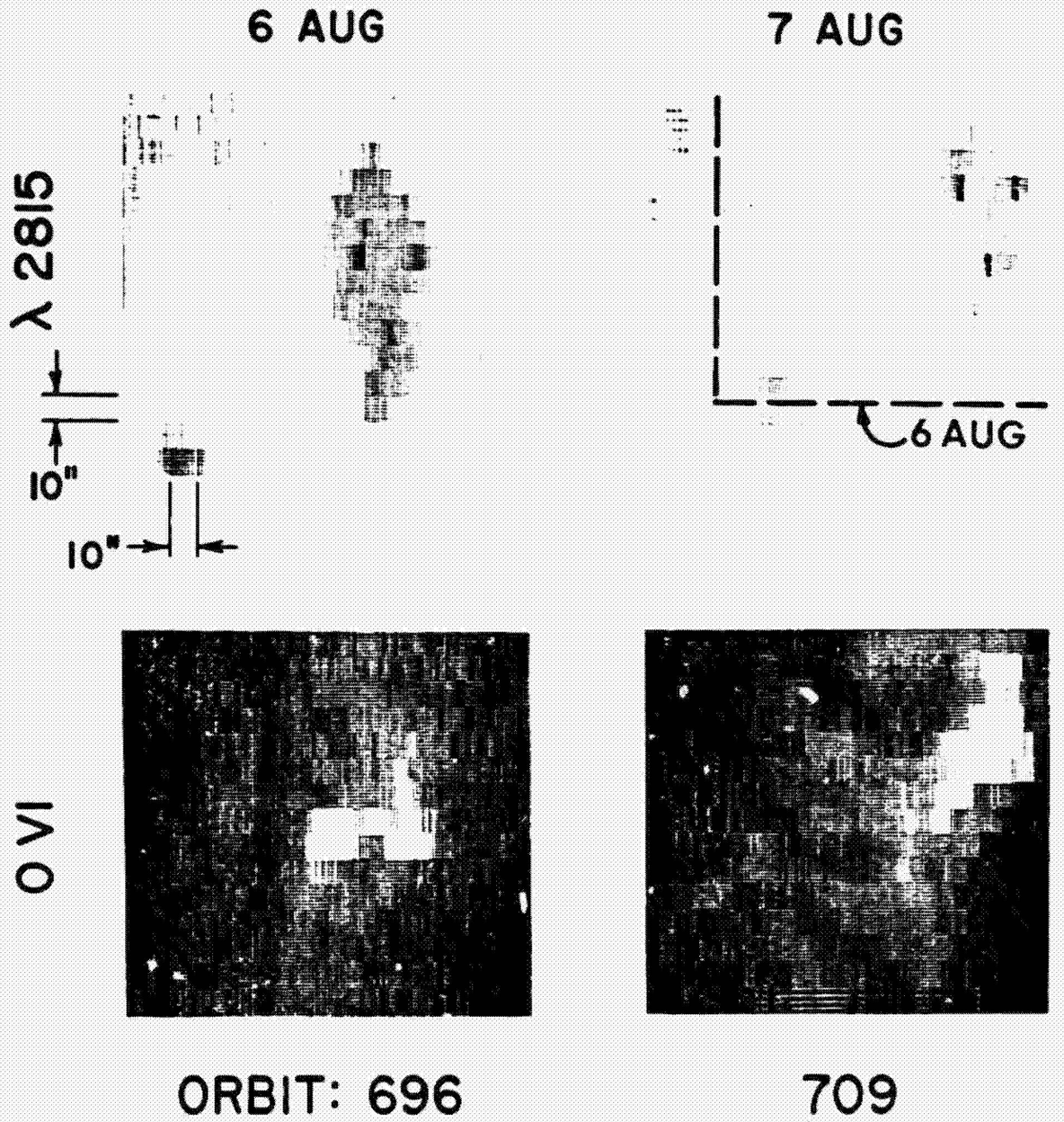

FIG. 18.—Illustration of step changes in field connectivity of spot evolution. The two upper pictures are satellite rasters made in the wings of Mg II k. The two lower pictures are taken simultaneously in O VI. The evolution of the sunspot group is continuous when observed in white light and discontinuous in O VI.

Figure 22 represents observations of an active region at the limb on 1975 July 7. The slit was parallel to the limb and probably intersected it slightly, as indicated by the presence of scattered light in the wings of the Ca II profiles. On the left portion of Figure 22, full and dotted lines correspond to profiles taken at positions separated by only 1". The emission maxima in Ca II and Mg II are displaced shortward with an amplitude corresponding to about 20 and 15 km s^{-1}, respectively. These maxima may in fact correspond to K_2v and k_2v, while K_2r and k_2r are barely visible and show up only as asymmetries in the line profile. Lα is not displaced and shows the geocoronal reversal with no apparent self-reversal. The distance between its emission peaks is only 0.022 nm, leading to an optical depth of only 500 at line center. On the right panel of Figure 22, solid and dotted lines show temporal variations for a 22 min interval. Orbital Doppler effects have not been corrected for on the figure; but if they are corrected for, a shift to the longward is still found for Ca II and Mg II with an amplitude of 5 km s^{-1}. Moreover, Ca II and Mg II lines have essentially the same intensity while Lα has increased by a factor of 2.

f) *Chromosphere-Corona Transition Lines*

The two lines Si III 120.65 nm ($3s\,^1S$–$3p\,^1P^o$) and O VI 103.19 nm ($2s\,^2P$–$2p\,^2P^o$) are formed in the chromosphere-corona transition region at 40,000 K and 350,000 K, respectively (Jordan 1969). They are observed with the LPSP instrument with a spectral resolution of 0.002 and 0.006 nm, respectively.

The shape of transition-region line profiles may indicate whether there is any propagation of either acoustic or magnetohydrodynamic waves (McWhirter 1977). The presence of such waves may be symptomatic of coronal heating mechanisms.

Figure 23 shows an average (single orbit) Si III profile at the center of the disk (quiet Sun) observed with a resolution of 1" × 40". The FWHM is 0.015 nm and, if we assume that the line is optically thin, the rms (line-of-sight) nonthermal velocity is 22 km s^{-1}. This value is 4 km s^{-1} higher than the values obtained by Nicolas *et al.* (1976) for the Si III lines at 128.9 and 189.2 nm.

Quiet and active Sun profiles of the O VI line at the center of the disk are given on Figures 24*a* and 24*b*. This line is optically thin, and the FWHM is 0.021 nm nearly identical for both quiet and active Sun; the rms line-of-sight nonthermal velocity is 30 km s^{-1}. A departure from a purely Gaussian profile can be noticed in both profiles. The line appears asymmetric and may indicate the effect of a velocity structure in the region of formation of the line.

Figure 24*c* shows a quiet limb O VI profile, averaged over several positions above the limb (+2" + 6"). The FWHM is now 0.026 nm, equivalent to a rms line-of-sight nonthermal velocity of 38 km s^{-1}. This is larger by 11 km s^{-1} than the value previously quoted by Moe and Nicolas (1977).

The chromosphere and transition region height distribution is shown on Figure 25 as derived from internal raster scans simultaneously in the wing of Mg II h, Mg II h_3, O V 121.8 nm, and N I 119.95 nm.

As is apparent from the figure, the h_3 chromosphere appears to have an additional contribution, which may likely be due to spicules that appear to peak at about the same height as the O VI component. Separate measurements of O VI (and for the far wing of Mg II h) show a similar behavior as O V. These results would argue for an inhomogeneous transition between chromosphere and corona (cf. Doschek, Feldman, and Tousey 1975).

TABLE 6

CHARACTERISTICS OF SPECIES IN THE EARTH'S ATMOSPHERE OBSERVED WITH THE LPSP INSTRUMENT

OSO 8 Channel	Component	Wavelength (nm)	Range of Altitudes in the Earth Atmosphere (km)
Mg II.....	O3	277.7–282.3	60–80
Mg II.....	OH	281.6	> 75
Lα.....	O2	120.6–122.3	90–110
Lα.....	H	121.6	> 500
Lβ.....	O2	101.7–103.2	150–200
Lβ.....	H	102.5	> 500

g) *Aeronomy Investigations*

At orbital sunsets and sunrises, the solar UV light is absorbed by successively denser layers of the Earth's atmosphere. Vertical distribution of number densities of several components may be studied by this technique as indicated in Table 6. The light in the Ca channels is not attenuated and provides a pointing reference.

The measurement of the width and depth of the hydrogen geocoronal absorption was undertaken during several orbit days. This is a new and very promising observational technique to measure simultaneously the exospheric temperature at each point of the orbit and the atomic hydrogen density at the exobase, which may solve the question of what mechanism(s) control(s) the hydrogen distribution at the exobase. The preliminary results of aeronomy investigation have been published in Vidal-Madjar *et al.* (1976).

VI. CONCLUSION

We have described here the actual performance of one of the most complex solar physics instruments launched into space and the main results obtained with the first high-resolution multichannel UV and visible spectrometer placed in orbit by *OSO 8*. For the first time, an absolute pointing accuracy of nearly 1" could be achieved in orbit with real time operations. It undoubtedly represents the largest and most complex experiment of the French space program in solar physics. Although the bulk of the data has not yet

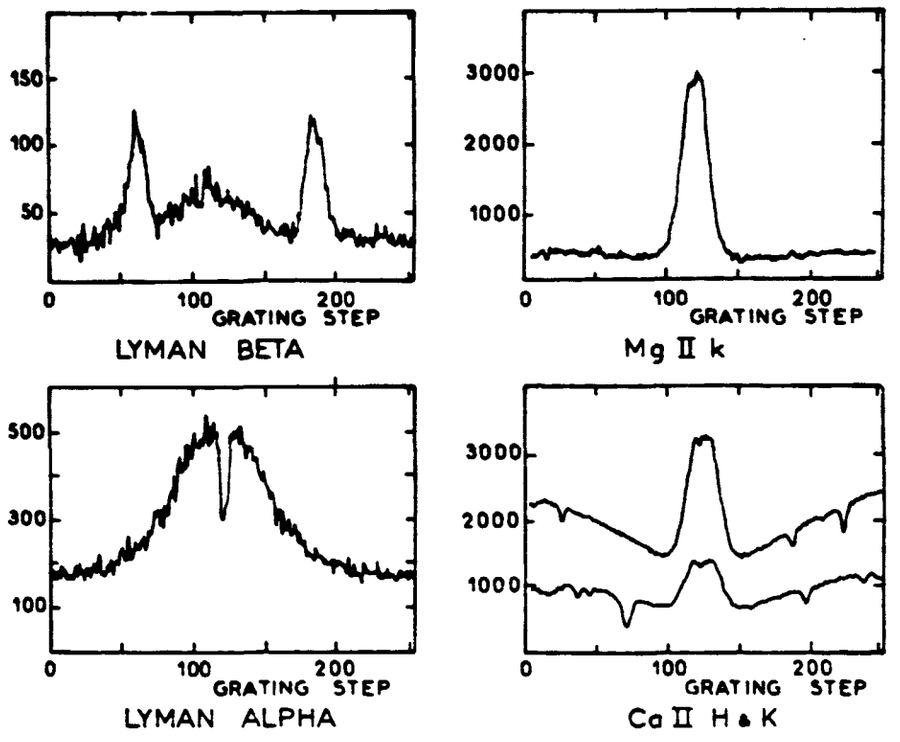

FIG. 19—Profiles of Ca II K, Mg II *k*, Lα, and Lβ observed simultaneously over an active region. All lines are free from the central self-reversal usually observed over quiet Sun areas. The two peaks in the Lβ profile are the two O I lines. For conversion into λ units, see Table 1. Wavelengths increase to the left.

been examined in detail, preliminary analyses show that the performance of the instrument was nominal and at times beyond nominal expectations. The results presented here are only isolated samples of what has been obtained in the first 18 months. The instrument continues to perform nominally and has begun its third year of operation. This will allow us to obtain more data on active regions and particularly on flares which were very rare during the first 18 months. Indeed, only one flare, that of 1977 April 19, has been observed so far (Jouchoux *et al.* 1977).

The operation of the instrument has been very exhausting, and we have benefited from the assistance of many people. Our experience with regard to the remote management of an entirely automated complex instrument is, we feel, of great value for similar experiments in the future.

The accomplishment of this experiment would not have been possible without the support of CNES and particularly of Dr. A. Lebeau, former Director of Programs and Plans, and Professor M. Levy, former President. We would like to thank collectively the NASA and CNES engineers who have contributed to this experiment.

The operations of the instrument from Boulder would not have been possible without the kind hospitality of LASP, in particular of its Director, Professor C. Barth. We also thank the LASP *OSO 8* staff for their contributions. We are indebted to NASA and LASP for access to space on the American calibration rockets. The excellent spirit of cooperation and the dedicated service of the *OSO 8* Control Center at the Goddard Space Flight Center was certainly a key to the success of real time acquisition and of the daily programming of observations in general. The observations of sunspots, active regions, and flaring regions could not have been done without the generous assistance of NOAA, Big Bear Solar Observatory, Meudon Observatory, Sacramento Peak Observatory, and Lockheed Research Laboratory. We wish to express our warmest acknowledgements to these numerous and often anonymous people who played such an important although thankless role in the daily work required by the continuous observation of the Sun during several years. Highly appreciated were the contribution of Drs. P. Bruston and M. Malinovsky of LPSP in the preparation and checkout of observing programs. Invaluable and continuous support in the daily operations was provided by M. Bruston (Mrs.) and N. Dionnau of LPSP. We also thank J. Borsenberger (Institut d'Astrophysique de Paris) and B. Phissamay (LPSP) for their important contribution.

Last but not the least, all of the Guest Investigators who have assisted our team in the operation and

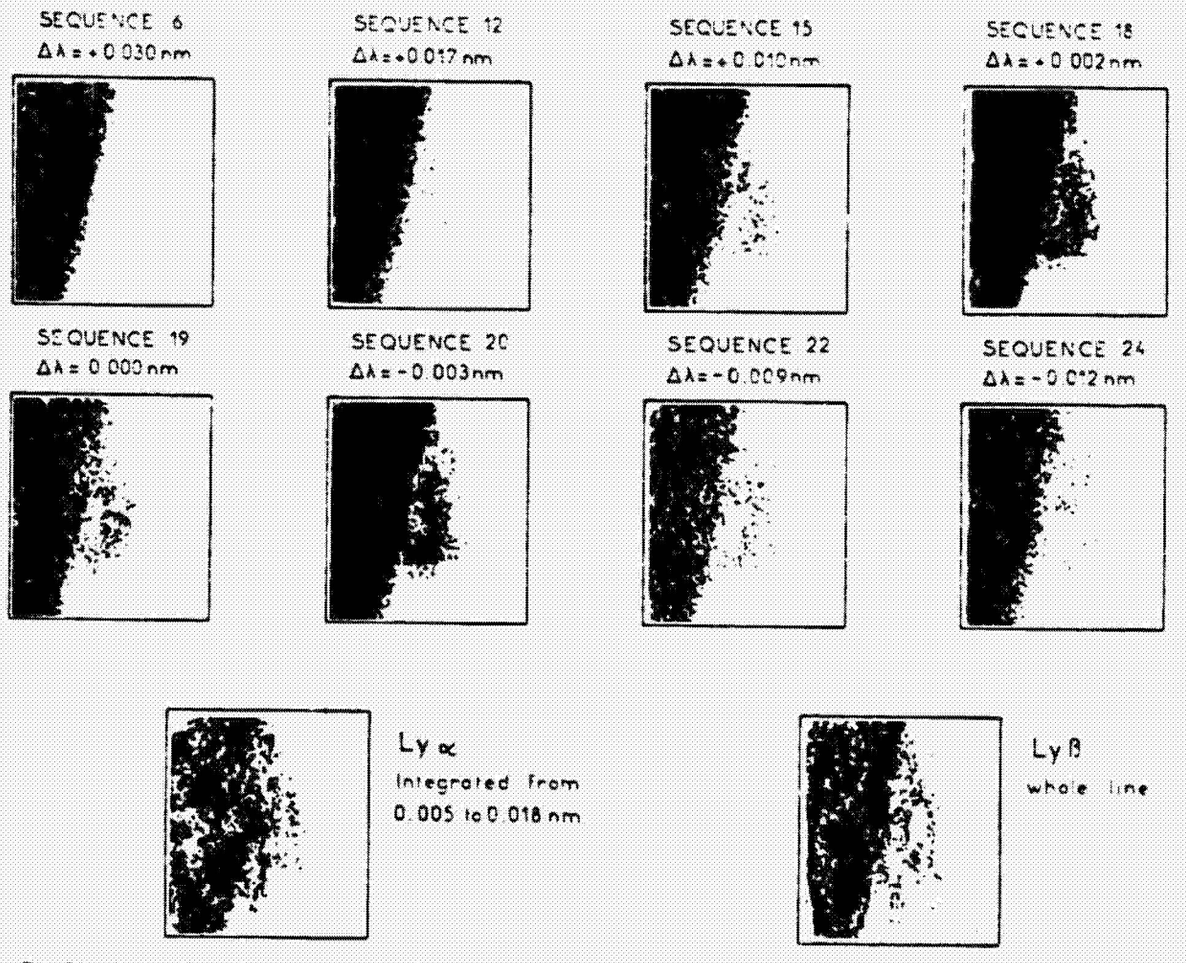

FIG. 20.—Series of satellite raster negative images, taken at different positions in the Ca K line ranging from −0.012 nm to +0.03 nm from line center. At the bottom are two simultaneous images of the loop prominence in Lα and Lβ. Image size is 2'3 × 2'7, repetition rate 82 s, resolution 10" × 10".

planning should be acknowledged here. They are: D. Dravins, S. Dumont, E. Frazier, K. Fredga, U. Grossman-Doerth, M. Hersé, S. Jordan, H. P. Jones, F. Kneer, P. McWhirter, W. Mattig, D. J. Mullan, J. C. Noens, J. Pasachoff, J. C. Pecker, G. Sharmer, G. Simon, J. O. Stenflo, M. von Uexuel, and A. Wyller.

The contribution, calibration, and operation of this instrument were funded under CNES contracts 70-220, 71-202, 73-202, 74-202, 75-202, 76-202, and 77-202. Special funding was provided by CNRS for the salaries of the seven LPSP scientists and programmers in charge of the operations at Boulder. The Guest Investigator Program was funded in the USA under NASA grant NSG 7130.

Additional acknowledgement must go to G. Sharmer for his extensive and supportive contributions which far exceeded his role as Guest Investigator.

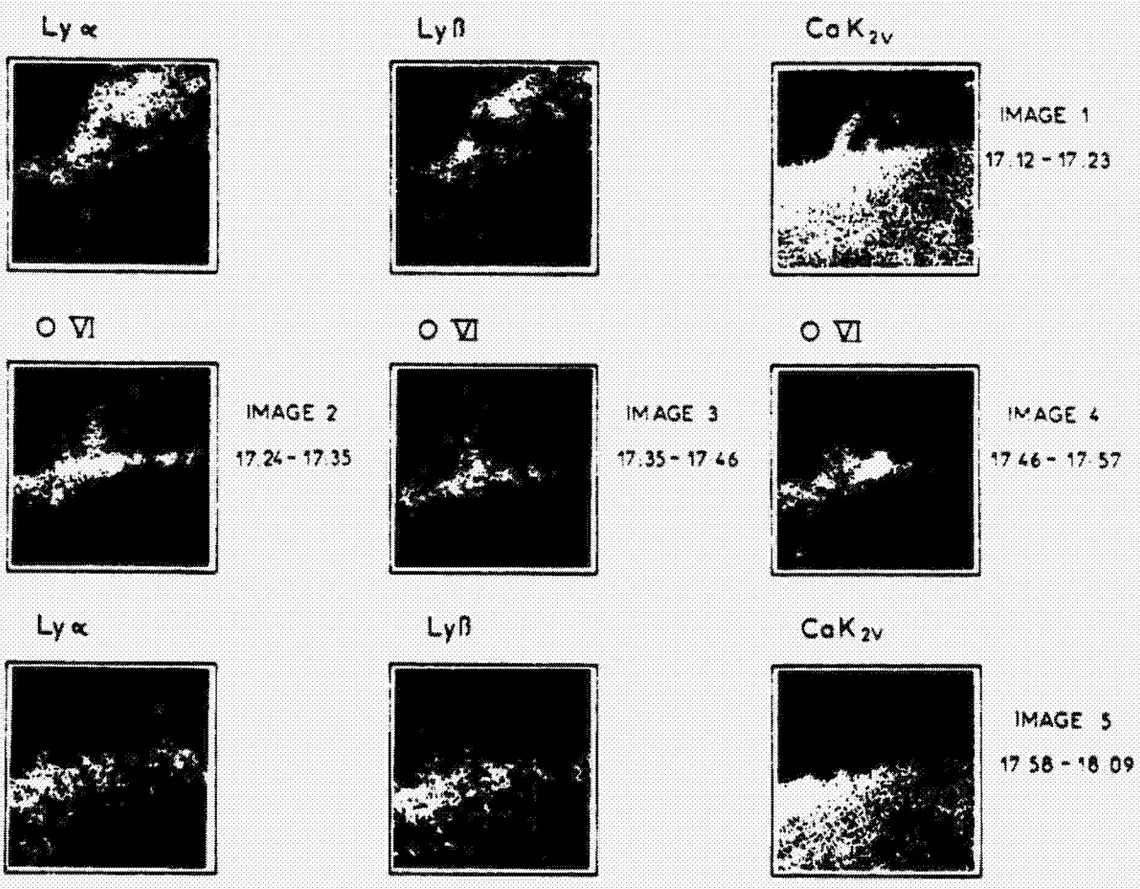

FIG. 21.—Development and evolution of an eruptive prominence associated with Active Region 14127 (McMath number) when it crossed the west limb.

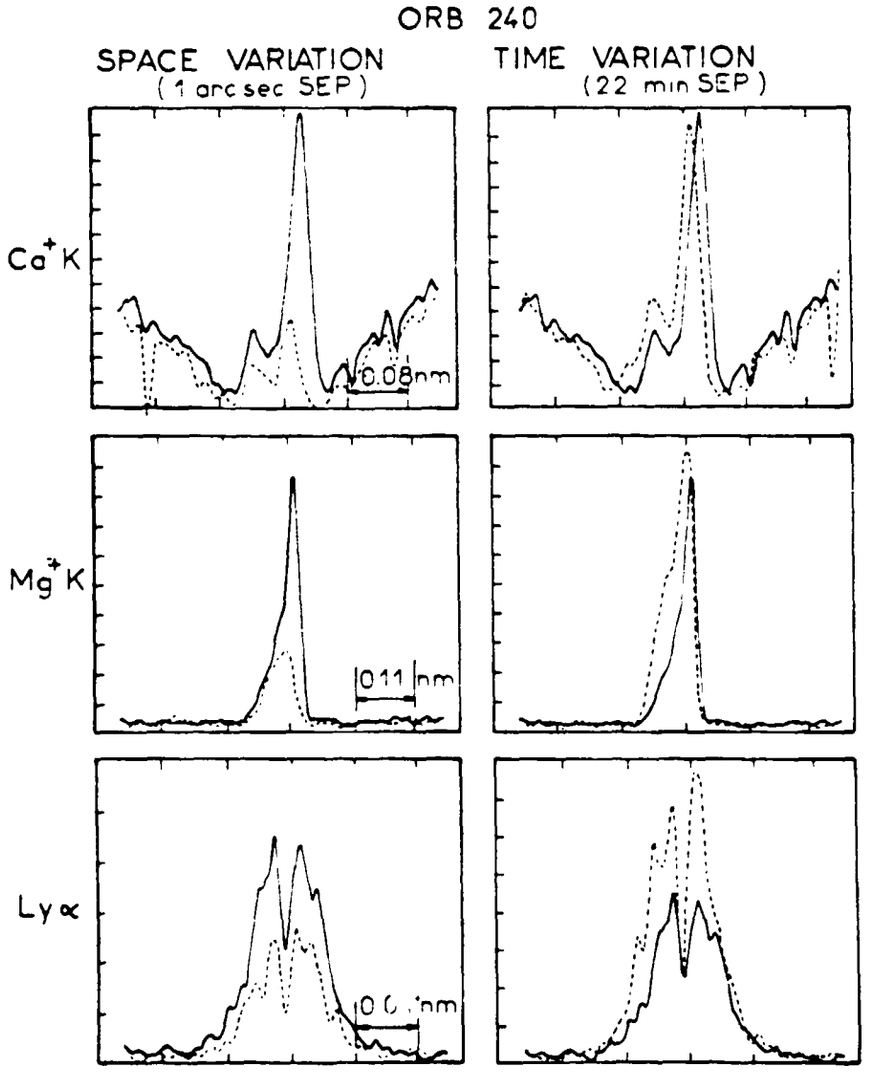

FIG. 22. Profiles taken over an active region visible at the limb on 1975 July 7. The set of profiles on the left (*solid* and *dashed lines*) correspond to two points 1" apart. On the right, solid and dashed profiles correspond to profiles taken 22 min apart, in time.

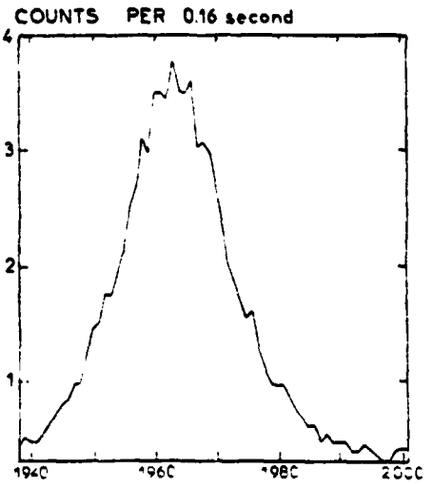

FIG. 23.—Profile of the Si III 120.6 nm line observed at Sun center with a resolution of 1" × 40". Wavelengths increase to the left. For conversion into λ units, see Table 1. Counts represent an average over one orbit

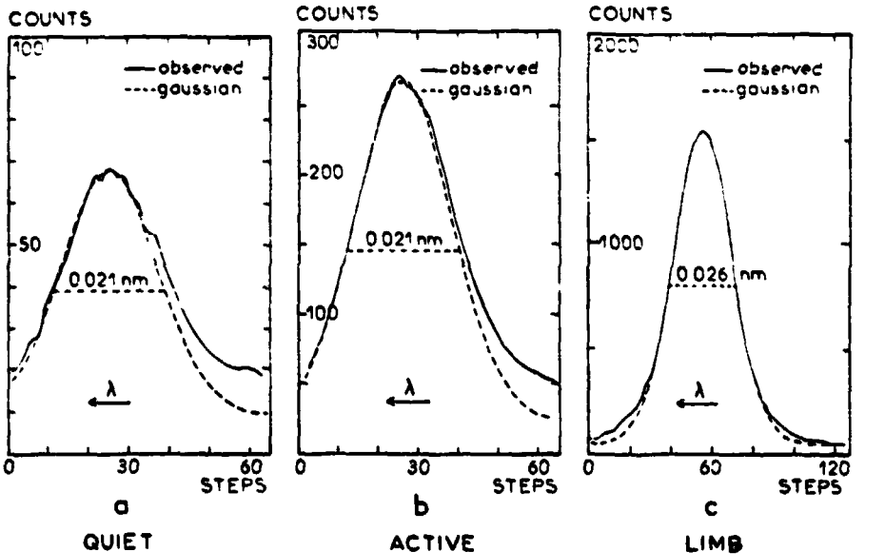

FIG. 24.—(*a*) Quiet and (*b*) active Sun profiles of O VI at Sun center. Each profile is an average of 20 individual profiles. The full lines represent the observations; the dashed line, a best Gaussian fit. The resolution is 1" × 40". Wavelengths increase to the left. For conversion into λ units, see Table 1. Profile (*c*) refers to the limb; it is also an average, but the individual profiles were observed at another orbit, and the units cannot be compared with those of profiles (*a*) and (*b*).

LPSP INSTRUMENT ON *OSO 8*

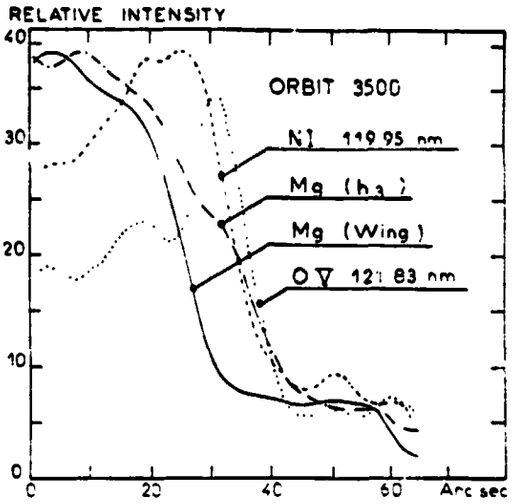

FIG. 25.—Limb "darkening" profiles, in Mg II *h*3, the far wing of Mg II *k*, N I 119.95 nm, and O V 121.83 nm. Distance is measured in arcsec (arbitrary origin).

REFERENCES

Artzner, G. E., Bonnet, R. M., Lemaire, P., Vial, J. C., Jouchoux, A., Leibacher, J., Vidal-Madjar, A., and Vite, M. 1977, *Space Sci. Instrum.*, **3**, 131 (Paper I).

Artzner, G. E., *et al.* 1978, in preparation.

Beckers, J. M., Bridges, C. A., and Gilliam, Lou B. 1976, Air Force Geophysics Laboratory Report AFGL-TR-76-0126 (II).

Bonnet, R. M. 1968, *Ann. d'Ap.*, **31**, 597.

Bradford, A. P., Hass, G., Osantowski, J. F., and Toft, A. R. 1969, *Appl. Optics*, **8**, 1183.

Brault, J. M., and Testerman, L. 1972, unpublished.

Doscheck, G. A., Feldman, U., and Tousey, R. 1975, *Ap. J. (Letters)*, **202**, L151.

Engvold, O., and Livingston, W. 1971, *Solar Phys.*, **20**, 375.

Foukal, P. V., Huber, M. C. E., Noyes, R. W., Reeves, E. M., Schmahl, E. J. Timothy, J. G., Vernazza, J. E., and Withbroe, G. L. 1974, *Ap. J. (Letters)*, **193**, L143.

Hinterreger, H. E. 1976, *J. Atmos. Terr. Phys.*, **38**, 791.

Huber, M. C. E., Dupree, A. K., Goldberg, L., Noyes, R. W., Parkinson, W. H., Reeves, E. M., and Withbroe, G. L. 1973, *Ap. J.*, **183**, 291.

Jordan, C. 1969, *M.N.R.A.S.*, **142**, 501.

Jouchoux, A., Skumanich, A., Bonnet, R. M., Lemaire, P., Artzner, G. E., Leibacher, J., Vial, J. C., and Vidal-Madjar, A. 1977, paper presented at the 150th Meeting of the American Astronomical Society, Atlanta.

Jouchoux, A., and Hansen, E. 1978, in preparation.

Kohl, J. L., and Parkinson, W. H. 1976, *Ap. J.*, **205**, 599.

Lemaire, P., and Skumanich, A. 1973, *Astr. Ap.*, **22**, 61.

Levasseur, A. C., Meier, R. R., and Tinsley, B. A. 1976, *J. Geophys. Res.*, **81**, 5587.

Linsky, J. L. 1970, *Solar Phys.*, **11**, 355.

Livingston, W. C., and White, O. R. 1978 (to be published).

McWhirter, R. W. P. 1977, in *Proceedings of IAU Coll. 36, The Energy Balance and Hydrodynamics of the Solar Chromosphere and Corona*, ed. R. M. Bonnet and P. Delache (Nice), p. 220.

Minnaert, M., Mulders, G. F. W., and Houtgast, J. 1940, *Photometric Atlas of the Solar Spectrum from λ3612 to λ8771* (Amsterdam: North-Holland).

Moe, O. K., and Nicolas, K. R. 1977, *Ap. J.*, **211**, 579.

Nicolas, K. R., Bruecknер, G. E., Tousey, R., Tripp, D. A., White, O. R., and Athay, R. G. 1976, submitted to *Solar Phys.*

Reeves, E. M. 1976, *Solar Phys.*, **46**, 53.

Rottman, G. E. 1977, private communication.

Salvetat, P. 1975, in *Technology of Scientific Space Experiments*, ed. CNES (Paris, May 1975), p. 445.

Skumanich, A., Smythe, C., and Frazier, E. N. 1975, *Ap. J.*, **200**, 747.

Vernazza, J. E. 1972, thesis, Harvard University.

Vernazza, J. E., Foukal, P. V., Huber, M. C. E., Noyes, R. W., Reeves, E. M., Schmahl, E. J., Timothy, J. G., and Withbroe, G. L. 1975, *Ap. J. (Letters)*, **199**, L123.

Vial, J. C., *et al.* 1978, in preparation.

Vidal-Madjar, A. 1977, private communication.

Vidal-Madjar, A., Laurent, C., Bonnet, R. M., and York, D. G. 1977, *Ap. J.*, **211**, 91.

Vidal-Madjar, A., Roble, R. G., Mankin, W. G., Artzner, G. E., Bonnet, R. M., Lemaire, P., and Vial, J. C. 1976, in *Atmospheric Physics from Spacelab*, ed. J. J. Berger *et al.* (Dordrecht: Reidel), p. 117.

White, O. R., and Suemoto, Z. 1968, *Solar Phys.*, **3**, 523.

G. ARTZNER, R. M. BONNET, P. GOUTTEBROZE, A. JOUCHOUX, P. LEMAIRE, J. C. VIAL, and A. VIDAL-MADJAR: Laboratoire de Physique Stellaire et Planétaire-C.N.R.S., P.O. Box 10, 91370 Verrieres-le-Buisson, France

J. LEIBACHER: Lockheed Palo Alto Research Laboratory, 3251 Hanover St., Palo Alto, CA 94040

A. SKUMANICH: High Altitude Observatory, NCAR, Boulder, CO 80307

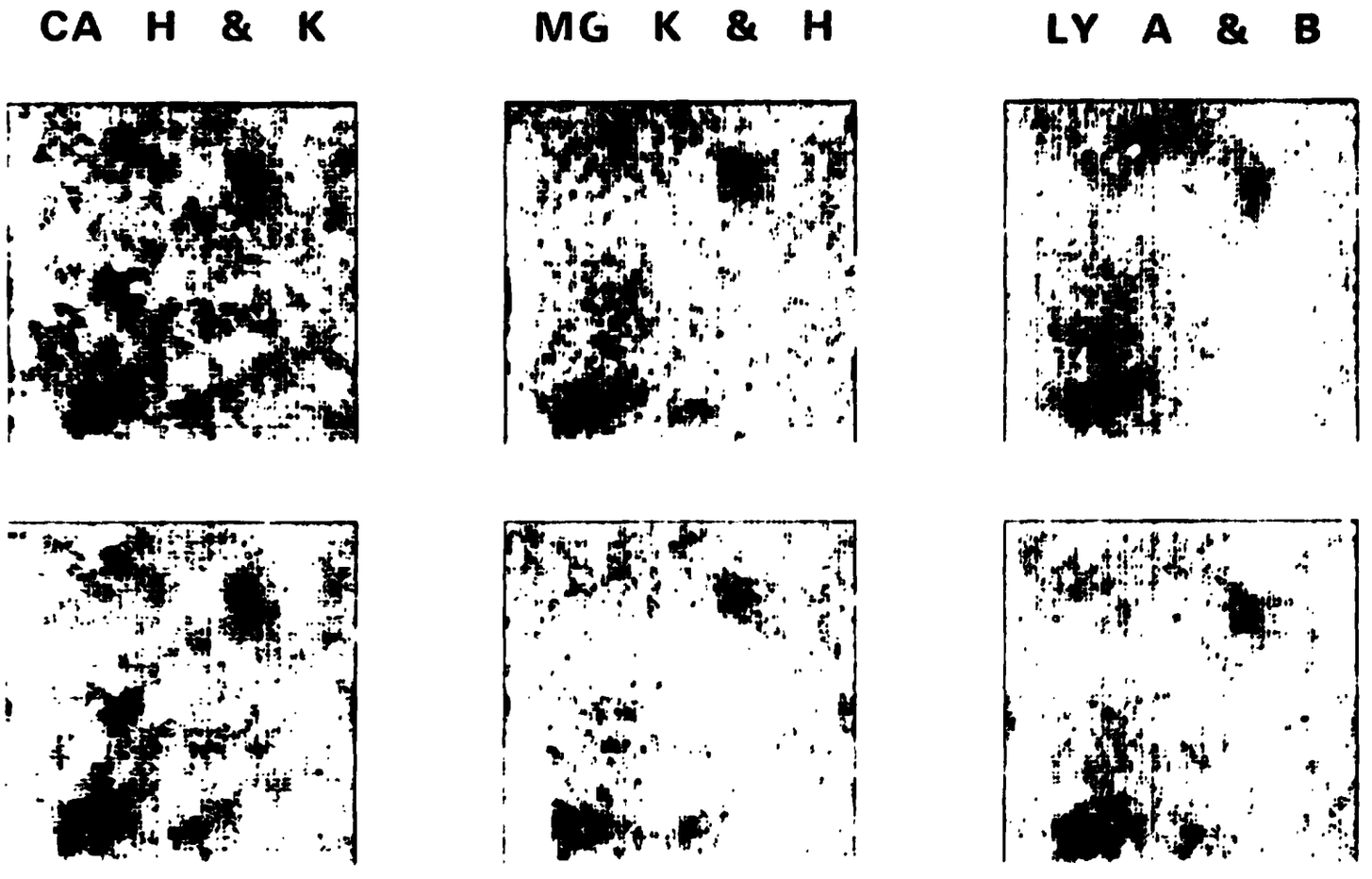

FIG. 8.—Internal raster images of the quiet Sun chromospheric network in Ca II K and H, Mg II *h* and *k*, L*α*, and L*β*. The field is 64″ × 64″, the slit size 1″ × 1″.

BOSSET *et al.* (*see* page 1044)

Attachment D

THE ASTROPHYSICAL JOURNAL, 224: L83–L85, 1978 September 1

SIMULTANEOUS TIME-RESOLVED OBSERVATIONS OF THE H Lα, Mg *k* 2795 Å, AND Ca K SOLAR LINES

G. ARTZNER, J. LEIBACHER,* J. C. VIAL, P. LEMAIRE, AND P. GOUTTEBROZE
Laboratoire de Physique Stellaire et Planétaire
Received 1978 February 22; accepted 1978 June 15

ABSTRACT

Observations indicate that the temporal variations of wavelength of the reversal of the solar H Lα and Mg *k* lines are correlated.

Subject headings: Sun: atmospheric motions — Sun: chromosphere — Sun: spectra

I. INTRODUCTION

The solar photospheric and chromospheric lines exhibit ubiquitous quasi-periodic oscillations of intensity and wavelength. The presence or absence of periodic fluctuations higher in the solar atmosphere has been investigated by measuring the intensity variations of spectral lines formed between 10^4 K and 1.5×10^6 K (Vernazza *et al.* 1975), the microwave emission of the Sun around 10^6 K (Avery 1976), the intensity and position of the C II 1336 Å line formed around 20,000 K (Chipman 1977), the intensity and position of the C IV 1550 Å line formed around 100,000 K (Bruner 1977), and the line profile of the Fe XIV λ5303 coronal line (Tsubaki 1977).

We report here the first observations of the solar HLα 1216 Å line formed near 25,000 K with temporal, spectral, and spatial resolution adequate for the study of solar velocity fields.

II. OBSERVATIONS

The LPSP instrument on board *OSO 8* is described by Artzner *et al.* (1977). The observations reported here, mostly at disk center, had 1″ × 3″, 1″ × 10″, or 1″ × 20″ spatial resolution, a spectral scanning increment of, respectively, 2.4, 2.3 and 1.6 km s^{-1} for the Lα, Mg *k* and Ca K lines, and a time resolution of from 10 to 40 s. A sequence of observations consists of 100 to 180 successive spectra scanning the Lα line over ±0.53 Å, the Mg *k* line over ±1.4 Å, and the Ca K line over ±1.1 Å.

In order to discriminate between actual solar oscillations and pointing variations, we have measured the pointing stability by three different methods (Bonnet *et al.* 1978). As a result, we estimate that the pointing drifts randomly at a rate smaller than 1″ per 3 minutes of time.

As a check of the instrumental stability over 1 hour and of the procedure to compensate for the Doppler-Fizeau component of the velocity of the spacecraft, we have averaged Lα spectra during three consecutive 20 minute intervals of the 60 minute daylight portion of an orbit. The constant position of the geocoronal line demonstrates that the wavelength drifts by less than 4 mÅ over one orbit. The observed spectral resolution does not vary, but the shape of the geocoronal absorption is wider during the third part of the orbit day than during the first part. This measured geophysical effect, most likely due to the heating of the terrestrial atmosphere between local sunrise and sunset, will be investigated elsewhere and gives us confidence in the ability of the instrument to detect minor changes in the shape and position of spectral lines during 1 hour.

The low measured dark current (1.1 counts s^{-1}) enables us to make use of data taken through orbit 380, when the sensitivity was 35 counts s^{-1} at the blue Lα peak with 0.01 Å and 1″ × 10″ resolution.

Note that the simultaneously measured counting rates may vary from 10 (Lα wing) to 100,000 (K2v peak of Ca K), because of the combined increase of solar flux and instrumental sensitivity from 1216 to 4000 Å.

III. DATA ANALYSIS

Any plot of the data exhibits quasi-periodic oscillations of the Ca K, Ca H, Mg *k* 2795, and Mg h 2803 Å lines. These are reported in Artzner *et al.* (1978). As indicated by Bonnet *et al.* (1978), the Lα signal for a constant solar input is modulated in phase with the rotation of the spacecraft wheel, with a period of the order of 10 s. Therefore a mathematical procedure (as used by Artzner *et al.* 1978) applied to the raw, noisy, uncorrected Lα data will fail to reveal the true time behavior of this line, because it will essentially reflect the "10 second modulation" of the signal. As the mean intensity of the Lα line, measured over 10.24 or 20.48 s, is much less sensitive to this modulation than the velocity measurements, we have integrated the Lα profiles over ±0.41 Å and we have computed the average power spectrum (for 16 sequences) of the time variation of this quantity (Fig. 1). The result agrees with the observations of Vernazza *et al.* (1975). For each sequence we have measured the standard deviation of the values of the integrated intensity (Table 1). For the sequences with low average numbers of counts per profile, the intensity variation is found to be primarily due to statistical noise, but for the sequences with higher count rates, the standard deviation is considerably larger than photon statistics alone would imply.

* Lockheed Research Laboratories, Palo Alto.

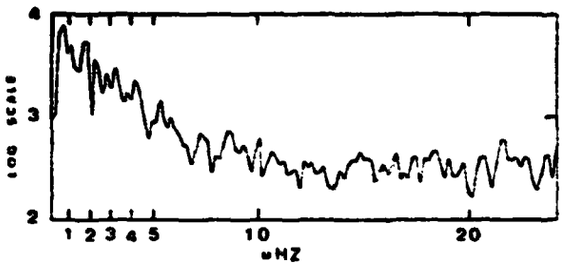

FIG. 1.—Temporal variations of the Lα intensity; bandwidth ±0.41 Å. Average of 16 power spectra.

TABLE 1

Lα 1216 Å LINE (bandpass ±0.41 Å)

Duration (minutes)	Average Number of Counts per Profile	Standard Deviation around Average
40	200	23
49	210	14
55	230	16
42	240	13
38	270	16
28	290	14
37	290	20
37	300	21
39	330	16
33	340	20
40	350	27
42	370	28
56	400	24
47	450	62
53	520	35
56	520	29

As of now, we have analyzed 21 orbits of the Lα data. The analysis has been conducted in such a way as to be insensitive to the 10 s modulation: we classify into three classes the Mg *k* spectra according to the relative strength of the k_2 peaks and then compare average Lα spectra corresponding to each of the three classes. Class I has a high ratio of (Mg k_{2v} intensity/Mg k_{2r} intensity), while classes II and III have successively lower values of this ratio. This procedure reduces statistical noise and should reduce the effect of the "10 second" modulation, because the solar oscillations observed in Mg *k* and the spinning of the spacecraft should have a random relationship. As a result, after correcting for the Doppler component of the velocity of the spacecraft, average class I, II, and III profiles are computed, not only for the Mg *k* line but also for the simultaneously observed H Lα, Ca K, Ca H, and Mg *h* lines.

1. For the Mg *k* channel, the average class I profile actually has a strong (blue peak, red peak) ratio, as a verification of the procedure.

2. A very similar effect is seen for the Mg *k*, Ca H, and Ca K channels.

3. For the Lα line, the average class I and class III profiles are identical in the wing, but shifted in the central reversal. The integrated intensity of the average "class I" Lα profile is equal to the integrated intensity of the average "class III" Lα profile, whereas the integrated intensity of the average "class I" Mg *k* profile is stronger than for the average "class III" profile.

We have fitted to the Lα and Mg *k* line profiles a six-parameter formula, I, λe, $W e$, A, λa, $W a$,

$$I(\lambda) = I \exp\left[-\left(\frac{\lambda - \lambda e}{W e}\right)^2\right] \times \left\{1 - A \exp\left[-\left(\frac{\lambda - \lambda a}{W a}\right)^2\right]\right\}. \quad (1)$$

The parameters λe and $W e$ refer to the wings and the parameters λa and $W a$ to the position and width of the central reversal.

The data points within ±35 mÅ of the geocoronal line were excluded from this fit. The zero of the wavelength scale is, for the Lα observations, fixed by the geocoronal absorption (no correction for the solar rotation is needed, as the observations reported in Tables 2 and 3 are at disk center). The zero of the wavelength scale for the Mg *k* line, at the present stage of data reduction, may be affected by a systematic error of ±0.01 Å. For the sake of comparison, the wavelengths have been converted in meters per second. The numbers quoted do not imply that such velocities are present in the solar atmosphere; the derivation of actual solar velocities is beyond the scope of this *Letter*.

Table 2 shows the results of these fits for the three

TABLE 2

POSITION AND INTENSITY OF SPECTRAL FEATURES OF AVERAGE SPECTRA*

	High (Mg k_{2v}, Mg k_{2r}) Ratio Class I	Average Ratio Class II	Low (Mg k_{2v}, Mg k_{2r}) Ratio Class III
Lα			
λa–H telluric (central reversal)	+3800 m s^{-1}	+2300 m s^{-1}	+950 m s^{-1}
λe–He telluric (wings)	+1100 m s^{-1}	+1100 m s^{-1}	+780 m s^{-1}
Ie	8.9	8.9	9.0
Mg *k*			
λa central	+4150 m s^{-1}	+2950 m s^{-1}	+1720 m s^{-1}
λe emission	+330 m s^{-1}	+730 m s^{-1}	+1350 m s^{-1}
Arbitrary units Ie emission	315	283	269
Faint Mn I photospheric line zero average	+75 m s^{-1}	−25 m s^{-1}	+50 m s^{-1}
H geocoronal absorption (zero average)	−60 m s^{-1}	+120 m s^{-1}	−60 m s^{-1}

* Classified according to the K_{2v}/K_{2r} ratio; three equal classes for each time sequence.

classes of profiles defined above. From the same set of data, by averaging of faint and bright sequences, we have computed typical La and Mg *k* faint and bright profiles, and applied the same fit with a six-parameter formula (Table 3). From the comparison of Tables 2 and 3, it appears that, for the La and Mg *k* lines, if the position of the central reversal is related to the atmospheric velocity fields, the instantaneous, time-resolved velocity fluctuations are greater than the large-scale (chromospheric network) permanent velocity features.

We have also computed three average profiles by sorting out at random the observed profiles into three classes to derive an estimate of the statistical precision of our measurements. We find the La, photospheric line, and geocoronal line velocities are accurate to about ± 100 m s^{-1}, while the Mg *k* velocities are accurate to ± 25 m s^{-1}. The La intensity values are accurate to ± 0.1 in our units, and the Mg *k* intensities to ± 2.

TABLE 3

POSITION AND INTENSITY OF SPECTRAL FEATURES OF AVERAGE SPECTRA*

	Average of 5 Brightest Sequences out of 16	Average of 5 Faintest Sequences out of 16
La		
λa–H telluric central reversal	+2600 m s^{-1}	+2100 m s^{-1}
λe–H telluric wings	+900 m s^{-1}	+330 m s^{-1}
Ie	12, 5	5, 4
Mg *k*		
λa central reversal	+3000 m s^{-1}	+3060 m s^{-1}
λe emission	+1300 m s^{-1}	+450 m sec
Ie	391	241

* Brightest sequence versus faintest sequence.

IV. CONCLUSION

At this stage of OSO *8* data reduction, we cannot yet present the power spectrum of the spatially resolved solar La line velocity fluctuations; nevertheless, we have demonstrated that the La central reversal does exhibit wavelength fluctuations positively correlated with the oscillations of the chromospheric Ca K and Mg *k* lines.

Temporal variations in the derived velocity of the central reversal feature of 2500 m s^{-1} in Mg *k* are accompanied by variations in the same sense of approximately 2800 m s^{-1} in the central reversal feature of La.

This *Letter* is the continuation of efforts of teams on the *OSO 8* project at Verrières-le-Buisson, Greenbelt, Los Angeles, and Boulder. Special acknowledgment goes to A. Jouchoux, who organized special observing sequences for this program. The computations were carried out on the CDC 7600s of NCAR and CNES. The CNES funded the fabrication and operations of the instrument under contracts 70-220, 71-202, 72-202, 73-202, 74-202, 75-202, 76-202, and 77-202.

REFERENCES

Artzner, G. E., Bonnet, R. M., Lemaire, P., Vial, J. C., Jouchoux, A., Leibacher, J., Vidal-Madjar, A., and Vite, M. 1977, *Space Sci. Instr.*, 3, 131.
Artzner, G., Leibacher, J., Vial, J. C., Lemaire, P., and Gouttebroze, P. 1978, *Astr. Ap.*, submitted.
Avery, L. W. 1976, *Solar Phys.*, 49, 141.
Bonnet, R. M., *et al.* 1978, *Ap. J.*, 221, 1032.
Bruner, E. C., Jr. 1977, *Proc., November 7–10 OSO 8 Workshop* (LASP), p. 427.
Chipman, E. G. 1977, *Solar Phys.*, 55, 277.
Tsubaki, T. 1977, *Solar Phys.*, 51, 121.
Vernazza, J. E., Foukal, P. V., Huber, M. C. E., Noyes, R. W., Reeves, E. M., Schmahl, E. J., Timothy, J. G., and Withbroe, G. L. 1975, *Ap. J. (Letters)*, 199, L123

G. ARTZNER, P. GOUTTEBROZE, J. LEIBACHER, P. LEMAIRE, and J. C. VIAL: Laboratoire de Physique Stellaire et Planétaire, P.O. Box 10, F-91370, Verrières-le-Buisson, France

Attachment E

Abstract of Paper presented at the 153rd Meeting of the American Astronomical Socity. Published in the Bulletin of the A.A.S., 1978, 10, 671.

A Dynamical Representation of the Solar Chromosphere, J.W. LEIBACHER, Lockheed and P. GOUTTEBROZE, Laboratoire De Physique Stellaire et Planetaire = We present investigations of the non-linear hydrodynamic state of a model solar atmosphere and the time dependent, ionized calcium and magnesium resonance line profiles emitted by the chromosphere. We calculated the one dimensional response to an excitation 1.6 Mm below the visible surface using a finite difference code, and the resulting motions exhibit the well known 300 second oscillation of the photosphere and 200 second oscillation of the chromosphere. Both oscillations have the chracter of standing waves. We shall discuss the formation of these oscillations and their dependence upon parameters of the calculation. Time sequences of resonance line profiles display asymmetry and intensity variations that result from both oscillations. This work was supported by NASA contracts NAS8-32356 and NASW-3053, the Lockheed Independent Research Program and the Centre National d'Etudes Spatialies.

ATTACHMENT F

SOLAR ATMOSPHERIC DYNAMICS

II. FORMATION OF OPTICALLY THICK CHROMOSPHERIC LINES

by

Pierre GOUTTEBROZE

Laboratoire de Physique Stellaire et Planétaire du C.N.R.S.

and

John W. LEIBACHER

Lockheed Palo Alto Research Laboratory

submitted to

The Astrophysical Journal

....., 1979

ABSTRACT

Two of the most representative chromospheric lines, Mg II k and Ca II K are used to study the formation of optically thick lines in a time-dependent, one-dimensional model of the solar atmosphere, which was discussed by Leibacher, Gouttebroze and Stein . (1979). Time sequences of these line profiles are calculated for two kinds of atmospheric motions : propagation of a pulse through the atmosphere and free oscillations. The mechanisms of formation (especially the displacements of the emitting layers) are studied for different parts of the profiles. Finally, the deformations of the profiles are analyzed using methods also suitable for observations, and the resulting parameters are compared to physical variables in order to evaluate the diagnostic methods.

INTRODUCTION

Among the known motions of the solar atmosphere, the so-called 300 second oscillations, which are now known to originate from the sub-photospheric regions of the sun, have been the object of numerous studies. On the contrary, while some early observations of the Ca II K resonance line (Jensen and Orrall, 1963) showed periodic variations in the core, formed in the chromosphere, with shorter periods (170 seconds), we remain far from an understanding of these chromospheric oscillations. Nevertheless, the observations of the Ca II K line continued to provide knowledge about chromospheric motions (see for instance Wilson and Evans, 1971, Liu, 1974, Beckers and Artzner, 1974, Cram, 1974). More recently, chromospheric motions have been seen in other lines : especially U.V. emission lines with the OSO-8-Colarado experiment (see, e.g. Chipman, 1977, 1978, White and Athay, 1979a, b, Athay and White, 1979) Mg II and L α lines with the OSO-8-LPSP experiment (Bonnet et al. 1978, Artzner et al. 1978). Among the theories developed to interpret these observations, the more detailed are probably those of Heasley (1975) and Cram (1976) who studied the deformations of the Ca II lines during the propagation of a pulse through the atmosphere. Recently, Durrant, Grossmann-Doerth and Kneer (1976), discussed the temporal evolution of Ca II K line profiles and concluded in favour of a mechanism of chromospheric oscillations similar to that proposed by Leibacher (1971). This encouraged us to undertake a more detailed study of chromospheric hydrodynamics (Leibacher, Gouttebroze and Stein,

1979, hereafter Paper I) and to compute the emergent intensities for various spectral features relevant to chromospheric studies. These features are continua (Lyman continuum or centimeter microwaves), optically thin emission lines, and optically thick lines. The other aim of this study was to provide the framework for an interpretation of the optically thick lines (Mg II, Ca II and L α) observed with the OSO-8 LPSP experiment, which is planned in a further paper of this series. In the present paper, we investigate the Mg II k and Ca II K resonance lines and discuss variations of these lines produced by either a propagating pulse or free oscillations.

II - THE INITIAL SOLAR-TYPE ATMOSPHERE

As a first step in the computations, we must define a solar-type atmospheric model in hydrostatic equilibrium, providing a medium for the propagation of the waves. This atmosphere must cover a wide range of depths in order to include both the region where the five-minute oscillations originate in the convective zone and photosphere, and the whole chromosphere, which is the object of the present investigation, from the temperature minimum up to the base of the corona. The definition of such a model atmosphere is subject to two general constaints : those arising from the frequencies and amplitudes of the actually observed oscillations, which will be referred to as "hydrodynamical constaints", and those provided by the intensities observed in the various lines and continua of the solar spectrum, which may be summarized as "radiative transfer constraints".

a - Hydrodynamical constraints

First of all, the variation of the temperature with height in the convective zone is prescribed by the outward flux of energy, following the mixing-length theory. Once this variation is known the position of the bottom of the atmosphere (assumed rigid for computational purposes), is determined by the five-minute oscillations. Five minutes represent four times the time of propagation of the waves between the bottom and the top of the convective zone (the top corresponding to the photospheric layer whose acoustic cut-off period is shorter than five minutes).

A similar requirement exists for the chromosphere. As explained in Paper I, the eigen-frequencies of chromospheric oscillations are sensitive to the temperature structure of the chromosphere. The observed periods of oscillation are not so well defined for the chromosphere as for the photosphere or the convection zone, and range from about 150 to 250 seconds : For instance, Jensen and Orrall(1963) found a period of about 170 seconds for the K 3 absorption feature of Ca II, Liu (1974) a rather broad distribution about 180 seconds, and Beckers and Artzner (1974) a repetition rate of 200 $\pm$ 50 seconds. These variations may be attributed to the inhomogenity of the solar chromosphere.

b - Radiative transfer constraints

The solar spectrum is known with some accuracy over a large range of frequencies, which allows the determination of the average temperature structure of the photosphere and chromosphere,

through the use of semi-empirical models. These methods and some recent models have been reviewed by Avrett (1977). Some discrepancies remain between different semi-empirical model atmospheres based on different kinds of data, which allows some degrees of freedom in the choice of atmospheric parameters. For instance, models based on continuum data, such as those of Gingerich et al. (1971) or Vernazza, Avrett and Loeser (1976) exhibit temperature minima between 4100 and 4200 K. On the other hand, atmospheric models derived from the shape of the Mg II or Ca II resonance lines, taking into account partical frequency redistribution effects, have a somewhat higher temperature minimum of about 4400 or 4500 K, as in that of Ayres and Linsky (1976).

In the higher chromosphere, the increased importance of inhomogeneities gives riseto larger variations between the various temperature models. Above 9000 K (the upper chromosphere) a constraint is provided by the non-LTE calculations of hydrogen ionization required for the determination of electron and hydrogen densities in hydrostatic equilibrium. These computations include the determination of intensities in the Lyman α and β lines, which may be compared to observations (owing to inhomogeneities in these regions, an agreement within a factor of 2 or 3 for the integrated intensities may be considered as satisfactory).

In order to reproduce the observed width of chromospheric lines (and especially the separation between the red and blue peaks of the Mg II or Ca II lines), our atmospheric model must include a non-thermal isotropic velocity field which increases

with altitude. These motions produce a "microturbulent" pressure which must be included in the hydro-static or -dynamic equations, in order to get a self-consistent representation of the atmosphere. It should be noticed that the inclusion of this effect may alter significantly the depth scales in the chromosphere, and consequently the eigen-frequencies of oscillation.

c - *Computational methods*

Our atmosphere is defined by the electron temperature (Te) and microturbulent velocities (v_T) as functions of mass integrated along a vertical line (m). From this basic set of parameters, we obtain the corresponding altitudes, densities, pressures, and electron-to-hydrogen density ratios by solving iteratively the equations of hydrostatic equilibrium, hydrogen and metal ionization. A difference-equation method is used to solve the equations of hydrostatic equilibrium, taking into account the gas, electronic and microturbulent pressures. To determine the ionization of hydrogen, we consider a 3-level and continuum atom, and solve self-consistently the equations of statistical equilibrium and radiative transfer in the L α, L β, H α and Lyman continuum transitions. The photoionization rates in the Balmer and Paschen continua are fixed by setting the radiation temperatures to 5000 and 4800 K, respectively, in the parts of the atmosphere which are optically thin in these transitions. Deeper in the atmosphere, they are assumed to be equal to the local electronic temperature. The effects of partial frequency redistribution are taken into account in the computation of

the Lyman lines. The other elements contributing to the electron density are treated in the LTE approximation (their contribution is really important only in the temperature minimum region, where hydrogen is scarcely ionized).

d - The adopted model

As explained above, the present hydrodynamical calculations require a model atmosphere extending from deep within the convection zone to the low corona, which constitutes a range of depths far more extensive than is usually the case for radiative transfer computations. For this reason, the atmosphere used here is a synthesis of several models from different origins, with local modifications. First, our convective zone is taken from Baker and Temesvary (1966). Our photosphere and chromosphere are similar to those of Vernazza, Avrett and Loeser (1973 and 1976) with the following modifications : first, the temperature minimum region is raised to 4500 K, following Ayres and Linsky (1976), in order to get a better fit to the observed Ca II and Mg II resonance line wings. The temperatures are slightly lowered in in the upper chromosphere (by less than 200 K) and the so-called Lyman β-plateau (by about 2000 K) for two reasons : first, the large temperature excursions produced by waves in these regions give strongly non-linear variations of the source functions, so that the averaged intensity is higher than the intensity corresponding to the average-temperature model ; secondly, some dissipation of mechanical energy occurs in these regions (provided that the waves have sufficient amplitudes) which

produces an increase of the average temperatures with time. A similar lower L β-plateau was proposed by Lites, Shine and Chipman (1978). The microturbulent velocities adopted here are also lower (by about 20 percent) in the chromosphere than those of Vernazza, Avrett and Loeser (1973), since an extra broadening of the average profiles may be expected from the atmospheric motions. A summary of the initial and computed atmospheric parameters is given in Table 1.

III - HYDRODYNAMICAL COMPUTATIONS

As described in Paper I, we have calculated the one-dimensional, non-linear dynamical state of this model atmosphere for various excitations and boundary conditions, as well as for different treatments of the energy equation and ionization balance. We have included the effect of an isotropic, unresolved velocity field of "micro-turbulence" which is required for the radiative transfer, in the hydrodynamic calculations. Vertical variation of this velocity field, which remains constant in time, contributes to the mechanical support of the atmosphere. Thus at a given (gas) pressure in the atmosphere, the density is lower than it would have been in the absence of the "micro-turbulence". To discuss the formation of optically thick chromospheric lines, we have selected three time sequences illustrating : a) the propagation of a pulse through an initially motionless atmosphere, b) well established chromospheric and photospheric oscillations,

whose amplitudes correspond to those observed, and c) a similar set of oscillations, whose amplitude was reduced substantially to investigate the effect of non-linearities upon the hydrodynamic and line formation results. The pulse introduced at the bottom of the atmosphere for experiment a) was one half cycle of a sinusoid in velocity, lasting 100 seconds and reaching a maximum velocity of 0.01 km/sec. That is to say the bottom boundary of the atmosphere was raised by 318 metres. Experiments b) and c) were excited by five cycles of a 300 second motion of the bottom boundary, whose amplitude was respectively 6.7 and 1.05 m/s, corresponding to the total vertical motions of 640 metres and 100 metres.

Experiment a) might represent the impulse generated by a granule and is of additional interest here to compare our results with previous work (viz. Cram, 1976). The momentum transfer and heating of the chromosphere result in a very substantial difference between the mean state of the dynamical atmosphere and the initial atmosphere, so that this excitation is not appropriate for the study of the long term fluctuations of the line formation process. Experiments b) and c) result in a much more efficient transfer of energy to the resonant oscillations, so that for comparable resulting amplitudes in the oscillations negligible heating occurs and the mean atmosphere remains very similar to the initial atmosphere. Thus we have some hope that the resulting line profiles bear some resemblance to the observations.

C-2

As we concern ourselves here primarily with effects arising from simultaneous variations of the velocity and the state variables and with the effect of non-linearities, we consider a simplified energy equation to expedite the calculations. Radiative transfer (and loss) are neglected in the internal energy of the gas, and ionization variations are considered to be small fluctuations about the mean state. Locally, the state variables are related adiabatically, and the adiabatic exponent γ (the ratio of specific heats) reflects the state of collisionally controlled ionization in the initial atmosphere. When the gas is completely ionized or completely neutral, γ is 5/3. However, when an abundant species is partially ionized, changes in the internal energy of the gas primarily produce changes in the ionization -because of the large ratio of the ionization energy to the thermal energy- and thus the temperature fluctuations are substantially reduced. γ is reduced to 1.1 in the hydrogen convection zone. Above the temperature minimum, where the ionization is maintained by radiative, rather than collisional, processes which are slow compared to the dynamical time scales (Kneer and Nakagawa, 1976), we hold the ionization constant.

The dynamical aspects of these experiments have been discussed in Paper I. We present in Figures 1a, b and c the variation of the velocity and temperature for the intervals during which we have investigated the line profiles. Two essential points should be recalled. First, during the propagation of energy, velocity and pressure (and hence temperature) vary in phase, as is seen in experiment A. However, they vary

in quadrature for both trapped and evanescent oscillations. This difference of relative phase has a significant effect on the spectral diagnostics. Second, since for established oscillations the chromospheric velocity field is primarily non-propagating, the chromosphere moves more or less in phase, without important vertical velocity gradients, so that even though the particle velocities are substantial fractions of the sound speed mechanical dissipation is not significant. In addition, the absence of large vertical gradients reduces the importance of averaging along the line of sight inherent in spectral line formation, so that there is good reason to suppose a priori that line shifts will reflect the chromospheric velocities.

IV - COMPUTATION OF LINE PROFILES

Let us now study the temporal variations of the Mg II k and Ca II K profiles corresponding to the atmospheric motions described above. For that purpose, we compute temporal sequences of profiles corresponding to the three hydrodynamical experiments. In every case, the moving atmospheres are sampled every 10 seconds. For experiment a), the computations are restricted to the interval from 200 to 400 seconds, when the primary pulse travels through the photosphere and chromosphere. For the "standing oscillations" experiments b) and c), we concentrate our attention on the interval from 1600 to 2600 seconds, where a sequence of typical chromospheric oscillations occurs.

Because of the short time constants associated with the de-excitation of atomic levels, especially for the resonance lines,

compared to the dynamical time scales, we use a quasi-static approximation to compute the line profiles. On the other hand, the photoionization rates depend mainly on the continua, and principally on the hydrogen Lyman continuum, which are expected to vary slowly, as seen in the preceding section. We thus take these intensities as constant, and equal to those of the initial atmosphere.

The computation of line source functions and profiles requires a simultaneous solution of the radiative transfer equations for the lines and statistical equilibrium equations for the atomic level populations. The radiative transfer equations are expressed in lagrangian coordinates, as in our previous computations (Gouttebroze, 1977, hereafter G 77). Methods using this "comoving frame" formulation have been described by Noerdlinger and Rybicki (1974) and Mihalas et al (1976). The large numbers of profiles corresponding to long time sequences, e.g. 100 profiles both for Mg II and Ca II in experiment b), lead us to make some drastic simplications in order to keep the computer time within reasonable limits. We make three principal simplications : first, we reduce the frequency mesh, for intensity integration to 25 points instead of the 39 used in G 77 (for moving atmospheres, we must use symmetric frequency meshes, so that these numbers correspond for a static atmosphere to 13 and 20 points, respectively). This reduction is the main source of uncertainty, but it allows a significant reduction of the computer time used in matrix inversions. We use the Eddington approximation for the integrations over direction.

Secondly, we use average net radiative rates for transitions other than the one computed. We first calculate the complete set of lines corresponding to the average atmosphere, self-consistently. We then compute the time sequence of profiles for the transition under study, assuming that the net radiative rates in other transitions remain equal to the average-atmosphere rates. The computing time for an instantaneous profiles is thus equal to that required by a 2-level atom calculation. This change has negligible effects in the case of Mg II, the k line formation process being close to that of a 2-level atom transition. The effect on the Ca II lines is somewhat more important (although not essential), this simplification being equivalent to neglect of the influence on the K line of variations in the Ca II infrared triplet. Finally, we replace the exact redistribution R_{IIA} (for the scattered fraction which is coherent in the atom's frame) by the R_{IIN} function of Argyros and Mugglestone (1971), which requires only the computation of an exponential and a Voigt function. This procedure is particularly efficient when a fast Voigt function routine is used. Our numerical experiments on the Mg II k line have shown that this change accounts for an error of a few percent in the emergent intensities, much less than from the first approximation.

For Mg II, we use a 3-level and continuum model atom described in G 77. The Ca II model atom has 5 levels and a continuum, and includes the H and K resonance lines, and the infrared triplet. The atomic parameters are taken from Shine

and Linsky (1974), except for the line broadening parameters for which we use the empirical values of Ayres (1977).

Before looking at the results of these computations, it may be useful to bear in mind some simple considerations about the effects of the variations of the physical parameters (velocity, temperature and density) on the lines. The velocity acts by shifting the absorption (and emission) profile by the Doppler effect. The relation between the frequency of a spectroscopic feature and the velocity at a given lagrangian altitude is thus straightforward when this feature is formed in a limited part of the atmosphere (which is the case for optically thin lines or, as shown below, for the central reversals of the Ca II and Mg II lines). The temperature and the density vary generally in phase and both contribute to increase the intensity. For a two-level atom (a situation not too far from that of our resonance lines), the intensities depend upon two parameters : first, the Planck function B which, in the ultraviolet and at chromospheric temperatures, is given by

$$B \approx \frac{2h\nu^3}{c^2} \exp\left(-\frac{h\nu}{kT}\right)$$

(the symbols have their usual meaning) ;
secondly, the ratio ε of collisional to radiative de-excitation rates :

$$\varepsilon \approx N_e \frac{C_{21}}{A_{21}}$$

which depends mainly on the electron density N_e (and thus the density ρ of the gas) provided that C_{21} does not vary rapidly with temperature. As limiting cases, the emission in an optically thin line depends linearly on εB, the photon creation term, while the intensity goes to B when one gets closer to L.T.E. An interesting intermediate case is that of a semi-infinite isothermal atmosphere (whose temperature and density vary in phase everywhere) : the emergent intensity at line center then varies as $B\sqrt{\varepsilon}$.

To evaluate the relative contributions of density and temperature fluctuations to the intensity fluctuation, one may consider an elementary isentropic pressure increase dp, for which density and the temperature increase such that :

$$\frac{dNe}{N_e} = \frac{d\rho}{\rho} = \frac{1}{\gamma}\frac{dp}{p} \quad \text{and} \quad \frac{dT}{T} = \frac{\gamma - 1}{\gamma}\frac{dp}{p} .$$

The intensity variation is :

$$\frac{dI}{I} = \frac{d(\varepsilon^{\eta}B)}{\varepsilon^{\eta}B} = \eta\frac{d\varepsilon}{\varepsilon} + \frac{dB}{B} ,$$

where η is 0, 1/2 or 1 depending on the problem under consideration as discussed above.

With $\frac{d\varepsilon}{\varepsilon} = \frac{1}{\gamma}\frac{dp}{p}$,

and $\frac{dB}{B} = \frac{h\nu_0}{kT}\ \frac{\gamma - 1}{\gamma}\frac{dp}{p}$,

for $\gamma = \frac{5}{3}$, $\nu_0 = 10^{15}$ Hz ($\lambda_0 = 3000$ Å), T = 6000 K, we obtain

$$\eta \frac{d\varepsilon}{\varepsilon} = 0.6 \frac{dp}{p} \eta ,$$

and

$$\frac{dB}{B} = 3.2 \frac{dp}{p} .$$

In chromospheric conditions, the effects of the temperature variations on intensities are thus generally far more important than those arising from density changes.

It should be emphasized that velocity and temperature changes do not act independently. For instance, an increase of temperature in an internal slab produces a more important increase of intensity when it is coupled with a Doppler shift, because the photons created escape more easily from the atmosphere. Such an effect occurs during the passage of a pulse, as described in the next section.

V - VARIATION OF LINE PROFILES ASSOCIATED WITH THE PROPAGATION OF A SINGLE PULSE

The temporal sequences of profiles obtained between 200 and 390 seconds are shown in Figure 2a and b for the Mg II k and the Ca II K line, respectively. The behavior of the two lines is roughly the same : the profiles being initially symmetrical, the blue peak begins to increase with respect to the red peak (around 250 s for Ca II, and 280 s for Mg II), reaches a maximum (around 300 s for Ca II, 330 s for Mg II),

after which the asymmetry reverses (around 330 s for Ca II, 360 s for Mg II). In the Ca II sequence, a new "blue asymmetry" (i.e. with a ratio I(K2V) / I(K2R) larger than 1) appears about 380 s, due to the passage of the secondary pulse. These changes may be roughly interpreted as follows (with the help of the "contribution functions" of Figure 5) : At rest, the k2 peaks are formed principally in the low chromosphere (around 1000 km for Mg II k). The pulse travelling upwards through the atmosphere produces an increase of temperature and density (and thus photon creation) coupled with an upward velocity. When the pulse has reached the formation region of k2 (at rest), it begins to produce an emission of photons shifted to the blue. Only the most blue-shifted photons then escape through the motionless overlying atmosphere, with its centered absorption profile, which produces an increase of the blue peak intensity. On the contrary, the red peak continues to be formed principally in the low chromosphere with small velocities and remains almost steady, which produces a blue asymmetry. Before the pulse reaches the k3 formation region, the central intensity begins to increase due to the incoherent scattering within the line core of photons created by the passage of the pulse in underlying regions. When the pulse reaches the "k3 slab", the wavelength of the reversal is shifted to the blue with respect to the mean position of the peaks, which results in a red asymmetry. These results are consistent with those that Cram (1976) obtained for the Ca II K line. The delay of about 30 seconds between the events in the Ca II and Mg II

lines corresponds to the time for the pulse to travel, from the formation altitude of a part of the Ca II profile, to the formation altitude of the corresponding part of the Mg II profile.

In order to analyse these variations of profiles more closely, we tried to determine more accurately the positions and intensities of the peaks and central absorption of the lines by fitting parabolae to these three features. The variations of the three intensities for the Mg II k line are shown in Figure 3. The intensity increase resulting from the passage of the pulse, the delay between changes in k2V and k3, and the variation of asymmetries appear clearly.

Having simultaneously the values of the physical parameters (particularly the velocities, temperatures and electron density) and the positions and intensities in the lines, we investigated the correlations between these two kinds of parameters, in order to establish the diagnostic possibilities of these "optically-thick" transitions. The correlation between the shift of k3 and the velocity of the slab where the optical depth at line center is equal to 1 in the average atmosphere is remarkably good for Mg II (Figure 4a), and not so good but nevertheless reliable, for Ca II (Figure 4b). The central reversal of these optically thick lines is thus a possible diagnostic tool to determine the vertical velocities in some parts of the chromosphere. On the contrary, we failed in our attempt to find a similar relation between the position of the k2 peaks and the velocity at a definite lagrangian altitude.

The reason appears more clearly when one looks at the contribution functions.

The contribution functions used here represent the contribution at geometrical depth z to the vertical emerging intensity, per unit of z :

$$C(z,\nu) = S(z,\nu)\ \kappa(z,\nu)\ \exp\left|-\ \tau(z,\nu)\right|$$

(S : source function ; ν : frequency ; κ : absorption coefficient, τ : optical depth). These functions for the central reversal and the peaks are shown in Figures 5a and b, respectively, for the Mg II k line. The contribution functions for k3 are sharply peaked at a definite and rather constant lagrangian altitude, i.e. the main part of the emission comes from a thin slab of the chromosphere, which is always about the same. For Ca II K3, these functions (not represented here, but similar to those of Figure 12e related to oscillations) cover a wider, though limited (about 500 km), range of depth, so that the Doppler shift of the reversal is the result of an average of the velocities across this region. For the peaks, on the contrary, the contribution functions are spread over regions as thick as 1000 to 1500 km (for Mg II as well as for Ca II), covering the main part of the chromosphere, where the density varies by several orders of magnitude. This prevents us from using the displacements of the peaks as a practical tool to determine chromospheric velocities. Nevertheless, Figure 5b shows an interesting peculiarity of the blue peak : its contribution function exhibits a sharp peak which follows, during nearly 100 seconds, the passage of

the pulse. This might have applications in the diagnosis of such pulses from spectroscopic data.

The phase difference between velocity and temperature fluctuations represents an important characteristic that distinguishes between different types of waves. As shown above, the velocity in the k3 slab is closely related to the Doppler shift of k3. Unfortunately, the determination of the temperatures from the intensities is not so straightforward : due to the scattering effect mentioned above the intensity in k3 depends on the temperatures and densities in a large region of the atmosphere with a thickness corresponding approximately to the thermalization length. Thus, the temperature-intensity correlation is accurate only when the temperatures are approximately in phase throughout the chromosphere, as will be the case in the next section. In the case of a pulse propagation, the temperature and velocity variations are approximately in phase, but the k3 intensity begins to increase about 40 or 50 seconds before than the pulse has reached the corresponding slab. This effect may be seen in Figure 6, where we plot the reduced k3 intensity :

$$\tilde{I}(t) = \frac{I(t) - I_{min}}{I_{max} - I_{min}}$$

and the corresponding reduced wavelength and temperature.

VI - VARIATIONS OF LINE PROFILES ASSOCIATED WITH NON-PROPAGATING OSCILLATIONS

Let us now examine the variations of the Ca II and Mg II resonance line profiles emerging from the freely oscillating atmospheres defined by the experiments a) and c) of § III. The profiles were calculated between 1600 and 2590 seconds, and thus begin 100 seconds after the end of the excitation phase. Figure 7a shows the whole sequence of Mg II profiles corresponding to the large amplitude oscillations. The intensities are varying with a quasi-periodicity of about 200 seconds, as expected: the maximum corresponding to the minimum of the altitude (the pressure and the temperature of the gas then reach their maxima). At this minimum altitude point, the velocity changes quickly, the gas moving downwards before beginning to move upwards. For such general, one-dimensional motions, the decrease of density with altitude produces an increase of the velocity amplitude. If the gas moves downwards, the formation region of k3 is shifted to the red with respect to the underlying emitting layers, which results in a blue asymmetry. Conversely, a similar upward motion produces a red asymmetry. Changes of a blue to a red asymmetry associated with maxima of intensity may be seen on Figure 7a around sequence numbers 169, 191, 209, 229 and 248. We obtain similar results with other experiments. Figures 7b, c and d show the last 20 sequences, corresponding approximately to a cycle, for large amplitude oscillations (Mg II and Ca II), and small oscillations

(Mg II). 7b and c show that the oscillations are practically in phase in Mg II and Ca II, the change of asymmetry occurring between sequence numbers 248 and 249 in each case. This contrasts with the result obtained for a pulse propagation. Another feature visible on Figure 7c is the presence of profiles with a single peak (sequences 243 to 245) which are associated with large velocity gradients and relatively low chromospheric emission. Profiles of this kind occur frequently on the Sun. One may notice that both singly-peaked and doubly-peaked profiles are explained by the same theory of line formation without difficulty. (Nevertheless, we must recognize that singly-peaked profiles are less frequent in our computations than in the observations ; this might certainly be modified through adjustments in the initial model atmosphere).

Applying the same method of least square fit to the peaks and reversal as in the preceding section, we obtain the variations of intensities shown on Figure 8a and b for the large and small amplitude oscillations, respectively. In the case of large amplitude, the variations of intensity are sharply peaked, with positive excursions reaching an order of magnitude, while the variations remain almost sinusoidal in the other case. (One should notice that the variation of k3 is in phase with that of the average of the two peaks).

As seen above, an important property of non-propagating oscillations is that velocities and temperatures vary in quadrature. As the temperatures are approximately in phase throughout the chromosphere, and thus the intensities, we obtain a similar

phase difference between the intensity and the Doppler shift of k3. This is shown in Figure 9 which represents these two quantities in reduced form : one may see that the instants of maximum acceleration correspond approximately to the extrema of the intensity.

In data analyses, it is a current practice to use the Fourier transform for the determination of phase shifts. The results of such an analysis for the variations of shift and intensity in k3, are summarized in Figure 10 : the power spectra of the shift and the intensity have a peak at 5 mHz, as expected, and several harmonics (the harmonic at 10 mHz is particularly strong in the case of the intensity). The phase difference between the components of the Doppler shift and intensity is close to 90° for the frequencies corresponding to the fundamental and the first harmonic, in accordance with the direct comparison of the parameters in Figure 9.

In Figure 11, we compare the Mg II k profile emitted by a "mean atmosphere" -obtained by averaging the physical parameters (temperature, density, velocity) over the 100 sequences- with the average of the 100 profiles of the sequence. The first aim of this comparison is to investigate the effects of non-linear averaging of the intensities which is expected to be important for the ultraviolet spectrum. This effect appears clearly for the average intensity which is about 25% higher in the peaks than that emitted by the average atmosphere. Another aim is to try to explain discrepancies between the observed profiles and those computed from static atmospheres.

As a general feature, observed Mg II k profiles have broader peaks and less deep central reversals than the calculated ones. From that point of view, the motion-averaged profile of figure 11 is far more satisfying than the static profile. Another puzzling feature is the average blue asymmetry of the observed profiles. Although our motion-averaged profile has a blue peak slightly higher than the red one, the difference is small and does not compare well with the observations. In our one-dimensional scheme, the addition of a mean downflow would be required to explain the observed average asymmetry. Nevertheless, many effects, arising in particular from multi-dimensional hydrodynamics and radiative transfer, remain to be investigated before concluding in favour of the reality of such a downflow. The formation process of the peaks and reversal appears when one examines the contribution functions, defined as in § V (Figure 12). The atmosphere undergoes a series of short, high temperature, contraction phases and long, low temperature exapansion phases. The central reversals are formed, approximately, at a constant lagrangian altitude (Figures 12d and e) with sharp intensity maxima in the neighborhood of the minimum altitude times. As was the case for the pulse propagation studied above, the regions of formation of the k2 peaks move over a range of lagrangian altitudes of about 1000 km. During the "cool" expansion phase, the maximum contribution for both peaks is located in the low chromosphere (around 1000 km for Mg II K) (Figure 12b). As one gets closer to the maximum contraction phase, the region of formation of the blue peak moves upwards with

increasing intensities (Figure 12a). At t' is point, the intensity in the blue peak decreases rapidly and a red peak appears in the high chromosphere, close to the formation region of the k3 reversal (Figure 12c). Then, the region of formation of this red peak moves downwards with decreasing intensities, wh' :h is the beginning of a new expansion phase. As in the pulse propagation experiment (§V), the central reversal is formed in a narrow range of quasi-constant lagrangian altitudes and thus produces a good correlation between the Doppler shift of these reversals and the velocity in the corresponding layers. This is valid for Ca II as well as for Mg II, which gives a diagnostic tool to determine the velocities at two different altitudes and thus discriminate propagating from non-propagating waves. As seen in § V, the k3 intensity diagnostic :· not so easy to use : although some general correlation exists between temperature and intensity, the latter is the resu.t of a non-local transfer process and thus depends on both temperatures and densities throughout a wide range of altitudes. The fact that the oscillatory motions are in phase throughout this range gives rise to a good correlation, which however is of very limited diagnostic value.

VII - CONCLUSION

We have constructed a time-dependent, one-dimensional model of the solar chromosphere satisfying radiative transfer (line profiles) and hydrodynamical (oscillation periods in the range 150 to 250 seconds) requirements. The aim of computing Ca II

REFERENCES

Argyros, J.D. and Mugglestone, D.,1971, *J. Quant. Spectrosc. Rad. Transf.*, 11, 1633.

Artzner, G.,Leibacher, J.W.,Vial, J.C.,Lemaire, P.,Gouttebroze, P. 1978, *Ap. J.*, 224, L83.

Athay, R.G. and White, O.R., 1979, *Ap. J. Suppl.*, 39, 333.

Avrett, E.H., 1977, in "*The Solar Output and its Variations*" p. 327 (Ed. by O.R. White; Colorado Ass. Univ. Press : Boulder)

Ayres, T.R. and Linsky, J.L., 1976, *Ap. J.*, 205, 874.

Ayres, T.R., 1977, *Ap. J.*, 213, 296.

Baker, N.,Temesvary, S., 1966, *Tables of Convective Stellar Envelope Models*, (2nd ed. ; NASA Institute for Space Studies, New-York).

Beckers, J.M. and Artzner, G., 1974, *Solar Phys.*, 37, 309.

Bonnet, R.M.,Lemaire, P.,Vial, J.C.,Artzner, G.,Gouttebroze, P., Jouchoux, A.,Leibacher, J.W.,Skumanich, A. and Vidal-Madjar, A., 1978, *Ap. J.*, 221, 1032.

Chipman, E.G., 1977, *Solar Phys.*, 55, 277.

Chipman, E.G., 1978, *Ap. J.*, 224, 671.

Cram, L.E., 1974, *Sol. Phys.*, 37, 75.

Cram, L.E., 1976, *Astr. Ap.*, 50, 263.

Durrant, C.J.,Grossmann-Doerth, U. and Kneer, F.J., *Astr. Ap.*, 51, 95.

Gingerich, O.,Noyes, R.W.,Kalkofen, W. and Cuny, Y., 1971, *Solar Phys.*, 18, 347.

and Mg II line profiles was twofold : first, to describe the effects of different kinds of motions (pulse propagation and free oscillations) on the profiles and characterize their differences ; secondly, to check the reliability of the diagnostic tools used to analyze these lines. We concluded that the measurement of the Doppler shifts of the central reversals is a reliable means to determine the velocities in some atmospheric layers, while a much more careful treatment is needed to interpret intensity variations. We plan to continue this study of the chromospheric dynamics, first, by comparing the present results to sequences of observed Mg II k and Ca II K profiles ; then, by extending the computations to continua and other lines, especially the Lyman lines of hydrogen, and optically thin lines formed in the high chromosphere and transition region.

We wish to thank G. Artzner, R.M. Bonnet, J.P. Delaboudinière, P. Lemaire, D.T. Roethig, R.F. Stein, R.N. Thomas and J.C. Vial for useful discussions. The Centre National d'Etudes Spatiales computer was used for numerical calculations. Program development and analysis of the results utilized the computer facilities of the LPARL Space Astronomy Group. One of us (J.W.L.) wishes to acknowledge support by NASA contracts NAS W-3053 and NAS 8- 32356 , as well as the Lockheed Independent Research Fund.

Gouttebroze, P., 1977, (G 77), *Astr. Ap.*, 54, 203.

Heasley, J.N., 1975, *Solar Phys.*, 44, 275.

Jensen, E. and Orrall, F.Q., 1963, *Ap. J.*, 138, 252.

Kneer, F. and Nakagawa, Y., 1976, *Astr. Ap.*, 47, 65.

Leibacher, J.W., 1971, Ph. D. Thesis, Harvard University.

Leibacher, J.W., Gouttebroze, P., and Stein, R.F., 1979, (Paper I), *Ap. J.* (submitted).

Lites, B.W. Shine, R.A. and Chipman, E.G., 1978, *Ap. J.*, 222, 333.

Liu, S.Y., 1974, *Ap. J.*, 189, 359.

Mihalas, D., Shine, R.A., Kunasz, P.B. and Hummer, D.G., 1976 *Ap. J.*, 205, 492.

Noerdlinger, P.D. and Rybicki, G.B., 1974, *Ap. J.*, 193, 651.

Shine, R.A. and Linsky, J.L., 1974, *Solar Phys.*, 39, 49.

Vernazza, J.E., Avrett, E.H. and Loeser, R., 1973, *Ap. J.*, 184, 605.

Vernazza, J.E., Avrett, E.H. and Loeser, R., 1976, *Ap. J. Suppl.* 30, 1.

White, O.R. and Athay, R.G., 1979a, *Ap. J. Suppl.*, 39, 317.

White, O.R. and Athay, R.G., 1979b, *Ap. J. Suppl.*, 39, 347.

Wilson, P.R. and Evans, C.D., 1971, *Solar Phys.*, 18, 29.

PIERRE GOUTTEBROZE : Laboratoire de Physique Stellaire et
Planétaire, boîte postale 10, 91370 Verrières-le-Buisson, France
JOHN W. LEIBACHER : Lockheed Palo Alto Research Laboratory,
3251 Hanover Street, Palo Alto, California 94304, U.S.A.

TABLE 1

INITIAL ATMOSPHERIC PARAMETERS

m (g/cm^2)	T (K)	v_T (km/s)	h (km)	N_H (cm^{-3})	N_e/N_H
7.90 (-6)	1 000 000	8.0	2 745	6.83 (+8)	1.20
7.95 (-6)	1 000 000	7.9	2 438	6.88 (+8)	1.20
8.05 (-6)	316 000	7.7	2 076	2.19 (+9)	1.20
8.08 (-6)	158 000	7.6	2 035	4.37 (+9)	1.20
8.10 (-6)	79 400	7.6	2 021	8.60 (+9)	1.20
8.12 (-6)	39 800	7.5	2 014	1.68 (+10)	1.20
8.18 (-6)	20 000	7.4	2 003	3.42 (+10)	1.05
8.40 (-6)	19 000	7.0	1 977	3.73 (+10)	1.04
8.80 (-6)	17 800	6.2	1 935	4.28 (+10)	1.02
8.85 (-6)	12 600	6.1	1 931	6.18 (+10)	9.12 (-1)
8.90 (-6)	9 000	6.0	1 928	9.04 (+10)	7.37 (-1)
1.00 (-5)	7 410	5.9	1 884	1.26 (+11)	6.41 (-1)
1.26 (-5)	6 790	5.7	1 812	1.83 (+11)	5.14 (-1)
1.58 (-5)	6 640	5.5	1 749	2.50 (+11)	4.03 (-1)
2.51 (-5)	6 520	5.1	1 635	4.60 (+11)	2.23 (-1)
3.98 (-5)	6 430	4.7	1 536	8.15 (+11)	1.19 (-1)
1.00 (-4)	6 310	4.0	1 359	2.33 (+12)	3.76 (-2)
2.51 (-4)	6 190	3.3	1 200	6.39 (+12)	1.45 (-2)
6.31 (-4)	6 030	2.5	1 054	1.74 (+13)	6.92 (-3)
1.58 (-3)	5 780	1.8	920	4.73 (+13)	2.93 (-3)
3.98 (-3)	5 370	1.0	797	1.32 (+14)	8.65 (-4)
1.00 (-2)	4 920	1.0	686	3.63 (+14)	2.57 (-4)
2.51 (-2)	4 570	1.0	582	9.78 (+14)	1.48 (-4)
5.01 (-2)	4 510	1.0	508	1.98 (+15)	1.32 (-4)

1.00 (-1)	4 500	1.0	435	3.96 (+15)	1.20 (-4)
2.00 (-1)	4 570	1.0	361	7.80 (+15)	1.14 (-4)
3.98 (-1)	4 740	1.0	285	1.50 (+16)	1.17 (-4)
1.00	5 040	1.0	179	3.54 (+16)	1.26 (-4)
2.51	5 570	1.0	64	8.05 (+16)	1.70 (-4)
3.98	6 170	1.0	0	1.15 (+17)	3.63 (-4)
5.01	6 920	1.0	- 35	1.30 (+17)	1.24 (-3)
6.31	8 320	1.0	- 77	1.35 (+17)	8.91 (-3)
7.94	9 550	1.0	- 125	1.45 (+17)	3.17 (-2)
1.00 (+1)	10 300	1.0	- 181	1.66 (+17)	5.65 (-2)
1.58 (+1)	11 500	1.0	- 306	2.24 (+17)	1.14 (-1)
2.51 (+1)	12 700	1.0	- 455	3.03 (+17)	1.92 (-1)
3.98 (+1)	13 700	1.0	- 626	4.24 (+17)	2.59 (-1)
6.31 (+1)	14 700	1.0	- 819	5.98 (+17)	3.25 (-1)
1.00 (+2)	15 800	1.0	- 1 036	8.40 (+17)	3.97 (-1)
1.58 (+2)	16 900	1.0	- 1 278	1.19 (+18)	4.59 (-1)
2.51 (+2)	18 100	1.0	- 1 550	1.70 (+18)	5.19 (-1)
3.98 (+2)	19 400	1.0	- 1 851	2.44 (+18)	5.75 (-1)

FIGURE CAPTIONS

Figure 1

Normalized velocities and temperatures as functions of time (seconds) for 15 selected lagrangian altitudes (kilometers) indicated at the left of the figure. The extrema of the velocities are written in the right side.

a) propagation of a pulse ;

b) large amplitude oscillations ;

c) small amplitude oscillations.

Figure 2

Time sequence of line profiles, computed every 10 seconds, during the passage of a pulse through the atmosphere. The sequence n° 21 corresponds to t = 200 seconds.

a) Mg II k line ;

b) Ca II K line.

(in abscissa : relative wavelength in angströms).

Figure 3

Time variations of intensities in the Mg II k line (time in seconds, intensity in erg $s^{-1}cm^{-2}sr^{-1}Hz^{-1}$).

Square symbols : central reversal (k3). Triangles : blue peak (k2V). Crosses : red peak (k2R).

Figure 4

Comparison of time variations of the position of the central reversal, converted into velocity (squares) with the velocity of the slab corresponding to an optical depth unity at line center (velocities in km/s).

a) Mg II k ;

b) Ca II K.

Figure 5

Mg II contribution functions versus eulerian altitude (in km) for 20 time sequences (pulse propagation).

a) k3 (the dots correspond to constant lagrangian altitudes) ;

b) k2 (solid line : blue peak, dotted line : red peak).

The contribution functions are shown to 1% of their peak value.

Figure 6

Time variations of reduced Mg II k3, intensity (squares), Doppler shift (triangles) and reduced temperature (crosses) in the k3 formation slab (pulse propagation).

Figure 7

Sequences of line profiles during chromospheric oscillations, separated by 10 seconds. Sequence n° 161 corresponds to t = 1600 seconds.

a) and b) large amplitude oscillations and Mg II k line ;

c) large amplitude oscillations and Ca II K line.

Figure 8

Time variation of Mg II k line intensities in the k3 reversal (squares), k2V (triangles) and k2R (crosses) peaks.

a) large amplitude oscillations ;

b) small amplitude osccillations.

Figure 9

Reduced intensity (squares) and wavelength (triangles) versus time for the Mg II k3 reversal (large amplitude oscillations).

Figure 10

Fourier transform of the time variations of Doppler shifts and intensity of Mg II k3 (large amplitude oscillations). Squares : power spectrum for Doppler shifts (arbitrary units) ; triangles : power spectrum of intensity ; crosses : phase difference between Doppler shift and intensity components (degrees).

Figure 11

Comparison of time-averaged profi the Mg II k line (squares) with the profile corresponding to the average atmosphere (triangles) (intensities in erg $s^{-1}cm^{-2}sr^{-1}Hz^{-1}$, wavelength in anstroms) (large amplitude oscillations).

Figure 12

Time sequences of contribution functions versus eulerian altitude in kilometers (large amplitude oscillations). The dots indicate constant lagrangian altitudes.

a) Mg II k2V ;

b) same as a) normalized at each time to show more clearly the low chromospheric contribution which dominates the "quiet" profile ;

c) Mg II k2R ;

d) Mg II k3 ;

e) Ca II K3.

FIG. 1a

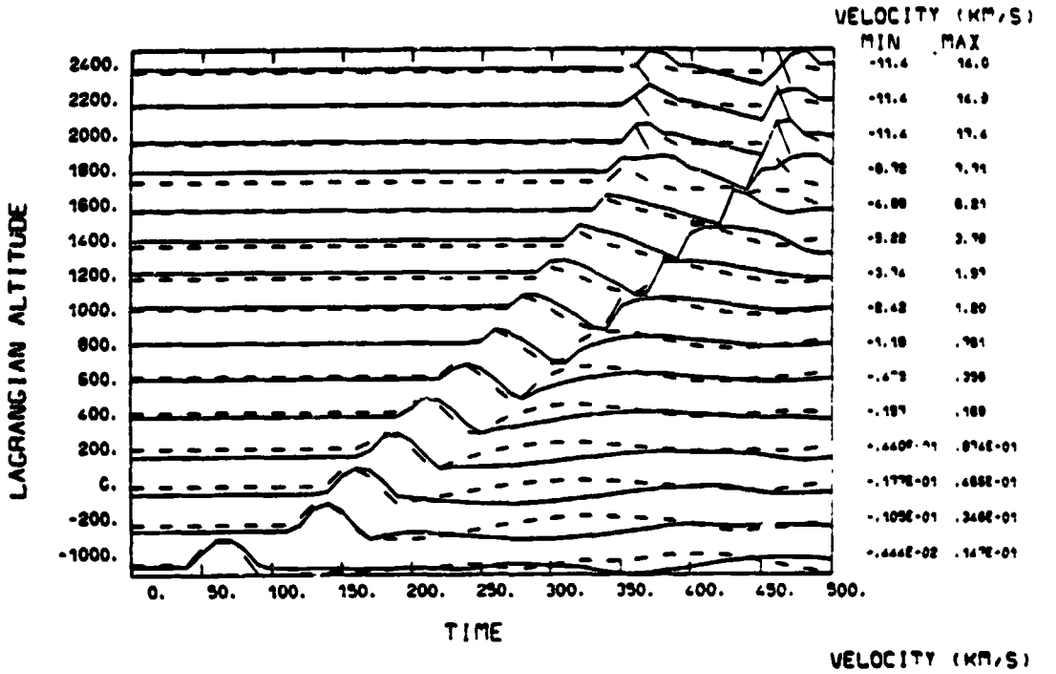
VELOCITY (KM/S)
MIN MAX
LAGRANGIAN ALTITUDE
2400.
2200.
2000.
1800.
1600.
1400.
1200.
1000.
800.
600.
400.
200.
0.
-200.
-1000.
0. 50. 100. 150. 200. 250. 300. 350. 400. 450. 500.
TIME

1b

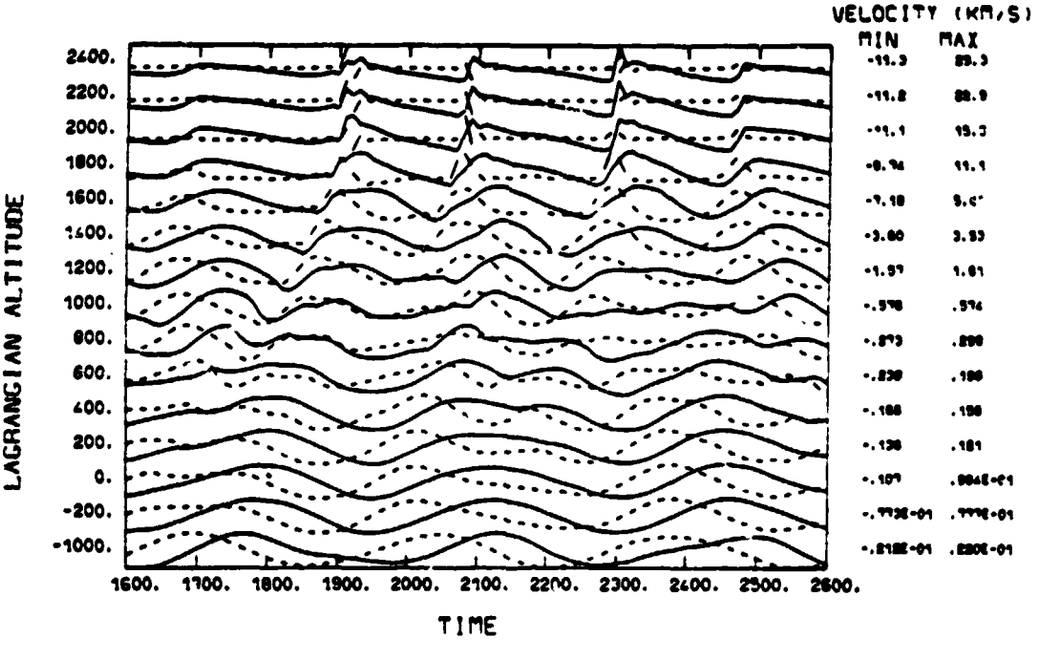
VELOCITY (KM/S)
MIN MAX
LAGRANGIAN ALTITUDE
2400.
2200.
2000.
1800.
1600.
1400.
1200.
1000.
800.
600.
400.
200.
0.
-200.
-1000.
1600. 1700. 1800. 1900. 2000. 2100. 2200. 2300. 2400. 2500. 2600.
TIME

1c

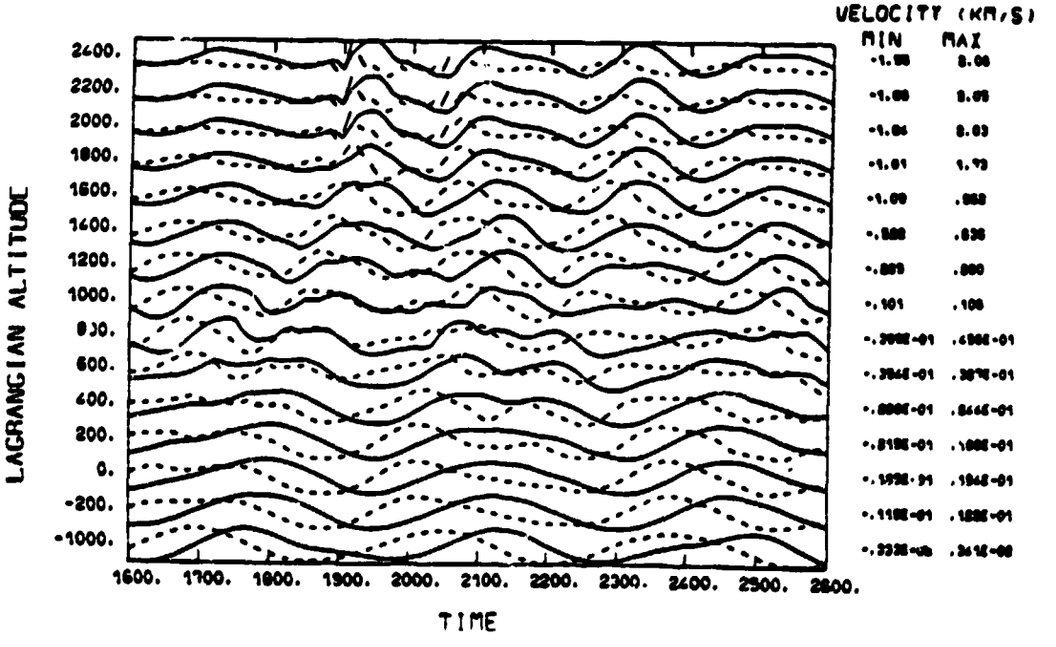
VELOCITY (KM/S)
MIN MAX
LAGRANGIAN ALTITUDE
2400.
2200.
2000.
1800.
1600.
1400.
1200.
1000.
800.
600.
400.
200.
0.
-200.
-1000.
1600. 1700. 1800. 1900. 2000. 2100. 2200. 2300. 2400. 2500. 2600.
TIME

FIG. 2 a

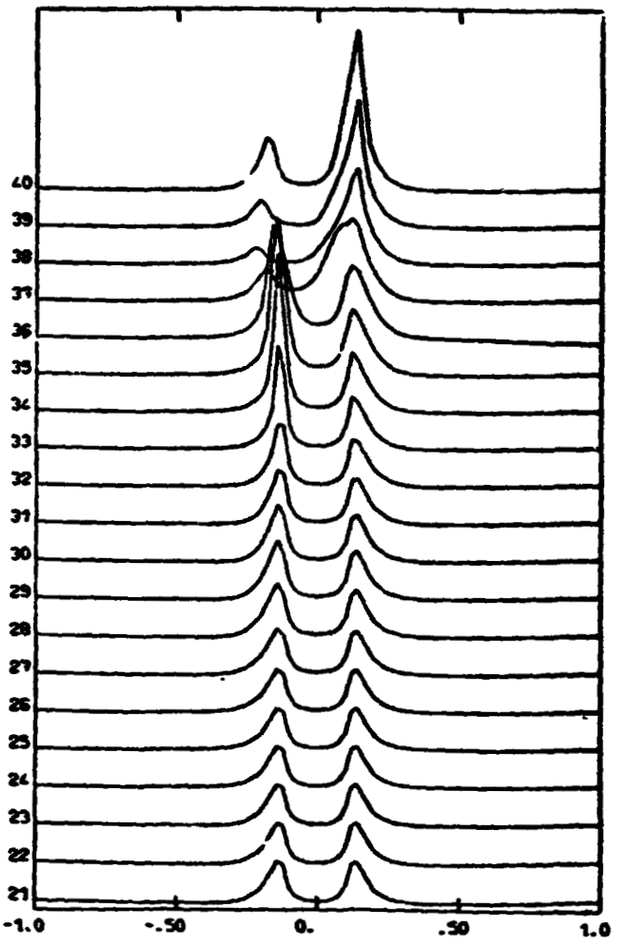
40
39
38
37
36
35
34
33
32
31
30
29
28
27
26
25
24
23
22
21
-1.0
-.50
0.
.50
1.0

2 b

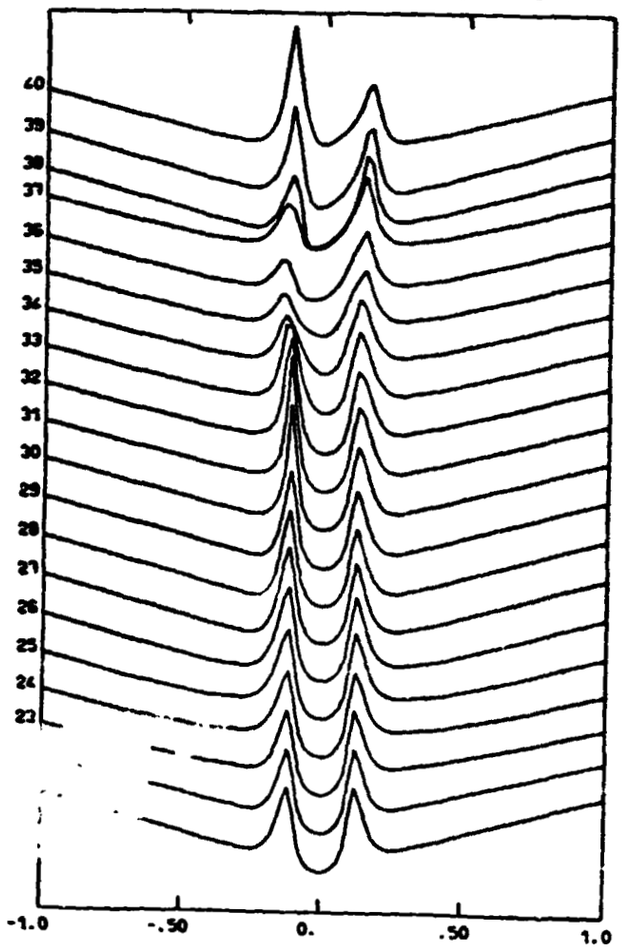
40
39
38
37
36
35
34
33
32
31
30
29
28
27
26
25
24
23
-1.0
-.50
0.
.50
1.0

FIG. 3

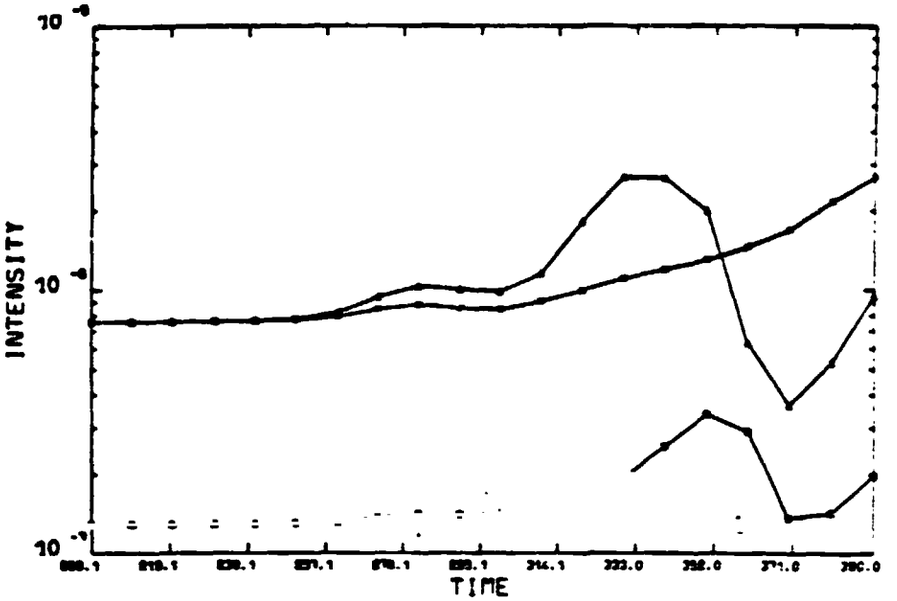

FIG. 4a

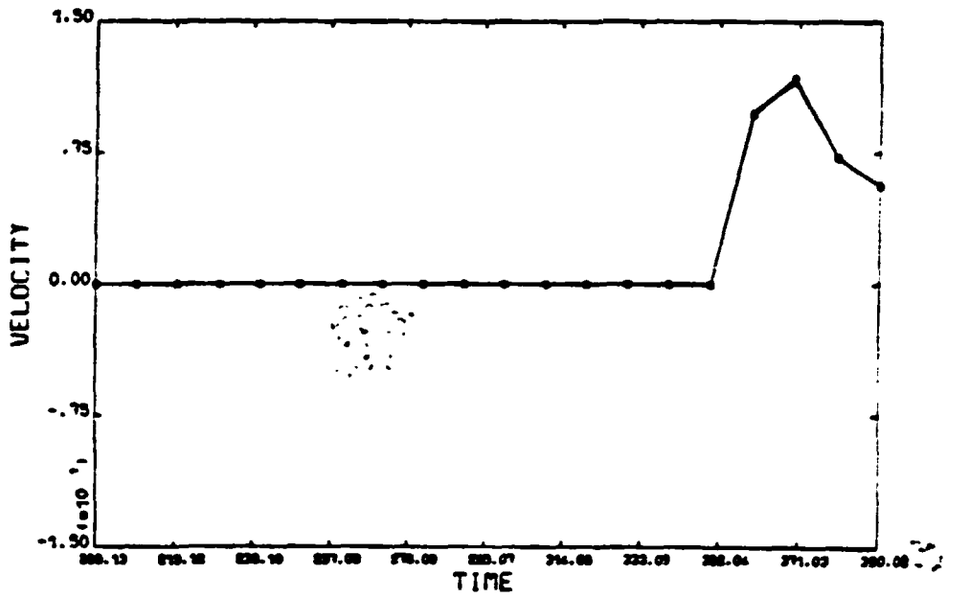

4b

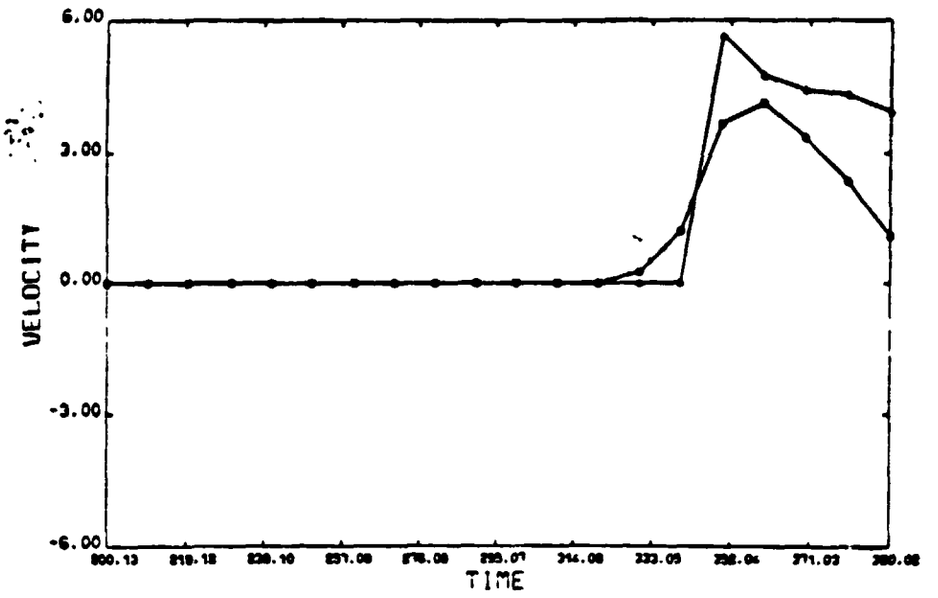

FIG. 5 a

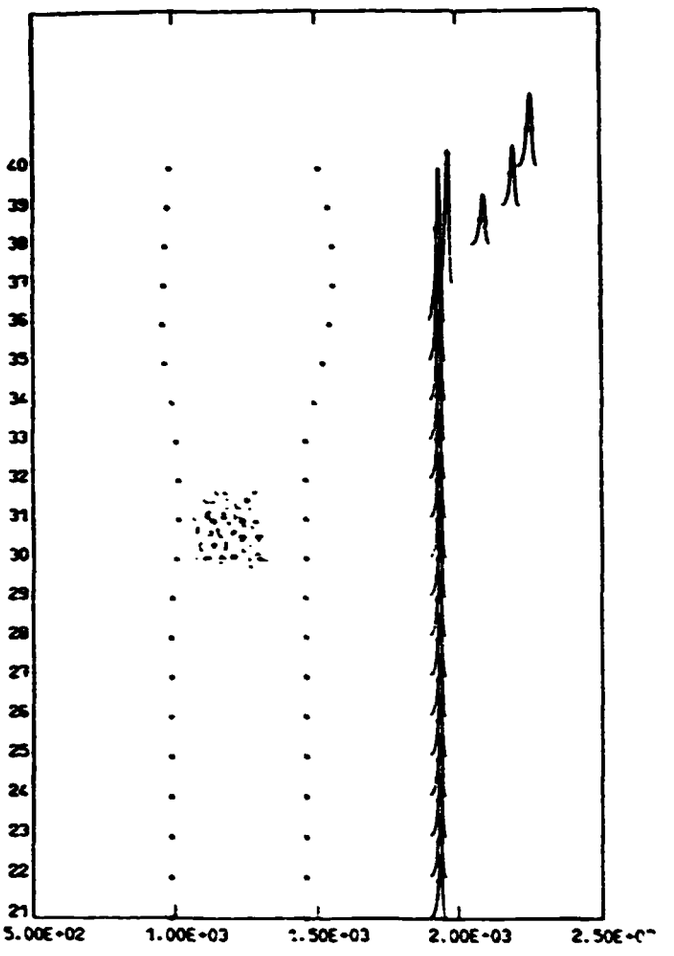
40
39
38
37
36
35
34
33
32
31
30
29
28
27
26
25
24
23
22
21
5.00E+02
1.00E+03
1.50E+03
2.00E+03

5 b

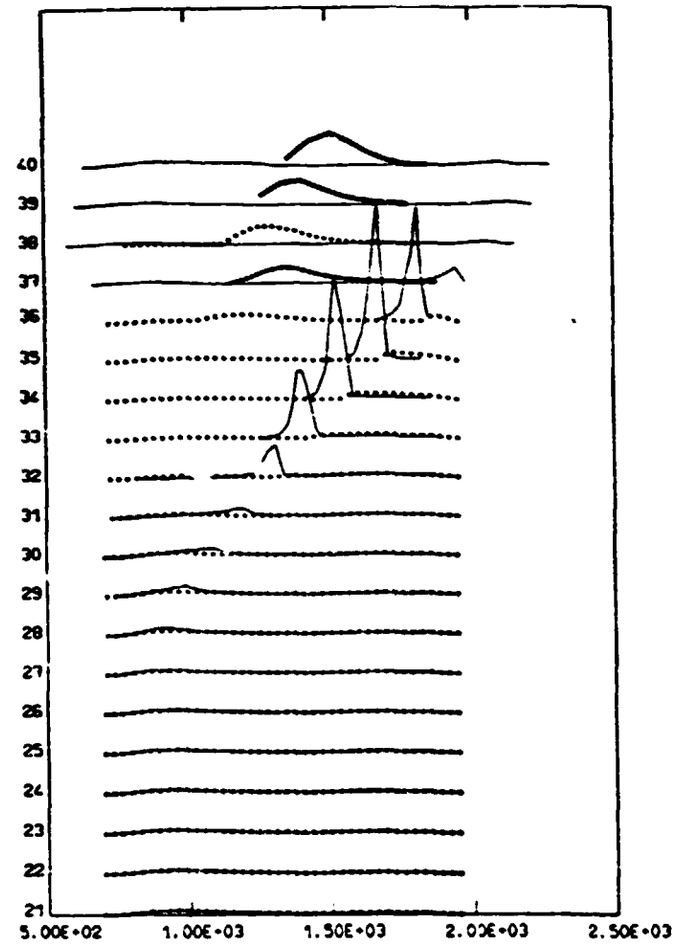
40
39
38
37
36
35
34
33
32
31
30
29
28
27
26
25
24
23
22
21
5.00E+02
1.00E+03
1.50E+03
2.00E+03
2.50E+03

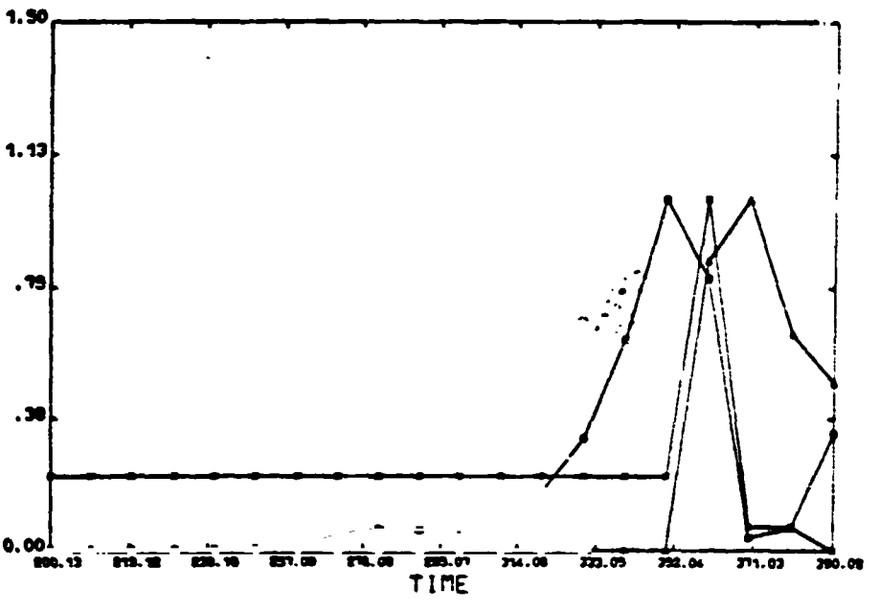

FIG. 6

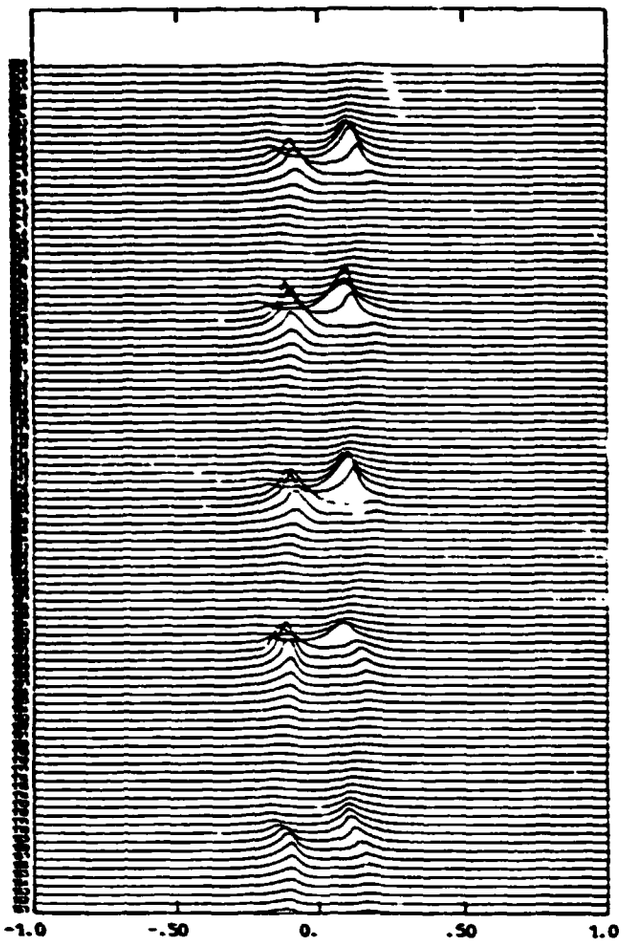
-1.0
-.50
0.
.50
1.0

FIG. 7a

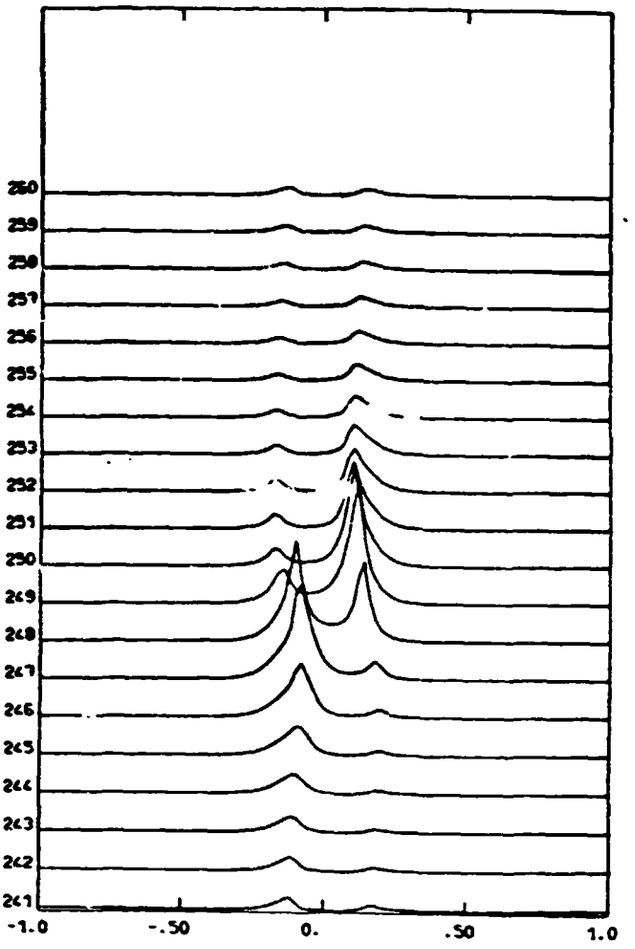
260
259
258
257
256
255
254
253
252
251
250
249
248
247
246
245
244
243
242
241
-1.0
-.50
0.
.50
1.0

7b

7c

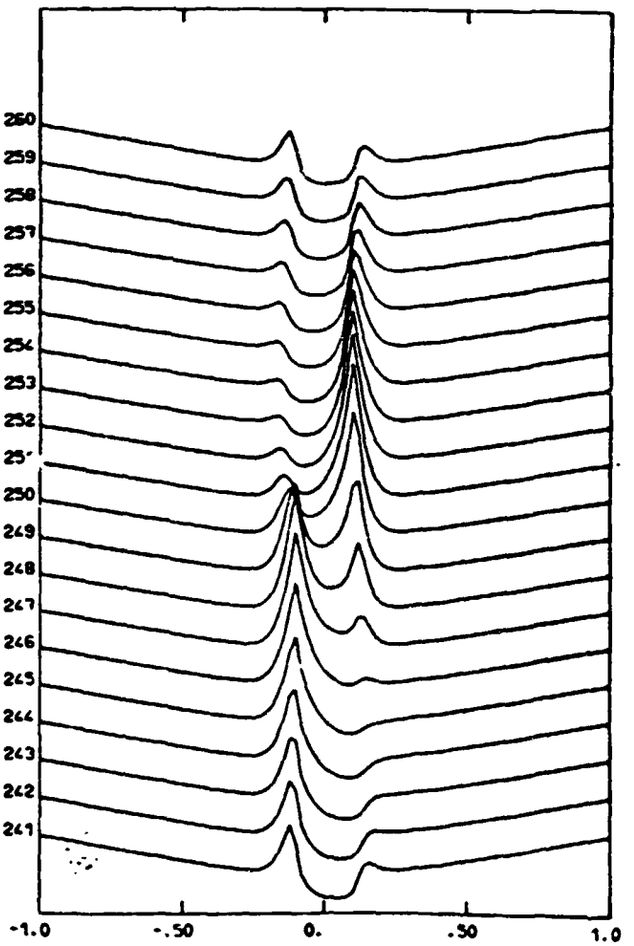
260
259
258
257
256
255
254
253
252
250
249
248
247
246
245
244
243
242
241
-1.0
-.50
0.
.50
1.0

FIG. 8a

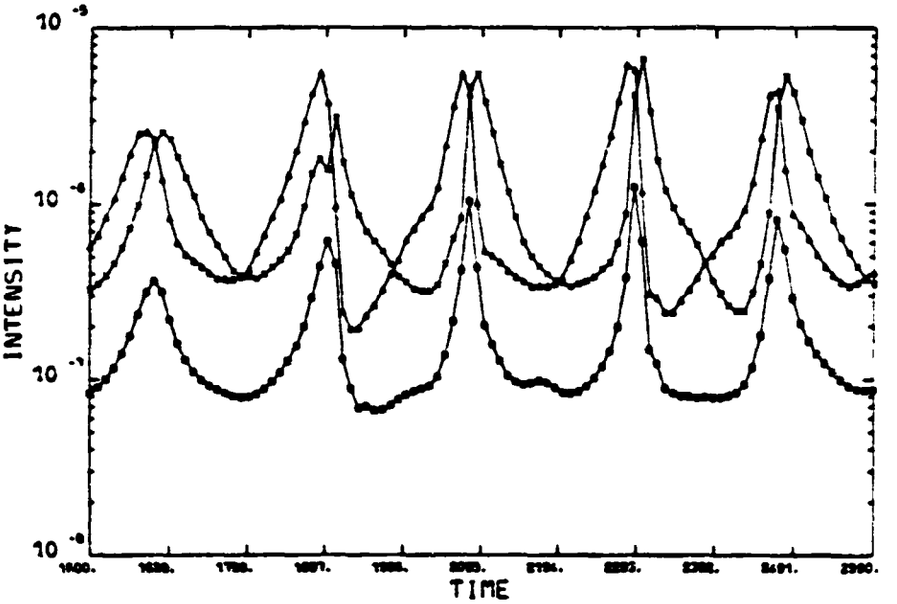

8b

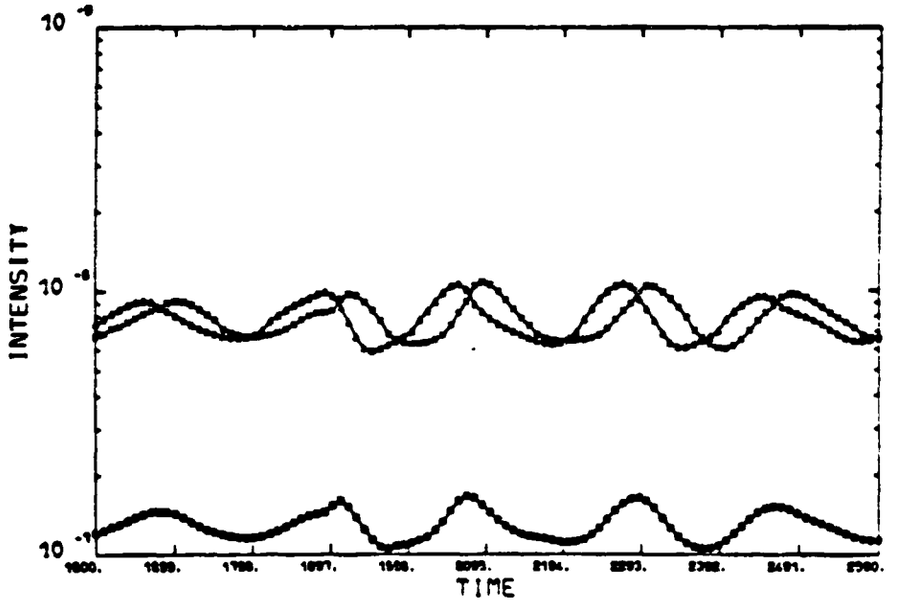

energy to the corona away from active regions and its dissipation there, has become increasingly attractive. While it is tempting to consider coronal models that are scaled down analogs of flare models where energy is released gradually, we should recall that it has been the requirement of rapid energy release that has driven the search for flare mechanisms, and that processes which are too slow to describe flares, and have been discarded, may be relevant for the quasi-steady heating of the corona.

Although we are not discussing generation mechanisms here, we should point out that the observed fields are roughly in equipartition with the kinetic energy density at the top of the convection zone (Deckers and Weiss, 1978). The seed field for amplification by the convective motions presumably results from the dynamo interaction between rotation and convection in deeper layers. Thus, the magnetic field associated heating will vary with the spindown time of a star, which in general will be unrelated to the evolutionary time scale determined by nucleosynthesis.

In the convection zone β (= gas pressure/magnetic pressure) is large and convective velocities move the magnetic lines of force with little resistance. Magnetic fields provide (at least) three broad mechanisms for transmitting energy from the convection zone to the corona: 1) waves propagating along lines of force, 2) currents induced in the corona by waves, twists and motions of the magnetic foot points, and 3) emerging flux carrying stored energy upwards. Dissipation of magnetic energy occurs primarily as the dissipation of induced currents. Alfven waves, where the magnetic energy is in the form of Alfven waves, viscous damping and wave mode coupling also occur.

Alfven Waves

The field may serve (more or less passively) as a medium for transmitting the shaking or twisting of field lines (Wentzel, 1978; Uchida and Kaburaki, 1974; Hollweg, 1980). Twisting or jiggling of a magnetic line of force can be produced directly by convective motions or by thermal over-stability in the convectively unstable layer. The disturbance will then propagate away as a wave, or if slow enough, as a quasi-static change in the field. Several magneto-acoustic-gravity wave modes exist. One can understand the essence of magnetic waves by considering only Alfven waves. Their restoring force is magnetic tension, so they act like waves on a string—the magnetic field line—with motion transverse to the field. The temperature, density, pressure and magnetic field strength ($B_0 + \zeta B$) are constant. Energy propagates along the field at the Alfven speed

$$a = B/\sqrt{4\pi\rho}.$$

Because of its density dependence, the Alfven speed increases by a factor of 10^3 between the photosphere and the corona, so that substantial reflection of Alfven waves will occur. Since the magnetic field in the corona is inhomogeneous, the internal Alfven waves will be slightly modified and propagate as surface waves with the average

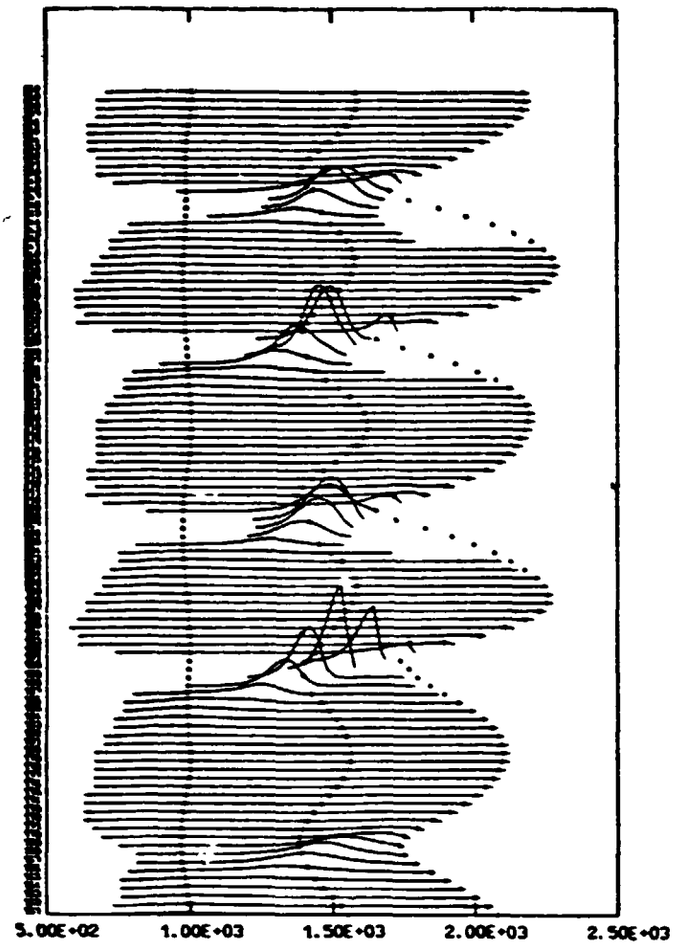

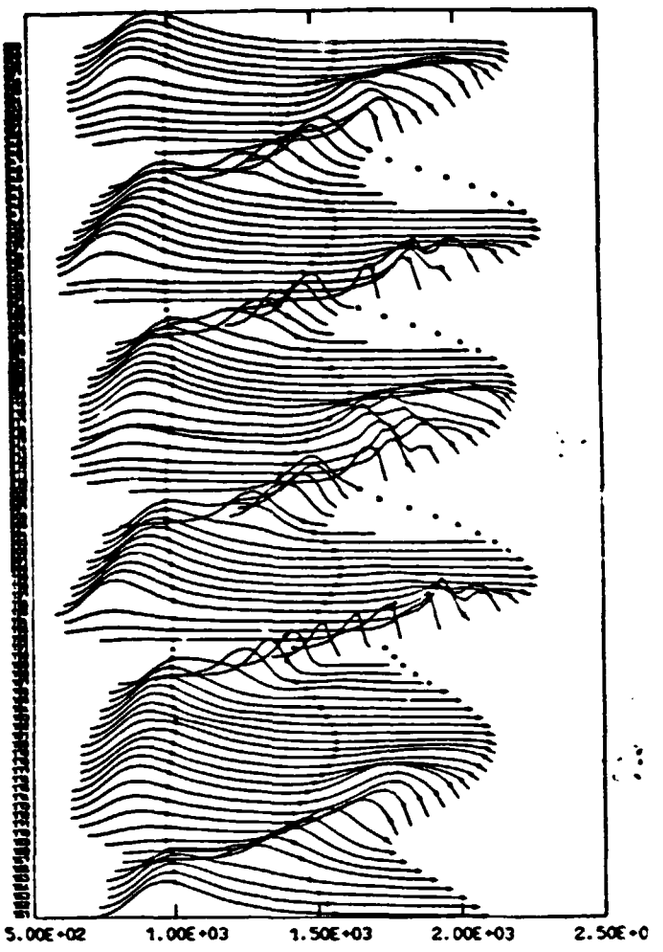

FIG. 12a

12b

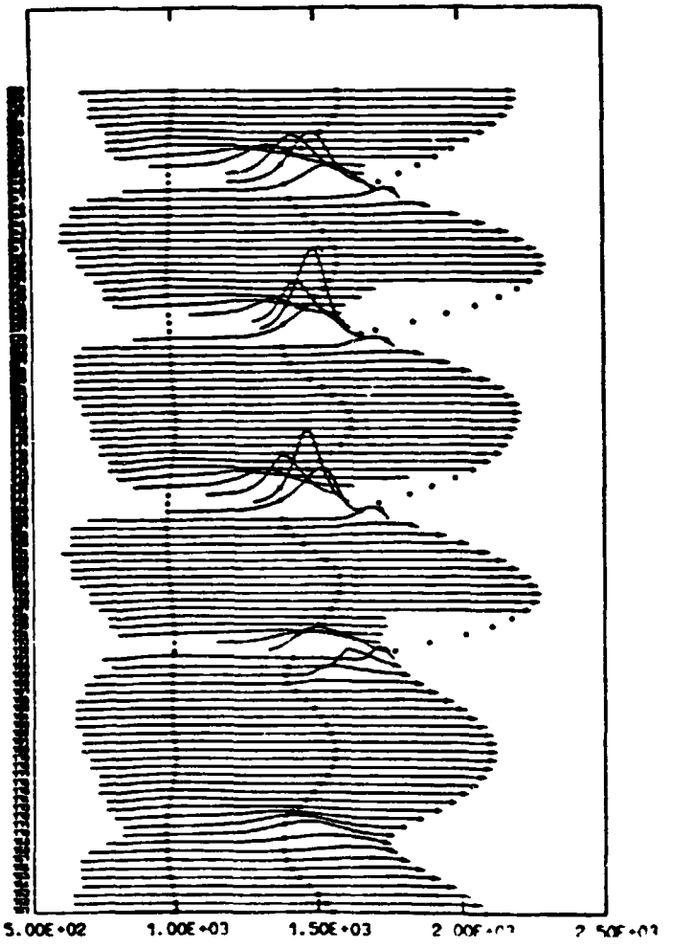

12c

FIG. 12 d

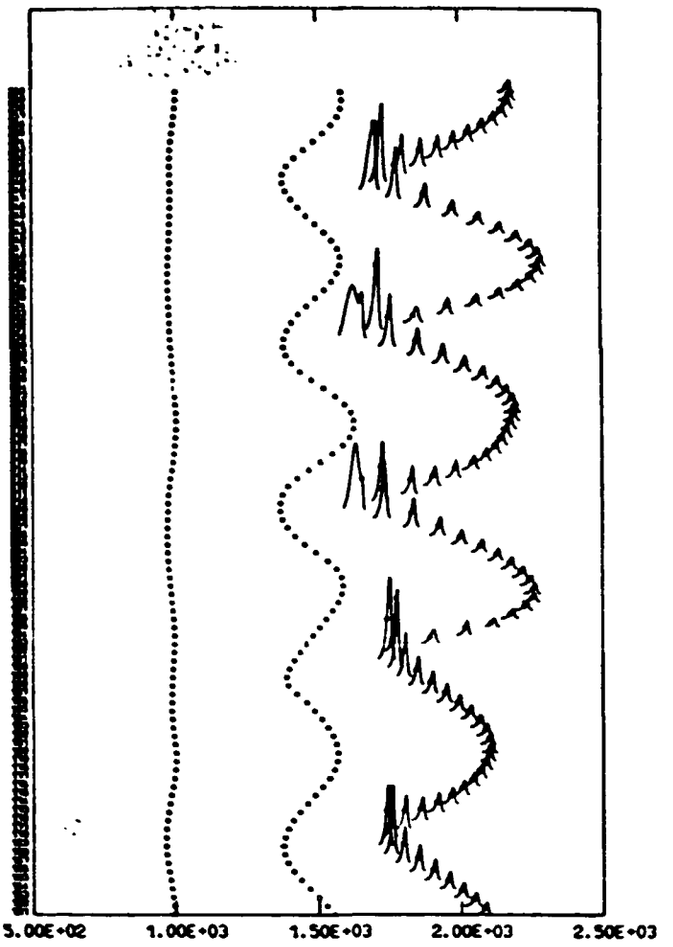
5.00E+02
1.00E+03
1.50E+03
2.00E+03
2.50E+03

12 e

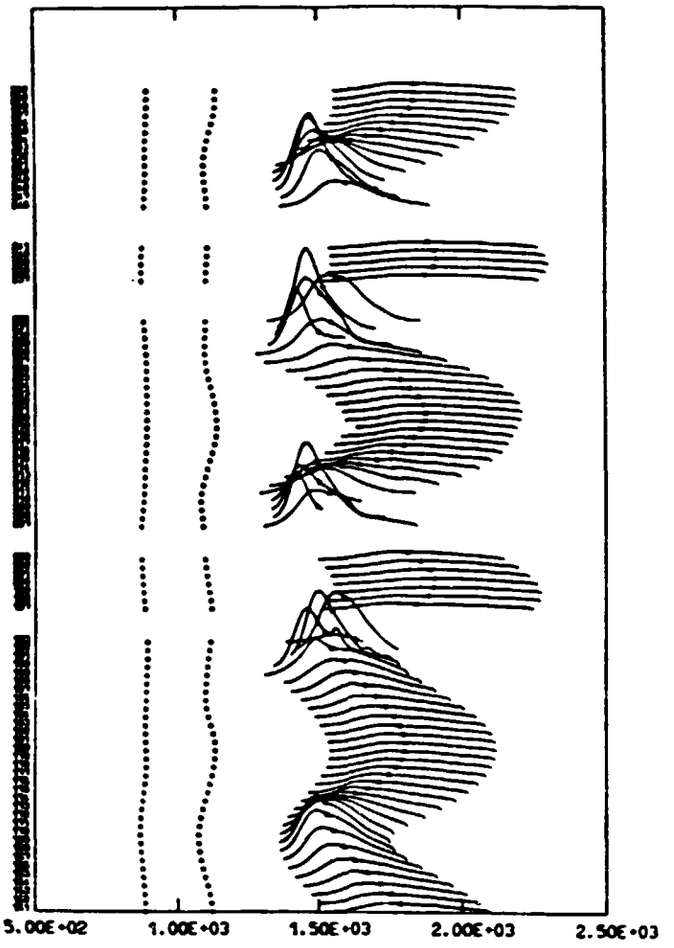
5.00E+02
1.00E+03
1.50E+03
2.00E+03
2.50E+03

ATTACHMENT G

SMALL SCALE DISSIPATIVE PROCESSES IN STELLAR ATMOSPHERES

J. W. Leibacher
Space Astronomy Group
Lockheed Palo Alto Research Laboratory
Palo Alto, California

R. F. Stein
Department of Astronomy and Astrophysics
Michigan State University
East Lansing, Michigan

ABSTRACT

The outer atmospheres of stars must be heated by some non-thermal energy flux to produce chromospheres and coronae. We discuss processes which convert the non-thermal energy flux of organized, macroscopic motions into random, microscopic (thermal) motions. Recent advances in our description of the chromosphere velocity field suggest that the acoustic waves observed there transmit very little energy, and hence are probably incapable of heating the upper chromosphere and corona. The apparent failure of this long held mechanism and the growing appreciation of the importance of strong magnetic fields in the chromosphere and corona have led to hypotheses of heating by the dissipation of currents (both oscillatory and quasi-steady). This follows discoveries in laboratory and ionospheric plasmas and work on solar flares, that instabilities can concentrate currents into thin high current density filaments where they dissipate rapidly.

INTRODUCTION

The major advances in understanding the Sun and other stars during the second half of this century have resulted from our appreciation of violations of the paradigm: stellar structure (both interior and atmospheric) is determined by thermal energy transport (i.e., radiation, convection and to a much lesser extent conduction). It now appears that the outer atmospheres of virtually all stars are substantially hotter than radiative equilibrium would have predicted and that stellar winds are important energy losses for the outer atmosphere. The conventional wisdom has become: a thermodynamic engine converts internal, thermal energy (maintained by thermal energy transport) to external, macroscopic energy which then propagates, or is transported, with little interaction with the material through which it propagates, upwards into the corona. Generally, production of propagating energy is not very efficient, $\leq 10^{-3}$. However, where the bulk of the total outward energy flux escapes from the star, i.e., within the outer several

photon mean free paths, the macroscopic energy now represents a substantial proportion of the energy density, and dissipation of this energy can substantially change the temperature structure. In addition, the mechanical energy density directly contributes to the momentum balance, and hence structure, of the overlying atmosphere. Dissipation of the macroscopic energy results from microscopic processes (viscosity, conductivity and resistivity) which reduce gradients and increase random internal motions; i.e., increase entropy. By dissipation, we understand the ultimate transformation of macroscopic, organized energy to microscopic disorganized ones, and we don't discuss the transformation of one propagation mode to another, which "dissipates" the mode, but not the non-thermal energy.

We shall discuss the wave modes (acoustic, internal gravity and Alfven) which have been considered, and the role they appear to play in the Sun, as well as the less fully studied hypothesis of heating by current dissipation. We do not discuss the generation of this propagation energy here, and the reader is referred to Stein and Leibacher (1979, 1980).

Finally, we should point out that the identification of the various candidates for propagating the required non-thermal energy flux has proceeded from observations of the time dependent, horizontally inhomogeneous structure of the Sun. The Sun is where we learn the physics to understand the stars. On the other hand, the variation of non-thermal heating with stellar type provides a stringent test for all generation, propagation and dissipation theories. We should note several recent reviews of heating mechanisms: Cram (1977), Cram and Ulmschneider (1978), Rosner, Tucker and Vaiana (1978)—particularly the Appendix—and Wentzel (1978).

ACOUSTIC (PRESSURE) WAVES

Propagating pressure fluctuations were the first non-radiative flux suggested to account for the corona's high temperature. These steepen to form discontinuities due to the dependence of their propagation speed on temperature: the upwardly moving, hotter part of the wave propagates faster than the downwardly moving cooler part. The steepening is accelerated in a stellar atmosphere, since the wave amplitude increases as the density decreases, to keep the energy flux constant in the absence of dissipation and refraction. When the steepening progresses to the point that the wave changes appreciably over a collision mean-free-path, diffusion (viscosity and conductivity) acts against further steepening, converting the organized motion of the wave into thermal motions, and a shock wave is said to exist. In stellar coronae, the high thermal conductivity of the hot plasma is generally more important than viscosity. As the pressure jump across the wave increases, the dissipation (or entropy increase) grows very rapidly: initially as the third power of the pressure jump. It is important to note that it is the sharp gradient, or discontinuity, produced by the wave which produces the dissipation;

the existence of large velocities (comparable with the sound speed) is not sufficient. In particular, long period vertical motions will raise and lower the atmosphere more or less in phase, with the velocity varying exponentially—not sinusoidally with height—and even at large amplitudes "phase" is not propagated vertically. Radiative exchange (losses from hot, compressed gas and gains by the cool, rarefied gas) also will dissipate the flux of an acoustic wave.

Short period waves (10 - 100 seconds), created by turbulent motions in the convection zone, should be capable of providing the heating required near and immediately above the temperature minimum (Ulmschneider, Schmitz, Kalkofen and Bohn 1978, and references therein). However, they rapidly dissipate their energy and do not appear capable of any heating higher up. These waves lose a very substantial part of their energy by radiative damping in the photosphere before forming shock waves. Thus, the flux available for heating is a small number which is the difference of two large numbers (the generation and radiative damping), a situation which amplifies numerical as well as physical uncertainties.

Although the dissipation of these waves is fairly well understood, the total power emitted and its temporal spectrum remains uncertain. Extrapolations to other stars have been suggested (Renzini, Cacciari, Ulmschneider and Schmitz, 1976), but the predicted, very rapid increase in the chromospheric emission with luminosity for solar type stars does not appear to occur (Linsky and Ayres, 1979). Short period waves remain "unobservable" because their wavelengths are comparable to the widths of the regions emitting the spectral lines used as diagnostics, however they do contribute to the non-thermal width of spectral lines.

Longer period acoustic waves are seen as spatially resolved displacements of photospheric and chromospheric lines. Theory and observation have achieved rare agreement in the description of the "five minute oscillations" as acoustic waves trapped within certain ranges of temperature (Leibacher, 1977; Zirker, 1979). These standing waves transmit virtually no energy: neither in the cavity where upward and downward propagating waves, of equal flux, interfere constructively, nor outside the reflecting boundaries of the cavity where the mode may continue to exist by "tunneling" as an evanescent wave. Thus, although the velocity amplitudes may be substantial, since pressure and velocity vary nearly in quadrature, little energy would be propagated. In addition, since there is no vertical phase propagation, the large vertical gradients required for diffusive dissipation do not occur.

The radiative losses of the upper chromosphere and corona appear to exceed the most optimistic estimates of the acoustic flux (Athay and White, 1978; Bruner, 1979): assuming that the total non-thermal width of chromospheric lines is due to acoustic waves propagating upwards at the maximum possible energy propagation (group) velocity. For other stars, the situation is likely to be similar: short period waves lose a majority of their flux by radiation and dissipate the

remainder in a relatively short distance. Longer period waves develop substantial amplitudes only if they are trapped, and propagate little energy.

INTERNAL GRAVITY (BUOYANCY) WAVES

Buoyancy restoring forces, in a convectively stable atmosphere, will drive predominantly horizontal motions known as internal gravity waves (IGW). These waves are abundant in the earth's atmosphere, and will be generated by slow motions, such as penetrative convection, and velocity shear, such as that associated with the variation of the super-granulation velocity with altitude. Because of their short vertical wavelengths, they are not prominent in the observed macroscopic motions of the Sun, but they presumably make a significant contribution to the unresolved, "microscopic" velocity field. Dissipation through ordinary viscosity and conductivity will occur, and as they propagate upwards and their amplitude grows, the waves will "break" and produce shorter wavelength IGW turbulence along their fronts—like whitecaps. Large amplitude waves can drive mean flows, and conversely IGW's can be absorbed by a steady flow whose velocity equals the wave's phase velocity. The wave energy goes into the mean flow, and it is not dissipated in the sense of returning to thermal energy. Radiative damping tends to make a wave isothermal, which destroys the buoyancy driving force, and hence is particularly effective in dissipating IGW's.

The energy propagation speed for IGW's is $\leq$ the sound speed, so the arguments of Athay and White (1978) for the energy flux carried if the excess line broadening were all taken as propagating mechanical energy, also apply for IGW's. However, because their velocity is primarily horizontal, only a small part of their amplitude contributes to line broadening at disk center.

MAGNETIC FIELDS (CURRENTS)

Recent observations have vastly increased our appreciation of the importance of magnetic fields on the Sun, and hence other stars. Strong fields have been found away from active regions: the super-granulation network consists of strong (greater than 1000 gauss), concentrated (less than a magameter horizontal extent) fields, and flux emerges at all latitudes. X-ray observations indicate that the corona consists almost entirely of filamentary and loop structures which have been identified as magnetic flux tubes. The role of magnetic fields in heating solar and stellar flares has long been known, as has their importance in maintaining the enhanced emission of active regions. While the important physical processes are becoming clearer, we are still far from an accepted model for these phenomena (Spicer and Brown, 1980). Nonetheless, as the difference between a spherically symmetric, one dimensional chromosphere or corona and reality becomes more obvious, the idea that the magnetic field plays an essential role in the transport of mechanical

energy to the corona away from active regions and its dissipation there, has become increasingly attractive. While it is tempting to consider coronal models that are scaled down analogs of flare models where energy is released gradually, we should recall that it has been the requirement of rapid energy release that has driven the search for flare mechanisms, and that processes which are too slow to describe flares, and have been discarded, may be relevant for the quasi-steady heating of the corona.

Although we are not discussing generation mechanisms here, we should point out that the observed fields are roughly in equipartition with the kinetic energy density at the top of the convection zone (Peckover and Weiss, 1978). The seed field for amplification by the convective motions presumably results from the dynamo interaction between rotation and convection in deeper layers. Thus, the magnetic field associated heating will vary with the spindown time of a star, which in general will be unrelated to the evolutionary time scale determined by nucleosynthesis.

In the convection zone β (= gas pressure/magnetic pressure) is large and convective velocities move the magnetic lines of force with little resistance. Magnetic fields provide (at least) three broad mechanisms for transmitting energy from the convection zone to the corona: 1) waves propagating along lines of force, 2) currents induced in the corona by waves, twists and motions of the magnetic foot points, and 3) emerging flux carrying stored energy upwards. Dissipation of magnetic energy occurs primarily as the dissipation of induced currents. Although, where the magnetic energy is in the form of Alfven waves, viscous damping and wave mode coupling also occur.

Alfven Waves

The field may serve (more or less passively) as a medium for transmitting the shaking or twisting of field lines (Wentzel, 1976; Uchida and Kaburaki, 1974; Hollweg, 1980). Twisting or jiggling of a magnetic line of force can be produced directly by convective motions or by thermal over-stability in the convectively unstable layer. The disturbance will then propagate away as a wave, or if slow enough, as a quasi-static change in the field. Several magneto-acoustic-gravity wave modes exist. One can understand the essence of magnetic waves by considering only Alfven waves. Their restoring force is magnetic tension, so they act like waves on a string—the magnetic field line—with motion transverse to the field. The temperature, density, pressure and magnetic field strength ($\underset{\sim}{B}_0 + \underset{\sim}{\delta B}$) are constant. Energy propagates along the field at the Alfven speed

$$a = B/\sqrt{4\pi\rho}.$$

Because of its density dependence, the Alfven speed increases by a factor of 10^3 between the photosphere and the corona, so that substantial reflection of Alfven waves will occur. Since the magnetic field in the corona is inhomogeneous, the internal Alfven waves will be slightly modified and propagate as surface waves with the average

Alfven speed. Where the local Alfven speed equals this average Alfven speed a resonance occurs, at which the transverse velocity and electric field become large.

The Alfven speed is independent of Alfven wave amplitude, since the density and magnetic field remain constant. Hence, Alfven waves do not steepen and shock. However, they can dissipate by microscopic processes (viscosity and resistivity). The damping lengths for both viscous and Joule heating increase as the cube of the magnetic field and the square of the wave period.

Viscous damping is more important than Joule heating in the corona and vice versa in the photosphere and chromosphere. In the corona the problem is turned around. The damping lengths are so long that dissipation is very small and attention has focussed on coupling to other modes which dissipate more rapidly. Surface Alfven waves have very large amplitudes at their resonant point, so most of their energy will be dissipated by Joule and viscous dissipation in the thin resonant layer. The damping rate is determined by the rate at which energy can propagate into the resonant layer. Mode coupling occurs when the Alfven wave amplitude becomes large, and a compressible, sound wave is formed which can dissipate efficiencly (Derby, 1978). Coupling also occurs in the presence of inhomogeneities, by producing an uncertainty in the wave number, of the order of the reciprocal of the inhomogeneity scale size. For two waves of the same frequency and wavenumbers differing by Δk, the coupling will be of order

$$1/L|\Delta k| \quad \text{(Melrose, 1974).}$$

In particular, Alfven waves propagating nearly along the field can couple efficiently to fast mode waves.

Current Dissipation

Slow motions of the magnetic foot points in the convection zone may force flux tubes against one another in the corona, which will induce currents between them perpendicular to the field direction. If the magnetic fields are oppositely directed, a neutral sheet will be produced. Buffeting of magnetic flux tubes in the photosphere by granule and supergranule motions will produce twists and Alfven waves which propagate up into the corona and induce currents there. Emerging magnetic fields may also carry energy stored as twists ($\underline{J} \times \underline{B} \neq 0$) up into the corona, where β is small. Any unbalanced magnetic force ($\underline{J} \times \underline{B}$) will cause the tube to move and relax (Parker, 1974). Field aligned currents can remain in the relaxed coronal flux tube (Parker, 1974; Hollweg, 1980).

Current or magnetic field dissipation is a diffusive process due to single or collective particle collisions. The heating rate is $Q = \eta J^2$, where J is the current density and η is the resistivity. The characteristic resistive diffusion time scale is $\tau_R = 4\pi L^2/\eta c^2$.

For typical coronal parameters $\tau_R \sim 10^4$ yrs; too long to be significant. This Joule dissipation time can be reduced either by reducing the width L of the region through which the currents flow or by increasing the resistivity by increasing the effective collision rate. To get significant current dissipation by any mechanism, the dissipation must occur in such small volumes that the transfer of the resulting heat to the rest of the corona is a serious problem.

Tearing Instability

The size of the current region can be reduced by the tearing instability in a sheared magnetic field. Parallel currents attract one another and tend to clump. The clumping of current produces a fluid flow that forces the sheared magnetic field into X-type neutral points Filamented currents are produced with small enough length scales so that the classical Coulomb collision resistive diffusion time becomes small and the magnetic field can tear and reconnect, and the currents can dissipate (Drake and Lee, 1977; Bateman, 1978, chapter 10).

This mechanism has been invoked for the violent energy release in flares. (See Spicer and Brown, 1980.) However, short wavelength tearing modes release less energy than the long wavelength instability thought to occur in flares, and so may produce a more tranquil heating appropriate for coronal flux tubes. The shorter wavelength modes distort the field lines more, which produces a greater restoring force, and also have a smaller volume of magnetic energy they can release. The tearing instability has a lower threshold than the current driven instabilities which lead to anomalous resistivity (discussed below).

Thermal Instability

Thermal instabilities can also reduce the size of the current region by producing current filamentation, because Coulomb resistivity decreases with increasing temperature. Hence, Joule heating will increase the temperature, which reduces the resistivity, which increases the current density, which leads to enhanced heating. Current filaments parallel to $\underset{\sim}{B}$ result. This instability can act as a trigger for other instabilities.

Anamolous Resistivity

When the current density, $J = n_e e V_{drift}$, becomes large enough that the drift velocity approaches the electron thermal velocity, then substantial numbers of electrons will tend to run away and generate several different types of electrostatic waves. These waves bunch the ions, so that the electrons collide with the electric field of a large collective charge rather than that of a single ion. This scattering of electrons by the waves increases the effective collision rate, the rate of momentum transfer and hence the resistivity. The enhanced resistivity due to electron scattering by plasma waves is called "anomalous resistivity", and since it occurs in conjunction with current filamentation

will shorten the resistive diffusion time tremendously (Papadopolous, 1977; Roesner, Golub, Coppi and Vaiana, 1978).

CONCLUSIONS

Short period acoustic waves (period < acoustic cut-off period) still appear to be the most satisfactory mechanism for heating the low chromosphere. These waves shock before reaching the corona, so increasing their flux only increases the temperature of the low chromosphere. Longer period waves are trapped by temperature gradients, and although their amplitudes can increase by constructive interference, they transmit little energy.

Internal gravity waves are probably present in stellar atmospheres, and while they may be important dynamically (line broadening, acceleration of steady flows), they probably do not contribute directly to heating.

Magnetic fields have recently received a great deal of interest, largely as a result of the discovery of very strong fields and the inhomogeneous structure of the corona. Progress has proceeded by invoking mechanisms previously considered for solar active regions and flares: Alfven waves dissipating motions excited by convective buffeting of flux tubes, anomalous resistivity dissipating field aligned currents induced by twisting of the field in and below the photosphere, and reconnection of field lines in regions of strong field gradients produced by the flux tube twisting and relative motions of different flux tubes.

For the new, magnetic field associated heating mechanisms, even more than the older, wave heating mechanism, small spatial structures are of fundamental importance and we must rely on solar observations and theory to lead the way to applications to other stars.

J. W. Leibacher would like to acknowledge support by NASA Contracts NASw-3053 and NAS5-23758, as well as the Lockheed Independent Research Fund. R. F. Stein acknowledges support by Air Force Contract F 19628-77-C-0068, NASA grant NSG-7293 and NSF grant AST-76-22479.

References

1. Athay, R. G. and White, O. R.: 1978, Astrophys. J. 226, pp. 1135: *Chromospheric and Coronal Heating by Sound Waves.*

2. Bateman, G.:1978, "MHD Instabilities" (Cambridge:MIT)

3. Bruner, E. C.:1977, Astrophys. J. 226, pp. 1140-1146: *Dynamics of the Solar Transition Zone.*

4. Cram, L. E.:1977, Aston. Astrophys. 59, pp. 151-159: *On the Heating of the Solar Chromosphere.*

5. Cram, L. E and Ulmschneider, P.: 1978, Astron. Astrophys 62, pp. 239: *Observational Tests of the Shock Heating Theory for Late-Type Stellar Chromospheres.*

6. Derby, N. F.: 1978, Astrophys. J. 224, pp. 1013: *Modulational Instability of Finite Amplitude Circularly Polarized Alfven Waves.*

7. Drake, J. F. and Lee, Y. C. 1977, Phys. Fluids, 20, pp. 1341: *Kinetic Theory of Tearing Instabilities.*

8. Hollweg, J. V. 1980, in "Proceedings of the Skylab Active Region Workshop", F. Q. Orral, Ed., Preprint: *Mechanisms of Energy Supply.*

9. Leibacher, J. W. 1977, in "Proc. OSO-8 Workshop", E. Hansen and S. Schaffner (Eds.), Boulder, Colorado, pp. 311-339: *Theoretical Aspects of the 300 Second and Related Oscillations of the Solar Atmosphere.*

10. Linsky, J. L. and Ayres, T. R. 1978, Astrophys. J. 220, pp. 619: *Stellar Model Chromospheres. VI. Empirical Estimates of the Chromospheric Radiative Losses of Late Type Stars.*

11. Melrose, D. B. 1977, Aust. J. Phys. 30, pp. 495-509: *Mode Coupling in the Solar Corona. III. Alfven and Magnetoacoustic Waves.*

12. Osterbrock, D. E. 1971, Astrophys. J. 134, pp. 347-388: *The Heating of the Solar Chromosphere, Plages and Corona by Magneto-hydrodynamic Waves.*

13. Papadopoulos, K. 1977, Rev. Geophys. and Spa. Phys. 15, pp. 113: *A Review of Anomalous Resistivity for the Ionosphere.*

14. Parker, E. N. 1974, Astrophys. J. 191, pp. 245-254: *The Dynamical Properties of Twisted Ropes of Magnetic Fields and the Nature of New Active Regions on the Sun.*

15. Peckover, R. S. and Weiss, N. O. 1978, Mon. Not. Roy. Astron. Soc. 182, pp. 189: *On the Dynamic Interaction Between Magnetic Fields and Convection.*

16. Renzini, A., Cacciari, C., Ulmschneider, P., and Schmitz, F. 1977, Astron. Astrophys. 61, pp. 39: *Theoretical Chromospheres of Late Type Stars. I. Acoustic Energy Generation.*

17. Rosner, R., Golub, L., Coppi, B., and Vaiana, G. S. 1978, Astrophys. J. 222, pp. 317: *Heating of Coronal Plasma by Anomalous Current Dissipation.*

18. Rosner, R., Tucker, W. H., and Vaiana, G. S. 1978, Astrophys. J. 220, pp. 643: *Dynamics of the Quiescent Solar Corona.*

19. Spicer, D. and Brown, J. C. 1980, in "The Sun as a Star", S. Jordan (Ed.), Preprint: *Solar Flare Theory: A Review.*

20. Stein, R. F., and Leibacher, J. W. 1974, Ann. Rev. Astron. Astrophys. 12, pp. 407-435: *Waves in the Solar Atmosphere*

21. Stein, R. F. and Leibacher, J. W. 1979, Proceedings of I.A.U. Colloquium 51 "Turbulence in Stars", D. Gray (Ed.), In press: *Mechanical Energy Transport.*

22. Stein, R. F. and Leibacher, J. W. 1980, in "The Sun as a Star", S. Jordan, Ed., In preparation: *Generation of Waves.*

23. Uchida, Y. and Kaburaki, O. 1974, Solar Phys. 35, pp. 451-466: *Excess Heating of Corona and Chromosphere above Magnetic Regions by Non-Linear Waves.*

24. Ulmschneider, P., Schmitz, F., Kalkofen, W. and Bohn, H. U. 1978, Astron. Astrophys. 70, pp. 787-800: *Acoustic Waves in the Solar Atmosphere. V. On the Chromospheric Temperature Plateau.*

25. Wentzel, D. G. 1978, Rev. Geophys. Spa. Sci. 16, pp. 757-761: *Heating of the Solar Corona.*

26. Zirker, J. B. 1979, Proceedings of the 17th Aerospace Sciences Meeting, New Orleans: *Solar Hydrodynamics.*

ATTACHMENT H

MECHANICAL ENERGY TRANSPORT

Robert F. Stein
Department of Astronomy and Astrophysics
Michigan State University
East Lansing, MI U.S.A.

and

John W. Leibacher
Space Astronomy Group
Lockheed Palo Alto Research Laboratory
Palo Alto, CA, U.S.A.

I. INTRODUCTION

Ladies and Gentlemen, we now reveal to you the secrets of how to create chaos out of order. The existence of a chromosphere or corona requires the existence of motions. A chromosphere or corona requires some non-radiative heat input. There has to be some kind of motion, either oscillatory or quasi-static, to transport the energy up to the chromosphere or corona. This ordered motion may be observed as chaos: microturbulence, macroturbulence, line asymmetries or shifts. Of course, it is necessary to actually compute the effects of motions on line profiles in order to see what will really happen.

We review the properties, generation and dissipation mechanisms of three kinds of waves: acoustic, gravity and Alfven waves. These are not the only kinds that can exist, but they will give you some idea of most of the range of wave properties, at least for the low frequency waves for which plasma effects are unimportant. They are pure cases. These different wave modes are distinguished by their different restoring force--pressure for acoustic waves, buoyancy for gravity waves, and magnetic tension for the Alfven waves. Their properties are summarized in Table I. From an observational viewpoint, the most important properties are the relation between temperature and density variations (which change the intensity) and fluid velocity (which shifts the line). Acoustic waves are compressive: In propagating waves the temperature and density vary in phase with the velocity, which is parallel to the energy flux. However, for standing or evanescent waves the temperature and density are 90° out of phase with the velocity. Gravity waves are slightly compressive: The temperature and density vary oppositely to each other and 90° out of phase with the velocity, which is parallel to the energy flux. Alfven waves are not compressive: The temperature, density, pressure and the total magnetic field strength remain constant and the motion is transverse to the energy flux. We will come back to these properties in more detail later.

There are basically two kinds of generation mechanisms: One is direct coupling from the convective motions to the wave motions, either inside the convection zone or penetrating into the photosphere; and the other is thermal overstability. There are only a few basic dissipation mechanisms also: Radiation can destroy the restoring force and damp a wave. The other major dissipation processes occur by collisions which diffuse momentum and energy, and produce viscosity, thermal conductivity, and resistivity. Sometimes, instabilities can clump the particles so that collisions occur with a large collective "particle" rather than an individual one. This increases the effective collision rate and enhances the diffusion of momentum and energy. These diffusive transport processes dissipate acoustic waves in shocks, gravity waves in shear layers, and Alfven waves by viscous or Joule heating.

II. ACOUSTIC WAVES

A. PROPERTIES

This material is well-known, so let us quickly run through the basics. As we said, the restoring force for acoustic waves is the pressure. The energy flux is

$$F = pu = \rho u^2 V_g,$$

and the group velocity is

$$V_g = s(1-N_{ac}^2/\omega^2)^{\frac{1}{2}},$$

where s is the sound speed. The acoustic cutoff frequency is

$$N_{ac} = s/2H = \gamma g/2s.$$

Acoustic energy propagation can occur only for $\omega > N_{ac}$ ($2\pi/200s$ for the sun). In the absence of dissipation or refraction the flux must be constant, and the sound speed is roughly constant throughout the photosphere and chromosphere and increases by a factor of 10 going up to the corona, hence the velocity amplitude will scale roughly as

$$u \propto \rho^{-\frac{1}{2}}.$$

Acoustic waves can propagate or be evanescent or standing. The essential difference is that propagating waves transport energy, but evanescent or standing waves don't. In propagating waves with vertical wavelength small compared to the scale height, the pressure, temperature and density vary in phase with the velocity:

$$\frac{\delta\rho}{\rho} = \frac{u}{s}, \quad \frac{\delta T}{T} = (\gamma-1)\frac{u}{s}, \quad \frac{\delta p}{p} = \gamma\frac{u}{s}.$$

In standing or evanescent waves although the pressure, temperature and density fluctuations are of the same order as in propagating waves, they vary 90 degrees out of phase with the velocity

$$\frac{\delta\rho}{\rho} = -i\frac{u}{s}, \quad \frac{\delta T}{T} = i(\gamma-1)\frac{u}{s}, \quad \frac{\delta p}{p} = -i(2-\gamma)\frac{u}{s}.$$

Since the energy flux is the average over a period of the pressure times the velocity, the average flux will be zero. Also the vertical phase velocity of evanescent waves will be infinite, so that the motions will be in phase all the way up and down through the atmosphere. Figure 1 shows a portion of the diagnostic diagram that Jacques Beckers showed yesterday, to remind you that the acoustic waves occur in the high frequency region. Later we will come to gravity waves, which occur in the low frequency region. (For more details, see Lighthill, 1978.)

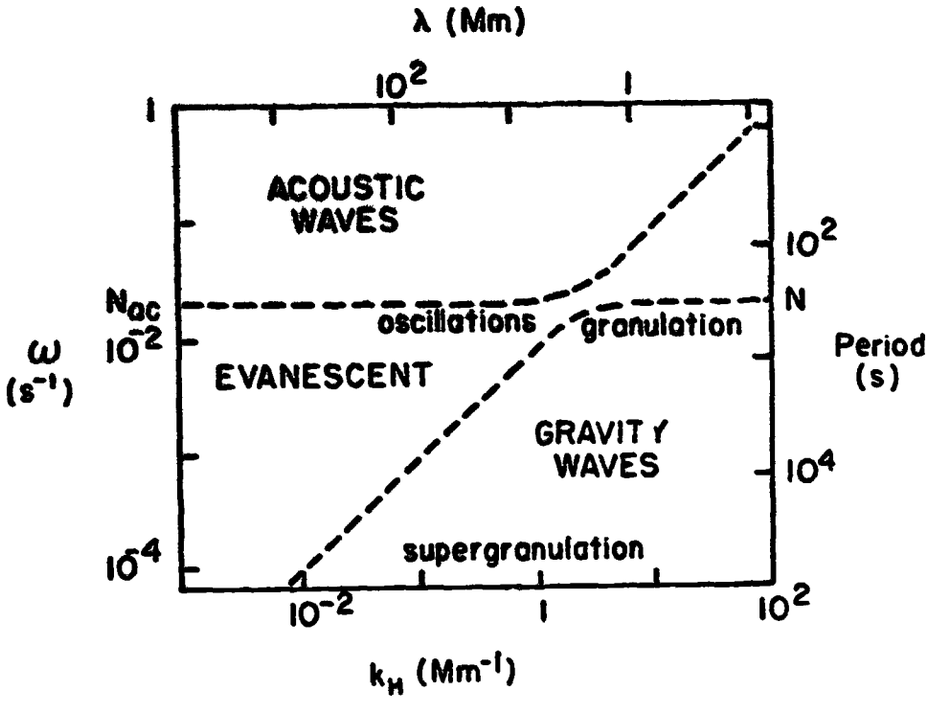

B. GENERATION

1. Direct Generation by Turbulent Motions

Acoustic waves may be generated directly by the turbulent convective motions. This is what is usually called the Lighthill mechanism. The radiated power is roughly the energy density in the turbulent motions divided by the time scale for the turbulent motions, times some efficiency factor. The turbulent energy density is ρu^2, the time scale is the eddy to turn over time, which is the length scale of the eddies divided by their velocity, $\tau = \ell/u$, and the efficiency factor is the wave number of the wave times the size of the eddy to some power, $(k\ell)^{2n+1}$.
Thus, the radiated power is

$$P \sim \frac{\rho u^3}{\ell} (k\ell)^{2n+1}.$$

The exponent n depends on the kind of emmission: If there is monopole emmission, which corresponds to a mass source, then n = 0; there is no mass source in the convection zone. If there is dipole emission, which corresponds to a momentum source, which corresponds to an external force, then n = 1; in a uniform medium there would be no external force and no dipole emission, but in stars there is an external gravitational field so there is some dipole emission. Finally, for quadruple emission, which corresponds to the action of the Reynolds stresses, n = 2, and that is the dominant process (Stein, 1967). For acoustic waves:

$$k = \omega/s \text{ and } \omega = \tau^{-1} = u/\ell,$$

so

$$k\ell = u/s = M,$$

the Mach number of the turbulent motions. What you get is the familiar result that the radiated power is proportional to the eighth power of the turbulent velocity:

$$P = \frac{\rho u^3}{\ell}\left(\frac{u}{s}\right)^5 \propto u^8.$$

The turbulent velocity that one chooses is very sensitive to the model that one takes for the turbulence, and therefore the emission is very uncertain. But if one makes some crude estimates for the sun,

$$\rho \sim 10^{-6},\ s \sim 10^6,\ u/s \sim 1/4,$$

then

$$F \sim P\ell \sim 10^7 \text{ ergs/cm}^2\text{s}.$$

One can also use mixing length theory to see how the flux will depend on stellar properties. From mixing length theory

$$u \sim \left(\frac{g}{T}\delta\right)^{1/2} \ell,$$

and

$$\Delta T \sim \beta\ell,$$

where

$$\beta = -\left[dT/dz - (dT/dz)_{AD}\right]$$

is the superadiabatic temperature gradient. Hence

$$F \sim \rho c_p \Delta T u \sim \rho c_p (g/T)^{1/2} \beta^{3/2} \ell^2,$$

so

$$u \sim \left(\frac{gF\ell}{\rho c_p T}\right)^{1/3}.$$

From hydrostatic equilibrium

$$\rho \propto \frac{P}{T} = \frac{g}{\kappa T}.$$

Assume $$\kappa \propto P^{0.7} T^{10} \propto g^{0.41} T^{5.88},$$

then $$F \sim \frac{\rho u^8}{s^5} \propto g^{-1} T_{eff}^{17}.$$

This means that the flux decreases very rapidly as you come down the main sequence, and increases rapidly as you go up to the giants and the supergiants. There are some problems with this. Linsky and co-workers find that the MgII flux is a good measure of the chromospheric emission and they claim that the ratio of the MgII flux to the total flux of the star is independent of g, which is contrary to what the Lighthill mechanism predicts (Basri and Linsky, 1979). Also if you look at the cool main sequence stars you find that the predicted flux is much less than the scaled chromospheric losses. The predicted wave flux may be increased by including effects of molecular hydrogen on the specific heats and the adiabatic gradient. Just how much is not known. Ulmschneider and Bohn are working on that now. But as of the moment there is still over an order of magnitude discrepancy in those results (Schmitz and Ulmschneider, 1979).

The turbulent motions may also directly excite the "five-minute" oscillation. In a steady state the amplitude of a given mode will be determined by the balance between turbulent generation by the Lighthill mechanism and dissipation by turbulent viscosity (Goldreich and Keeley, 1977):

$$\frac{\rho u_\lambda^3}{\lambda} (k\lambda)^5 = \nu k^2 \epsilon_k,$$

where

$$\nu = u_\lambda \lambda.$$

Hence, the energy density of an oscillation mode k will be

$$\epsilon_k = \rho \lambda^3 u_\lambda^2 k^3,$$

where λ is the size of the eddy whose turnover time equals the oscillation period, $u_\lambda/\lambda = \omega_k$. For a Kolmogorov turbulence spectrum, where

$$u_\lambda = u_H \left(\frac{\lambda}{H}\right)^{1/3},$$

and H is the scale height, which is assumed to be the size of the largest turbulent eddies which contain most of the turbulent energy, the oscillation mode energy density is

$$\epsilon_k = \rho u_H^2 \left(\frac{u_H}{s}\right)^{11/2} \left(\frac{\omega}{N_{ac}}\right)^{-5/2}.$$

2. Thermal Overstability

Overstability is an oscillating, thermal instability. There are several kinds of thermal instabilities. The one that works for acoustic waves is the κ- mechanism or the Eddington Valve. If you have an opacity which increases with temperature, then

when the gas is compressed, it gets hotter, the opacity goes up, it blocks the flow of radiation, so heat accumulates which raises the gas pressure, which means there is more pressure expanding the gas than would be obtained from just compressing the gas, and so it will have a stronger expansion than its compression and the amplitude will increase. When you actually calculate the growth rates as Ando and Osaki (1975) did, you find that they are very slow. The time scale for a mode to grow is about a thousand periods, and that is so long that the turbulent viscosity has a chance to destroy the overstability. On the other hand, as we have seen, the turbulent motion may also directly excite the modes. And since we certainly see them in the sun, we know something is exciting them. It ought to be pointed out that the calculations show that the fundamental mode is stable. It is, however, seen on the sun, although at a somewhat smaller amplitude than the higher modes. If the calculations are right, at least the fundamental mode must be excited by some other mechanism besides thermal overstability. So thermal overstability may or may not work for the five minute oscillation. Some people have proposed a mechanism of Doppler shifted line opacities as a generation mechanism for sound waves in stellar winds.

C. DISSIPATION

What about the dissipation of acoustic waves?

1. Radiation

In the first place photons can transfer energy from the hotter to the cooler regions of a wave which will reduce the restoring force and damp the wave. Calculations show that about 90% of the wave energy of the acoustic waves is removed in the photosphere. Radiative damping also alters the phase of the temperature and density relative to the velocity (Noyes and Leighton, 1963).

2. Shocks

The other damping mechanism, of course, is shocks. As the wave propagates its front steepens, and when the thickness of the wave front becomes comparable to the mean free path of the particles, one gets a shock. It should be remarked that a shock has to do with the steepness of the gradient, not with the size of the velocity. You can have a shock where the velocity amplitude is small compared to the sound speed. The distance a wave must travel for a crest to overtake a trough and a shock develop is

$$\Delta Z = 2H \ln \left(1 + \frac{\lambda}{2H} \frac{s}{u} \frac{1}{\gamma+1}\right).$$

Short period acoustic waves will dissipate near the temperature minimum, but longer period waves with periods around the acoustic cutoff period (200 sec) will dissipate higher up. And the five minute oscillation which is evanescent doesn't steepen at all until it gets high enough to become nonlinear. The dissipation length is

$$L \approx \begin{cases} \lambda/(M-1) & \text{weak shocks} \\ \lambda & \text{strong shocks,} \end{cases}$$

and the strength of weak shocks varies as

$$M = V_{shock}/s \propto \rho^{-1/4}$$

(Stein and Schwartz, 1972).

III. GRAVITY WAVES

A. PROPERTIES

In gravity waves the restoring force is buoyancy, which is similar to convection. The different thing about gravity waves is that, while for acoustic waves there is a natural speed, the sound speed, for gravity waves there is a natural frequency, the buoyancy or Brunt-Vaisala frequency at which a blob will oscillate if displaced:

$$N = \left(-\frac{g}{T}\beta\right)^{\frac{1}{2}},$$

where β is the superadiabatic temperature gradient. In an isothermal atmosphere

$$N \rightarrow (\gamma - 1)^{\frac{1}{2}} g/s.$$

Gravity waves only propagate at frequencies less than this natural buoyancy frequency, and the buoyancy frequency is only real and nonzero in convectively stable regions. You cannot have gravity waves propagating in a convectively unstable region. They cannot propagate or be generated inside the convection zone, only by motions in the stable photosphere. Gravity waves propagate energy in a particular direction, which depends on frequency. The cosine of the angle between the flux and the vertical is

$$\cos\theta = \omega/N.$$

For the sun, for values that are appropriate for the granulation,

$$\tau_{granulation} \approx 10\text{-}20 \text{ min and } N_{Tmin} \approx 0.03 \approx 2\pi/3\text{min},$$

the direction of gravity wave energy propagation is

$$\cos\theta \approx 1/5, \quad \theta \approx 75^{\circ}.$$

Figure 2 shows what you would see if you looked at a schlieran photograph of gravity waves produced by an oscillating source. The solid lines are the wave crests and the dashed lines are the wave troughs. The lines intersect at the source. Energy is propagating radially outward at the angle theta and the velocity of the fluid is also radial, parallel to the energy flux, but the phase propagates perpendicular to the energy,

$$\underset{\sim}{v} \;//\; \underset{\sim}{F} \perp \underset{\sim}{k}.$$

You see different waves moving across the fan, while the fan extends out further and further with time as the energy gets out further and further. The group velocity of gravity waves is

$$V_g = \frac{N}{k} \sin\theta.$$

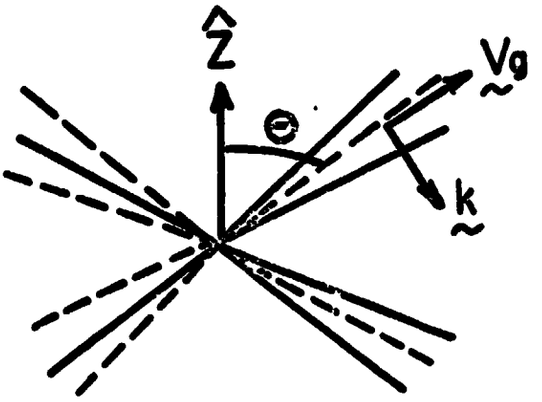

Figure 2: Gravity Wave Crests (——) and troughs (---).

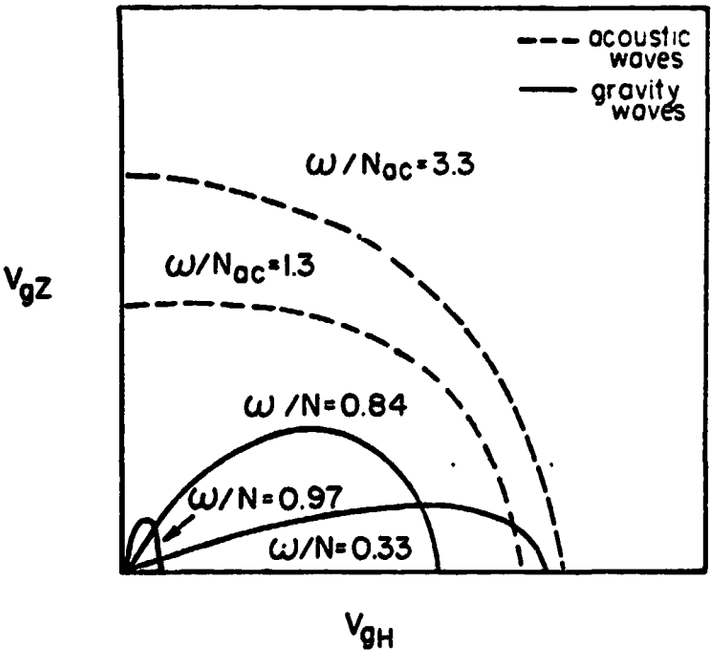

Figure 3: Group Velocity for gravity and acoustic waves.

For solar granulation N/k ~ 1 km/s. Figure 3 shows the group velocity for gravity (and acoustic) waves as a function of frequency and direction. Notice that one would observe low frequency, long wavelength waves first. The phase relations between temperature, density, pressure and velocity for low frequency gravity waves are similar to evanescent acoustic waves:

$$\frac{\delta\rho}{\rho} = i\frac{u}{s}, \quad \frac{\delta T}{T} = -i\frac{u}{s}, \quad \frac{\delta p}{p} = \frac{\omega}{sk_H}\frac{u}{s} << \frac{u}{s}.$$

Pressure fluctuations are in phase with velocity but very small, while temperature and density are 90° out of phase with velocity (Pittway and Hines, 1965; Lighthill, 1978, Chapter 4).

B. GENERATION

Gravity waves are ubiquitous in the atmosphere of the earth; they are produced by any slow motion. Therefore, they should also be present in the Sun. There are two common generation mechanisms.

1. Penetrative Convective Motions

One of the main ways gravity waves will likely be produced is by the penetrative convective motions. One can think of the penetrative convection as blobs pushing on the boundary of the stably stratified layer. The amplitude of the wave produced will be comparable to the amplitude of the penetrative motion,

$$|u_{wave}| = |u_{penetration}|.$$

This has been verified in laboratory experiments (Townsend, 1966). However, since only frequencies that are less than the buoyancy (Brunt-Väisälä) frequency can propagate, only that part of the penetrative convective power that satisfies $\omega = \underline{k}\cdot\underline{V} < N$ will contribute to the production of gravity waves. This mechanism is similar to the Lighthill mechanism, but with an efficiency much smaller one.

If you make a rough estimate for the solar granulation, taking a velocity of 1 km/sec and the appropriate length scales, then

$$F \sim \rho u^2 V_{gz} \sim 3\times10^{-7} \times 10^{10} \times \frac{1}{3}10^5 \sim 10^8 \text{ erg/cm}^2\text{s}.$$

This flux will, however, be greatly reduced by the strong radiative dissipation of gravity waves, which we discuss below.

2. Shear

Gravity waves can also be produced by the shear that will arise from the supergranule motions. Supergranule flows have a cellular structure. Conservation of mass requires that a gradient of the vertical momentum flux produces a horizontal momentum flux. Braking is large in the photosphere and produces a large horizontal flow there. Even though the horizontal momentum flux is small in the chromosphere, the chromospheric horizontal velocity is large, because of the small density. The horizontal

supergranule flow is observed to decrease from ~ 0.8 km/s in the low photosphere to ~ 0.4 km/s in the low chromosphere and then increase to ~ 3 km/s in the mid-chromosphere (November, et al. 1979). Where the size of shear becomes comparable to the buoyancy frequency,

$$\frac{d\, U_H\,(z)}{dz} \geq \min\left[\, N, N^2\, \tau_{cool} \,\right]$$

(where τ_{cool} is the radiative cooling time) the shear layer becomes unstable and radiates gravity waves. Most of the energy is radiated near

$$k = N/\sqrt{2}\; U_H,$$

and the growth times are of order

$$\gamma = 10^{-1}\, dU_H/dz$$

(Lindzen, 1974). This mechanism will operate in the low photosphere where the cooling time is short and in the high chromosphere where the shear is large.

C. DISSIPATION

How do gravity waves dissipate?

1. Wave Breaking

Gravity waves steepen, but instead of forming a shock front they form a thin shear layer, where the fluid velocity changes direction over a very short distance. When that shear becomes comparable to the buoyancy frequency, $dU/dz = N$, turbulence will develop along that wave front. Small scale motions are produced which dissipate the wave motion and damp the wave. To find the condition on the wave amplitude for breaking to occur, we need to calculate du/dz. Let $\underline{u} = (u, 0, w)$ where u is the horizontal and w the vertical component of the velocity. For gravity waves the Boussinesq approximation holds, so

$$\nabla \cdot \underline{u} = 0,$$

which implies that

$$\frac{dw}{dz} = - i\, k_H\, u.$$

The wave equation for gravity waves is

$$\frac{d^2 w}{dz^2} + \left(\frac{N^2}{\omega^2} - 1\right) k_H^{\,2}\, w = 0,$$

so

$$\frac{du}{dz} = \frac{i}{k_H}\,\frac{d^2 w}{dz^2} = -i\left(\frac{N^2}{\omega^2} - 1\right) k_H w.$$

Hence, the condition for gravity wave breaking is

$$N^{-1}\,\frac{du}{dz} = \left(\frac{N^2}{\omega^2} - 1\right)\frac{k_H w}{N} > 1$$

or

$$\omega > \frac{N}{k_H}\left(\frac{N^2}{\omega^2} - 1\right)^{-1}$$

2. Radiative Damping

As we mentioned, there is very severe radiative damping of the gravity waves. Radiation tends to make a wave isothermal, which destroys the buoyancy restoring force. The radiative cooling rate is

$$\gamma_R = \tau_R^{-1} = \frac{16\kappa\sigma T^3}{\rho c_v}\left(1 - \frac{\kappa}{k}\cot^{-1}\frac{\kappa}{k}\right)$$

$$\rightarrow \frac{16\kappa\sigma T^3}{\rho c_v} \times \begin{cases} 1 - \frac{\tau}{2}\frac{\kappa}{k} & \text{optically thin} \\ \frac{1}{3}\left(\frac{k}{\kappa}\right)^2 & \text{optically thick.} \end{cases}$$

where κ is the inverse of the photon mean free path (Spiegel, 1957). The optically thin damping time $\rho c/16\kappa\sigma T^3$, increases rapidly with height and exceeds 10 min above

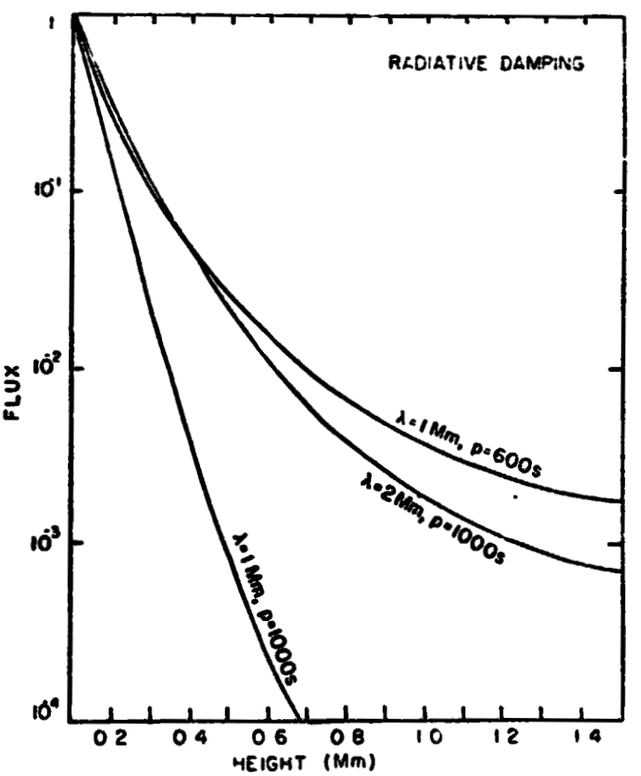

700 km above $\tau_{5000} = 1$. Damping is severe when the radiative cooling time is shorter than the wave period. The long period, short wavelength waves are the most highly damped. Figure 4, from Barbara Mihalas' thesis (1979), shows the fraction of flux remaining at each height for several wavelengths and periods. In order of magnitude, the flux decreases by 10^3 between the bottom of the photosphere and the mid-chromosphere, for parameters appropriate to granule produced gravity waves. On the other hand, gravity waves generated by penetrative motions a few hundred kilometers above the bottom of the photosphere suffer reduced radiative dissipation and can transmit 2% of their flux to the chromosphere. Since the radiation which produces the damping of gravity waves also allows for easier penetration of the convection, the wave flux reaching the chromosphere from penetrative convective motions high up in the photosphere is only slightly less than that from the bottom of the photosphere with its severe radiative damping.

3. Critical Layers

Gravity waves have one other property which is very different from sound waves: they can interact very strongly with the mean horizontal fluid flow. In particular, they can give the fluid a horizontal acceleration. A layer where the horizontal fluid flow velocity is equal to the horizontal phase speed of the wave, is a "critical layer." Here in the fluid frame, the doppler shifted frequency goes to zero, $\omega - \underset{\sim}{k}.\underset{\sim}{u} \to 0$, so the waves propagate along the critical layer, $\cos i = (\omega - \underset{\sim}{k}.\underset{\sim}{u})/N \to 0$, and their energy is absorbed. Such a critical layer can arise from the horizontal supergranulation flow or may be produced by absorption of horizontal gravity wave momentum. For the sun, the horizontal gravity wave phase speed is about 1.5 km/s, which will match the horizontal supergranulation flow somewhere in the mid-chromosphere. The transmission through a critical layer is

$$T = \frac{F_{trans.}}{F_{inc.}} = \exp\left\{-2\pi\left(Ri - \frac{1}{4}\right)^{\frac{1}{2}}\right\},$$

where the Richardson number,

$$Ri = N^2/(dU/dz)^2 ,$$

is the order of 50. Hence, the absorption at critical layers is very large (Booker and Bretherton, 1967; Acheson, 1976). Such critical layers will occur in the chromosphere and will produce localized dissipation of gravity waves there.

The important thing to emphasize about gravity waves is that because they propagate energy mostly horizontally and because of radiative damping, one does not expect too much heating from them. But they are a source of chaos and may contribute substantially to any microturbulence, because they are certain to be there. Their horizontal wavelengths are comparable to granules, $\leq$ 1Mm, and their vertical wavelengths are only 1/4 as large, which is comparable to the scale height or smaller.

IV. ALFVEN WAVES

A. PROPERTIES

Moving on apace, we now come to Alfven waves. Here the restoring force is magnetic tension. The group velocity is the Alfven velocity,

$$V_g = a = B/\sqrt{4\pi\rho}.$$

Unlike the sound speed, the Alfven speed increases substantially between the photosphere and the corona, by a factor of 10^3. The flux is

$$F = \rho u^2 a = \frac{\delta B^2}{4\pi} a,$$

and is parallel to the magnetic field. In the absence of dissipation or refraction, the flux remains constant, so the velocity amplitude scales as

$$u \propto \rho^{-1/4} B^{-1/2}.$$

The velocity is perpendicular to the magnetic field, i.e. transverse to the direction of energy propagation. Hence Alfven waves act like a vibrating string. There is no compression,

$$\delta T = \delta\rho = \delta p = 0,$$

so there are no opacity changes. Only Doppler shifts affect the line profiles. The total magnetic field strength, $|B_o + \delta B|$, is constant, so the wave is polarized in part of the arc of a circle, along which the magnetic vector swings back and forth (see e.g., Bazer and Fleischman, 1959; Barnes and Hollweg, 1974).

Most people up until recently have considered uniform magnetic fields. But we know that in the corona the magnetic field is very inhomogeneous. Luckily it turns out that waves in inhomogeneous fields are rather similar to the internal waves in a uniform field. If you consider a thin flux tube surrounded by plasma in a weaker field, several different modes occur (Roberts and Webb, 1978; Wilson, 1979; Wentzel, 1979a). First, there is an axisymmetic mode which is just the torsional Alfven wave, propagating along the flux tube at the Alfven speed inside the tube, $c = a_i$. Second, there is another axisymmetic mode which is like the slow mode, a sound wave propagating along the flux tube with

$$c^2 = a_i^2 s_i^2/(a_i^2 + s_i^2).$$

It has a short wavelength and its amplitude is concentrated at the surface of the tube. For these waves to excite waves outside the tube, the phase velocity inside the tube would have to be greater than the sound or the Alfven speed outside. In general that is only possible for these modes when the inside density is less than the outside density. Third, there are other modes which are not axisymmetric, and act like vibrating string modes. Their phase velocities are essentially an average of the Alfven speed inside and outside the tube,

$$c^2 = (B_i^2 + B_e^2)/ 4\pi (\rho_i + \rho_e).$$

These modes can have a resonance where the phase velocity of the tube mode equals the local Alfven speed. At that resonant point the amplitude of the perpendicular (to the magnetic field) velocity and electric field becomes large. Other perturbed quantities are unaffected by the resonance. Thus, even in an inhomogeneous corona the waves are similar, although not identical, to those in a homogeneous corona. The main difference is that for these tube or surface wave modes there exists a resonance at places in the flux tube where c = a.

B. GENERATION

What about Alfven wave generation?

1. Convective Motions

Alfven waves can be generated by the convective motions, similar to the Lighthill mechanism for the sound waves. But, because the magnetic field channels the motions, monopole rather than quadrupole emission occurs. The radiated power is

$$P = \frac{\rho u^3}{\ell} (k\ell).$$

For Alven waves,

$$k = \frac{\omega}{a}, \quad \omega = \frac{u}{\ell},$$

so

$$k\ell = \frac{u}{a} = M_B.$$

Thus

$$P = \frac{\rho u^3}{\ell} \left(\frac{u}{a} \right)$$

(Kulsrud, 1965: Kato 1968). Rough estimates for the sun $\rho \sim 10^{-6}$, $u \sim 10^5$, $a \sim 10^6$ predict an Alfven wave flux from strong field regions of

$$F \sim P\ell \sim 10^8 \text{ erg/cm}^2\text{s}.$$

However, anything which jiggles a magnetic field line will also generage Alfven waves, so granules will generate Alfven waves and supergranules will generate Alfven waves. Granules have larger velocities and so are more important. They produce a flux

$$F = \rho u^2 a.$$

For typical granule velocities of 1 km/s,

$$F = 3\times10^{-7} \times 10^{10} \times 10^6 = 3\times10^9 \text{ ergs/cm}^2\text{s}.$$

(See, however, Hollweg, 1979.)

What we are really interested in is the average flux, so we have to include the fact that the flux tubes will spread with height and that the Alfven speed increases with height. The waves produced by granular motions have fairly long wavelength so

they see the change in Alfven speed roughly as a discontinuity. In this case the transmission coefficient is

$$T = \frac{4a_1a_2}{(a_1+a_2)^2} \approx 4\frac{a_1}{a_2} \approx 10^{-3}.$$

The average flux is

$$F = F_o \frac{A_{photo}}{A_{corona}} \approx \frac{a_{photo}}{a_{corona}},$$

where A is the flux tube area. Since the magnetic flux is constant along a flux tube, BA = constant, so $A_a \propto \rho^{-1/2}$. Thus, the average flux will be

$$F = F_o (\rho_{corona}/\rho_{photosphere})^{1/2}$$

$$\approx 10^{-4} F_o$$

$$\approx 3\times10^5 \text{ erg/cm}^2\text{s},$$

which is fairly substantial, enough to heat the corona.

I have not made a distinction between Alfven waves and magnetohydordynamic waves. In a strong field the Alfven and the fast mode are similar and the slow mode is an acoustic wave propagating along the flux tube.

2. Thermal Overstability

Alfven waves may also be generated by thermal overstability. This is not the mechanism, but the Cowling-Spiegel mechanism (Cowling, 1957; Moore and Spiegel, 1966). Here buoyancy acts as a driving force which tends to destabilize the system and make it depart from equilibrium. Magnetic tension acts as a restoring force which tends to bring it back to equilibrium and radiative transfer decreases the destabilizing effect of the buoyancy force. Since there will be less destabilizing effect on the way back than there was on the way out from equilibrium, the magnetic tension will return the system to equilibrium faster than it departed, and the wave amplitude will grow. Because the buoyancy must be destabilizing this mechanism works only in convectively unstable regions. One can calculate the growth rate by equating the rate of working of this buoyancy force with the kinetic energy of the waves (Parker, 1979). The buoyant force is

$$F_B = \Delta\rho g \approx \rho g \frac{\Delta T}{T}.$$

The temperature fluctuation is the temperature difference between the adiabatically displaced fluid in the wave and mean temperature at its displaced level, reduced by diffusive radiation cooling:

$$\Delta T \approx A\lambda\beta \frac{t}{\tau_{cool}},$$

Where A is the wave amplitude, λ is the wave length, β is the superadiabatic temperature gradient, t is the period, and the diffusive radiation cooling time is

$$\tau_{cool} = \frac{\lambda^2}{c\ell_{mfp}} \frac{E_{gas}}{E_{rad}} = \frac{\kappa\lambda^2}{c} \frac{\rho c_p T}{aT^4} = \frac{\rho c_p}{\kappa\sigma T^3} (\kappa\lambda)^2,$$

which is assumed to be much greater than the period. The growth time γ^{-1}, is the time it takes the buoyant work, vF_B, to supply the wave energy $\frac{1}{2}\rho v^2$, where $v = A\omega = A\lambda/t$:

$$\gamma^{-1} v F_B = \frac{1}{2}\rho v^2.$$

Thus

$$\gamma = \frac{g\beta}{T\omega^2\tau_{cool}} = \frac{t_{osc}^2}{t_{eddy}^2\tau_{cool}}.$$

How does this growth rate depend on stellar properties? For an opacity

$$\kappa = \ell_{mfp}^{-1} \propto \rho^{1.7} T^9,$$

hydrostatic equilibrium gives

$$P = \frac{g\rho}{\kappa} \propto g^{.6} T^{-6},$$

so

$$\kappa \propto g/T.$$

The wave frequency is

$$\omega^2 = a^2/\lambda^2 = B^2/\rho\lambda^2 \propto B^2 g^{-.6} T^{+7} \lambda^{-2},$$

and the cooling rate is

$$\tau_{cool}^{-1} = \frac{4F}{\rho c_p T \kappa\lambda^2} \propto g^{-1.6} T^{11} \lambda^{-2},$$

From mixing length theory,

$$\tau_{eddy}^{-2} = \frac{g\beta}{T} = \left(\frac{gF}{\rho c_p T \ell^2}\right)^{2/3}$$

$$\propto g^{1.6} T^{5.25},$$

where $\ell = H \propto T/g$. Hence the growth rate varies with stellar gravity, surface temperature, and magnetic field as

$$\gamma \propto g^{3/5} T^{9.25} B^{-2}.$$

C. DISSIPATION

1. Viscous and Joule Heating

How do Alfven waves dissipate? Alfven waves don't steepen and form shocks, because the Alfven speed is independent of wave amplitude, since the magnetic field strength is constant and they are not compressive. They can still dissipate by particle collisions which produce Joule or viscous heating. However, the damping lengths

are large, although they may be comparable to coronal loop dimensions. The Joule and viscous heating rates are

$$Q_J = \eta J^2 = \eta c^2 k^2 (\delta B)^2/(4\pi)^2$$

and

$$Q_V = \mu k^2 u^2.$$

The damping rate is

$$\gamma = Q/2E,$$

where

$$E = \rho u^2 = \delta B^2/4\pi ,$$

and the damping length is

$$L = a/\gamma.$$

For Joule heating

$$L_J = 8\pi a^3/\eta c^2 \omega^2$$

$$= 10^{20} n^{-3/2} T^{3/2} B^3 P^2 \text{ cm},$$

where the resistivity is

$$\eta = \frac{m_e \nu_{coll}}{ne^2} = \frac{\pi e^2 m^{1/2}}{(kT)^{3/2}} \ln \Lambda = 10^{-7} T^{-3/2}.$$

For viscous heating

$$L_V = 2\rho a^3/\mu\omega^2$$

$$= 10^{23} n^{-1/2} T^{-5/2} B^3 P^2 \text{cm},$$

where the viscosity is

$$\mu = \frac{1}{3} n m_p v_e^2/\nu_{coll} = 10^{-15} T^{5/2}.$$

Viscous damping is more important than Joule heating in the corona and visaversa in the photosphere and chromosphere. If the fields are weak, then the Joule dissipation will be significant in the photosphere. Hence Alfven waves can only get through from the photosphere up into the corona in strong field regions. That used to be a serious problem before we knew that fields come in little patches of high field strength. Now it is not. For typical coronal loop parameters ($n \sim 10^{10} \text{cm}^{-3}$, $T \sim 2 \times 10^{6} \text{K}$, $B \sim 100 \text{G}$, $L \sim 10^{10} \text{cm}$) the viscous damping length is

$$L_V \sim 10^8 P^2 \text{cm},$$

which is comparable to the loop length for short period waves.

Because the corona is inhomogeneous, the Alfven waves are really tube modes and have a resonance where the tube phase speed is equal to the local Alfven speed. In this resonant region the wave amplitude is large. Hence large currents and large Joule heating will occur in the narrow resonant layer. The rate of heating is controlled by the rate at which energy can flow into that resonant region, and has been calculated by Ionson (1978) and Wentzel (1979b):

$$\gamma = \pi\omega k_r \Delta r \quad (\Delta a^2/a^2) \quad (2 + \rho_i/\rho_e + \rho_e/\rho_i)^{-1}.$$

They thought this was the rate at which waves were radiating energy away. It isn't. It is the rate of energy flow into the resonant region (Hollweg, 1979). There is a problem of how the energy released in this very small resonant region volume is transferred to the rest of the large coronal volume where it is needed. Nobody has figured out how that is done. This is a problem for just about every type of Alfven wave dissipation, except for the Joule and the viscous dissipation. The reason is that in order to rapidly dissipate the Alfven wave energy the currents must be clumped, and so the dissipation occurs in a small region.

2. Mode Coupling

In the presence of inhomogenieties the Alfven wave will couple to other wave modes. Coupling will be large between wave modes whose wave vectors' difference is comparable to the inverse of the inhomogeniety scale length. The coupling ratio between two modes is roughly

$$|\Delta kL|^{-1},$$

where Δk is the difference in k between the two modes and L is the length scale of the inhomogeniety (Melrose, 1977). In a strong field the major coupling occurs between Alfven and fast mode waves that are propagating in the direction of the magnetic field, because both of them are propagating nearly at the Alfven speed, so they will stay together. The difference in wave vector is

$$\Delta k = \Delta\left(\frac{\omega}{c}\right) = \frac{\omega}{c}\,\frac{\Delta c}{c},$$

where c is the phase speed of the mode. For propagation close to the magnetic field direction

$$c_+^2 = a^2 + s^2\,\theta^2,$$

$$c_-^2 = s^2\left(1 - \frac{s^2}{a^2}\,\theta^2\right).$$

$$c_A^2 = s^2\,(1 - \theta^2).$$

So

$$\frac{\Delta c}{c} = \frac{c_+ - c_A}{a} = \left(1 + \frac{1}{2}\,\frac{s^2}{a^2}\,\theta^2\right) - \left(1 - \theta^2/2\right)$$

$$\approx \theta^2/2.$$

and

$$\Delta k/k \approx \theta^2/2.$$

Thus the coupling ratio is

$$\approx 2\,(kL)^{-1}\,\theta^{-2}.$$

When $\theta < (\omega/\Omega_i)^{1/2}$, where Ω_i is the ion-cyclotron frequency, ion cyclotron effects increase Δk. So the maximum coupling occurs at this critical angle and is

$$|\Delta kL|^{-1} \approx (kL)^{-1}\,(\Omega_i/\omega)$$

(Melrose, 1977). There will not be much coupling if the waves are not propagating along the field direction, nor will there be much coupling between the Alfven and slow modes. The fast mode, if it gets any energy, will form shocks and dissipate, so that this is a round about way in which the Alfven waves can dissipate their energy.

3. Alfven Wave Decay

The Alfven waves can also decay. If a set of waves satisfy the resonance condition,

$$\omega_o = \omega_1 + \omega_2,$$

$$\underset{\sim}{k}_o = \underset{\sim}{k}_1 + \underset{\sim}{k}_2,$$

which is essentially energy and momentum conservation, then one wave can decay into two. In this case a forward moving Alfven wave can decay into a backward moving Alfven wave and a slow mode pressure wave, at the rate

$$\gamma \approx \omega \left(\frac{a}{s}\right) \frac{k}{\Delta k} \left(\frac{\delta B}{B}\right)^2.$$

(Kaburaki and Uchida, 1971). For a broad spectrum of incident waves, only those that stay in resonance for a decay time, i.e. have $\Delta k/k \sim \Delta\omega/\omega \leq \gamma/\omega$, can decay. So the decay rate is

$$\gamma \approx \omega \left(\frac{a}{s}\right)^{1/2} \left(\frac{\delta B}{B}\right).$$

(Sagdeev and Galeev, 1969). There seems to be some disagreement between the calculated decay rates and the fact that one sees the Alfven waves in the solar wind at the earth.

4. Current Dissipation

Finally, I want to talk a little about current dissipation. Currents are produced not only by Alfven waves, but by any twisting motion of the magnetic flux tubes, for instance a quasi-static twisting motion. Current or magnetic field dissipation is a diffusive process due to single or collective particle collisions. The characteristic resistive diffusion time scale is

$$\tau_R = \frac{2E}{Q_J} = \frac{2B^2}{8\pi\eta J^2} = 4\pi L^2/\eta c^2.$$

For typical coronal parameters $\tau_R \sim 10^4$ yrs, too long to be significant. This Joule dissipation time can be reduced either by reducing the width L of the region through which the currents flow or by increasing the resitivity by increasing the effective collision rate. If some instability or resonance filaments the current so the current density is high in a small region, then there can be significant dissipation of the currents. If that occurs and if the current density $J = n_e e v_{drift}$ becomes large enough so that the drift velocity approaches the electron thermal velocity then substantial numbers of electrons will tend to run away and generate several different types of electrostatic waves. These waves bunch the ions, so that the electrons collide with the electric field of a large collective charge rather than that of a single ion. This scattering of electrons by the waves increases the effective collision rate, the rate of momentum transfer and hence the resistivity. The enhanced resistivity due to electron scattering by plasma waves is called "anomalous resistivity," and since it occurs in conjunction with current filamentation will shorten the resistive diffusion time tremendously (Papadopolous, 1977; Rosner et al, 1978; Hollweg, 1979). Also if the current density becomes large it will develop large shears or gradients in the magnetic field, which will lead to tearing mode instabilities. Parallel currents attract one another and tend to clump. The clumping of current produces a fluid flow that forces the sheared magnetic field into X-type neutral points. Filamented currents are produced with small enough length scales so that the classical, Coulomb collision, resistive diffusion time becomes small and the magnetic field can tear and reconnect and the currents can dissipate (Drake and Lee, 1977). This mechanism has been invoked for the violent energy release in flares (see Spicer & Brown, 1980). However, shorter wavelength tearing modes distort the field lines more, which produces a greater restoring force, and also have a smaller volume of magnetic energy they can release, so they may produce a more tranquil quasi-static heating appropriate for coronal flux tubes. The tearing instability has a lower threshold than the current driven instabilities which lead to anomalous resistivity. To get significant current dissipation by any mechanism, the dissipation must occur in such small volumes that the transfer of the resulting heat to the rest of the corona is a serious problem.

V. CONCLUSION

In conclusion, there are many kinds of different wave motions in the sun; acoustic, gravity, Alfven waves, and other kinds of magneto-acoustic-gravity wave modes; maybe even higher frequency waves like whistlers. All of these ordered motions may contribute to the chaos observed in stellar atmospheres. In order to develop diagnostics, somebody has to take self-consistent calculations of these waves with the right velocities, temperatures, densities and pressures and calculate the effects on the line profiles of each wave mode.

To summarize the major roles of the waves we have discussed today: Acoustic waves can heat the low chromosphere but not the corona. The evidence is partly observational: the observed nonthermal line widths due to waves in the upper chromosphere are too small, and also theoretical: increasing the driving amplitude at the bottom of the atmosphere only increases the dissipation of the acoustic waves in the chromosphere, but doesn't increase the flux through the transition region to the corona.

For gravity waves the motion is mainly horizontal. Their amplitudes will be comparable to the amplitudes of the penetrative convection (granulation). They may contribute to the observed microturbulent velocities, but they are unlikely to be important in the heating.

Alfven waves will dissipate primarily by highly clumped currents in very small regions, so there is the problem of how to get that energy from the small volume where the dissipation occurs to the larger volume of the corona. The nice thing about Alfven waves is that they are observed in the solar wind, and they seem to be important in providing an energy and momentum input to the wind. Someplace between the photosphere and the earth, where the wind is observed, those Alfven waves must be produced.

TABLE I.

WAVE MODE	ACOUSTIC	GRAVITY	ALFVEN
PROPERTIES	Pressure $\underline{u} \;//\; \underline{F} \;//\; \underline{k}$ $V_g \sim s$ Propagating: $\frac{\delta T}{T} \sim \frac{\delta \rho}{\rho} \sim \frac{\delta p}{p} \sim u/s$ Evanescent $\frac{\delta T}{T} \sim \frac{\delta \rho}{\rho} \sim \frac{\delta p}{p} \sim i\,\frac{u}{s}$	Buoyancy $\underline{u} // \underline{F} \perp \underline{k}$ $\cos\theta = \omega/N$ $\frac{\delta p}{p} \sim \frac{\omega}{k_H s}\,\frac{u}{s} << u/s$ $\frac{\delta \rho}{\rho} \sim \frac{\delta T}{T} \sim i\,u/s$	Magnetic Tension $\underline{u} \perp \underline{F},\ \underline{F} // \underline{B}$ $V_g = a$ $\delta T = \delta p = \delta \rho = 0$ $\lvert \underline{B}_o + \delta \underline{B} \rvert = \text{const.}$
GENERATION	Convective Motions Thermal Overstability	Penetrative Convection	Convective Motions Thermal Overstability
DISSIPATION by single or collective partical collisions	Shocks radiation	Shear Critical Layers Radiation	Viscous and Joule Heating Plasma Instabilities Mode Coupling

R.F.S. is grateful for support from N.S.F. grant AST-76-22479, NASA grant NSG 7293, and Air Force contract F19678-77-C-0068. J.L.L. is grateful for support from NASA contract NASw-3053 and NAS-5-23758, and the Lockheed Independent Research Fund.

REFERENCES

Acheson, D. J., 1976, J. Fluid Mech. 77, 433.
Ando, H., and Osaki, Y., 1975, Publ. Astron. Soc. Jap. 27, 581.
Barnes, A., and Hollweg, J. V., 1974, J. Geophys, Res. 79, 2302.
Basri, G. S., and Linsky, J. L., 1979, Astrophys. J. (in press).
Booker, J. R., and Bretherton, F. P., 1967, J. Fluid Mech. 27, 513.
Cowling, T. G., 1957, Magnetohydrodynamics, Interscience, New York.
Drake, J. F., and Lee, Y. C., 1977, Phys. Fluids 20, 1341.
Goldreich, P., and Keeley, D. A., 1977, Astrophys. J., 212, 243.
Hollweg, J. V., 1979, Proc. Skylab Active Region Workshop, ed. F. Q. Orrall, NASA. (in press)
Ionson, J.A., 1978, Astrophys, J., 226, 650.
Kaburaki, O., and Uchida, Y., 1971, Publ. Astron., Soc. Jap. 23, 405.
Kato, S., 1968, Publ. Astron. Soc. Jap. 20, 59.
Kulsrud, R., 1965, Astrophys. J., 121, 461.
Lighthill, J., 1978, Waves in Fluids Cambridge University Press, Cambridge, England.
Lindzen, R. S., 1974, J. Atm. Sci. 31, 1507.
Melrose, D. B., 1977, Aust. J. Phys. 30, 495.
Mihalas, B., 1979, Thesis, University of Colorado.
Moore, D. W., and Spiegel, E.A., 1966, Astrophys. J., 143, 871.
Noyes, R. W., and Leighton, R. B., 1963, Astrophys. J., 138, 631.
November, L. J., Toomre, J., Gebbie, K. B., and Simon, G. W., 1979, Astrophys. J., 227, 600.
Papadopoulos, K., 1977, Rev. Geophys. Space Phys. 15, 113.
Parker, E. N., 1979, private communication.
Phillips, O.M., 1966, The Dynamics of the Upper Ocean, Cambridge University Press, Cambridge, England.
Pitteway, M. L. V., and Hines, C. O., 1965, Can. J. Phys. 43, 2222.
Roberts, B., and Webb, A. R., 1978, Solar Phys. 56, 5.
Rosner, R., Golub, L., Coppi, B., and Vaiana, G. S., 1978, Astrophys. J., 222, 317.
Sagdeev, R. Z., and Galeev, A. A., 1969, Plasma Physics, Benjamin, N. Y.
Schmitz, F., and Ulrichneider, P., 1979, Astron. and Astrophys. (in press).
Spicer, D. S., and Brown J. C., 1980, The Sun as a Star, NASA/CNRS (in press).
Spiegel, E. A., 1957, Astrophys. J., 126, 202.
Stein, R. F., 1967, Solar Phys. 2, 385.
Stein, R. F. and Schwartz, R. A., 1977, Astrophys. J., 177, 807.
Townsend, A. A., 1966, J. Fluid Mech. 24, 307.
Wentzel, D. G., 1979, Astron. and Astrophys. 76, 20.
____ 1979b, Astrophys. J. (in press).
Wilson, P. R., 1979, Astron. and Astrophys. 71, 9.

ATTACHMENT .

SOME EFFECTS OF STRONG ACOUSTIC WAVES ON STRONG SPECTRAL LINES

Pierre Gouttebroze (Laboratoire de Physique Stellaire et Planetaire, Verrières-le-Buisson, France)

John Leibacher (Lockheed Palo Alto Research Laboratory, Palo Alto, CA)

We have studied the formation of optically thick lines in time dependent, non-linear hydrodynamic model of the solar chromosphere. Models of the 200 second, chromospheric oscillation indicate that the emission peaks of self-reversed profiles such as those of MgII and CaII are formed at very different depths depending on the phase of the oscillation, while the central absorbtion feature is emitted at a very nearly constant mass depth. The figure shows the MgII k line emitted by the mean atmosphere, including "microturbulence" (triangles) and the mean profile (squares). In addition to the substantial intensity increase interior to the emission peaks, one should note that the peaks are broadened only towards line center; i.e. the intensity fluctuations are symmetric outside of the peaks and strengthen more than they weaken within the peaks. A more detailed version has been submitted to the Astrophysical Journal.

J. L. wishes to acknowledge support by NASA contracts NASw-3053 and 5-23758.

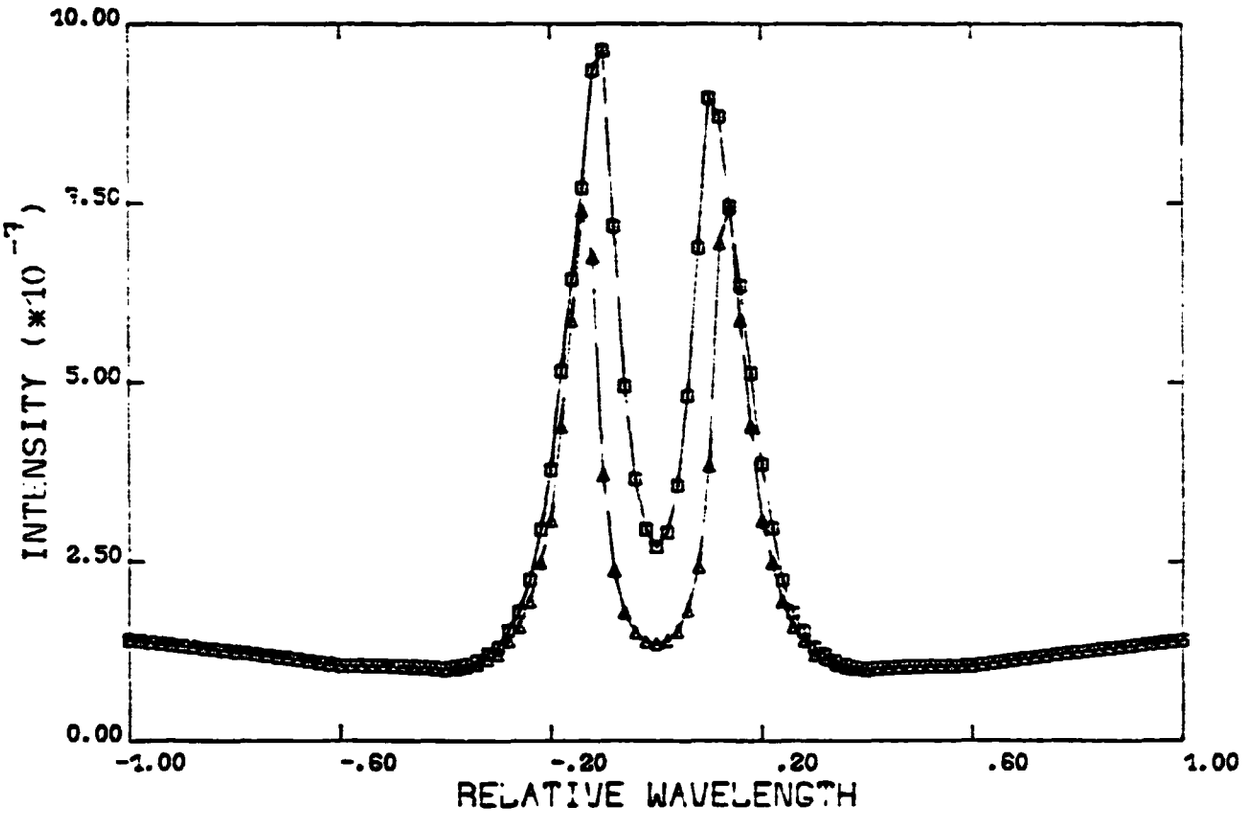
10.00
7.50
5.00
2.50
0.00
INTENSITY (*10^-7)
-1.00
-.60
-.20
.20
.60
1.00
RELATIVE WAVELENGTH